EXPRESSION, SUBCELLULAR LOCALIZATION AND FUNCTIONAL CHARACTERIZATION OF RBM5 AND RBM10 DURING THE DIFFERENTIATION OF C2C12 SKELETAL MYOBLASTS (SKELETAL MYOGENESIS)

by

Twinkle Jasmine Masilamani

A thesis submitted in partial fulfillment
of the requirements for the degree of
Doctor of Philosophy (PhD) in Biomolecular Sciences

The Faculty of Graduate Studies
Laurentian University
Sudbury, Ontario, Canada

© Twinkle J. Masilamani, 2016

THESIS DEFENCE COMMITTEE/COMITÉ DE SOUTENANCE DE THÈSE
Laurentian Université/Université Laurentienne
Faculty of Graduate Studies/Faculté des études supérieures

Title of Thesis Titre de la thèse	EXPRESSION, SUBCELLULAR LOCALIZATION AND FUNCTIONAL CHARACTERIZATION OF RBM5 AND RBM10 DURING THE DIFFERENTIATION OF C2C12 SKELETAL MYOBLASTS (SKELETAL MYOGENESIS)
Name of Candidate Nom du candidat	Masilamani, Twinkle
Degree Diplôme	Doctor of Philosophy
Department/Program Département/Programme	Biomolecular Sciences
Date of Defence Date de la soutenance	March 26, 2015

APPROVED/APPROUVÉ

Thesis Examiners/Examinateurs de thèse:

Dr. Leslie Sutherland
(Supervisor/Directrice de thèse)

Dr. Celine Boudreau-LarivièreDr. Robert
(Committee member/Membre du comité)

Dr. Robert Lafrenie
(Committee member/Membre du comité)

Approved for the Faculty of Graduate Studies
Approuvé pour la Faculté des études supérieures
Dr. David Lesbarrères
M. David Lesbarrères
Acting Dean, Faculty of Graduate Studies
Doyen intérimaire, Faculté des études supérieures

Dr. Joe Quadrilatero
(External Examiner/Examinateur externe)

Dr. Jeffrey Gagnon
(Internal Examiner/Examinateur interne)

ACCESSIBILITY CLAUSE AND PERMISSION TO USE

I, **Twinkle Masilamani**, hereby grant to Laurentian University and/or its agents the non-exclusive license to archive and make accessible my thesis, dissertation, or project report in whole or in part in all forms of media, now or for the duration of my copyright ownership. I retain all other ownership rights to the copyright of the thesis, dissertation or project report. I also reserve the right to use in future works (such as articles or books) all or part of this thesis, dissertation, or project report. I further agree that permission for copying of this thesis in any manner, in whole or in part, for scholarly purposes may be granted by the professor or professors who supervised my thesis work or, in their absence, by the Head of the Department in which my thesis work was done. It is understood that any copying or publication or use of this thesis or parts thereof for financial gain shall not be allowed without my written permission. It is also understood that this copy is being made available in this form by the authority of the copyright owner solely for the purpose of private study and research and may not be copied or reproduced except as permitted by the copyright laws without written authority from the copyright owner.

Abstract

RNA-binding proteins (RBPs) are a highly regulated, evolutionarily conserved and functionally distinct family of proteins involved in key RNA metabolic processes. The RNA-binding motif protein RBM5 is an anti-proliferative, pro-apoptotic, putative tumor suppressor. A paralogue of RBM5, RBM10, which shares 50% identity with RBM5, functions in development. RBM5 and RBM10 are spliceosomal components involved in alternative splicing. *RBM5* and *RBM10* are ubiquitously expressed with higher levels in muscle (heart and skeletal) and pancreas. Most of the studies on RBM5 and RBM10 have been focused on cancer cells. Several factors such as 1) abundance in muscle, 2) developmental and temporal regulation, 3) alternative splicing activity and 4) association with functional events related to muscle development led us to hypothesize that both RBM5 and RBM10 are involved in skeletal muscle differentiation. The mechanism of action through which these two RBPs effect differentiation is hypothesized to involve alternative splicing of muscle differentiation-specific mRNAs. RBM5 and RBM10 expression and intracellular distribution was analyzed during muscle differentiation in the C2C12 murine model using qPCR, end-point PCR, immunoblotting and confocal microscopy. Also, RBM5 and RBM10 levels were transiently down-regulated using siRNA either separately and/or together and the associated changes in cell phenotype, expression of myogenic proteins plus a few alternative splicing events were analyzed. We observed a decrease in RBM5 and RBM10 protein expression levels in the differentiated myotubes compared to the myoblasts and myocytes, which indicates a time-dependent potential regulatory role during differentiation. Further, changes in RBM5 and RBM10 protein expression without modulating the levels of mRNA variants suggests post-transcriptional and/or post-translational regulation. Stage-specific differential localization suggests multiple functions related to mRNA biogenesis. RBM5-depleted cells showed a reduction in the total cell number during differentiation, and exhibited a delay in differentiation, fusion and maturation with down-regulated expression of myogenin and myosin heavy chain (MyHC). This implies that RBM5 is necessary to maintain the cell population to execute the myogenic differentiation process in a timely manner. RBM10-depleted cells showed an increase in total cell number immediately after transfection, and

exhibited a delay in differentiation with a decrease in inclusion of exon 11 in *Dtna* mRNA. This indicates that RBM10 is required to maintain the necessary cell population before induction and acts as a splicing regulator during differentiation. RBM5- and RBM10- depleted cells differentiated and matured slowly, and had an increase in Mef2c γ exon inclusion. Therefore, these two RBPs are associated with the alternative splicing of Mef2cγ during differentiation. This is the first study to analyze the expression and the function of these two RBPs in a murine skeletal muscle differentiation model, and has implicated them in myogenesis, paving a way for further characterization. Future studies can investigate the involvement of RBM5 and RBM10 in disease states such as muscular dystrophy and rhabdomyosarcomas, given the known functions of RBPs in tumorigenesis in other cell types.

Keywords

RBM5, RBM10, Skeletal Myogenesis, C2C12, Development, Differentiation, Alternative Splicing, RNA-binding proteins

Acknowledgments

I acknowledge the guidance and support of Drs. Leslie Sutherland, Céline Larivière and Robert Lafrenie. I extend my sincere gratitude to Advanced Medical Research Institute of Canada (AMRIC). I thank my family and friends for their continued love and support. I acknowledge the funding support from Vanier Canada Graduate scholarship.

Table of Contents

List of Tables

List of Figures

List of Abbreviations

aa : amino acid

ANOVA : analysis of variance

AS : alternative splicing

BSA : bovine serum albumin

BrdU : 5-bromo 2'-deoxyuridine

DGC : dystrophin glycoprotein complex

DMEM : Dulbecco's modified eagle medium

DM : differentiation medium

DTNA : dystrobrevin

FBS : fetal bovine serum

GM : growth medium

hnRNP : heterogeneous ribonucleoprotein

HPF : high power field

HRP : horseradish peroxidase

HS : horse serum

IF : immunofluorescence

IHC : immunohistochemistry

KD : knockdown

MEF2 : myocytes enhancer factor 2

miRNA : micro RNA

MRF : myogenic regulatory factor

MyHC : myosin heavy chain

NICD : notch intracellular domain

Na_2VO_3 : sodium orthovandate

NaF : sodium fluoride

NaN_3 : sodium azide

NLS : nuclear localization signal/sequence

NMD : non-sense mediated decay

NSCLC : non-small cell lung carcinoma

NTC : no template control

PAGE : poly acrylamide gel electrophoresis

PBS : phosphate buffered saline

PCR : polymerase chain reaction

PVDF : polyvinylidene difluoride

RBM : RNA-binding motif

RBP : RNA-binding proteins

RIPA : radio immunoprecipitation assay

RNAi : RNA interference

RNP : ribonucleoprotein

RRM : RNA recognition motif

SDS : sodium dodecyl sulphate

SEM : standard error of the mean

siRNA : small interfering RNA

TBS : tris buffered saline

TARP : talipes equinovarus, atrial septal defect, Robin sequence and persistent left superior vena cava

UTR : untranslated region

VSMC : vascular smooth muscle cell

List of Appendices

Chapter 1

1 Introduction

1.1 RNA-Binding Proteins

During RNA biogenesis, multiple factors are involved in regulating all of the steps from generation to degradation of mature mRNA transcripts. One of the major factors involved in this control are the RNA-binding proteins (RBPs). RBPs bind to nascent transcripts to form ribonucleoprotein complexes (RNPs). These RNPs are essential components in many RNA metabolic processes including splicing, capping, polyadenylation, transport, localization, stability and translation (Glisovic et al., 2008). The predominant mechanisms of RNP activity are post-transcriptional control, which is accomplished by (a) binding of RBPs to the 3' or 5' untranslated regions (UTR) of RNA leading to transcriptional repression or activation, and (b) RBPs acting as splicing factors leading to alternative splicing of mRNAs, thereby resulting in expression changes of important genes (Kishore et al., 2010). Thus, RBPs play an important role in RNA metabolism by regulating a number of gene expression changes in a cell.

RBPs are highly significant, evolutionarily conserved and functionally relevant amongst species. Most of the functions of RBPs are in developmental processes, specifically, in germ-line and early embryo development (Naryzhny et al., 2006, Colegrove-Otero et al., 2005). They are also involved in the development of neuron, muscle, hypodermis and excretory cells and determine the timing of development (Lee and Schedl, 2006). Additional associated functions of RBPs are in cell attachment, cell migration, cell cycle checkpoint control, DNA damage responses and miRNA biogenesis (Lunde et al., 2007). Because RBPs are implicated in multiple cellular events, it is not surprising that their expression is highly regulated. It is worth highlighting that altered expression, mutation and improper functioning of RBPs can cause cancer (Kim et al., 2009, Wurth, 2012), muscular atrophies (Lukong et al., 2008), cardiovascular diseases (Musunuru, 2003) and neurodegenerative diseases (Lukong et al., 2008).

There are close to 860 RBPs in humans (Castello et al., 2012) and many of them are associated with major cellular processes. Cell-specific RBPs are required for regulation of cell growth, proliferation, differentiation, and development and are spatio-temporally regulated (Kishore et al., 2010). Two such important RBPs are the RNA-binding motif proteins RBM5 and RBM10. These two proteins are implicated in many processes including cell proliferation and apoptosis in tumor cells.

1.2 RBM5

The *RBM5* gene, first cloned as Gene15 (Wei et al., 1996), is located on chromosome 3p21.3 and encodes the RBM5 protein. *RBM5* was originally identified as one of the 19 genes belonging to the tumor suppressor locus that is deleted in lung carcinomas (Timmer et al., 1999). RBM5 is also known as LUCA-15 (Drabkin et al., 1999) and H37 (Oh et al., 1999).

1.2.1 Alternatively spliced variants

A number of alternatively spliced variants have been identified for RBM5 (Figure 1.1). Full-length human *RBM5* mRNA variant (NM_005778.3) is approximately 3kb containing 25 exons. This variant encodes an 815 amino acid (aa) RBM5 isoform with a molecular weight of ~113 kDa. Deletion of exon 6 produces the *RBM5△6* variant, which encodes a ~17 kDa isoform due to a frame-shift mutation (Mourtada-Maarabouni et al., 2003). Two other variants retain introns: *RBM5+5+6* retains introns 5 and 6; and, *RBM5+6* retains intron 6. Both of these variants putatively encode ~17 kDa and 21.5 kDa proteins, respectively, however the transcripts could be destroyed by non-sense mediated decay (NMD) (Sutherland et al., 2005). A truncated transcript of *RBM5+5+6*, termed *RBM5+5+6t* or clone26, so named because of the presence of stop codon at intron 6, has also been identified (Sutherland et al., 2000, Sutherland et al., 2005). A non-coding RNA of antisense orientation termed *RBM5-AS1* (previously termed LUST) is a 1.4kb fragment, antisense to introns 6 to 4 (Rintala-Maki and Sutherland, 2009). This fragment also includes Je2, a 326bp sequence initially identified in bone marrow by Sutherland et al. (2000). Therefore, generation of various transcripts by alternative splicing shows that RBM5 undergoes post-transcriptional modifications.

The mouse *Rbm5* full-length variant (NM_148930.3) is 3104bp long. The cDNA is 90% and the protein is 97% identical to human RBM5. Using end-point PCR, Ozuemba (2011) identified that homologs to the human *RBM5* variants *RBM5*, *RBM5+6*, *RBM5+5+6* and *RBM5-AS1* were present in mouse tissues such as brain, skin, skeletal muscle and heart.

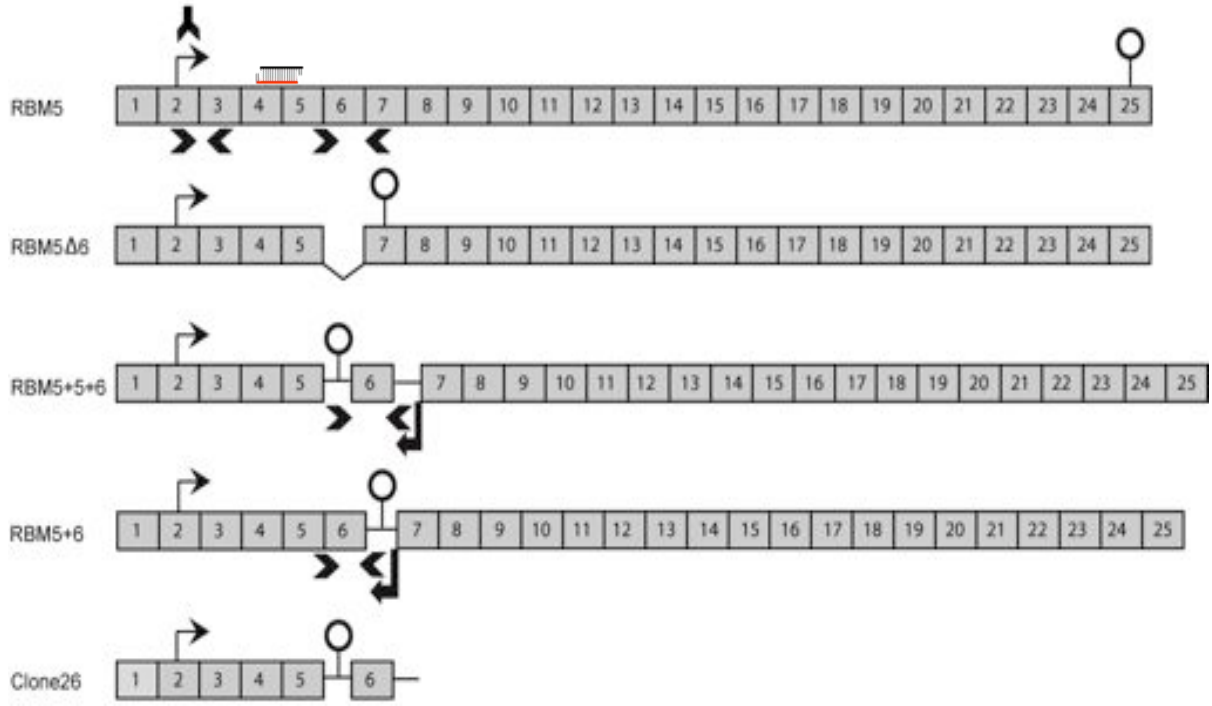

Figure 1.1 The various alternatively spliced human *RBM5* mRNA variants. Diagram illustrating the alternatively spliced variants of *RBM5* with the start and stop codon positions in the protein coding sequence. The antisense variant *RBM5-AS1* is not included here. Location of primers used in reverse transcription and qPCR, antibody and siRNA used in this study are indicated schematically. Primers and siRNA were designed using mouse-specific *Rbm5* mRNA sequence (NM_148930.3). Not drawn to scale. Adapted from Sutherland et al., 2005.

Start and stop codons

Primers used in qPCR

Gene-specific primer (mFactorXF) used in reverse transcription

Antibody, LUCA-15UK

siRBM5 (siRNA), target site (end of exon 4 and beginning of exon 5)

1.2.2 RBM5 function

RBM5 functions as a pro-apoptotic, anti-proliferative, putative tumor suppressor. It has been observed that changes in RBM5 expression affected approximately 35 genes associated with apoptosis and cell proliferation (Maarabouni and Williams, 2006). RBM5 is a putative tumor suppressor, particularly in lung carcinoma (Sutherland et al., 2010). *RBM5* is one of the 19 genes (370kb) undergoing allelic loss and homozygous deletion in lung cancer (Timmer et al., 1999). A recent study identified RBM5 as an important component in spermatid differentiation (O'Bryan et al., 2013). RBM5 was purified along with spliceosomal B complexes demonstrating that it is one of around 200 proteins involved in pre-mRNA splicing (Schmidt et al., 2014).

1.2.2.1 Apoptosis

Apoptosis, or programmed cell death, is a major player in tumorigenesis. Cancer cells evade apoptosis by up-regulating expression of anti-apoptotic proteins and down-regulating expression of many pro-apoptotic related proteins. When the full-length RBM5 was experimentally overexpressed in A549 cells (human alveolar basal epithelial adenocarcinoma) (Shao et al., 2012), Jurkat cells (human T-cell leukemia) (Sutherland et al., 2000), MCF-7 cells (human breast adenocarcinoma) (Rintala-Maki et al., 2004) or PC3 cells (human prostate cancer) (Zhao et al., 2012), the cells died of apoptosis. In A549 cells, RBM5 regulated apoptosis by up-regulating the expression of the apoptotic protein Bax (Shao et al., 2012). When RBM5 was overexpressed in cisplatin-resistant A549/DPP cells, induction of apoptosis was through the mitochondrial intrinsic apoptotic pathway involving Cytochrome-c, Caspase-3 and Caspase-9 activation (Li et al., 2012). In Jurkat cells, RBM5 overexpression led to apoptosis by activation of the extrinsic pathway via Fas, TNF-α and TRAIL (Sutherland et al., 2000). In MCF-7 cells, apoptosis was induced through the TNF-α mediated pathway (Rintala-Maki et al., 2004). In PC3 cells, overexpression of RBM5 led to apoptosis by increasing the expression of p53, B3H-only proteins, cleaved Caspase-3 and cleaved Caspase-9 (Zhao et al., 2012). RBM5 up-regulated the expression of BH3-only proteins, Bim, Bid and Bad, which affected the mitochondrial membrane potential and

triggered the mitotic apoptotic pathway. Thus, up-regulated RBM5 expression in tumor cells promotes apoptosis, thereby inhibiting tumor progression. Similarly, when RBM5 was overexpressed *in vivo*, there was increased apoptosis in lung adenocarcinoma xenografts (Shao et al., 2012).

A recent study identified a mis-sense mutation in RBM5, which affected its ability to bind various mRNA targets, consequently resulting in male sterility in mice (O'Bryan et al., 2013). This mutation of arginine to proline at the 263 amino acid position (R263P) caused testicular atrophy, spermatid differentiation arrest and sloughing of germ cells due to the loss-of-function allele. Besides affecting expression of many genes involved in these pathways, the RBM5 mutant activated the Caspase pathway; the levels of cleaved Caspase-3 and Caspase-9 were high leading to apoptosis and sloughing of the male germ cells.

Interestingly, the alternatively spliced variants of *RBM5* were able to differentially regulate the expression of major apoptotic genes resulting in different effects (Maarabouni and Williams, 2006). The variants hold significant functions in tumorigenesis. As explained above, full-length *RBM5* is pro-apoptotic, however, *RBM5△6* (Mourtada-Maarabouni et al., 2003) and *RBM5-AS1* (Je2 cDNA antisense fragment) (Mourtada-Maarabouni et al., 2006) are anti-apoptotic. Overexpressed *RBM5-AS1* decreased the expression of full-length *RBM5* and changed the expression of six apoptotic genes in CEM-C7 cells (Mourtada-Maarabouni et al., 2006). For example, *RBM5-AS1* expression up-regulated the expression of Bax, down-regulated the expression of BCL-2 and BCL-XL, increased the release of Cytochrome-c and increased the activation of Caspase-9 and Caspase-3 (Mourtada-Maarabouni et al., 2006). In CEM-C7 and Jurkat T- cells, *RBM5-AS1* overexpression inhibited apoptosis via the Fas and TNF-α mediated extrinsic apoptotic pathway (Mourtada-Maarabouni et al., 2001, Sutherland et al., 2001). In contrast, overexpression of *RBM5+5+6t* is cytotoxic and in Jurkat cells leads to Fas-mediated apoptosis (Sutherland et al., 2000) indicating that this variant has similar functions to the full-length *RBM5*.

1.2.2.2 Cell cycle arrest and cell proliferation

Most tumor suppressors are negative regulators of cell growth. RBM5 has an anti-proliferative function in tumor cells. When RBM5 was overexpressed in human breast

cancer cells, NCI-H740 (small cell lung cancer), H1299 (non-small cell lung carcinoma), A9 (mouse fibroblasts) and HT1080 (human fibrosarcoma) cells, there was growth suppression indicating anti-proliferative functions (Kobayashi et al., 2011). There was also a significantly lower proliferation index in RBM5 transfected PC-3 cells (Zhao et al., 2012). Cell proliferation and cell cycle arrest are associated events. Cell proliferation is associated with initiating the cell cycle by activating the early events in G1 (Berridge, 2007). RBM5 causes cell cycle arrest in G1 when overexpressed in CEM-C7 cells (Mourtada-Maarabouni et al., 2003). In A549 cells, the effect of RBM5 overexpression was through down-regulating expression of Cyclin A and retinoblastoma proteins leading to cell cycle arrest at G1 (Shao et al., 2012). When RBM5 was overexpressed in H1299 cells, suppression of cell growth was mediated via the p53 pathway (Kobayashi et al., 2011). Accordingly, RBM5 overexpression prevented formation of tumors in nude mice and inhibited the growth of human breast cancer cells and A9 mouse fibrosarcoma cells (Oh et al., 2002). Thus, both *in vitro* and *in vivo*, the effects of RBM5 indicate tumor specific anti-proliferative functions.

1.2.2.3 Splicing regulation

One way of modulating protein expression is by alternative splicing of mRNA. As stated earlier, most RBPs are associated with post-transcriptional regulation by controlling alternative splicing because of their RNA-binding capacity. The function of RBM5 in regulating alternative splicing is confirmed by target identification and binding studies. RBM5 interacts with spliceosomal A complex (Bonnal et al., 2008, Fushimi et al., 2008). Specifically, RBM5 is associated with spliceosomal complexes such as U2AF65 and U2AF35. RBM5 controls splice-site pairing and directly binds to pre-mRNA (Bonnal et al., 2008). RBM5 is a component of spliceosomal B complex (Schmidt et al., 2014).

Besides affecting expression of apoptotic genes, RBM5 is shown to alternatively splice a few other apoptotic-related mRNAs. RBM5 is involved in the exclusion of exon 9 of *CASP-2* by binding to a splice site in intron 9 (Fushimi et al., 2008). RBM5 has also been shown to regulate the exclusion of exon 6 in FAS and the exclusion of exon 7 in c-FLIP (Bonnal et al., 2008). When RBM5 was overexpressed in HeLa cells it induced alternative splicing changes in activation-induced cytidine deaminase (AID) such as skipping of exon

4 by inhibiting the splicing of intron 3, as RBM5 possibly competes with the U2AF65 and a weak U2AF35 binding site at the 3' splice site of the mRNA (Jin et al., 2012). RBM5 is involved in regulating the alternative splicing of abscisic acid-insensitive3 (ABI3). Specifically, RBM5 decreases splicing of *ABI3-β* and increases splicing of *ABI3-α*, which is important for seed maturation in *Arabidopsis thaliana* (Sugliani et al., 2010). RBM5 is also involved in skipping exons 40 and 72 of the *Dystrophin* mRNA in humans (O'Leary et al., 2009). RBM5 is a splicing regulator in spermiogenesis (O'Bryan et al., 2013). RBM5 bound to many splicing regulators such as the hnRNPs (heterogeneous nuclear ribonucleoproteins) hnRNP A2/B1, hnRNP K, hnRNP M and hnRNP UL1, the SR proteins (serine/arginine-rich splicing factor) SFRS1/ASF/SF2 and PSIP1, the splicing factor SFPQ, and the RNA helicase DDX5 and U1A, implicating a role in mRNA splicing during spermatid differentiation. In addition, other protein-binding partners included polyadenylate-binding protein 1 (PABP1), DEAD box helicase 4 (DDX4), paraspeckle component 1 (PSPC1) and embryonic lethal abnormal vision-like protein 1 (ELAV1), implying a role in RNA metabolism during sperm development. The pre-mRNAs that are spliced significantly by the R263P mutant were suppression of tumorigenicity 5 (*St5*) (increase in exon 3 skipping), ankyrin repeat and SOCS box containing 1 (*Asb1*) (exon 3 and exon 4 skipping) and phospholipase A2, groupX (*Pla2g10*) (intron retention). Apparently, RBM5 was involved in promoting exon inclusion in a variety of mRNA.

Besides these functions, RBM5 was down-regulated in metastasis, especially in stage I solid tumors (Ramaswamy et al., 2003). In lung and breast epithelial cells (BEAS-2B, MCF-10A), as well as in lung cancer cells (A549), knocking down RBM5 up-regulated proteins involved in cell adhesion, migration and motility such as Rac1, β-catenin, collagen and laminin, promoting metastasis (Oh et al., 2010). Thus, an additional function in metastatic processes has been suggested for RBM5.

1.2.3 RBM5 expression profile

RBM5 is ubiquitously expressed in human primary tissues, with the highest expression in heart, skeletal muscle and pancreas (Drabkin et al., 1999). Tissue-specific and spatio-temporal expression was observed; for example, RBM5 expression was high in adult thymus and fetal kidney but was lowest in fetal thymus and adult kidney (Drabkin et al.,

1999). Further, RBM5 levels were higher in adult thymus than in fetal thymus, higher in fetal kidney than in adult kidney and higher in older fibroblasts and cultured lymphocytes than in younger cells (Geigl et al., 2004). This shows that RBM5 expression is developmentally regulated. A recent study showed that the expression level of *Rbm5* was highest in adult mouse testis, followed by ovary and brain, when compared with the levels in epididymis, uterus, kidney, lung, spleen, skeletal muscle, stomach and liver (O'Bryan et al., 2013). This group also reported that RBM5 is expressed in somatic, germ and differentiating cells, such as spermatogonia, spermatocytes and round spermatids. A recent report by Loiselle and Sutherland (2014) using H9c2 rat myoblasts revealed that RBM5 was expressed in skeletal and cardiac lineage specific differentiation.

As previously mentioned, alterations in gene expression characteristically reveals association with many diseased states. RBM5 is no exception. Aberrant expression and mutations in RBM5 have been associated with tumorigenesis and male sterility, respectively. Importantly, down-regulated expression of RBM5 was seen in pancreatic ductal adenocarcinoma (Peng et al., 2013), cancerous prostatic tissue (Zhao et al., 2012), lung adenocarcinoma (Shao et al., 2012), non-small cell lung carcinoma (NSCLC) (Liang et al., 2012), human vestibular schwannomas (Welling et al., 2002), stage III serous ovarian carcinoma (Kim et al., 2010) and biliary tract cancer (Miller et al., 2009). Reduced RBM5 expression was also reported in A549 cells (Oh et al., 2006) and cisplatin-resistant A549 cells (Li et al., 2012). In most cases, RBM5 was down-regulated, however, RBM5 was shown to be up-regulated in breast and ovarian cancer. Interestingly, this overexpression in breast cancer was associated with Her-2 overexpression (Rintala-Maki et al., 2007), which shows that there are other associated factors contributing to the expression and functional relevance of RBM5.

The *RBM5* mRNA variants have the ability to modulate expression of their own other variants, especially the antisense variants. Accordingly, when *RBM5-AS1* was overexpressed, there was an increase in *RBM5+5+6* levels but a decrease in *RBM5+5+6t* levels (Rintala-Maki and Sutherland, 2009). In addition, *RBM5-AS1* (Je2) regulates the expression of full-length RBM5 (Mourtada-Maarabouni et al., 2002, Rintala-Maki and Sutherland, 2009). Internal control mechanisms are in place to regulate expression and thus

function. Therefore these variations in expression and their regulation suggest that RBM5 gene expression and post-transcriptional modifications are likely in many systems of study.

Thus far, only one mutation corroborates RBM5's association with male sperm cell development. Mice with a mis-sense mutation (R263P) have abnormal spermatid differentiation and are sterile (O'Bryan et al., 2013). There was no reduction in RBM5 mRNA or protein levels in the knockout mice having this mutation. Furthermore, besides human studies, animal gene expression studies reveal that Ras-transformed Rat-1 rat embryonic fibroblastic cells have reduced RBM5 levels (Edamatsu et al., 2000). This study also showed that the *Rbm5+5+6t* variant is expressed in rat fibroblasts.

1.2.4 RBM5 structure

A characteristic feature of RBPs is the presence of RNA-binding domains (RBDs). The RBDs bind to either double-stranded (ds) RNA or single-stranded (ss) RNA either in a sequence or structure dependent manner. Some well-characterized functional domains are RNA Recognition Motifs (RRMs), Zinc Finger (ZF) domains, Serine-Arginine (SR) domains, Glycine-rich patch (G-patch) domains, K-Homology (KH) domains, Octamer repeats (OCRE), DEAD/DEAH box and Piwi/Argonaute/Zwille (PAZ) domains (Lukong et al., 2008). The presence of these motifs is necessary to recognize different RNAs, particularly to form RNA-protein interactions which contribute to distinct functions; RNA helicase activity (DEAD/DEAH box), splicing (ZF and KH domains), translation, transcription, chromatin remodeling (KH domain), RNAi (PAZ domain) and promoters of protein-protein interactions (SR domain) (Wurth, 2012).

Like all typical RBPs, RBM5 contains two RRM domains, two ZF domains (RanBP2 and C2H2), one SR domain, one glutamine-rich domain, one G-patch and one OCRE domain (Figure 1.2). Similarly, these various domains in RBM5 have been associated with various functions such as (a) RNA-protein interactions resulting in involvement in splicing, (b) protein-protein interactions involved in binding with other hnRNP/SR related proteins and (c) a localization sequence necessary for transport between the nucleus and cytoplasm. *In silico* analysis using the PROSITE database can be used to identify probable motif regions. Subsequently, the importance of these predicted sequence regions have been analyzed by

mutagenesis and deletion experiments. The RRMs are located in exon 6 (98-178 aa position) and exon 10 (231-315 aa position). The presence of two RRMs provides better recognition of target RNA sequences and enhanced binding kinetics by forming a RNA-binding pouch. Furthermore, Zhang et al. (2014) showed that deletion of both RRM domains inhibit cancer cell proliferation, are needed for apoptosis by activation of Caspase-3 and contribute to alternative splicing of Caspase-2. The RanBP2-type ZF is located in the N-terminal region between the 181-209 aa residues, while the C2H2-type ZF motif region is located between 647-677 aa residues in the C-terminus (Mourtada-Maarabouni et al., 2003). These two ZF motif regions are responsible for binding to specific RNA targets and thus are involved in splicing. The OCRE is located between 452-511 aa residues and is involved in regulating alternative splicing (Bonnal et al., 2008). The continuous Glycine-rich region is located in the C-terminal position between 741-787 aa residues and functions in RNA splicing (Li and Bingham, 1991). Besides these RNA-binding associated motifs, RBM5 has two bipartite nuclear localization signals (NLS) and an arginine-rich N terminal region (RS-domain) suggesting localization to the nucleus. The Glutamine-rich domain located in the N-terminal region (362-385 aa) is a protein-protein interaction site (Mourtada-Maarabouni and Williams, 2002). Thus, detailed structural analyses of RBM5 have revealed a number of sequence-specific regions, which help to predict RBM5 function.

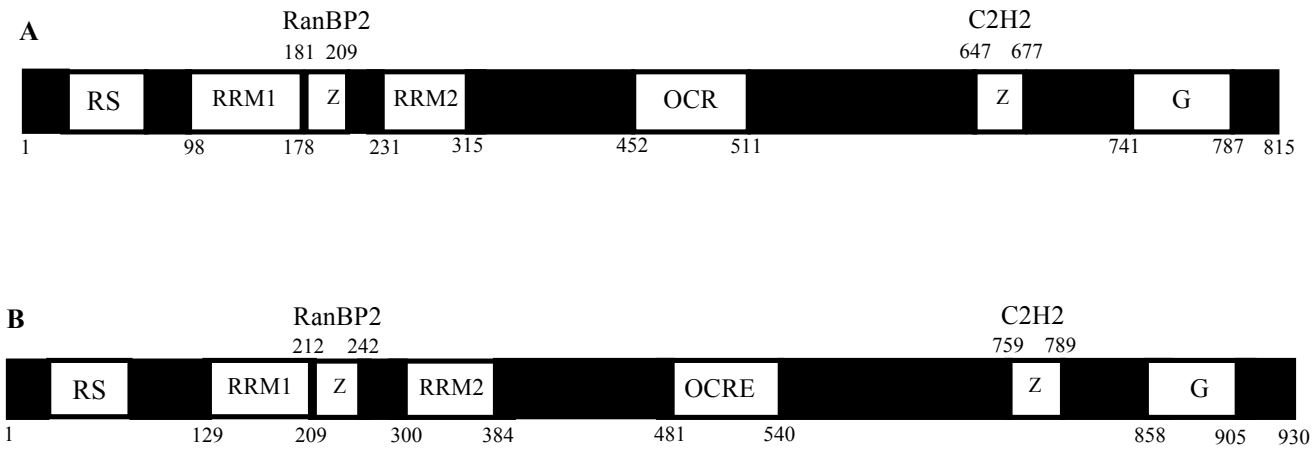

Figure 1.2 Protein domains of RBM5 and RBM10. Schematic description of the protein domain structures of the human **A**) RBM5 (UniProt ID P52756, NCBI accession number NP_005769.1) and **B**) RBM10 isoform1 (UniProt ID P98175, NCBI accession number NP_005667.2)**.** RBM5 and RBM10 are RNA-binding proteins containing several motif regions associated with binding to RNA in a sequence or structure specific manner. The following are the description of each domain: RS= Arginine-Serine rich domain, RRM= RNA recognition motif, Z= Zinc finger motif (RanBP2 and C2H2), OCRE= Octamer repeat domain and G= Glycine-rich patch. The numbers indicate their corresponding amino acid positions.

1.2.5 RBM5 binding

The first *in vitro* binding studies performed on RBM5 were by Drabkin et al. (1999). They showed that the RRM domains bind to poly (G) RNA thus demonstrating that RBM5 was indeed a RBP. A year later, Edamatsu et al. (2000) confirmed this poly (G) RNA-binding and further identified that the binding capacity was stronger to the RBM5 N-terminal fragment than to the RBM5 C-terminal fragment. Later, it was shown that the RRM domain binds to 5' CUCUUC 3' and 5' GAGAAG 3' sequences (Song et al., 2012). The OCRE domain of RBM5 interacts with the U5 snRNP and regulates FAS alternative splicing by associating with splice-site selection (Bonnal et al., 2008). The RanBP2 ZF motif binds to the GGU motif region of ssRNA (Nguyen et al., 2011). RBM5 also binds to UC rich sequences; for instance, it has been shown to bind to the 5' CUCUUUUCCUAAGAACUUGGCUCUUCUCU 3' region of intron 9 of Caspase-2 mRNA. Furthermore, Niu et al. (2012) have shown that two splicing factors, the DEAH-box polypeptide 15 (DHX15) and PRP19 are the nuclear binding partners of RBM5. Specifically, the G-patch domain of RBM5 interacts with DHX15 and is responsible for the helicase activity of DHX15. These binding studies have provided us with a clear picture of the role, the mode of action and the mechanistic regulation of RBM5.

1.2.6 RBM5 subcellular localization

Nuclear localization signals (NLS) are necessary for importing proteins into the nucleus. NLS are specific sequences, which bind to receptors such as importin α. Importin α and importin β form complexes with the protein "cargo", which is transported into the nucleus and released resulting in protein translocation into the nucleoplasm (Freitas and Cunha, 2009). NLS are of two types, monopartite and bipartite. Monopartite NLS are shorter basic amino acid sequences that are present as a single stretch of amino acids. Bipartite NLS are longer sequences containing two stretches of basic amino acids with a linker sequence between (Lange et al., 2007). RBM5 has two bipartite NLS. RBM5 was found in the nuclei of human fibrosarcoma HT1080 cells (Drabkin et al., 1999). Additionally, this group also detected a stronger nuclear signal in the C-terminal fragment compared to the N-terminal fragment stating that NLS in the C-terminal region could be the major constituent for the

nuclear localization. Immunohistochemistry (IHC) of RBM5 in prostate tissues revealed the presence of RBM5 in both the nucleus and cytoplasm. However, higher levels of RBM5 were detected in the cytoplasm of cancer tissues than in normal prostatic tissues (Zhao et al., 2012). Localization studies for RBM5 have been done in adult male mouse testis (O'Bryan et al., 2013). RBM5 was localized to spermatogonia, spermatocytes and round spermatids (O'Bryan et al., 2013). Furthermore, RBM5 is seen to co-localize to the nucleus with hnRNPA2/B1 and SFPQ (splicing factors) in male germ cells such as spermatocytes and spermatids. Functional association of RBM5 with nuclear binding partners DHX15 and PRP19 further strengthens the nuclear localization claim for RBM5 (Niu et al., 2012). Gupta (2006) showed that RBM5 had a sub-nuclear distribution specifically in nuclear speckles in human umbilical vein endothelial cells (HUVEC), SV-40 large T-antigen transformed and immortalized cells (HT-6), NIH3T3 and HepG2 cells. It is evident from these localization studies that the location of RBM5 within the cell is an important criteria for a specific mechanistic role.

1.3 RBM10

Another RBP, a paralogue of RBM5, is RBM10. The *RBM10* gene, located on the X chromosome at Xp11.23, encodes for the RBM10 protein. *RBM10* was first cloned from bone marrow (Nagase et al., 1995). The rat homologue, S1-1 has been studied extensively (Inoue et al., 1996, Inoue et al., 2008).

1.3.1 Alternatively spliced variants

In humans, *RBM10* is alternatively spliced to form RBM10 mRNA variant1 (*RBM10v1*, NM_005676.4), which is 3412 bp long and RBM10 variant2 (*RBM10v2*, NM_152856.2), which is 3178 bp long, which encode for ~100 kDa and ~95 kDa proteins, respectively (Wang et al., 2012) (Figure 1.3). The two human RBM10 isoforms contain 852 aa (NP_690595.1) and 930 aa (NP_005667.2). There are 24 exons in *RBM10v1* and exon 4 (77 aa residues) is alternatively spliced in *RBM10v2*. The protein sequences of RBM10v1 and RBM10v2 have 49% and 53% homology to RBM5 (Sutherland et al., 2005). These two variants are extensively studied, however, a third variant (AK024839) exists, which was detected in primary smooth muscle cells of the coronary artery (Wang et al., 2012). Thus,

similar to RBM5, RBM10 is alternatively spliced and hence post-transcriptionally modified which is probably associated with functional relevance.

The mouse RBM10 isoform 1 (NP_663602.1) is 96% identical to human RBM10 (Johnston et al., 2010). In mouse, three RBM10 isoforms containing 930 aa, 929 aa and 853 aa have been identified (Figure 1.4). The murine RBM10v2 (NP_001161247.1) is not the same as the human RBM10v2. The mouse RBM10v2 isoform has one aa (valine) deletion and in the other isoform RBM10v3 (NP_001161248.1), exon 4 coding for 77 aa is alternatively spliced. [The current study focuses on Rbm10v1 and Rbm10v3 for the purpose of more accurate comparisons to the human variants].

1.3.2 RBM10 function

Initially, there were limited studies describing RBM10 function. However, recently, numerous studies have identified multiple functions for RBM10. RBM10 is implicated in apoptosis, alternative splicing and development and has been associated with cancer (Imielinski et al., 2012) and neurological diseases (Zhang et al., 2007). The rat RBM10 orthologue, S1-1 functions in the regulation of transcription and alternative splicing (Xiao et al., 2013), which shows that it is an important RBP implicated in RNA-associated functions.

1.3.2.1 Apoptosis and cell proliferation

RBM10 is pro-apoptotic. RBM10 can modulate apoptosis in tumor cells (Wang et al., 2012). Specifically, in Jurkat and MCF-7 cells, RBM10 induced apoptosis via the TNF-α mediated extrinsic pathway. When RBM10v1 was overexpressed, it significantly altered TNF-α, TNFRSF9 and TNFSF7 levels. When RBM10v2 was overexpressed, Caspase-4 and TRAIL expression were affected (Wang et al., 2012). In breast cancer cells, expression of RBM10 is correlated with the expression of apoptotic Caspase-3 (Martin-Garabato et al., 2008), and with Bax, p53 and VEGF (Martinez-Arribas et al., 2006). In addition to RBM10, two other RBM genes located on X-chromosome (RBM3 and RBMX) are associated with the expression of the apoptotic protein Bax and the angiogenic factors VEGF and CD105 (Martinez-Arribas et al., 2006). The human RBM10v1 is closely

associated with RBM3 and p53, whereas RBM10v2 is associated with higher proliferation. When the rat homologue, S1-1 was overexpressed it resulted in reduced proliferation and increased the rate of apoptosis in vascular smooth muscle cells (VSMC) (Mueller et al., 2009). Their involvement in VSMC indicates potential roles in oxidative stress management and atherogenesis.

1.3.2.2 Splicing regulation

Similar to RBM5, RBM10 is a splicing regulator and interacts with spliceosomal complexes. In Hela cells, RBM10 was recovered from PRPF40A-U2 complexes and was identified as a component of the U2 snRNPs (Makarov et al., 2012). RBM10 was further shown to interact with spliceosomal A and B complexes (Agafonov et al., 2011). RBM10 has overlapping functions with RBM5 in alternative splicing. For instance, knockdown (KD) of RBM5, RBM6 and RBM10 together resulted in inclusion of exon 6 during alternative splicing of Fas (Bonnal et al., 2008). RBM10 was shown to act as a splicing repressor, specifically causing exon 18 skipping in Discs large homolog 4/ post-synaptic density protein 95 (*Dlg4/Psd-95*) mRNA in primary neurons (Zheng et al., 2013). Additionally, RBM10-induced alternative splicing changes can be inferred from experiments where RBM10 was overexpressed or silenced in HEK293 cells leading to expression changes in a number of genes. When RBM10 was overexpressed, 19 genes were up-regulated and 49 genes were down-regulated and when RBM10 was silenced, 171 genes were up-regulated and 105 genes were down-regulated (Wang et al., 2013). Broadly, RBM10 is involved in splicing by (a) recognizing splice sites and/or pairing, and (b) interacting with snRNPs, and pre-mRNAs and removing introns. For instance, using photoactivable-ribonucleoside-enhanced cross-linking and immunoprecipitation (PAR-CLIP), Wang et al. (2013) found that RBM10 bound close to the 5’ and/or 3’ splicing sites upstream or downstream of introns. Using RNA-sequencing, they identified 304 and 244 exon splicing changes that were significantly enhanced after RBM10 was deleted or overexpressed, respectively. Notably, RBM10 expression was involved in promoting exon skipping. Thus, from studies that analyzed the interactions and splicing changes, we can conclude that RBM10 is an important splicing regulator.

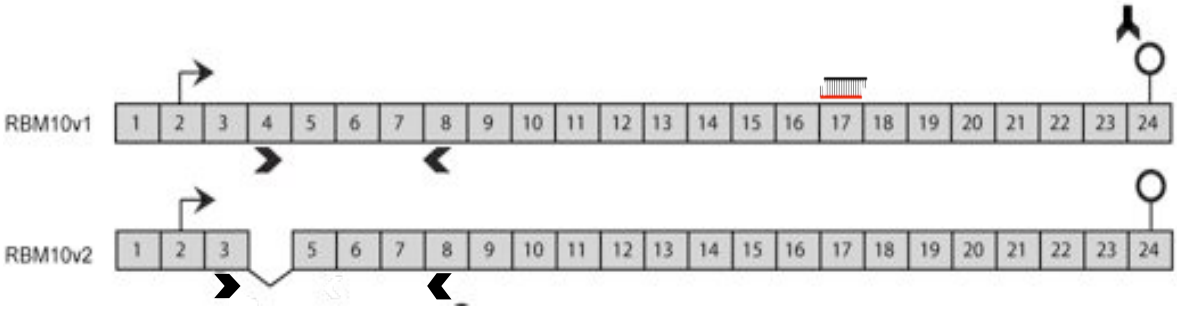

Figure 1.3 Alternatively spliced human *RBM10* mRNA variants. Diagram illustrating the two alternatively spliced variants of RBM10, with start and stop codons positions in the protein coding sequence. Location of end-point PCR primers, antibody and siRNA used in this study are schematically represented. Primers and siRNA were designed using mouse-specific *Rbm10* mRNA sequences (NM_145627.2, NM_001167775.1). Not drawn to scale. Adapted from Sutherland et al., 2005.

Primers used in end-point PCR

siRBM10 (siRNA), target site (exon 17)

Antibody, Bethyl

Start and stop codons

Figure 1.4 Sequence alignment of the three murine RBM10 isoforms. Amino acid alignment using Multalign illustrates the three RBM10 isoforms. The murine RBM10v2 is not the human equivalent RBM10v2 but is RBM10v3, which is the exon 4 (77 aa) alternative spliced isoform. Sequences with high (red) and low (blue) consensus.

1.3.2.3 Development

The association of RBM10 with mammalian development is evident from studies correlating RBM10 mutations with an X-linked developmental anomaly called TARP syndrome (Talipes equinovarus, atrial septal defect, Robin sequence and persistent left superior vena cava) in males (Gripp et al., 2011, Johnston et al., 2010). Limb deformities, neurological defects, cardiovascular defects and mandibular malformations are characteristics of this lethal defect. Therefore, the RBM10 loss-of-function due to mutational abnormality in TARP, clearly demonstrates its critical role in development.

1.3.3 RBM10 expression profile

Tissue-specific expression, invariably similar to RBM5 was detected, namely higher levels of expression in heart, skeletal muscle and pancreas (http://www.kazusa.or.jp/huge/gfimage/northern/html/KIAA0122.html). RBM10 expression is up-regulated in primary chondrocytes that were induced to hypertrophy (James et al., 2007). RBM10 is expressed in quiescent, non-dividing cells such as Purkinje cells (cerebellum), cells of villi and Paneth cells of the small intestine and in non-proliferating cells of the heart, skeletal muscle, intestine, kidney, spleen and adrenal glands; as well as in dividing cells such as spermatogonia (testis) (Inoue et al., 2008). Interestingly, higher expression was observed in cells undergoing transcription such as the spermatogonia and Purkinje cells than in the primary and secondary spermatocytes or the granulocytes, respectively (Inoue et al., 2008). The murine *Rbm10* gene is expressed during embryonic development, specifically in mid-gestation embryos (Johnston et al., 2010). The highest expression was seen in the brachial arches, limb and tail bud regions between E9.5 to E11.5 in these embryos. Similar to RBM5, RBM10 showed differential down-regulation in a lineage-specific manner in differentiating skeletal and cardiac H9c2 myoblasts (Loiselle and Sutherland, 2014). Indeed, during skeletal myoblast differentiation, the *Rbm10v2* mRNA levels decreased when compared to day zero (D0). However, the mRNA levels did not change during cardiac myoblast differentiation. The protein levels of both the RBM10v1 and RBM10v2 isoforms decreased significantly during skeletal differentiation and only the RBM10v2 isoform decreased significantly during cardiac myoblast differentiation. In addition, variant-dependent expression has been reported. For instance,

in human breast tumor specimens, the expression of one variant was dependent on the other variant (Martinez-Arribas et al., 2006). In contrast, changes in the expression or detection of only one variant have also been reported. In human lung cancer cell lines, the RBM10v2 isoform is not detected (Loiselle and Sutherland, 2014). In rat H9c2 differentiating myoblasts, the levels of only the RBM10v2 were high on day two (D2) compared to the levels in the differentiated myotubes (day seven) (Loiselle and Sutherland, 2014).

More studies have identified RBM10 mutational defects associating with major developmental anomalies and cancer. As mentioned previously, a non-sense and frame-shift mutation in RBM10 causes the TARP syndrome (Gripp et al., 2011, Johnston et al., 2010). This non-sense mutation in the RRM2 domain and the frame-shift mutation in the C-terminal region alters the conformation of the protein. Furthermore, an in-frame deletion of 239 aa, including a region comprising the C2H2 domain, a portion of G-patch and one NLS, leads to a potential loss-of-splicing functions in the nucleus that was associated with a familial X-linked intellectual disability, which has overlapping phenotypes observed in TARP syndrome (Wang et al., 2013). Finally, truncating and mis-sense mutations are found in lung adenocarcinomas (Imielinski et al., 2012) and pancreatic intra-ductal papillary mucinous neoplasms (Furukawa et al., 2011).

1.3.4 RBM10 structure

RBM10 is structurally related to RBM5, which is evident from the presence of two RRM domains, two ZF domains (RanBP2 and C2H2), one G-patch, one SR domain and one OCRE domain (Sutherland et al., 2005) (Figure 1.2). Most of the structural studies for RBM10 were performed on the rat S1-1 protein. The RRM domains of S1-1 are each approximately 80-90 aa and contains two critical ribonucleoprotein (RNP) motif regions (RNP1 and RNP2), one each in the C-terminal and N-terminal regions (Xiao et al., 2013). The RBM10v2 isoform, which has exon 4 alternatively spliced out, lacks the RNP2 motif of RRM1 (Xiao et al., 2013).

The probable motif regions of the murine RBM10v1 and RBM10v3 isoforms were mapped to amino acid locations using PROSITE (Figure 1.5). RRM1 domains were predicted at residues 129-209 (RBM10v1) and 37-132 (RBM10v3), and RRM2 was predicted at

residues 300-384 and 223-307 for RBM10v1 and RBM10v3, respectively. In RBM10v1, the RanBP2 ZF motif was located at residues 212-242, the C2H2 ZF motif at 759-789 aa and the G-patch at 858-904 aa positions. In RBM10v3, the RanBP2 ZF motif was located at residues 135-165, the C2H2 ZF motif at 682-712 aa and the G-patch at 781-827 aa positions. These sequence specific regions enable prediction of functions.

1.3.5 RBM10 binding

The first *in vitro* binding studies for RBM10 were done for S1-1. The rat homologue S1-1 has been shown to bind poly (G) and (U) ribonucleotides (Inoue et al., 1996). S1-1 bound to 130 mRNA clones encoding for cytokines and proto-oncogenes (Bhattacharya et al., 1999). S1-1 binds to the 3' UTR of the AT1 receptor (renin-angiotensin system) mRNA and is responsible for its stability and mRNA transcription (Mueller et al., 2009). RanBP2 possibly interacts with the AGGUAA sequence in the 5' splice sites (Wang et al., 2012), which is different from the interaction reported for RBM5.

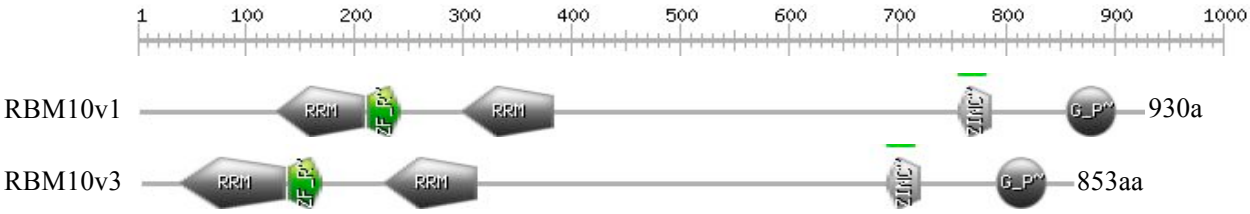

Figure 1.5 Domain structures of the mouse RBM10 isoforms. Schematic representation of the motifs and their corresponding locations predicted for the two isoforms, using PROSITE database. RBM10v1 is a 930 aa protein consisting of the following motifs; RRM1 at 129-209, RRM2 at 300-384, RanBP2 ZF at 212-242 and C2H2 ZF at 759-789 and G-patch at 858-904. RBM10v3 is an 853 aa protein with the following motifs; RRM1 at 37-132, RRM2 at 223-307, RanBP2 ZF at 135-165 and C2H2 ZF at 682-712 and G-patch at 781-827.

1.3.6 RBM10 subcellular localization

RBM10 localizes in the nucleus in certain cells. Using immunoelectron microscopy, Inoue et al. (2008) determined that S1-1 (RBM10) was located in nuclear domains as punctate nuclear bodies and as diffused granules. RBM10 was present in the interchromatin space and perichromatin fibrils. In the nucleoplasm, RBM10 was absent in the nucleoli. They detected RBM10 in the nucleus of spermatogonia, Purkinje cells, cells of villi and Paneth cells (small intestine). In tissues such as heart, skeletal muscle, intestine, kidney, spleen and adrenal gland, RBM10 was present predominantly as punctate structures in the nucleus (Inoue et al., 2008). Xiao et al. (2013) studied the pattern of RBM10 localization in many different tissue types and cell lines. RBM10 localized to the nucleus in rat ARL cells (liver epithelial cells) and NIH3T3 cells (Xiao et al., 2013). Initially, it was believed that the RBM10 sequence contained two NLS signals necessary for nuclear localization (Inoue et al., 2008), however, it was recently shown that an additional NLS is present in the OCRE region (NLS3) and all three NLS function in a dependent manner (Xiao et al., 2013). The other two NLS are located between amino acids 743-759 (NLS1) and in the RRM1 domain regions (NLS1). Interestingly, RBM10 was found in both nuclear and cytoplasmic fractions in neutrophils, HeLa cells, HL-60 cells (premyelocytic leukaemia cell line), cirrhotic liver cells and hepatocellular carcinoma cells. Further, a K756A mutation in NLS1 leads to localization to the cytoplasm (Xiao et al., 2013). Recently, Inoue (2013) have observed nuclear and cytoplasmic localization in normal chorion and complete hydatidiform moles (disease of the chorionic villi). These observations, therefore, indicate that RBM10 subcellular localization potentially relates to its specific regulatory functions.

Most of the studies on RBM5 and RBM10 were focused on tumor cell lines with little information on their role in normal cells, specifically muscle, even though these RBPs were highly expressed in both skeletal and cardiac muscles. In order to functionally characterize these two proteins in different biological systems, it is necessary to define their potential specificity in both normal as well as transformed systems. In addition to the relatedness of the functional events associated with muscle development, such as cell cycle arrest,

apoptosis and alternative splicing, the involvement of RBM10 in development therefore suggests a prospective role for these two RBPs in myogenesis.

1.4 Skeletal myogenesis

There are three types of muscles in vertebrates; cardiac, skeletal and smooth muscles (Buckingham, 2001). Skeletal muscles are voluntarily controlled by the somatic nervous system via neuro-muscular junctions, which are necessary for neuronal firing and contractile response, whereas the contractile response of both smooth and cardiac muscle types are controlled involuntarily by the autonomic nervous system (Exeter and Connell, 2010). The process of skeletal muscle development is termed "Skeletal Myogenesis" (Bentzinger et al., 2012). Myogenesis constitutes four specific phases; specification, determination, migration/commitment and differentiation (Perry and Rudnick, 2000). All four phases involve establishing the muscle-specific lineage from progenitor cells to developing a fully formed functional muscle fiber (Bentzinger et al., 2012). The somites, which produce the progenitors cells, are established from the mesodermal layer. Each mesodermal layer contributes to a specific location and type of muscle to be formed (Buckingham, 2002, Buckingham, 2006). Each phase in the myogenic program is monitored and accurately co-ordinated to generate the skeletal muscle (Buckingham and Rigby, 2014).

1.4.1 Myogenic differentiation

The final of the four phases in myogenesis is differentiation. Various changes occur during differentiation; the mono-nucleated myoblasts stop proliferating, withdraw from the cell cycle, elongate, migrate, align and fuse to form the multinucleated myotubes (Sabourin and Rudnicki, 2000). Myotubes mature to form myofibers. Mature myofibers are comprised of contractile units of the muscle, the sarcomeres, which contain actin and myosin myofilaments (Burattini et al., 2004). Myoblast proliferation and differentiation are distinct, temporal processes (Moran et al., 2002). Therefore, differentiation is tightly regulated with the end-result being the formation of multi-nucleated myofibers, which can contract and are adapted for specific functions.

Satellite cells are quiescent cells, different from myofibers, that reside in the spaces between the sarcolemma and basal lamina (Montarras et al., 2013). These cells are involved during injury, regeneration and repair. When stimulated (injury/trauma) these quiescent cells become activated and proliferate and undergo the regular process of differentiation to become adult myofibers (Charge and Rudnicki, 2004, Chang and Rudnicki, 2014). Young neonatal mice have 30% satellite cells of the total cell number, which decrease with age to 4% in adult and 2% in aged mice. This age-dependent decrease in the satellite cell population is associated with the increase in oxidative myofibers (Hawke and Garry, 2001). The adult muscle regeneration process, which involves the activation, proliferation and migration of the satellite cell to the site of injury to form the functional myofiber is governed by additional and varied gene expression changes (Yusuf and Brand-Saberi, 2012).

1.4.2 C2C12 model

Many *in vitro* tools such as primary cells and secondary cell lines such as C2C12, H9c2, L6E9 and L8 cells are available to study the fundamental cellular processes that occur during myogenesis (Miller, 1990). The most frequently used, well-established cell line is the C2C12 myoblast cell line. This *in vitro* mouse model is extensively used to study the process of myogenic differentiation. Blau et al. (1985) established this cell line as a subclone from the thigh muscle of a C3H mouse after injury (Yaffe and Saxel, 1977). Since then, scientists have used C2C12 cells in numerous transcriptomic and proteomic studies to identify the molecular mechanisms of the myogenic program (Casadei et al., 2009, Tannu et al., 2004). C2C12 myoblasts stop proliferating when the growth factors are depleted and this induces differentiation. According to Dedieu et al. (2002) fusion starts two days after differentiation induction and the rate of fusion is high by the fourth day and reaches a maximum level of cells being fused (60%) on the eighth day following induction. The C2C12 differentiation system is a model that represents a part of the skeletal myogenesis, beginning from the myoblast stage and ending in myofibre formation. While there are some differences between *in vivo* mouse myogenesis and C2C12 differentiation, the C2C12 model provides insight in to the dynamic steps involved in skeletal differentiation and has been widely used. *In vivo*, the differentiation process ends in fully formed mature myofibres, governed by additional gene expression changes (Abmayr and Pavlath, 2012).

C2C12 cells are a heterogenous group of phenotypes including mono-nucleated myoblasts and quiescent cells, which are dormant resting cells and are termed as reserve cells (Deato and Tjian, 2007, Riquelme et al., 2015). When the C2C12 cell population is subjected to differentiation, these reserve cells are those cells that escape differentiation and remain as undifferentiated cells (Yoshida et al., 1998).

1.4.3 Myogenic gene expression changes

Muscle-specific gene expression changes occur during differentiation (Heywood et al., 1983, Merlie et al., 1977). Comparative genomic and proteomic profiling studies comparing early and late stages of muscle differentiation have identified alterations in numerous molecular players involved in cell signalling, cell cycle, apoptosis, contraction, cell-architecture, mobility/motility, transcriptional related genes/proteins (Figure 1.6). The known protein list is exhaustive and has been extensively reviewed (Knight and Kothary, 2011, Molkentin and Olson, 1996). For the scope of this dissertation, a brief introduction on three specific events and a few associated essential proteins is presented here. Because of the relatedness of these events to RBM5 and RBM10 functions, the events that are elaborated are related to cell cycle withdrawal, apoptosis and alternative splicing.

1.4.3.1 Cell cycle

The first step in differentiation induction is cell cycle arrest (Walsh and Perlman, 1997). Gene expression changes occurring in transcription factors and cell cycle proteins during myogenesis are highly coordinated. The myogenic regulatory factors (MRFs), which are transcription factors, are the main key players. The four major MRFs are myogenic factor 5 (Myf5), MyoD, Myogenin (MyoG) and muscle regulatory factor 4 (MRF4) (Olson et al., 1991, Rudnicki et al., 1993). These MRFs belong to the family of basic helix-loop-helix (bHLH) muscle-specific transcription factors. First, MRFs heterodimerize with E proteins (E12/E47, HEB, E2-2) and then, the DNA-binding domain present in the MRFs bind to the DNA motif regions called the E-box on the promoters of many genes and activate transcription (Londhe and Davie, 2011). Each MRF is functionally activated during each stage of differentiation and therefore has a specific role during myogenesis (Sabourin and Rudnicki, 2000): Myf5 and MyoD are involved in determination and in cell cycle

regulation during differentiation (Rudnicki et al., 1993), MyoG in myotube formation (Faralli and Dilworth, 2012) and MRF4 in the terminal stage (myofibrillogenesis) of differentiation (Kassar-Duchossoy et al., 2004). MRF4 is also involved in postnatal myofiber regulation (Walters et al., 2000).

Furthermore, some MRFs have redundant (Myf5 and MyoD) as well as conserved functions such as regulating transcription of specific subsets of muscle-specific genes (Kablar et al., 1997). Inhibition of MyoD, Myf5 and MyoG prevent fusion and varying degrees of delay are observed based on the day of inhibition of MRF expression (Dedieu et al., 2002). MRFs co-ordinate with another set of myogenic protein, the myocyte enhancer factor 2 (MEF2) family of MADS box factors, and together regulate most muscle-specific genes (Dodou et al., 2003). Cell cycle proteins such as p21, p57 and p27 are regulated during differentiation (Chan et al., 2011). p21, a cyclin-dependent kinase inhibitor causes cell cycle arrest by inhibiting cdk-2 (cyclin dependent kinase-2). p21 is activated by MyoD, which leads to cell cycle withdrawal (Guo et al., 1995) in concurrence with p57 (Zhang et al., 1999). It is also known that MyoG is expressed after p21 is expressed (Halevy et al., 1995). Therefore after induction of differentiation, the levels of p21 are regulated, which invariably causes cell cycle arrest at G1 and also enables myotube formation by inducing MyoG expression. Cyclin D1 is expressed in proliferating myoblasts and p21 is expressed before fusion (Tannu et al., 2004). In addition, hypophosphorylated retinoblastoma protein associates with MyoD transactivating E-box-possessing muscle-specific promoters to maintain the differentiated state (Sabourin et al., 1999).

It is important to note that the expression of the MRFs *in vivo* is governed by their location and timing during development (Sabourin and Rudnicki, 2000). For instance, during the development of the mouse embryonic musculature, Myf5 is the first MRF expressed in the somites in the trunk. MyoG is expressed next, followed by MRF4. MyoD is expressed later in the lateral part of the somites (Smith et al., 1994). MyoD expression begins on embryonic D10 and is expressed until birth (Borycki and Emerson, 1997). *In vivo*, development-associated signalling mechanisms regulate the progenitor cells to proliferate and for a certain population to differentiate, which requires cell cycle arrest to occur at G1 so that they can proceed through differentiation (Pownall et al., 2002). In addition, the

signalling mechanisms involving muscle regeneration are different from embryonic myogenesis (Mercer et al., 2005). In the C2C12 model, similar events have been shown to take place and the percentage of differentiated C2C12 cells ranges between 40% and 60% (Yoshida et a., 1998) and the remaining are the satellite cell-like reserve cells (Miller, 1990). *In vivo*, the quiescent cells (satellite cells) that are located in the basal lamina express a distinct set of genes that regulate the expression of myogenic factors during muscle tissue injury and repair (Chang and Rudnicki, 2014; Charge and Rudnicki, 2004). Proteins such as paired box protein 7 (Pax7) and Myostatin maintain the satellite cells in a quiescent state and this state can be reversed by interacting with MEFs and MRFs, specifically MyoD and Myf5. MyoD inhibition controls the entry into S-phase in cell cycle; association with Myf5 activates the myoblasts (Buckingham et al., 2003). Immediately after injury (6 h), the expression of MyoD occurs in the activated satellite cells *in vivo* (Hawke and Garry, 2001). However, in the C2C12 model, MyoD appears to be expressed even in proliferating, non-differentiating (reserve) cells (Ferri et al., 2009), while MEF and MyHC are not expressed in the reserve cells until they are induced to differentiate (Blais et al., 2005).

Using microarray profiling of C2C12 cells induced to differentiate, Rajan et al. (2012) identified up to four-fold difference in expression of transcriptomes, with down-regulation being more common than up-regulation, and these changes were observed between 12 h and 24 h after induction. Exit from the cell cycle happened within two days after serum withdrawal (Shen et al., 2003).

1.4.3.2 Apoptosis

In addition to inducing irreversible cell cycle withdrawal, apoptosis is necessary for the progression of differentiation (Fernando et al., 2002). However, once differentiation occurs, the cells are resistant to apoptosis (Sandri and Carraro, 1999). During differentiation of C2C12 muscle cells, which contains a heterogenous pool of myoblasts and reserve cells, expression of the anti-apoptotic gene Bcl-2 and pro-apoptotic genes Bax, Bad and Bak are highly regulated (Schoneich et al., 2014). Activation of caspases such as Caspase-3, Caspase-9 and Caspase-12 are reported in a specific population of cells, during the early stage of differentiation (Schoneich et al., 2014). Other apoptotic regulators such as DAD1,

Caspase-11 and glycogen synthase kinase-3β are differentially expressed during differentiation (Shen et al., 2003). Apoptosis of the incompletely differentiated or undifferentiated cells occur at 48 hours after switching to DM and leads to a 20-30% loss of myoblasts (Mercer et al., 2005).

1.4.3.3 Alternative splicing

Alternative splicing is highly regulated during myogenesis, exhibiting a greater degree of control on proteins expressed during this important phase of development, and during repair and regeneration (Llorian and Smith, 2011). Bland et al. (2010) identified regulation of 95 alternative splicing events during C2C12 differentiation using splicing-sensitive microarray analysis. Of these 95 transitions, 69 (73%) had increased inclusion and 26 (27%) had increased exon skipping/exclusion. Functionally, these transitions were related to components of cytoskeletal, actin binding, cell junction, nucleotide kinase and integrin signalling pathways. The splicing transitions were conserved, coordinated and occurred in the proliferating myoblasts before the start of differentiation as well during the entire differentiation process. In addition, they also determined that 30% of the splicing events involved RBPs. Many *cis*-acting splicing regulators (FOX , MBNL, CUGBP1, hnRNP, PTB) that possess RNA-binding motifs showed expression level changes in response to alternative splicing transitions during myogenic differentiation in C2C12 cells. Interestingly, alternative splicing during myogenesis is implicated in a majority of muscle-related diseases such as dystrophies, spinal muscular atrophy and rhabdomyosarcoma (Garcia-Blanco et al., 2004, Spletter and Schnorrer, 2014).

α-Dystrobrevin is encoded by the *DTNA* gene. α-Dystrobrevin along with β-Dystrobrevin, dystrophin, sarcoglycan, syntrophins and dystroglycans form the dystrophin glycoprotein complex (DGC) (Ehmsen et al., 2002). DGC is essential for forming and maintaining the stability of synaptic clusters of nicotinic acetylcholine receptors. DGC is a structural component on the sarcolemma and is associated with muscular dystrophies (Metzinger et al., 1997). Multiple transcripts are generated due to alternative splicing and the splicing of *DTNA* is highly regulated (Nakamori and Takahashi, 2011). Differing degrees of splicing regulation are observed between human and mice; there are variations in the spliced

transcripts, expression profiles, location and function (Nakamori and Takahashi, 2011, Nakamori et al., 2008). Bland et al. (2010) reported that *Dtna* has a 78% increase in exon inclusion during C2C12 differentiation and this splicing transition is part of the myogenic differentiation program because this transition was not present in BDM (2,3, butanedione monoxime)-treated differentiating C2C12 cells, in which differentiation was blocked. Exon 11 is the alternatively spliced exon and inclusion of exon 11 occurs during the mid- and late-stages of C2C12 differentiation. Alternative splicing of this skeletal muscle differentiation specific variant, which was significant after the C2C12 myoblasts were induced to differentiate, indicates potential functions during this time-point.

MEF2 proteins are a family of transcription factors involved in differentiation, especially during the terminal-stages of differentiation such as fusion and maturation (Black and Olson, 1998). MEF2 isoforms A, B, C, D are encoded by different genes and have overlapping as well as specific functions during myogenesis (Edmondson et al., 1994). Knockdown and knockout studies in zebrafish and mouse, respectively, revealed that Mef2c is involved in maintaining the integrity of the sarcomere and for postnatal maturation of skeletal muscle (Potthoff et al., 2007). Multiple alternatively spliced isoforms of Mef2c are generated by alternative splicing of the α, β and γ exons (Sekiyama et al., 2012). Mef2c(γ-) is more active in transcription than Mef2c(γ+) and the alternative splicing of this γ domain is not dependent on the splicing events containing α/β domains (Zhu and Gulick, 2004).

Integrins are extracellular matrix receptors with functions in cell adhesion, migration and signal transduction. There are 2 subunits, α and β. There are two alternatively spliced isoforms of β1 integrin, β1A and β1D, which have distinct functions (Cachaco et al., 2003). When both isoforms were separately overexpressed in C2C12 cells, the myogenic differentiation program was differentially affected (Cachaco et al., 2005). The integrinβ1A isoform, which is associated with primary myogenesis (Cachaco et al., 2003), is expressed in proliferating myoblasts and decreases during differentiation while integrinβ1D expression increases (Belkin et al., 1996).

1.4.3.4 Associated proteins

There are other signalling pathways that exert a critical role in myogenic differentiation, such as the Notch pathway (Kopan et al., 1994, Nye et al., 1994). When the Notch pathway is activated, it inhibits differentiation (Nofziger et al., 1999). This effect is caused by an overexpressed Notch intracellular domain (NICD), which regulates MyoG and Myosin light chain 2 expression (Nofziger et al., 1999). When Notch is activated, it inhibits the three major muscle specific proteins, MEF2C, MyoD and MyoG (Kopan et al., 1994). Furthermore, the Notch pathway is implicated in activation of satellite cells and post-natal myogenesis, for instance, differentiation and fusion occurs when Notch signals are inhibited (Conboy and Rando, 2002). This down-regulation of Notch is caused by an apparent increase in NUMB expression, leading to myotube formation during injury (Conboy and Rando, 2002). Another pathway that regulates MyoG and MEF2 expression is the Rho family of proteins (Charrasse et al., 2002). Rho levels are high in myoblasts and down-regulated during differentiation (Iwasaki et al., 2008).

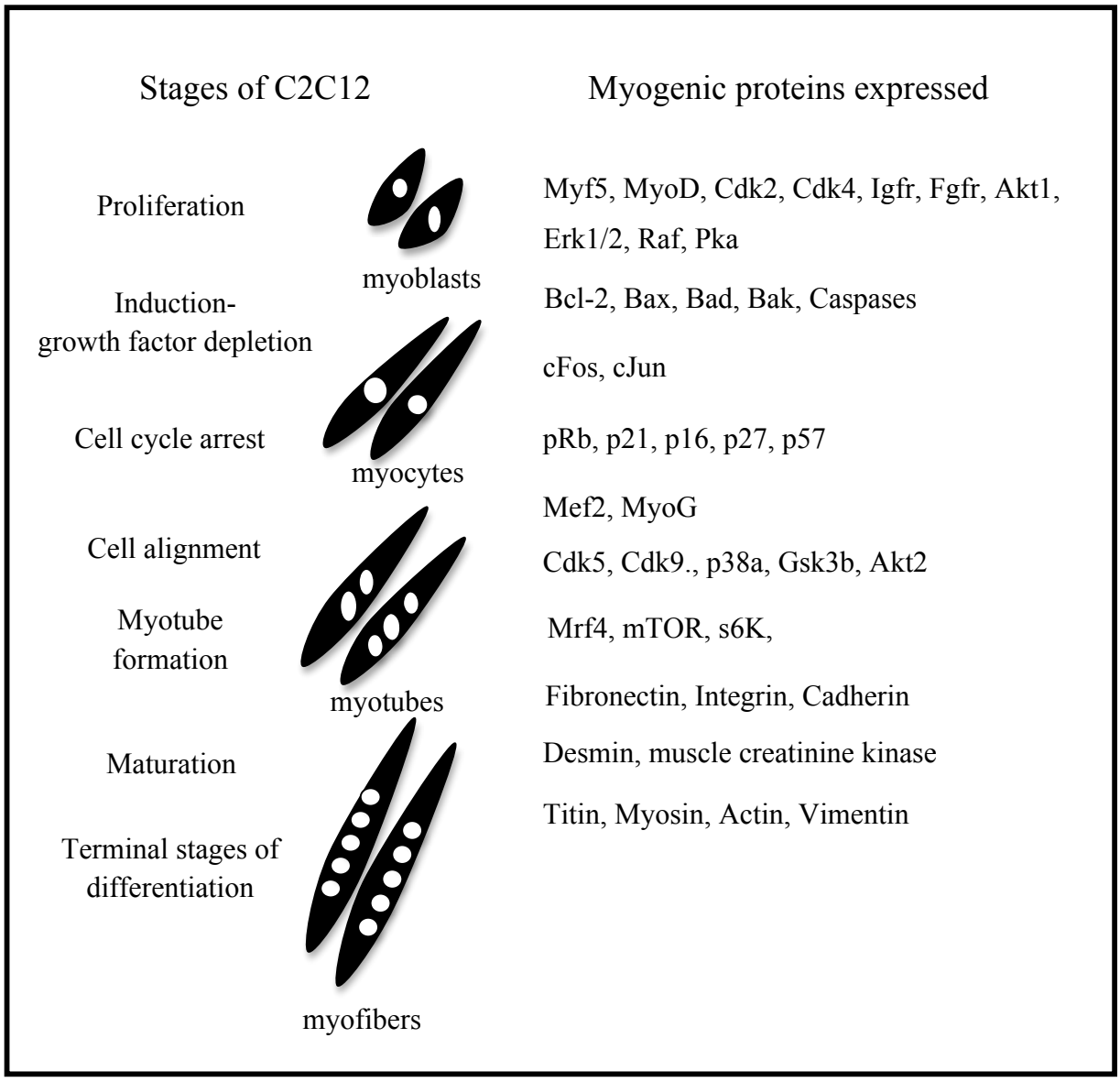

Figure 1.6 Expression of various proteins during C2C12 myogenic differentiation. Schematic representation of the approximate time-points of key events occurring during C2C12 myogenic differentiation and few of the associated proteins expressed at these various stages.

Many RBPs regulate myogenic genes post-transcriptionally during myogenesis (Apponi et al., 2011). They are important in regulating gene expression by splicing, maintaining mRNA stability, transport and translation. RBPs shown to be associated with myogenesis are; Human R antigen (HuR), KH-type splicing regulatory protein (KSRP), CELF (CUG-BP- and ETR-3- like factors) CUGBP1, nuclear poly (A)-binding protein1 (PABPN1), Lin-28 and Tristetraprolin (TTP). By binding to the U and AU-rich elements (AREs) of mRNA targets, HuR is involved in almost every aspect of RNA metabolism, including splicing, polyadenylation, transport from the nucleus to cytoplasm, translation and degradation (Hinman and Lou, 2008). KSRP regulates myogenesis as an alternative splicing regulator, and in mRNA decay, KSRP binds to ARE sequences (Apponi et al., 2011). CUGP1 functions in alternative splicing, translation and stability. PABPN1 functions as polyadenylation complex (Apponi et al., 2011). Lin-28 is involved in translation (Apponi et al., 2011). TTP plays a pivotal role in mRNA stabilization and degradation by binding to ARE regions (Apponi et al., 2011). Using *C. elegans* as the model system, many RNA targets binding to RBPs have been identified (Tamburino et al., 2013).

There are other RBM proteins shown to be associated with myogenesis. RBM38 is involved in cell cycle arrest and differentiation by binding to p21 (Miyamoto et al., 2009). RBM24, a paralogue of RBM38, regulates myogenesis via cell cycle regulation, not dependent on p21 (Miyamoto et al., 2009). These two RBM proteins have a similar expression profile, in particular, they are highly expressed in skeletal and cardiac muscle and are up-regulated during differentiation (Miyamoto et al., 2009). It was shown later that RBM24 binds to the 3'UTR of *MyoG* mRNA altering its stability, thereby inhibiting myogenesis (Jin et al., 2010). RBM4 and RBM20 are other important RBM proteins implicated in myogenesis (Lin and Tarn, 2011, Lin and Tarn, 2012). RBM4 functions as a positive myogenic regulator associated with both post-transcriptional and translational control during muscle differentiation. RBM4 is involved in alternative splicing of PTB, MEF2c, myocargin, α-tropomyosin, α-actinin, troponin T, vinculin, insulin receptor and ryanodine receptor (Lin and Tarn, 2011, Lin and Tarn, 2012). RBM20 is a splicing repressor in cardiac differentiation, specifically promoting intron retention, exon exclusion

and shuffling in *Titin* mRNA and in 31 other spliced genes (Li et al., 2013). These observations therefore indicate that regulation could be carried out in many different ways, affecting several mRNAs. In short, we can infer that there are numerous molecular players involved in differentiation to properly execute the myogenic program.

1.5 Subcellular localization of myogenic proteins

The location of major muscle-specific proteins in the cell is an important regulatory mechanism to streamline their expression and function. For instance, MyoD is localized in the nucleus, more specifically in the interchromatin domains during the early- and late-differentiation phase in C2C12 cells, but is seen only in the cytoplasmic space in the mitotic myoblasts (Ferri et al., 2009). Nuclear localization is seen in the interchromatin domains and not in the nucleolus. Myf5 exhibited different localization pattern during differentiation (Ferri et al., 2009). Myf5 was detected both in the nucleus and cytoplasm during early-, mid- and late- differentiation stages; however, Myf5 staining was more intense in the nucleus compared to the cytoplasm, indicating a strong nuclear presence during the entire differentiation process. In the nucleus, Myf5 was detected in the interchromatin domains and not in the nucleolus. Interestingly, the localization pattern for Myogenin, showed a stronger cytoplasmic presence in the myoblasts and as differentiation progressed, there was more nuclear distribution (Ferri et al., 2009). Similar to MyoD and Myf5, the distribution of Myogenin in the nucleus was focused in the interchromatin domains and not in the nucleolus. A distinct/stronger cytoplasmic presence was detected for MRF4, being distributed in the perinuclear space (Ferri et al., 2009). In addition, MRF4 was also present in the nucleus especially in the interchromatin domains. Therefore, nuclear localization is associated with the transcriptional role of these MRFs and nucleo-cytoplasmic shuttling of major muscle-specific myogenic factors during the differentiation process is not uncommon.

1.6 Rationale and hypothesis

There are close to 860 known RBPs. RBPs are necessary to recognize different sequences, to perform tight regulation/control and to coordinate gene expression changes. Therefore, RBPs have diverse functions; however, the functions of numerous RBPs are still

uncharacterized. Each stage of the myogenic program is highly controlled and new proteins in the pathway with distinct functions are constantly being identified. It is highly likely that some RBPs regulate the expression of myogenic transcription factors or other components that form part of the complex cascade of signaling events during myogenesis. In particular, RBPs may play important functions in muscle cell proliferation and differentiation, as well as in muscle development. Given that (a) *RBM5* and *RBM10* expression is high in skeletal muscle, (b) they have known functions related to cell cycle arrest, (c) they intervene in alternative splicing events, and (d) RBM10 is implicated in development, we hypothesize that RBM5 and RBM10 play an important role in skeletal myogenesis and that they exert their role by regulating alternative splicing of muscle differentiation specific mRNAs.

1.7 Objectives

The objectives of the study are firstly, to characterize the expression profiles of Rbm5, Rbm10 and their variants and isoforms in the C2C12 skeletal muscle differentiation model. Secondly, the study will involve experimentally repressing the expression of RBM5 and RBM10 and then allowing the cells to differentiate. The cell (myoblast to myotube) morphology will be studied in order to identify the phenotypic changes that result in response to knockdown in the differentiating cells. Thirdly, the study will assess molecular myogenic changes in the knockdowns by analyzing the expression of myogenic markers and a few alternative splicing events that occur during myogenesis.

Chapter 2

2 Materials and Methods

2.1 Cell culture

C2C12 myoblasts (ATCC® CRL-1772™, Manassas, VA, USA) were grown in growth medium (GM), which is Dulbecco's modified Eagle's medium (DMEM) (Life Technologies, Burlington, ON, Canada) supplemented with 10% fetal bovine serum (FBS) (Life Technologies) and 1% antibiotic-antimycotic (Life Technologies). The DMEM consisted of the necessary nutrient supplements with 4.5% glucose and 4 mM L-glutamine. The cells were incubated in a humidified incubator at 37°C, in a 5% CO_2 environment. The cells were maintained at 80-90% confluence during growth and the passage number did not exceed 20 for all the experiments (Table A1 in Appendix A). GM was changed every two days. When the cells reached 80% confluence, differentiation was induced using differentiation medium (DM), which is DMEM supplemented with 2% horse serum (HS) (Life Technologies) and 1% antibiotic-antimycotic (Sun et al., 2005). DM was changed every two days. For expression analysis, the cells were differentiated until day seven (D7); day zero (D0) representing the day on which the GM was replaced with DM (Figure 2.1). Cells were collected each day. For cell collection, the adherent cells were trypsinized using 2.5% Trypsin (Life Technologies) for 5 minutes, after which, the trypsin was inactivated using serum-containing GM and pelleted at 16 200 x g for 8 minutes. The supernatant was discarded and the cell pellets were stored in -80°C until further processing for RNA and protein extraction. Simultaneously, duplicate cultures of C2C12 cells were grown on coverslips, induced to differentiate and fixed for immunofluorescence staining.

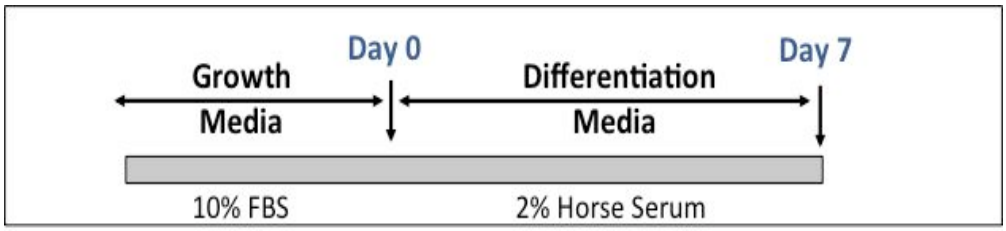

Figure 2.1 Time-line of expression analysis. Diagram showing the differentiation time-frame, and the growth and differentiation conditions. C2C12 myoblasts were grown in GM containing 10% FBS and differentiated on D0 using DM which contained 2% HS. Cells were collected every day until D7 for total RNA and protein extraction.

2.2 Transfection

2.2.1 siRNA

RNA interference (RNAi) was used to silence mRNA expression. Small interfering RNAs (siRNAs) (Dharmacon, GE Healthcare, Lafayette, CO, USA), which are 21 nucleotide double stranded RNAs with sequences specific to *Rbm5* and *Rbm10* were used to generate RBM5 and RBM10 knockdowns (KD) respectively. The siRNA for *Rbm5* with sense: 5'-GAGCGAUAUUCGAGAAAUGUU-3' and antisense: 5'-CAUUUCUCGAAUAUCGCUCUU-3' sequences, targeting sequence at the end of exon 4 and the beginning of exon 5, will transiently silence all *Rbm5* variants (Figure 1.1). The siRNA for *Rbm10* with sense: 5'-UAUUAGUGCUCUACGAGAUUU-3' and antisense: 5'-AUCUCGUAGAGCACUAAUAUU-3' sequences, targeting sequence at exon 17, will transiently silence both *Rbm10v1* and *Rbm10v3* variants (Figure 1.3). A scrambled siRNA (ON-TARGET*plus* #1, Dharmacon) with non-targeting sequences having at least 4 mismatches to any mouse gene was used as the negative control to eliminate off-target and non-specific effects. *In silico* analysis of these siRNAs was done through NCBI's BLAST to verify the sequence specificity. *In silico* analysis of these siRNAs revealed that the siRNAs were specific for the target mRNAs and that the scrambled siRNA did not target any mouse-specific sequence.

2.2.2 Transient transfection

C2C12 myoblasts were grown in six well plates with 2 ml GM. Optimization of siRNA concentration and the optimal cell density was done in order to increase KD efficiency. Briefly, the cells were transfected using a Tye 563 labeled siRNA duplex control (SR30002, OriGene Technologies, Rockville, MD, USA) to determine the optimal cell density and siRNA concentration.

For transfection, the cells were grown to 40-50% confluence and briefly washed twice with PBS pH 7.4 (Life Technologies) after which 1.5 ml of GM with no antibiotics was added to the cells. Transfection was carried out using a lipid-based delivery system. Five ml of

Lipofectamine 2000 (Life Technologies) was mixed with 245 ml of Opti-MEM (Life Technologies) and incubated at 22°C for 5 minutes. Subsequently, a final concentration of 10-25 nM of each siRNA (20 μM stock) was mixed with 245 ml of Opti-MEM and combined and all the reagents were incubated at 22°C for 20 minutes. This mixture was then added to the cells and the cells were maintained at 37°C in 5% CO_2. The medium was changed to GM with 1% antibiotic-antimycotic after 24 hours. Cells were collected to determine the KD levels at 24 and 48 hours post-transfection. In order to analyze the effect of KD during differentiation, cells were induced to differentiate 24 hours after transfection by changing GM to DM. The cells were differentiated until day four (D4) and cell pellets from two pooled wells were collected every day for RNA and protein extraction (Figure 2.2). Simultaneously, duplicate cultures of cells were grown on cover slips, transfected, induced to differentiate and fixed for immunofluorescence staining.

2.3 RNA extraction

RNA was extracted from the cells using Tri-Reagent (Molecular Research center Inc, Cincinnati, OH, USA) according to the manufacturer's instructions. Total RNA pellets were resuspended in 20 μl TE (10 mM Tris-HCl and 0.1 mM EDTA) and 1 μl of RNAse OUT (40 U/20 μl reaction mixture) (Life Technologies) was added to inhibit RNAse activity. The total RNA was quantified using a NanoDrop 2000 UV-Vis spectrophotometer (Thermo Scientific, Wilmington, DE, USA) and purity was assessed using the A260/A280 ratio; samples with ratios between 1.8 to 2 were used for downstream analyses. Furthermore, the integrity of the RNA samples was checked by electrophoresis of 1μg RNA on a 1% agarose gel stained with SYBR® Safe DNA gel stain (Life Technologies). Samples with a 2:1 ribosomal 28S/18S ratio were used in the qPCR and end-point PCR analysis. 20 μg of RNA was DNase treated (Turbo DNA-free™ Ambion kit, Life Technologies) according to manufacturer's instruction in a 50 μl total volume to remove DNA contamination.

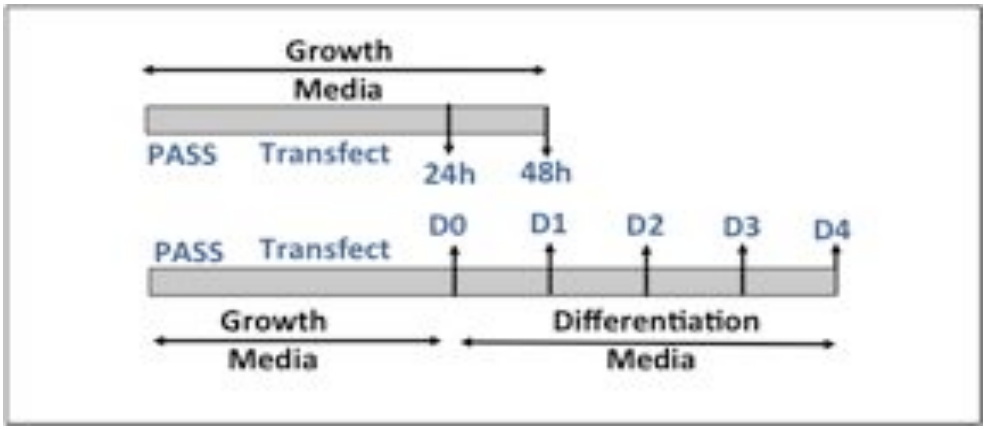

Figure 2.2 Time-line of knockdown analysis. Diagram showing the time-frame for transfection and differentiation induction post-transfection. C2C12 myoblasts were transiently transfected with specific siRNAs and the cells were collected at 24h and 48h post-transfection for total RNA and protein extraction. One set of the transfected myoblasts were induced to differentiate 24h after transfection and cells were collected every day until D4 for total RNA and protein extraction.

2.4 Reverse transcription (RT)

All the primers were obtained from Alpha DNA (Montreal, QC, Canada). Reverse-transcription was performed using 2 μg of DNase-treated RNA, 25ng of Oligo(dT) (500ng/ml stock), 0.5 mM dNTPs (10 mM stock) (Life Technologies), 1 x first-strand buffer (5 x stock), 10 mM DTT (0.1 M stock) and 10 U of Moloney murine leukemia virus (MMLV) reverse transcriptase (200U/μl stock) (Life Technologies) in a 40 μl reaction volume. A two-step RT was done; first denaturing the RNA at 65°C for 5 minutes followed by RT. RT conditions included incubation at 37°C for 2 minutes and addition of enzymes and continuation at 37°C for 50 minutes and the reaction was terminated by incubation at 70°C for 10 minutes. For gene-specific primers, SuperScript II (Life Technologies) was used for first-stand cDNA synthesis. For this reaction, 1 μg of DNase-treated RNA was reverse-transcribed using 0.5 μM of primers (10 μM stock), 0.5 mM dNTPs (10 mM stock), 10 mM DTT (0.1 M stock), 1 x first-stand buffer (5 x stock) and 10 U of SuperScript II (200U/μl stock) in a 20 μl reaction volume. RT was performed with the above mentioned conditions with the exception of carrying out the RT at 42°C for 2 minutes followed by incubation at 50°C for 50 minutes. The gene-specific primer mFactorXF (5' GTT CAA ATA CTC TAC TTG GTC C 3'), located in the intronic region (intron 6), reverse transcribes the two *Rbm5* intron-retaining variants *Rbm5+5+6* and *Rbm5+6* (Figure1.1), and mFactorXR (5' GAT AGC CTT TAA GAT AAA TGT A 3') reverse transcribes the antisense *Rbm5* variant *Rbm5-AS1* (Rintala-Maki and Sutherland, 2009).

2.5 End-Point PCR

End-point PCR for glyceraldehyde 3- phosphate dehydrogenase (*Gapdh*), *Rbm10v1*, and *Rbm10v3* was carried out using the primers listed in Table 1. Primers were designed using PrimerQuest from Integrated DNA Technologies Inc. cDNA synthesis and genomic DNA contamination was verified by doing a PCR for *Gapdh* using exon-exon spanning primers. End-point PCR for *Rbm10* variants was carried out to detect and quantify their relative mRNA expression levels during differentiation. The PCR reaction consisted of 100 ng of the cDNA template, 0.2 mM dNTPs (10 mM stock), 200 nM of forward and reverse

primers (10 μM stock), 1.25 U of Taq DNA polymerase and 1 x reaction buffer (New England Biolabs) in a 50 μl reaction volume. The DNA template was initially denatured for 5 minutes at 95°C and amplified for 26 cycles for *Gapdh* and 40 cycles for the *Rbm10* variants, with denaturation at 95°C for 30 seconds, annealing at 58°C for 30 seconds and extension at 72°C for 1 minute, followed by a final extension at 72°C for 10 minutes. A 452 bp Gapdh product was visualized on a 1% agarose gel. The use of genomic DNA contamination as template would generate a 646 bp fragment. End-point PCR using previously published primers (Table 1) was performed to detect the splicing transitions for three mRNAs: *Dtna* (Bland et al., 2010), *Integrin β* (Cachaco et al., 2003) and *Mef2cγ* (Hakim et al., 2010). The following thermal cycling conditions were used: initial denaturation at 95°C for 5 minutes, followed by 36 cycles for *Integrin β* and *Mef2cγ,* and 40 cycles for *Dtna* at 95°C for 30 seconds, respective primer-dependant temperature annealing for 30 seconds and 72°C for 45 seconds and a final extension at 72°C for 10 minutes, generating fragment sizes listed in Table 1. As negative controls, "RT-" samples, containing all reagents without reverse transcriptase and no template control (NTC) samples without cDNA template were included to detect any genomic DNA contamination or contaminants in the PCR master mix, respectively. No amplification of genomic DNA was seen. All of the PCR were performed in duplicates and all of the samples were electrophoresed on a 2% agarose gel in duplicates. The AlphaEase FC™ software program (Alpha Innotech, Genetic Technologies Inc, Miami, USA) was used to quantify the band densities.

Table 1
Primers used in end-point PCR

Transcript	Primer ID	5′-3′ Primer sequence	Tm °C	Amplicon size (bp)
Gapdh	Gapdh F	AACACAGTCCATGCCATCAC	60	452
	Gapdh R	TCCACCACCCTGTTGCTGTA	62	
Rbm10v1	mRBM10E4 F	AGCAAAGTGCAGAGGATTCCTACGAG	78	322
	mRBM10E8 R	TTGGGCACACCACATTTGAAGCAC	72	
Rbm10v3	mRBM10E3 F	AGGGCAAGCATGAGTATGACGACT	72	334
	mRBM10E8 R	TTGGGCACACCACATTTGAAGCAC	72	
Dtna	Dtna F	AAGTCCCTGAGCTGTGCTTC	62	391/220
	Dtna R	CGATCAGCCTGTGTTCTTCA	60	
Integrinβ	Integrinb F	GGCAACAATGAAGCTATCGT	58	363/282
	Integrinb R2	CCCTCATACTTCGGATTGAC	60	
Mef2cγ	Mef2c gamma F	TCCACCTCGGCTCTGTAACT	62	198/102
	Mef2c gamma R	ATCTCGAAGGGGTGGTGGTA	62	

Tm calculated by 4(G + C) + 2(A + T) °C (Wallace et al., 1979)

2.6 Real-time quantitative PCR (qPCR)

qPCR was carried out to quantify the mRNA expression levels of *Rbm5* variants during differentiation. Primers were designed using PrimerQuest from Integrated DNA technologies Inc. *In silico* analysis to check for specificity was performed using the BLAST tool from NCBI. Using cDNA synthesized with Oligo(dT) primer, qPCR was carried out for *Rbm5* (full length and all variants) and the reference genes *Gapdh*, hypoxanthine-guanine phosphoribosyltransferase (*Hprt*) and ribosomal protein S12 (*Rps12*). cDNA synthesized with mFactorXF as template was used for *Rbm5+5+6* and *Rbm5+6*. cDNA synthesized with mFactorXR as template was used for *Rbm5-AS1*. A NTC was used as the negative control. Using 21 ng of cDNA template, qPCR was carried out with 12.5 µl of iTaq™ SYBR® green super mix with ROX (Bio-Rad, Mississauga, ON, Canada), 300-400 nM of forward and reverse primers (stock 10 µM) in a 25 µl reaction volume using an ABI Prism 7900T (Applied Biosystems, Life Technologies). qPCR was performed for four biological replicates with a varying number of technical replicates (2 to 7) and the reaction conditions were: denaturation at 95°C for 30 seconds followed by 40 cycles of 95°C for 30 seconds and primer-dependent annealing temperature (Tables 2 and 3) for 60 seconds. A melt-curve analysis with data acquisition at 95°C for 15 seconds, 60°C for 15 seconds and 95°C for 15 seconds was carried out to determine primer specificity. The absence of a melting curve in the NTC sample indicated that there was no contamination of the reagents and as well, no stable primer-dimers were formed. A standard curve was generated using dilutions of the pooled cDNA samples throughout differentiation and expression levels were quantified using the ABI software (SDS 2.4), calculated based on the formula log 10^((Cq (sample)-y intercept)/(-slope)), where Cq (or Ct) is the cycle threshold value, and the y intercept and slope values are derived from the standard curve (Larionov et al., 2005).

Table 2
Primers used in qPCR for quantifying *Rbm5* mRNA variants

mRNA transcript	Primer ID	Primer Sequence [5´to 3´]	Tm °C	Amplicon length(bp)
Rbm5+5+6	mrintron5 F mrintron6 R	GGAACTGACTAACACGAGTATCC CTAGACTTGGTGAGTGAAGCAAC	68 68	146
Rbm5+6	mrRBM5E5/6 F mrintron6 R	GAGGAAAACAGTGTAAGCCGTG CTAGACTTGGTGAGTGAAGCAAC	66 68	107
Rbm5-AS1	mrintron5 F mrintron6 R	GGAACTGACTAACACGAGTATCC CTAGACTTGGTGAGTGAAGCAAC	68 68	146
Rbm5 (all)	mqRbm5E2/3 F mqRbm5E3 R	GACAAAAGAGTGAGTAGAACAGAACG ATCACCTCTCCGATCATCGCTTGA	74 72	131
Rbm5 (Full length)	mrRbm5E5/6 F rRbm5E7 R	GAGGAAAACAGTGTAAGCCGTG GCATTGCAATGTGCTTTCCTTGA	66 66	122

Table 3
Primers used in qPCR for optimizing reference genes for normalization

Gene	PubMed ID	Function	Primer Sequence [5´to 3´]	Tm °C	Amplicon length(bp)
Actb	NM_007393.3	Cytoskeletal protein	F: TCCTGACCCTGAAGTACCCCAT R: CTCGGTGAGCAGCACAGGGT	68 66	131
Gapdh	NM_008084.2	Metabolic enzyme	F: ATGTTTGTGATGGGTGTGAA R: ATGCCAAAGTTGTCATGGAT	56 56	131
Hprt	NM_013556	Enzyme	F: ATGGACTGATTATGGACAGGACTG R: TCCAGCAGGTCAGCAAAGAAC	70 64	124
Rps12	NM_011295.6	Ribosomal protein	F: AAGGCATAGCTGCTGGAGGTGTAA R: AGTTGGATGCGAGCACACAGAGAT	72 72	156
Tbp	NM_013684.3	Transcription factor	F: TGCACAGGAGCCAAGAGTGAA R: CACATCACAGCTCCCCACCA	64 64	134

2.7 Protein extraction

Protein extraction was carried out using radio immunoprecipitation assay (RIPA) cell lysis buffer [50 mM Tris-HCl pH 8.0, 150 mM NaCl, 0.5% NP-40, 100 mM NaF, 1 mM EDTA pH 8.0, 1 mM EGTA pH 7.5, 10 µl/ml of Protease inhibitor cocktail (Sigma-Aldrich)]. Briefly, cells were re-suspended in the cell lysis buffer, incubated on ice for 15 minutes and centrifuged at 16 200 x g for 15 minutes. The total protein in the supernatant was quantified using the Bio-Rad DC protein Assay kit (Bio-Rad). Absorbance was measured at 650 nm using a SpectraMax 340PC 384 absorbance microplate reader (Molecular Devices, Downingtown, PA, USA). Different dilutions of BSA were used for standard curve generation and r^2 values of > 0.9 were considered reliable.

2.8 Immunoblotting

Immunoblotting was carried out using rabbit anti-RBM5 at a 1:2 500 dilution (Sutherland et al., 2000), rabbit anti-RBM10 at a 1:500 dilution (A301-006A, Bethyl laboratories Inc, Montgomery, Texas, USA), mouse anti-α-tubulin at a 1:10 000 dilution (Sc-8035, Santa Cruz Biotechnology Inc.), mouse anti-MyoG at a 1:200 dilution (Sc-52903, Santa Cruz Biotechnology Inc.), rabbit anti-Myf5 at a 1:200 dilution (Sc-302, Santa Cruz Biotechnology Inc.) and rabbit anti-MyoD at a 1:200 dilution (Sc-304, Santa Cruz Biotechnology Inc.). Secondary antibodies conjugated to horseradish peroxidase (HRP) were goat anti-mouse IgG at a 1:10 000 dilution (Sc-2005, Santa Cruz Biotechnology Inc.) and goat anti-rabbit IgG at a 1:10 000 dilution (Sc-2004, Santa Cruz Biotechnology Inc.). 50 µg of cell lysate in RIPA was re-suspended in 2 x SDS gel loading buffer (100 mM Tris-HCl pH 6.8, 20% Glycerol, 4% SDS, 0.2% Bromophenol blue and 200 mM 2-Mercaptoethanol) and after denaturing for 5 minutes at 100ºC was subjected to electrophoresis through a discontinuous SDS-PAGE gel prepared as per standard protocol (Simpson, 2006). Proteins were transferred onto methanol pre-wetted 0.45 µm PVDF membranes (Amersham Hybond-P, GE Healthcare, Mississauga, ON) using a wet transfer system. Transfer and loading accuracy was verified by staining with Ponceau S for 5 min, after which the membranes were washed with water. The membranes were blocked in 5%

non-fat dried milk in TBS-T (0.01 M Tris HCl, 0.15 M NaCl and 0.05% Tween 20) for one hour to prevent binding of non-specific proteins and were subsequently incubated over-night at 4ºC with the respective primary antibodies re-suspended in 3% non-fat dried milk in TBS-T. After three washes in 1 x TBS-T, the membranes were then incubated with secondary antibodies re-suspended in 3% non-fat dried milk in TBS-T for one hour at 22ºC and the bands were visualised by exposure to X-ray film (Amersham hyper ECL film, GE Healthcare) using chemi-luminescent detection reagents (Amersham Western blotting detection reagents, GE Healthcare). A mild stripping procedure was used for stripping bound antibodies from the blot using buffer containing 0.02M glycine, 0.1% SDS and 0.1% Tween 20, at pH 2.2. The stripping efficiency was verified by re-probing secondary antibody-HRP again, after which the membranes were blocked and probed again with the appropriate antibodies. Each blot was stripped not more than three times. The AlphaEase FC™ software program was used to obtain the band intensities from the immunoblots. For this, the intensity of each protein band was quantified after subtracting the background. One limitation with this method is that if the bands are over exposed as observed in some of the blots, the intensity becomes saturated, which can affect quantification.

2.9 Immunofluorescence

For immunofluorescence (IF), cells were grown on glass coverslips in GM or DM as described previously. Cells were washed gently in PBS (pH7.4) to remove the medium and fixed for 10 minutes in 4% paraformaldehyde in PBS. Cells were permeabilized for 5 minutes by incubation in 0.5% Triton X-100 in PBS and then blocked for 15 minutes in 5% goat serum in PBS. For localization studies, sequential double immunofluorescence was performed by using the primary mouse anti-Mf-20 (Developmental Studies Hybridoma Bank, Iowa City, IA) for myosin heavy chain (MyHC) at 1:100 dilution and incubated for one hour at 22ºC, followed by either rabbit anti-RBM5 (Sutherland et al., 2000) or rabbit anti-RBM10 (A301-006A, Bethyl laboratories Inc) at a 1:10 dilution, and incubated overnight at 4°C. The secondary antibodies, Alexa fluor 594 anti-rabbit IgG and Alexa fluor 488 anti-mouse IgG (Molecular Probes, Life Technologies) were used at a 1:200 dilution for one hour. All antibodies were suspended in 5% BSA in PBS. For verification of the muscle skeletal prototype, the differentiating cells were labeled with Mf-20 as described

previously (Masilamani et al., 2014), followed by rhodamine phalloidin (Molecular Probes, Life Technologies) in PBS, which stains filamentous actin, at a 1:500 dilution. For KD studies, cells were stained with the primary mouse anti-Mf-20 (Developmental Studies Hybridoma Bank) at a 1:100 dilution and incubated for one hour at 22ºC followed by Alexa Fluor 488 anti-mouse IgG (Molecular Probes, Life Technologies) secondary antibody at a 1:200 dilution for one hour. The nucleus was stained using 5 mM DRAQ5^{TM} (Biostatus Ltd, Leicestershire, UK) at a 1:1 000 dilution in PBS for 30 minutes. The coverslips were then washed thrice in PBS and mounted on glass slides using 90% glycerol and sealed with nail polish. Control staining was performed to measure the level of detection of non-specific signals (Table 4).

2.10 Confocal LASER scanning microscopy (LSM)

Images of the fluorescent slides were taken using a Zeiss LSM 510 Meta confocal microscope (Carl Zeiss, Oberkochen, Germany). The LASER excitation wavelengths were set at 633 nm (DRAQ5), 488 nm (MyHC) and 543 nm (RBM5 or RBM10/rhodamine phalloidin). The same settings were kept for cells at different differentiation time-points. For expression and knockdown studies, the images were taken using the 25X objective and to assess localization, the objective was set at 63X and then electronically magnified. Images were acquired sequentially to avoid bleed-through from spectral overlapping. For the localization studies, the laser settings were set to optimize signal detection rather than to control for protein expression levels.

2.11 Measurement of cell parameters

The cells were analyzed using the Cell Counter plug-in from ImageJ (Schneider et al., 2012). For characterization of the differentiation morphology, 3 randomly chosen separate fields from one representative plate were counted for each day during differentiation. For the knockdown experiments, to determine the effect of KD on C2C12 cell count, differentiation, fusion and maturation, at least 8-12 randomly chosen separate fields were counted for each day and for each transfection condition. The numbers of nuclei was determined by DRAQ5 positive staining and counted for each separate field and indicated as the average nuclei number. The percentage of cells entering the differentiation phase is

represented as differentiation potential. The differentiation potential was calculated based on the ratio of nuclei in MyHC-positive cells/total number of nuclei in the field X 100 % (Shafey et al., 2005). The number of cells expressing the muscle-specific marker Mf-20 from all the fields was counted to assess the expression of MyHC and denoted as average number of MyHC-positive cells. The extent of fusion was determined as the fusion index. The fusion index, expressed as a percentage, is the ratio of the number of nuclei in myotubes (MyHC-positive cells with two or more nuclei)/(total number of nuclei in myoblasts and myotubes) X 100 % (Ferri et al., 2009). In addition, the average number of myotubes (MyHC-positive cells with two or more nuclei) per field were counted and plotted as a graph. The maturation efficiency was obtained by calculating the average number of myofibers (≥5 nuclei) per field.

2.12 Statistical analyses

All statistical analyses were performed using either Microsoft excel or Graph Pad prism® (GraphPad software Inc, La Jolla, CA, USA). For all qPCR analysis, the mRNA expression values were normalized to the geometric mean of three reference genes (*Gapdh*, *Hprt*, *Rps12*). The relative fold-change in mRNA expression during differentiation was calculated from the quantitiy normalized to the level on day 0 from 4 biological replicates with 2-7 technical replicates. Outliers were eliminated by inter-quartile range (IQR) analysis, based on the 25^{th} and 75^{th} percentile values. One-way ANOVA was used to calculate the statistical significance of the mRNA expression levels during differentiation. Pearson correlation (r) analysis was used to determine the relationship of expression of each Rbm5 variant during differentiation. For all end-point PCR analysis, the average fold-change was calculated after normalization to *Gapdh*. Fold-changes in expression for each day during differentiation compared to D0 were calculated from the normalized values from 4 biological replicates with 2-4 technical replicates to assess the mRNA expression levels. Statistical significance was calculated using one-way ANOVA. The protein expression levels were normalized to α-tubulin. The relative fold change in expression for each day during differentiation was calculated from the normalized value on D0 from 4 biological replicates with 2 technical replicates. One-way ANOVA followed by Bonferroni *post-hoc* test was used to calculate statistical significance of the expression levels during

differentiation (amongst multiple data sets). A *P* value of < 0.05 was considered statistically significant.

Cell morphology parameters in the KDs were measured using the cell counter plugin from ImageJ. Cell count, differentiation, fusion and maturation were determined by counting 8-12 randomly chosen sepatate fields from each plate for each day and each condition for the two trials. Statistical significance was calculated using unpaired Students' *t*-test. A *P* value of < 0.05 was considered statistically significant.

For quantification of exon inclusion, firstly, using densitometry, the band intensities of the control and KDs were quantified from 2-4 technical replicates. The values were normalized to the band intensity of *Gapdh*. Secondly, using the values, the percentage of inclusion was obtained by relative ratios of normalized inclusion/ normalized inclusion+exclusion X 100 % (Chen and Zheng, 2009).

Table 4
Controls for double immunofluorescence staining

Control	Conditions	First primary antibody	Second primary antibody
Normal	1^0 Antibody 2^0 Antibody Labeling	Rabbit anti-Rbm5 (or Rbm10) Goat anti-rabbit Alexa fluor 594 Red	Mouse anti-Mf-20 (MyHC) Goat anti-mouse Alexa flour 488 Green
No first 1^0Ab	1^0 Antibody 2^0 Antibody Labeling	None Goat anti-rabbit Alexa fluor 594 No labeling	Mouse anti-Mf-20 (MyHC) Goat anti-mouse Alexa flour 488 Green
No second 1^0Ab	1^0 Antibody 2^0 Antibody Labeling	Rabbit anti-Rbm5 (or Rbm10) Goat anti-rabbit Alexa fluor 594 Red	None Goat anti-mouse Alexa flour 488 No labeling

Adapted from (Burry, 2011)

Chapter 3

3 Results

Results obtained are divided into three sub-sections. The first sub-section details the establishment of the C2C12 differentiation model to study the expression and function of RBM5 and RBM10. The second sub-section describes the expression and cellular distribution of these two proteins in this model system. The third sub-section contains the results obtained when the cells were deprived of RBM5 and RBM10 and induced to differentiate.

3.1 Assessment of the differentiation landmarks

C2C12 myoblasts, a secondary cell line derived from mouse thigh muscle (Yaffe and Saxel, 1977), were employed for elucidating the role of RBM5 and RBM10 in skeletal myogenesis. C2C12 myoblasts are well-characterized and reproducible model systems normally used in the study of the myogenic differentiation program (Casadei et al., 2009, Tannu et al., 2004) and are thus ideal for studying the effect of RBM5 and RBM10 in a normal non-transformed system, especially differentiating cells in culture.

3.1.1 Cell morphology

To determine the growth and differentiation profile, the C2C12 cells were examined visually using immunofluorescent staining. Using DRAQ5 nuclear stain, mouse anti-MyHC specific antibody Mf-20 and rhodamine phalloidin for actin staining, the distinctive morphology of the mono-nucleated myoblasts, elongated myocytes and fused multi-nucleated myotubes were visualized (Figure 3.1). The cell nuclei were counter-stained with DRAQ5, which was visualized as a blue colour in our experiments. The red colour showed the characteristic pattern of filamentous actin (f-actin) and was clearly evident in all the cells stained with rhodamine phalloidin. The f-actin staining showed the muscle cell morphology and cytoskeleton and helped in distinguishing stained areas of cells from unstained areas. The Mf-20 antibody binds to the light meromyosin of the myosin heavy chain, which is present in the sarcomere (Bader et al., 1982). The green colour showed the

characteristics of the MyHC protein and was detected in the differentiating myocytes and myotubes.

As differentiation was induced, we expected to see a change in morphology, from single mono-nucleated myoblats to multi-nucleated myofibers. Cell proliferation stops as myoblasts starts to differentiate. Cell proliferation should cease on starvation/serum deprivation and we would expect to see that the number of myotubes will increase soon after differentiation is initiated (by D2) and that the number of myofibers will increase later as differentiation proceeds (>D4).

On D0, the cells showed the presence of DRAQ5-stained single nucleus. Between D0 and D1, the number of cells increased. The cells were becoming confluent as evident from the increase in the proportion of nuclei. As expected, by D2, the cell morphology changed; from being fusiform or star-shaped they became elongated and were compact. Initially, as the mono-nucleated myoblasts were proliferating there was no MyHC expression, however within two days after induction, the cells were positive for MyHC, one of the muscle differentiation-specific markers, which shows the induction of MyHC expression. On D3, fusion of cells was more evident because the MyHC-stained cells had two or more nuclei, which are called myotubes. As differentiation proceeded, the rate of cell fusion occurred faster, which was apparent from the increase in the number of nuclei arranged closely in a linear fashion in the myotubes and also an increase in the number of myotubes was detected. By D7, the number of myotubes was greater with an increase in the number of DRAQ5-stained nuclei inside the myotubes and the formation of myofibers (≥5 nuclei) was evident. Our IF staining results therefore show that co-ordinated events of differentiation are occurring phenotypically.

Next, we proceeded to quantitatively assess the cell morphological parameters such as the total number of nuclei, the number of MyHC-positive cells, differentiation potential, fusion index, the number of myotubes (≥ 2 nuclei) and the number of myofibers (≥ 5 nuclei). As mentioned above, when differentiation is induced, cell proliferation should stop. When the number of cells are counted by counting the DRAQ5-stained nuclei, we should see a stop in

proliferation before D2, because cell cycle withdrawal occurs within two days (Shen et al., 2003). Induction of MyHC expression should initiate differentiation.

Our results (Figure 3.2) showed that the total cell number was less on D0 and increased on D1 and remained similar on D2 indicating that cell proliferation stopped on D1. Specifically, the total number of cells increased from 70±18/ high power field (hpf) on D0 to 152±11/ hpf on D1 and was 153±10/ hpf on D2. The expression of MyHC, obtained from the count of MyHC-positive cells, occurred on D2, increased on D3, and reached a plateau thereafter. There were no MyHC expressing cells on D0 and D1, however on D2, there were 8±4 MyHC-positive cells/ hpf, which increased to 22±4 cells/ hpf on D3. Differentiation started on D2 and increased until D7. This was evident from the 5±2 % differentiating cells on D2 to the 19±6 % increase on D3. Fusion of the myocytes to form the multinucleated myotubes began on D3 and reached a maximum on D6. The number of fused cells increased from 9±2 % (D3) to 38±3 % (D6). Maturation potential, which followed fusion was indicated by the presence as well as an increase in the number of myotubes and myofibers. There were 8±1 myotubes/ hpf on D4, 9±0.3/ hpf on D5, 10±1.5/ hpf on D6 and 10±0 on D7. Myofiber formation started from D4. From these results it was clear that differentiation had occurred in the C2C12 murine myoblasts, which led to fusion and that the endpoint of differentiation has been reached in a timely manner.

During the entire differentiation process, a small fraction of cells were present that were mono-nucleated and did not undergo differentiation, which were the reserve cells (Miller, 1990). These cells did not express MyHC and were quiescent, which is what is observed normally (Yoshida et al., 1998). These MyHC-negative cells remained undifferentiated even after D4, however, during this time-point the MyHC-positive cells exhibited an increase in MyHC expression and were fusing.

These results therefore, (a) correlated with the previously reported observations, (b) signified that the distinctive morphology is skeletal, and (c) asserted that differentiation progressed properly from myoblasts to form myotubes and myofibers.

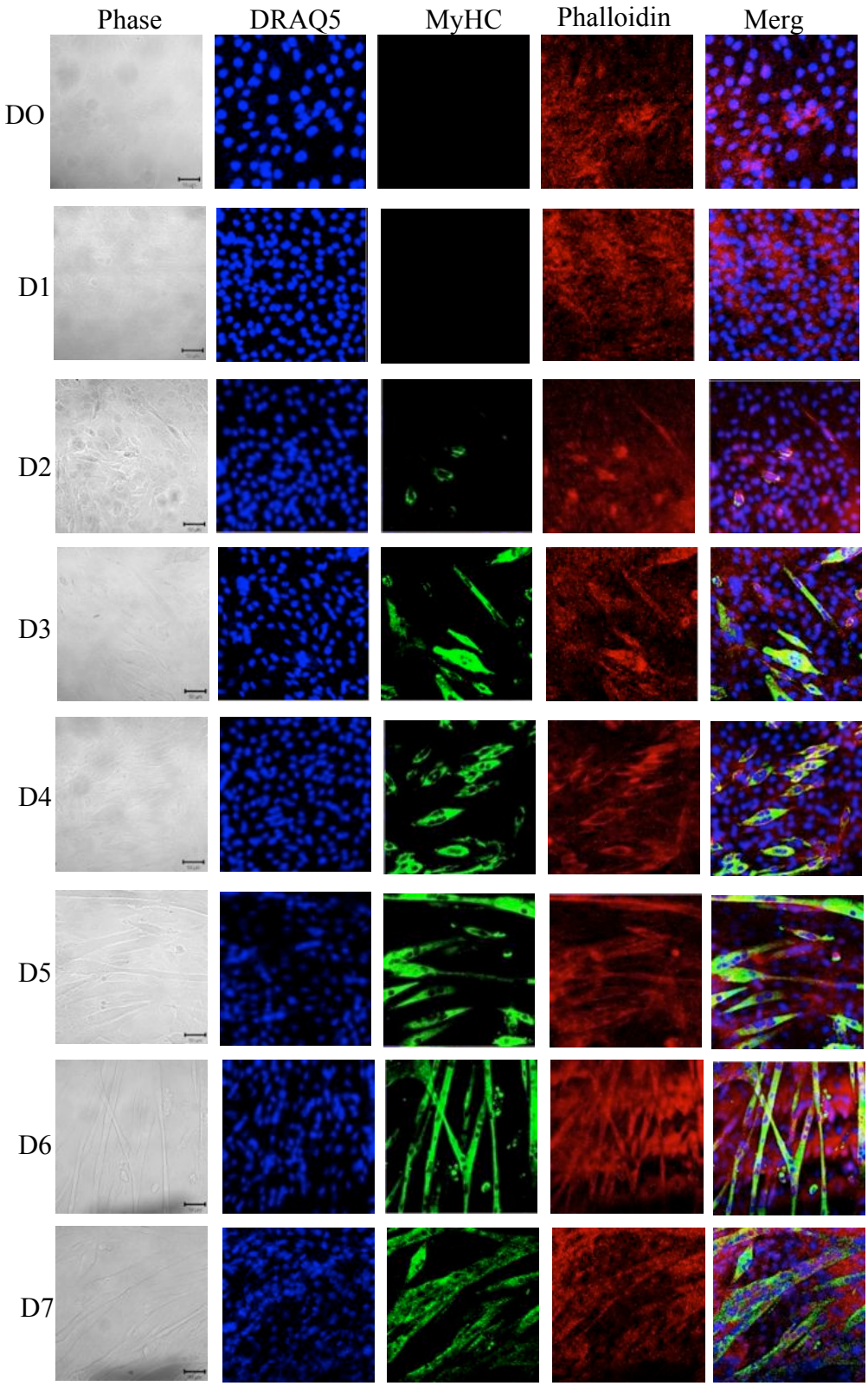

Figure 3.1 Visualization of the C2C12 differentiation morphology using IF. C2C12 myoblasts were grown to 80% confluency. On D0, the cells were induced to differentiate by removing growth factors (10% FBS to 2% HS) and were differentiated for 7 days (D0-D7). Cells were fixed, permeabilized and visualized by immunostaining. Phase contrast images and pictures of cells with DRAQ5, anti-mouse Mf-20 with fluorescein labeled secondary antibody and rhodamine phalloidin were taken using 25x objective, Scale Bar = 100µm.

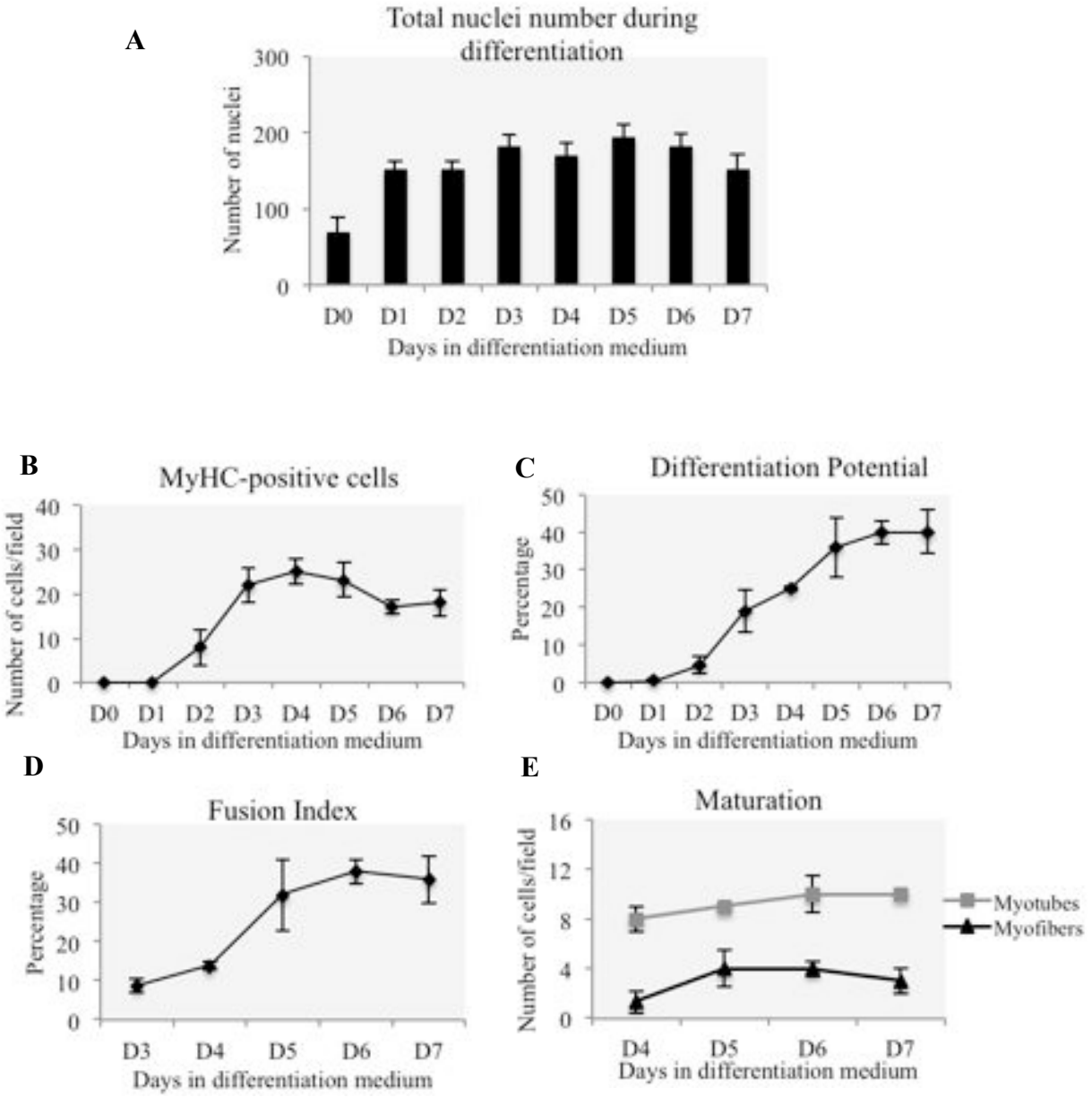

Figure 3.2 Characterization of the C2C12 differentiation morphology. Differentiating C2C12 **c**ells were fixed, permeabilized and visualized by IF staining. Pictures of cells stained with DRAQ5, anti-mouse Mf-20 with fluorescein labeled secondary antibody were taken every day and cell count analysis was performed. **A**) The average number of cells obtained by counting the total number of DRAQ5-stained nuclei per field, **B**) The average number of MyHC-positive cells, **C**) Differentiation potential, ratio of number of nuclei in MyHC-positive cells to the total number of nuclei in the field X 100, **C**) Fusion index, ratio of the number of nuclei in MyHC-positive cells (≥2 nuclei) to the total number of nuclei in myoblasts and myotubes X 100, **D**) Maturation potential showing the average number of myotubes and the average number of myofibers (≥5 nuclei) from all fields. Error bars represent SEM from 3 separate fields of view on each plate.

3.1.2 Expression of myogenic proteins

Most of the phenotypic changes that occur during differentiation are caused by gene expression changes at the molecular level (Moran et al., 2002). Changes in the expression levels of differentiation markers such as MyoD and MyoG are clear indicators of the differentiating status of the cells (Sabourin and Rudnicki, 2000). MyoD is a marker that is expressed in the early stages (determination/initiation) (Louis et al., 2008, Tomczak et al., 2004) and is necessary to maintain the cells in the differentiated state. MyoG is a characteristic differentiation protein marker that is not expressed during initiation but is present during the mid-stages of myogenic differentiation (Faralli and Dilworth, 2012). Expression of MyoG is the earliest indicator of differentiation.

Therefore, the expression levels of MyoD and MyoG were analyzed during the time course for differentiation using immunoblot analysis. Alpha-tubulin was used as a loading control, as it is a commonly used loading control and the expression does not change during differentiation (Blais et al., 2005, Smith et al., 2009, Jin et al., 2010, Ferri et al., 2009). Previous investigators have shown that MyoD can be expressed in C2C12 cells independent of differentiation status (Ferri et al., 2009). We expected to detect MyoD in the myoblasts and myotubes (Blais et al., 2005), and the levels to remain the same throughout differentiation (Shen et al., 2003). MyoG levels were expected to be absent in the myoblasts but detected 24 hours after switching to DM and should be present during differentiation (Blais et al., 2005).

As expected, MyoD (Dedkov et al., 2003) was expressed at D0 and the levels remained the same as differentiation proceeded (Figure 3.3). Next, as anticipated, MyoG (bottom band) (Favreau et al., 2004) was barely detected in undifferentiated myoblasts on D0 (Figure 3.4). Subsequently, MyoG levels increased after 24 hours of induction reaching the highest levels (four-fold) on D2 and then decreasing in the terminal-stages of differentiation. Transition from proliferation to differentiation after serum withdrawal indicates that the myoblasts are induced to differentiate. Accordingly, the absence of MyoG on D0 and high

levels on D2 indicated that induction of differentiation has occurred following the proliferation phase when the growth factors are removed.

Therefore, from our experiments we can conclude that the change in MyoD and MyoG levels paralleled previous findings, which show that the MRF expression is regulated, and the time-line of expression followed the pattern previously observed (Dedieu et al., 2002). These results corroborated molecularly that (a) the C2C12 cells are differentiating, (b) serum withdrawal induced the cells to differentiate and (c) the formation of myotubes was skeletal muscle specific.

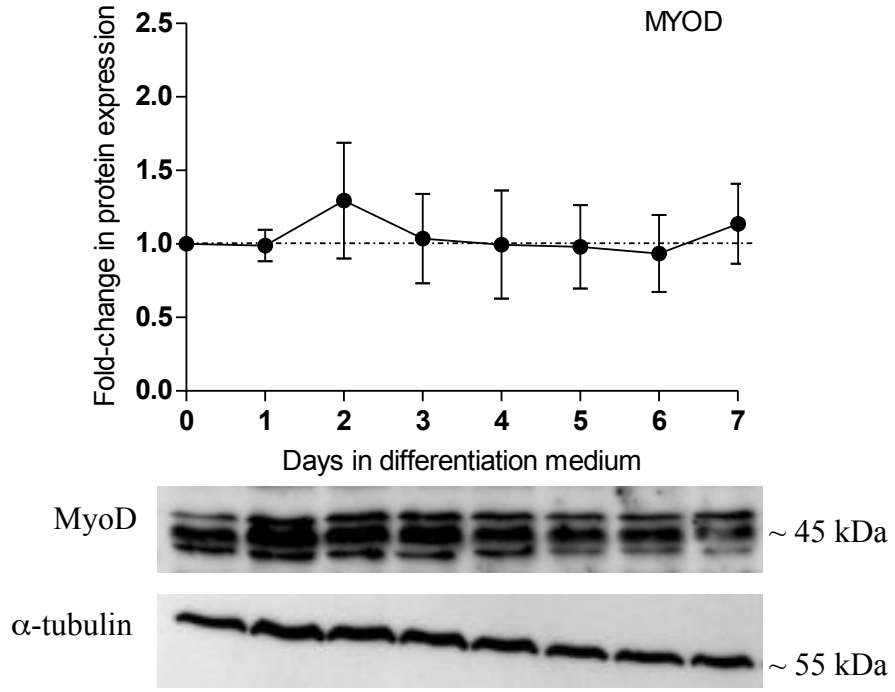

Figure 3.3 MyoD protein expression during C2C12 differentiation. MyoD is present on all days as differentiation proceeds. Using immunoblots, the MyoD (middle band) expression levels were quantified. The expression levels during the time-course of differentiation were analyzed using densitometry and plotted on a graph. α-tubulin was used for normalization. Error bars represent SEM from four biological replicates with technical duplicates for each. Raw data in Appendix A-Figure A1.

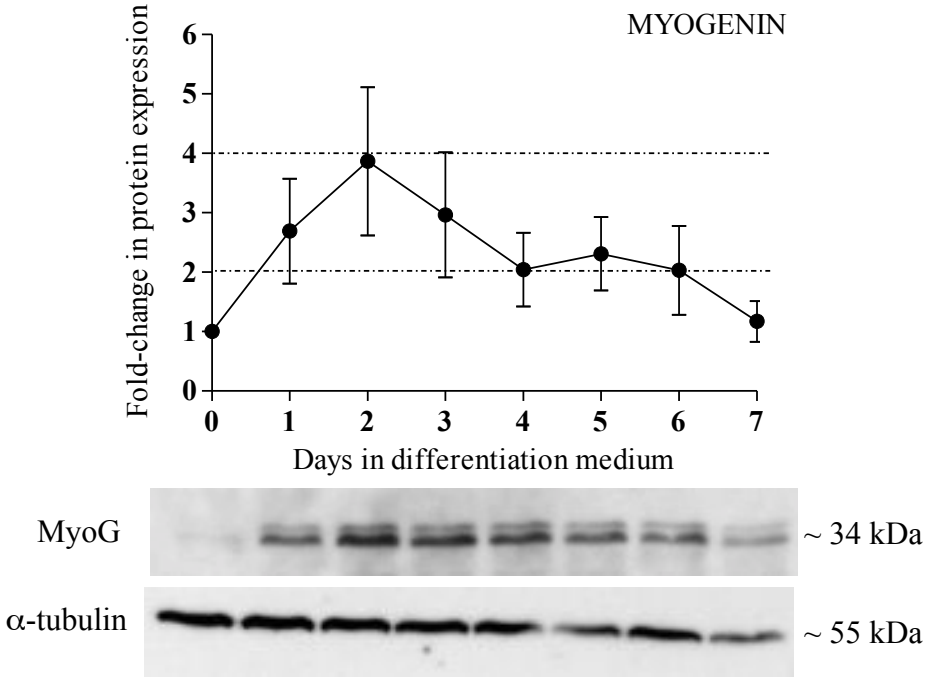

Figure 3.4 MyoG protein expression during C2C12 differentiation. MyoG is barely detectable on D0, is highest on D2 and decreases in the terminal-stages of differentiation. Using immunoblots, the MyoG (bottom band) expression levels were quantified. The expression levels during the time-course of differentiation were analyzed using densitometry and plotted on a graph. α-tubulin was used for normalization. Error bars represent SEM from four biological replicates with technical duplicates for each. Raw data in appendix A-Figure A1.

3.2 RBM5 and RBM10 expression and localization during C2C12 differentiation

After confirming the differentiation pattern morphologically and assessing the myogenic gene expression changes at the molecular level in the chosen C2C12 mouse model, protein expression levels of RBM5 and RBM10 were analyzed. Next, to determine the level of regulation of RBM5 and RBM10 expression, the levels of mRNA variants were assessed. In addition, using antibodies specific to each RBP, the sub-cellular distribution and the localization pattern were explored. Thus, this expression profile analysis serves as the first step to assess if RBM5 and RBM10 are potentially involved in skeletal myogenesis.

3.2.1 RBM5 and RBM10 are expressed in myoblasts, myocytes and myotubes

The presence of endogenous RBM5 and RBM10 protein in C2C12 cells during differentiation was assessed using immunoblots. The measurement of RBM5 protein levels during differentiation has not been done previously. However, based on previous northern blots of human skeletal muscle (Drabkin et al., 1999), we expected to detect RBM5 in myotubes. As, expected we detected RBM5 in myotubes. The specific protein band for RBM5, which is the full length translated RBM5 protein, migrated at ~113 kDa (Figure 3.5). Furthermore, the RBM5 band was detected during all seven days in the differentiating cells. Therefore, this experiment revealed that RBM5 was present in the murine myoblasts, myocytes and myotubes.

Using the same total protein, the specific protein bands for RBM10 were visualized. The measurement of RBM10 protein levels during differentiation has not been done previously. However, based on previous northern blots of human skeletal muscle (http://www.kazusa.or.jp/huge/gfimage/northern/html/KIAA0122.html), we expected to detect RBM10 in myotubes. As, expected we detected RBM10 in myotubes. Interestingly, although only one RBM10 mRNA transcript was present in the northern blots; we detected two RBM10 bands, one of which corresponds to the full-length translated RBM10 protein isoform (RBM10v1) and the other, the exon 4 alternatively spliced shorter isoform (RBM10v3) (Figure 3.6). Thus, two RBM10 isoforms were present in C2C12 cells and

migrated at ~130 kDa and ~117 kDa. Furthermore, both of the RBM10 isoforms were expressed during all seven days in the differentiating cells. Therefore, similar to RBM5, both RBM10v1 and RBM10v3 were present in the murine myoblasts, myocytes and myotubes.

In addition, it was evident that there was a difference in the expression of the RBM10 isoforms. The expression levels of RBM10v3 were higher than RBM10v1. We observed this on all days during differentiation. This is different from the observations seen in transformed cell lines; the RBM10v2 isoform (which is the mouse RBM10v3) was not expressed (Loiselle and Sutherland, 2014). Our results were similar to that observed in H9c2 cardiac- and skeletal- specific differentiation (Loiselle and Sutherland, 2014).

3.2.2 RBM5 and RBM10 expression decreases during differentiation

The band intensity of RBM5 and the two RBM10 isoforms was measured using densitometry. The intensity levels were normalized to the band intensity of the loading control, α-tubulin, as described previously. Fold-changes in expression for each day, compared to D0 were calculated to assess the protein expression levels. Based on the northern blots of human skeletal muscle, we expected to see high levels in the myotubes. However, our results indicate that the protein levels of both RBM5 and RBM10 decreased as differentiation progressed (Figures 3.5, 3.6). The amount of endogenous RBM5 and RBM10 was lower in differentiating myotubes than in proliferating myoblasts. There was a marked reduction in the protein levels during the later stages of differentiation but RBM5 and RBM10 were still detectable.

Certainly, the fold-change in RBM5 expression levels during differentiation was highly significant. Specifically, a decrease in RBM5 expression levels was noticed as the cells differentiated ($P < 0.0001$) (Figure 3.5). The reduction in the levels of RBM5 started on D2 and decreased thereafter, except on D5, which showed a slight increase. Interestingly, when compared to D0, the expression levels dropped 50% by D3 and > 50% by D7. Importantly, this reduction in expression was significant, as confirmed by Bonferonni *post-hoc* multiple comparison test, when each day was analyzed; D0 vs D3, D4, D5 D6 and D7, D1 vs D4,

D6 and D7, and D2 vs D6 and D7, showed statistically significant (varying *P* values) differences in RBM5 levels.

Based on the northern blots of human skeletal muscle, we expected to see high RBM10 expression in the myotubes. On the contrary, our results showed that there was a highly significant down-regulation in the fold-change in expression levels of the RBM10 isoforms during differentiation. The protein expression levels for both of the RBM10 isoforms decreased during the terminal-stages of myogenesis, the reduction being more pronounced for RBM10v1 ($P < 0.0001$) than for RBM10v3 ($P = 0.0374$) (Figure 3.6). The levels of both RBM10 isoforms decreased starting from D2. The level of RBM10v1 was significantly reduced from D2 to D7 whereas the level of RBM10v3 was significantly lower only on D7, as confirmed by Bonferonni *post-hoc* multiple comparison test. Indeed, significant (varying *P* values) differences in RBM10v1 levels amongst D0 vs D2, D3, D4, D5 D6 and D7; D1 vs D4, D6 and D7; D2 vs D7 were observed. Furthermore, when the reduction in fold-change was assessed, the expression was decreased by >50% by D7 for RBM10v1 and exactly 50% for RBM10v3 compared to D0.

To summarize, we detected RBM5, RBM10v1 and RBM10v3 in murine differentiating C2C12 myoblasts, and their presence was detected in all three myogenic cell types; myoblasts, myocytes and myotubes. The protein levels, however, were down-regulated during differentiation with a significant decrease by D7 when compared with D0. Finally, this similarity in the expression profile of both RBM5 and RBM10 proteins in differentiating C2C12 cells suggests a co-expression pattern for these two RBPs.

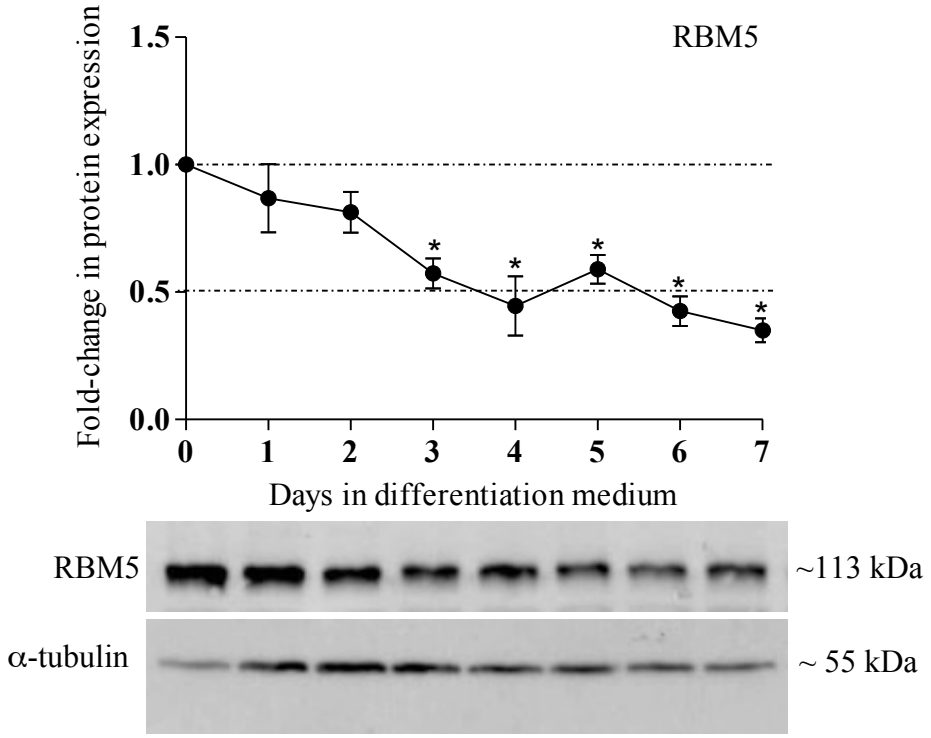

Figure 3.5 RBM5 protein expression during C2C12 differentiation. RBM5 is present in myoblasts, myocytes and myotubes. As differentiation proceeded RBM5 levels decreased and the decrease was significant from D3 onwards when compared with D0. Using immunoblots the RBM5 expression levels were quantified. The expression level during the time-course of differentiation was analyzed using densitometry and plotted on a graph. α-tubulin was used for normalization. Error bars represent SEM from four biological replicates with technical duplicates for each. Statistical significance was calculated using one-way ANOVA and Bonferonni *post-hoc* multiple comparison test,* P value < 0.05 were significant. Raw data in appendix A-Figure A2.

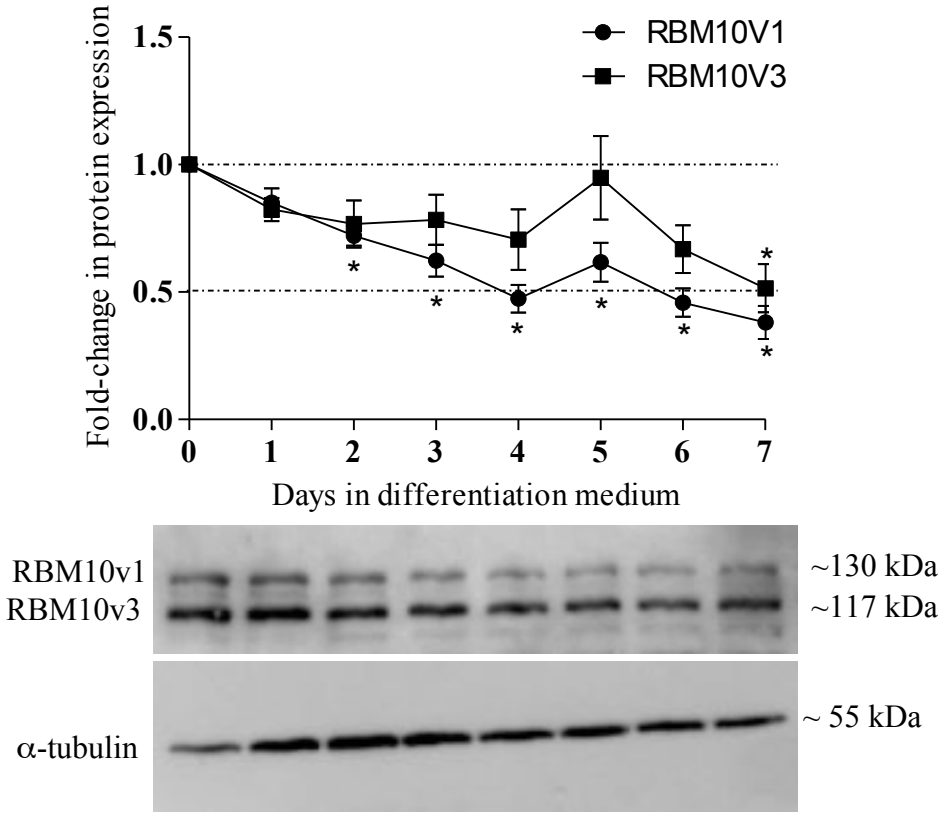

Figure 3.6 RBM10 protein isoforms expression during C2C12 differentiation. Both the RBM10 isoforms are present in myoblasts, myocytes and myotubes. As differentiation proceeded the levels decreased and the decrease was significant from D2 onwards when compared with D0 for RBM10v1. The decrease in expression in differentiating cells was significant on D7 compared with D0 for RBM10v3. Using immunoblots the expression levels of the RBM10 isoforms RBM10v1 and RBM10v3 were quantified. The expression level during the time-course of differentiation was analyzed using densitometry and plotted on a graph. α-tubulin was used for normalization. Error bars represent SEM from four biological replicates in technical duplicates. Statistical significance was calculated using one-way ANOVA and Bonferonni *post-hoc* multiple comparison test, * P value < 0.05 were significant. Raw data in appendix A-Figure A2.

3.2.3 *Rbm5* and *Rbm10* mRNA variants are expressed but their levels do not change in differentiating cells

To explore if the changes in protein expression were contributed by post-transcriptional modifications, the mRNA expression levels of the alternatively spliced variants of RBM5 and RBM10 were quantified. The *Rbm5* mRNAs that were measured in this study are *Rbm5* (full-length), *Rbm5+5+6*, *Rbm5+6* and *Rbm5-AS1*. These four RBM5 variants were analyzed because of their association with known functions such as cell cycle arrest, apoptosis and alternative splicing in other cell types (Mourtada-Maarabouni et al., 2006), which are the cellular events that underlie myogenesis.

3.2.3.1 *Rbm5* mRNA variants

The expression level of the *Rbm5* mRNA variants was quantitatively assessed using qPCR. Using the cDNA template reverse transcribed with Oligo(dT) and exon-specific primers located in exon 2/3 junction (forward primer) and exon 3 (reverse primer), the levels of all *Rbm5* variants were quantified (Figure 1.1). Next, using the same cDNA template, but primers located in exon 5/6 junction (forward primer) and exon 7 (reverse primer), the full-length *Rbm5* levels were quantified (Figure 1.1). Finally, for quantifying the other three variants, qPCR primers were located in the intronic regions for the intron retaining variants *Rbm5+6* and *Rbm5+5+6,* for which the cDNA template was synthesised using a gene-specific primer (mFactorXF) and in the antisense strand for *Rbm5-AS1*, for which the cDNA template was synthesized using a gene-specific primer (mFactorXR).

The coefficient of determination (R^2) of the standard curves showed that the Cq of dilutions are a proper fit to the curve and were in the range of 0.98-0.99 and the qPCR efficiencies calculated based on the slope of the standard curve were 1.96 (*Rbm5* full-length), 1.79 (Rbm5 all variants), 1.73 (*Rbm5+6*), 2.04 (*Rbm5+5+6*) and 1.96 (*Rbm5-AS1*). The geometric mean of three reference genes (*Gapdh*, *Hprt*, and *Rps12*) was used for normalization because these three genes were found to be stably expressed during C2C12 differentiation. These reference genes were chosen after proper validation using one-way ANOVA and NormFinder analysis (Masilamani et al., 2014) (See Appendix B). The R^2

values for these three reference genes were a good fit to the standard curve and were in the range of 0.98-0.99; in addition, the qPCR efficiencies were 2.2 (*Gapdh*), 2 (*Hprt*) and 2.19 (*Rps12*). RNA expression levels were calculated using the relative quantification method because of the variation in qPCR efficiencies.

Our results revealed that full-length *Rbm5*, *Rbm5+6*, *Rbm5+5+6* and *Rbm5-AS1* were detected in the C2C12 murine cells throughout the myogenic differentiation process (Figure 3.7). From this, we conclude that all the variants described in humans are present in mouse C2C12 cells. Based on our protein expression study results (Figure 3.5), we expected to see high Rbm5 mRNA levels in myoblasts than in myotubes. However, when the relative fold-change in expression for the day of differentiation was calculated relative to the quantity on D0, the levels of all the *Rbm5* variants (measured together) did not change during any day. Additionally, when each variant was measured individually, the levels did not change, which confirms the previous observation. Therefore, during differentiation, the mRNA levels remained relatively stable, except for small variations, which however, were not statistically significant. To conclude, during C2C12 differentiation, the *Rbm5* mRNA levels remained unchanged.

To determine if the variants regulated the expression of each other, using the fold-change in expression values we performed a pair-wise correlation using the Pearson correlation analysis (Mansson et al., 2004) (Table 5). A significant *P* value of 0.0003 with a R^2 value of 0.9 (closer to +1, positive correlation) indicates that the expression of all variants collectively is correlated to the expression of each *Rbm5* variant individually. This is indeed expected since it was found that there was a correlation in expression profile among all of the variants. However, no significant correlation was found when one variant was compared against the other. Therefore, in C2C12 myoblast differentiation, the *Rbm5* mRNA variants did not appear to have a regulatory relationship (linear positive correlation) on the co-expression of each other.

To summarize, we detected four *Rbm5* mRNA variants in the murine C2C12 differentiating cells and the variants were present at all differentiation time points (D0 to D7) in myoblasts, myocytes and myotubes. The levels were the same during the entire process, unlike the down- regulation observed in the RBM5 protein levels. Therefore, this implies

that the expression of RBM5 in differentiating C2C12 cells is not regulated at the transcriptional level but is subjected to post-transcriptional and/or post-translational regulation.

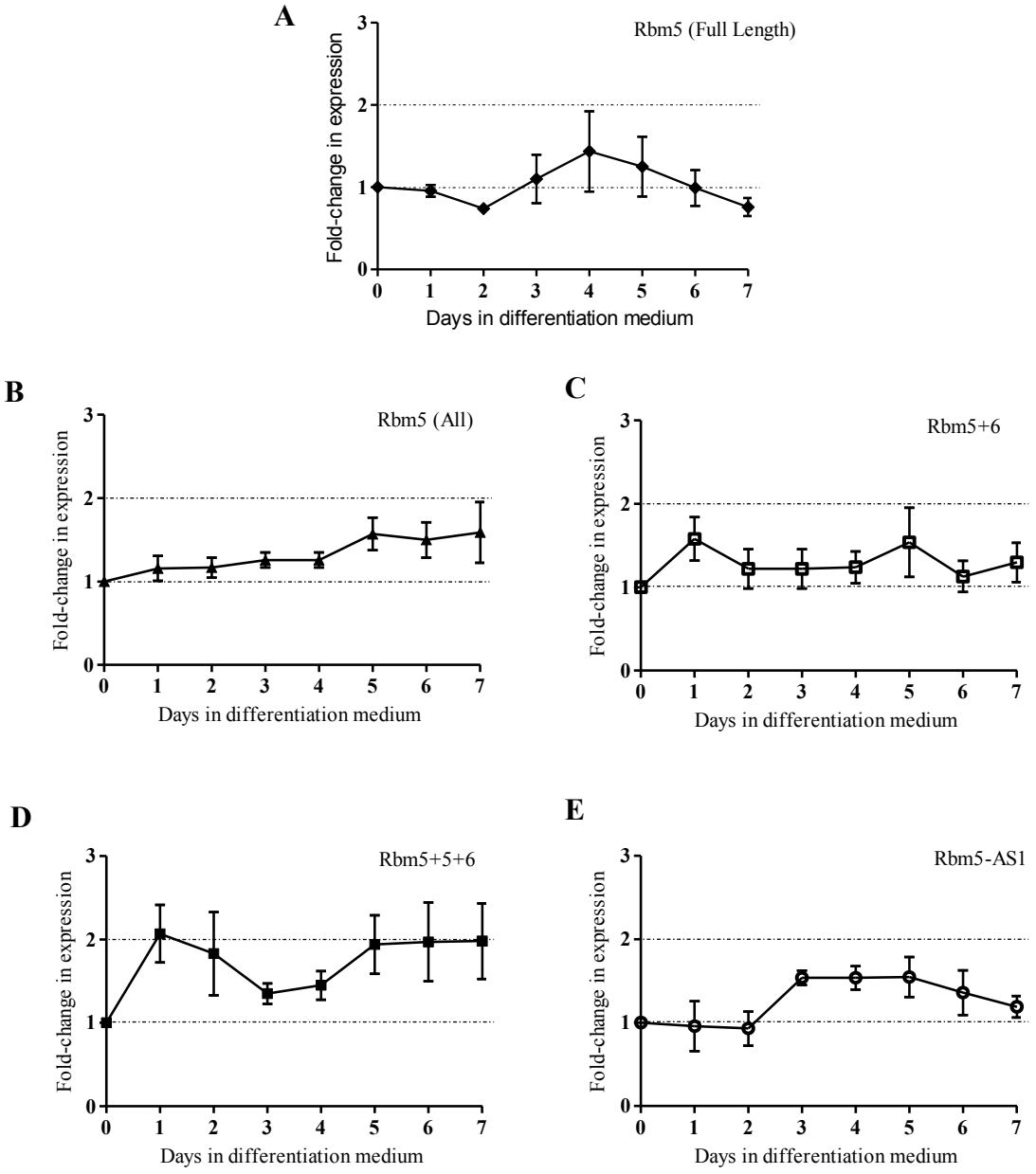

Figure 3.7 mRNA expression levels of *Rbm5* variants during differentiation. All the variants seen in human are expressed in the mouse C2C12 differentiating cells. No significant change in expression was observed during differentiation. Using qPCR the mRNA expression levels of **A**) *Rbm5* full length, **B**) *Rbm5* (all variants), **C**) *Rbm5+6*, **D**) *Rbm5+5+6* and **E**) *Rbm5-AS1* were quantified. The graph represents the levels during the time-course of differentiation from D0 to D7. Specific primers as listed in Table 2 were used for qPCR. The expression levels were normalized to the geometric mean of *Gapdh*, *Hprt* and *Rps12*. Error bars indicate SEM from four biological replicates with n=2-7 technical replicates. Statistical significance was calculated using one-way ANOVA.

Table 5
Pearson correlation for *Rbm5* mRNA variants

Parameter	Rbm5 All	Rbm5-AS1	Rbm5+5+6	Rbm5+6	Rbm5 FL
Pearson r	0.9511	0.5541	0.5143	0.1238	0.04382
95% confidence interval	0.7472 to 0.9914	-0.2473 to 0.9053	-0.2988 to 0.8947	-0.6365 to 0.7621	-0.6820 to 0.7262
P value (two-tailed)	0.0003	0.1542	0.1923	0.7703	0.9180
P value summary	***	ns	ns	ns	ns
Is the correlation significant? (alpha=0.05)	Yes	No	No	No	No
R square	0.9046	0.3070	0.2645	0.01532	0.001920

Significance: * $p < 0.05$, ** $p < 0.01$ and *** $p < 0.001$.

Pearson's correlation values closer to +1 or -1 indicate strong correlation.

3.2.3.2 *Rbm10* mRNA variants

The expression levels of the two *Rbm10* mRNA variants were analyzed using semi-quantitative RT-PCR (end-point PCR) with exon-specific primers (Figure 3.8). Specifically, the PCR was performed using a forward primer located on exon 4 along with the reverse primer located on exon 8, which would amplify only *Rbm10v1* because of the absence of exon 4 in *Rbm10v3* (Figure 1.3). PCR primers located on exon 3 (forward primer) and exon 8 (reverse primer) were used for *Rbm10v3*. Using densitometry, the band intensities were calculated and were normalized to the band intensity of *Gapdh*. *Gapdh* was used because the levels of *Gapdh* did not change during differentiation and hence was a suitable normalization control (Nishimura et al., 2008). Additionally, we have shown using qPCR that Gapdh is stably expressed during differentiation (Masilamani et al., 2014) (See Appendix B). Both the *Rbm10v1* and *Rbm10v3* variants were expressed in the myoblasts, myocytes and myotubes. Based on our protein expression results, we expected to see the myotubes with lower Rbm10 mRNA levels compared to the myoblasts. Interestingly, contrary to what was seen at the protein level, the mRNA expression levels for both of the variants remained the same. The expression did not change during the time-course of differentiation. Therefore, the expression of RBM10 in C2C12 cells does not appear to be regulated at the transcriptional level but is subjected to post-transcriptional and/or post-translational regulation.

One limitation of using end-point PCR is that it is a semi-quantitative approach and therefore in order to accurately assess the mRNA expression of both the RBM10 variants qPCR should be used. However, using qPCR for quantification of the two variants with 231bp nucleotide difference requires proper design and validation of many different primer pairs. Though it is possible to design qPCR primers located at the alternative exon (Exon4) and the constitutive exon (Exon5) for amplifying Rbm10v1, designing primers located in the exon-exon junction (Exon3/5) and the constitutive exon (Exon5) for RBM10v3 can lead to generation of false-positives and decrease in fidelity because of sequence similarity at the exon-exon junction (Brosseau et al., 2010).

To conclude, the apparent discrepancy between changing protein levels and the steady state mRNA levels for both RBM5 and RBM10 in the differentiating cells (myoblasts to myotubes) suggests that post-transcriptional and/or post-translational modifications contribute to the regulation of RBM5 and RBM10 during differentiation. Interestingly, both *Rbm5* and *Rbm10* had a similar pattern of expression. This further confirms their co-expression during differentiation, which possibly implies that they contribute to distinct functions in myogenesis.

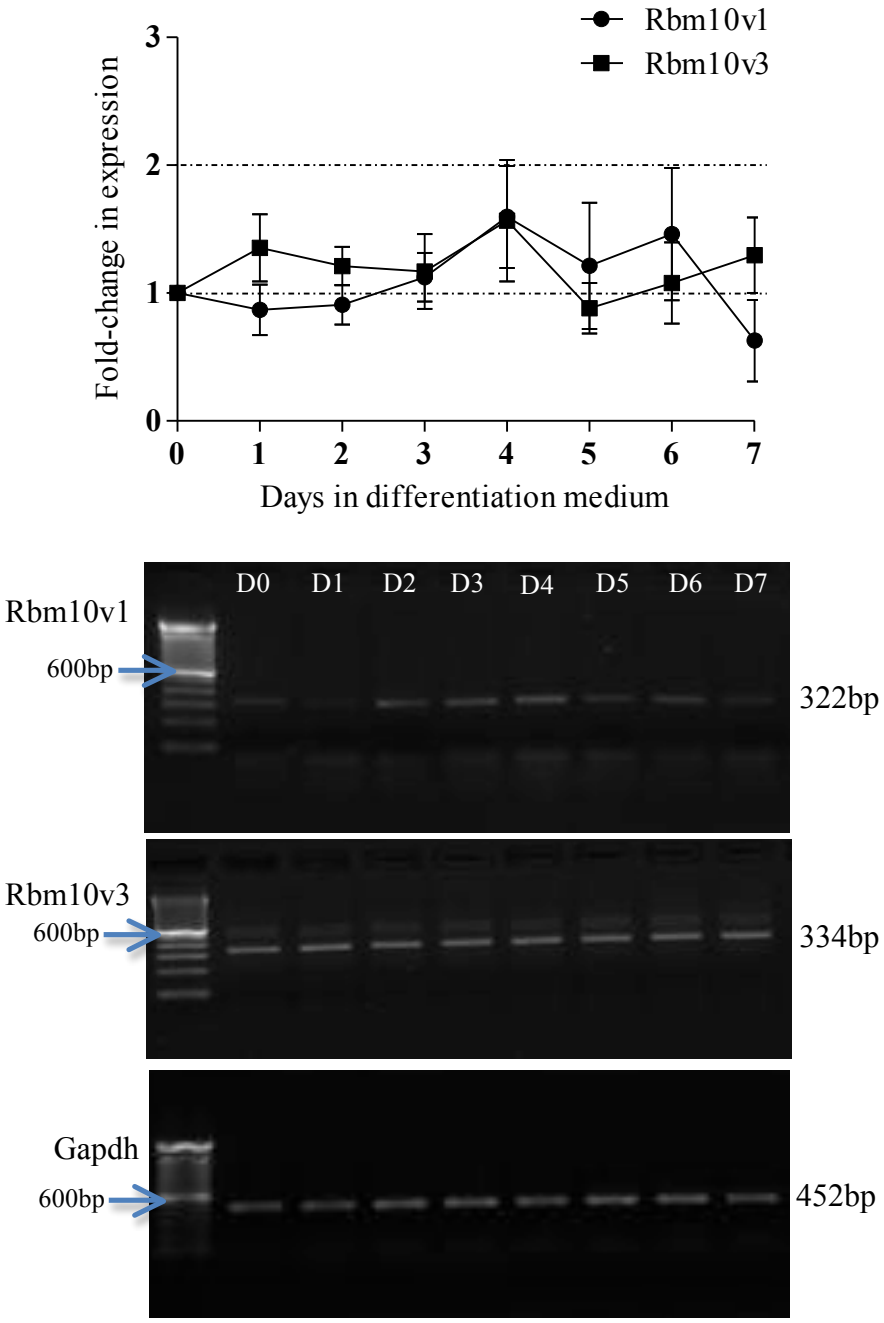

Figure 3.8 mRNA expression levels of *Rbm10* variants during differentiation. The two variants seen in human are expressed in mouse C2C12 differentiating cells. No significant change in expression was observed during differentiation. Using end-point PCR the mRNA expression levels of *Rbm10* variants *Rbm10v1* and *Rbm10v3* were analyzed. The graph represents the levels during the time-course of differentiation from D0 to D7. Specific primers as listed in Table 1 were used for end-point PCR. The expression levels were normalized to *Gapdh*. Error bars indicate SEM from four biological replicates. Statistical significance was calculated using one-way ANOVA. Raw data in appendix A-Figure A3.

3.2.4 RBM5 and RBM10 are differentially localized in differentiating C2C12 cells

To determine the subcellular location of RBM5 in the differentiating C2C12 cells, we carried out indirect double immunofluorescence (IF) microscopy using antibodies specific for MyHC and RBM5. The cell nuclei were counter stained with DRAQ5. The pattern of expression and cellular distribution was visualized under fluorescence using a confocal microscope. The same settings for image acquisition such as the intensity and exposure time were maintained through each day, for each experiment. Localization experiments do not control properly to allow quantification of signal intensity because of the structural difference of the cells. The confocal microscope settings were optimized to detect the localization of low levels of protein using immunofluorescence, which does not use the full range of intensity, which is therefore not quantitative.

In order to ensure proper detection and specificity, IF staining was verified by having controls (Figure 3.9). RBM5 immunoblots served as primary antibody controls, in which only bands specific for RBM5 were seen when using LUCA-15 UK antibody targeted against RBM5 (Appendix A, Fig A2). Next, controls with and without antibodies (primary and secondary) served as controls for staining specifically. All the signals detected were checked for specificity and cross-reactivity. Indeed, without RBM5 primary and secondary controls, there was no red color detected, which suggests that the MyHC antibody detected in the cytoplasm was specific. Similarly, when the cells were not stained with Mf-20 primary (MyHC) and secondary antibodies, only RBM5 (red color) was detected in the controls. No non-specific fluorescent signals were obtained.

To our knowledge, this is the first study to demonstrate localization pattern of RBM5 in mouse muscle cells. Based on previous reports in human fibrosarcoma HT 1080 cells (Drabkin et al., 1999), we mainly expected to see RBM5 in the nucleus. As expected, our results revealed that RBM5 accumulated in the nucleus on D0 as evident from the localized pattern of the red color (Figures 3.10, 3.11A). However, as the cells were differentiating, RBM5 was expressed both in the nucleus and cytoplasm (Figures 3.10, 3.11B, 3.12). Some of the MyHC-positive cells had RBM5 and MyHC in their cytoplasm as seen with yellow color in the merged fields, which is caused by overlapping red and green colors. Specifically, starting from D2 the transition from nucleus to cytoplasm was clearly evident

in the differentiating cells. Detection of RBM5 in the cytoplasm has been previously reported in prostatic tissues (Zhao et al., 2012), however, this is the first time, cytoplasmic (sarcomeric) presence was observed in muscle cells. Interestingly, we also observed that from D5 to D7, RBM5 was present in the nucleus in reserve cells (Figure 3.16). These are the single, mono-nucleated cells, which were not positive for MyHC even at the terminal-stages of differentiation (Blais et al., 2005).

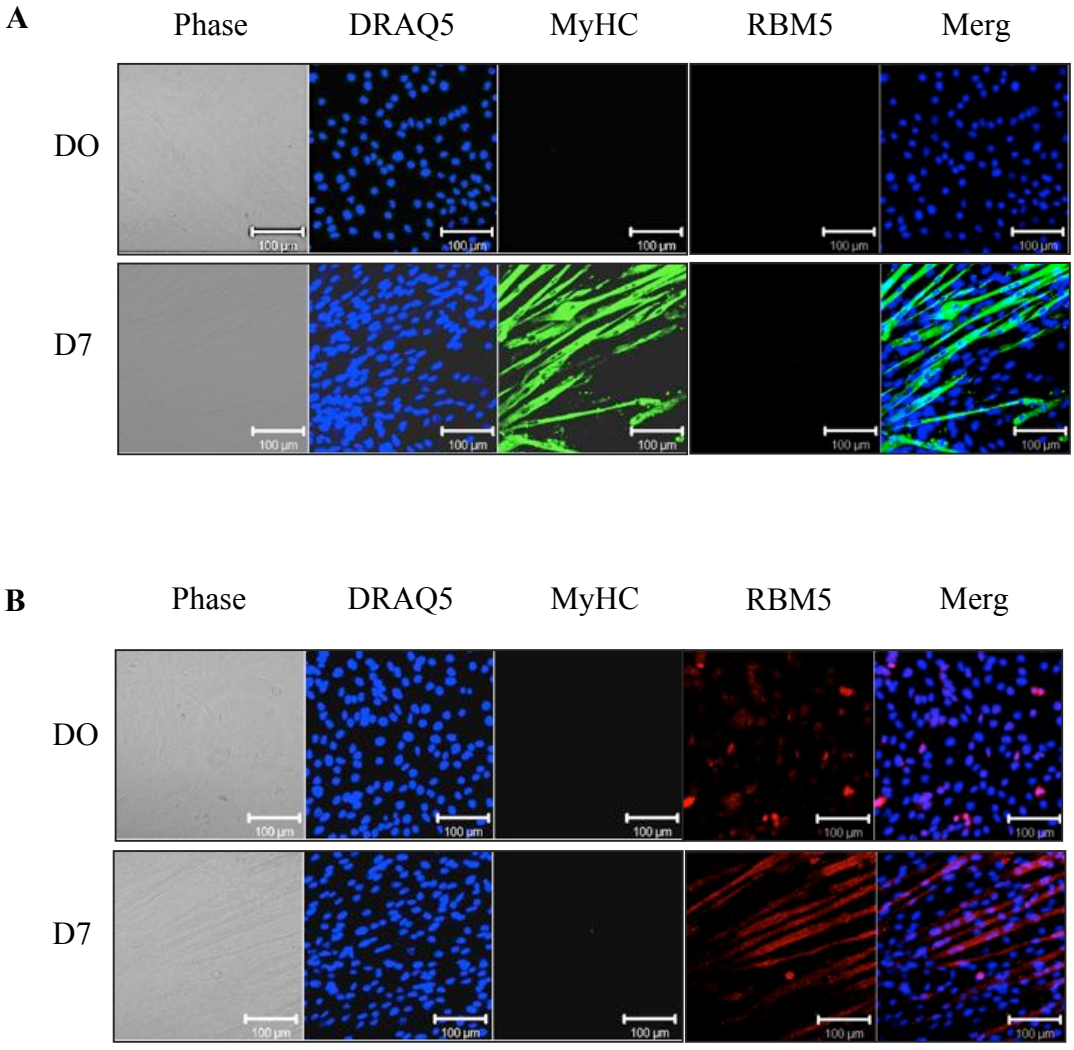

Figure 3.9 Controls for RBM5 and MyHC double IF staining. C2C12 myoblasts were induced to differentiate by changing GM to DM. The cells were grown on coverslips, fixed, permeabilized and stained. The staining procedure was verified using controls including **A**) no first rabbit anti-RBM5 primary antibody for D0 and D7 and **B**) no second mouse anti-Mf-20 primary antibody for MyHC for D0 and D7. Scale bar = 100µm.

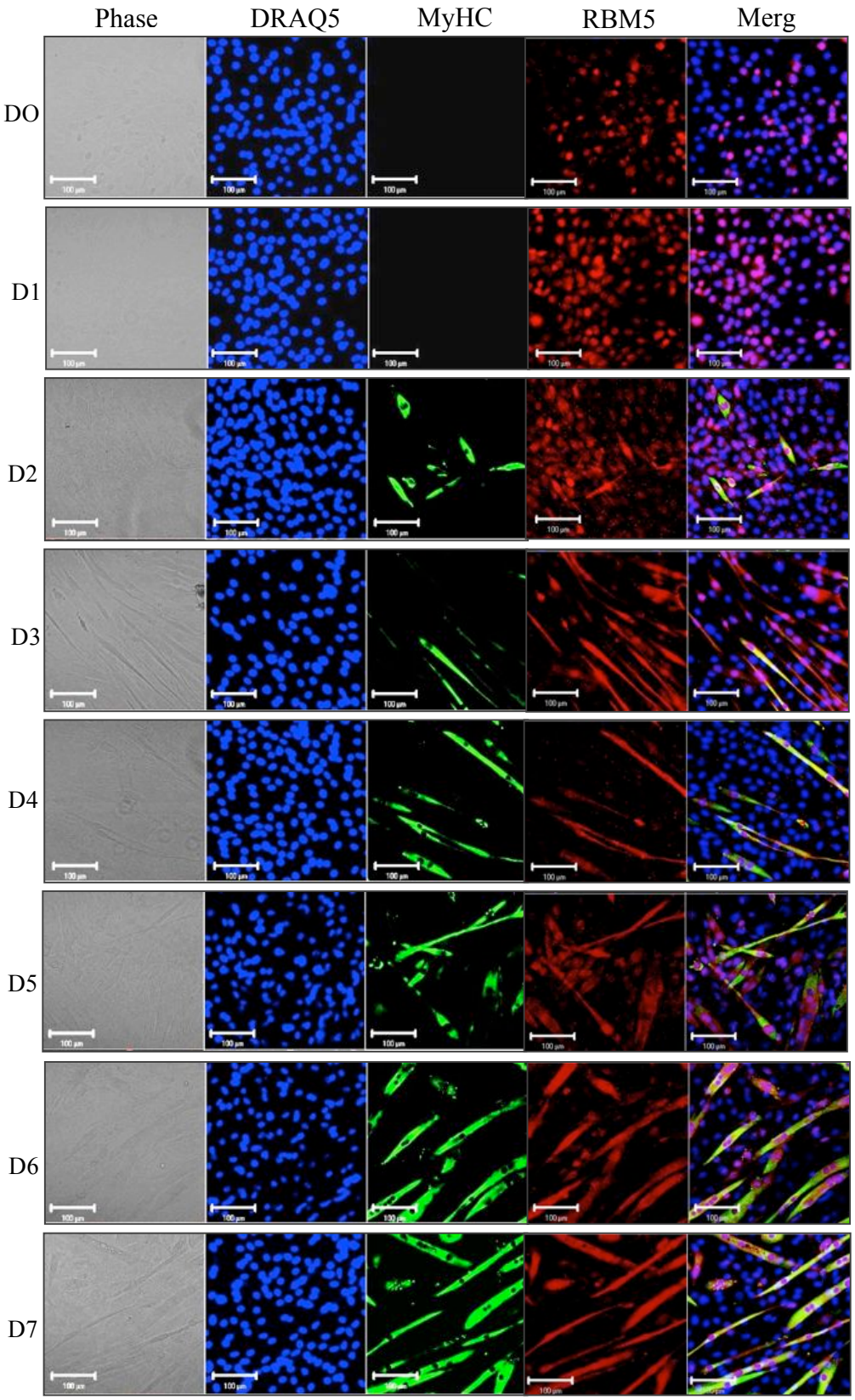

Figure 3.10 Intracellular distribution of RBM5 in differentiating C2C12 cells. RBM5 is differentially localized during C2C12 differentiation. C2C12 myoblasts were induced to differentiate for seven days, cells were fixed, permeabilized and stained. Phase contrast, DRAQ5, MyHC, RBM5 and merge panels showing the subcellular presence using IF staining. Scale Bar = 100µm

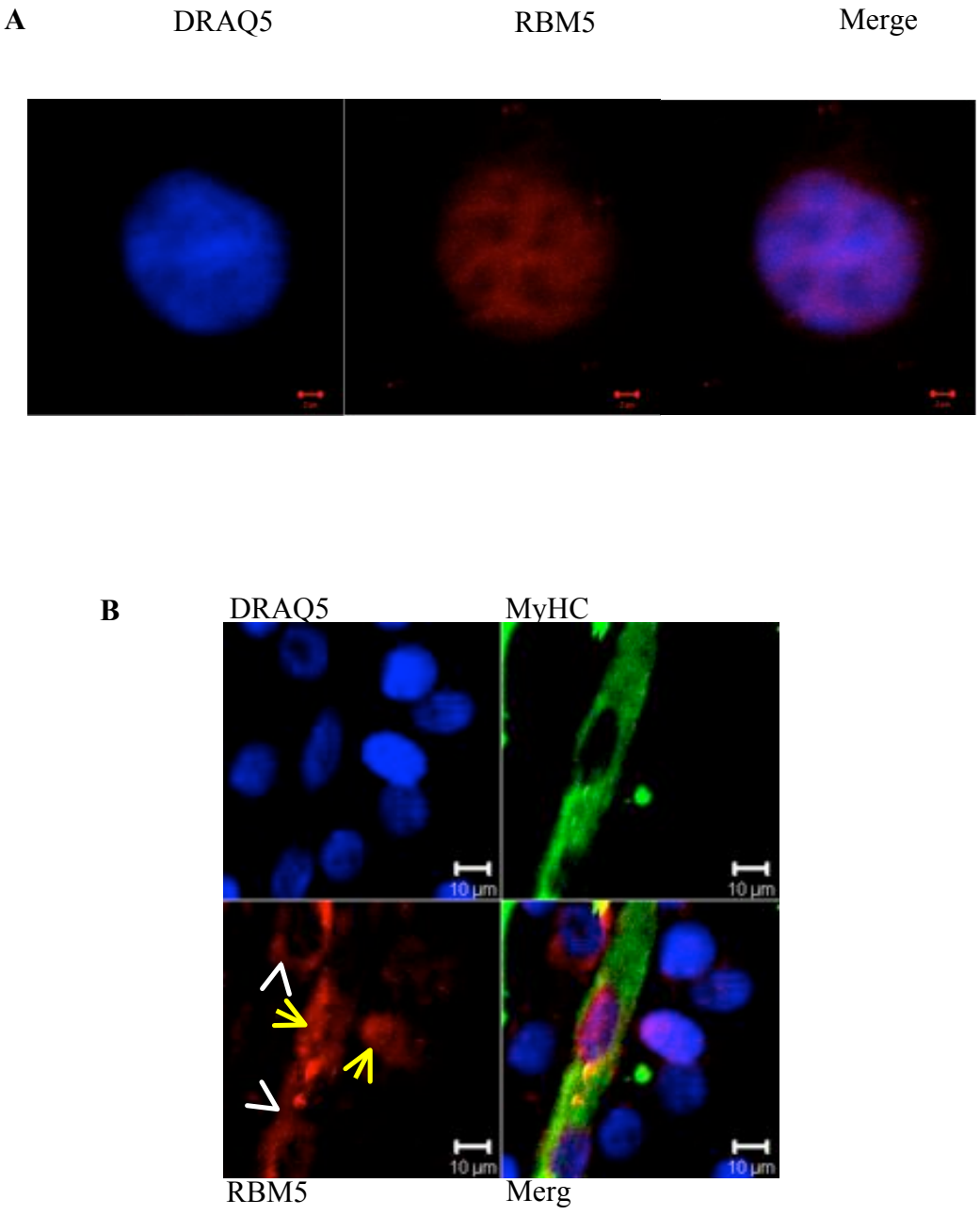

Figure 3.11 RBM5 cellular localization. RBM5 is detected in the nucleus in myoblasts, and in the nucleus and cytoplasm in myotubes. **A)** D0 showing nuclear localization, Scale Bar = 2µm and **B**) D7 showing both cytosolic and nuclear localization, Scale Bar =10µm. Arrow heads (white) indicate cytosolic presence and arrows (yellow) indicate presence in nucleus in differentiating myotubes. Images were obtained using 63x objective and then electronically magnified.

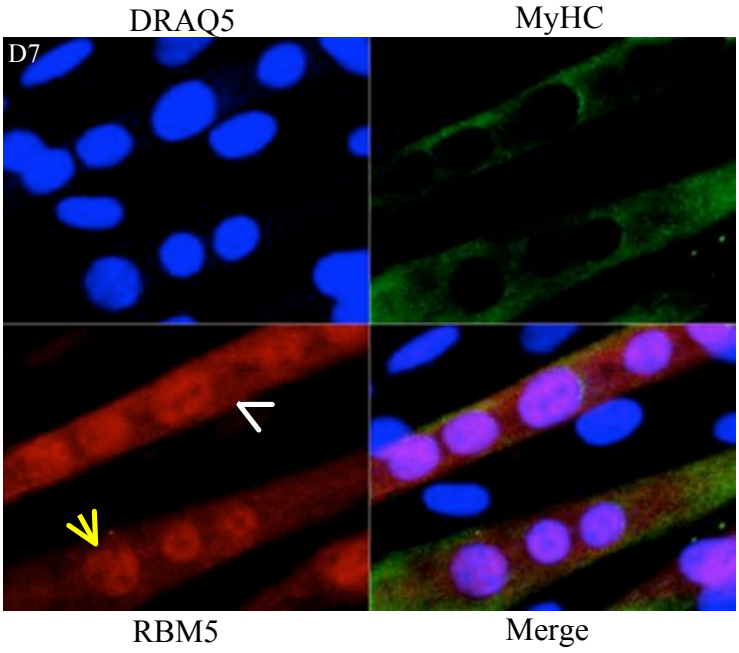

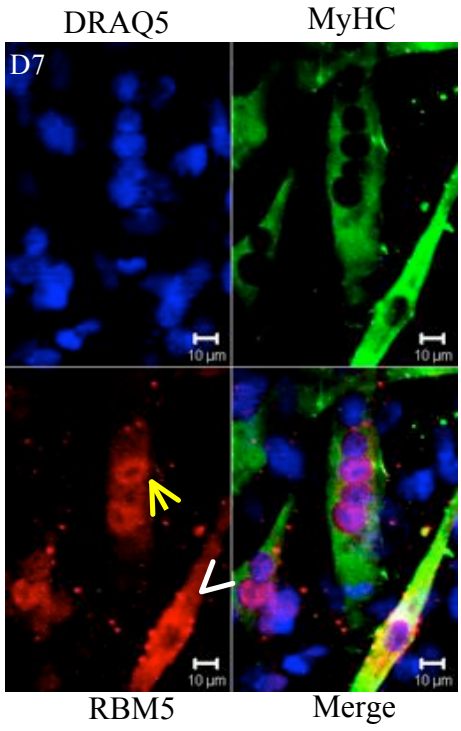

Figure 3.12 RBM5 cellular localization in differentiated myotubes. Detection of RBM5 in the nucleus and cytoplasm in D7 differentiated C2C12 cells. Arrowheads (white) indicate cytosolic presence and arrows (yellow) indicate presence in nucleus in differentiated myotubes. Scale Bar=10µm. Images were acquired using 63x objective and electronically magnified.

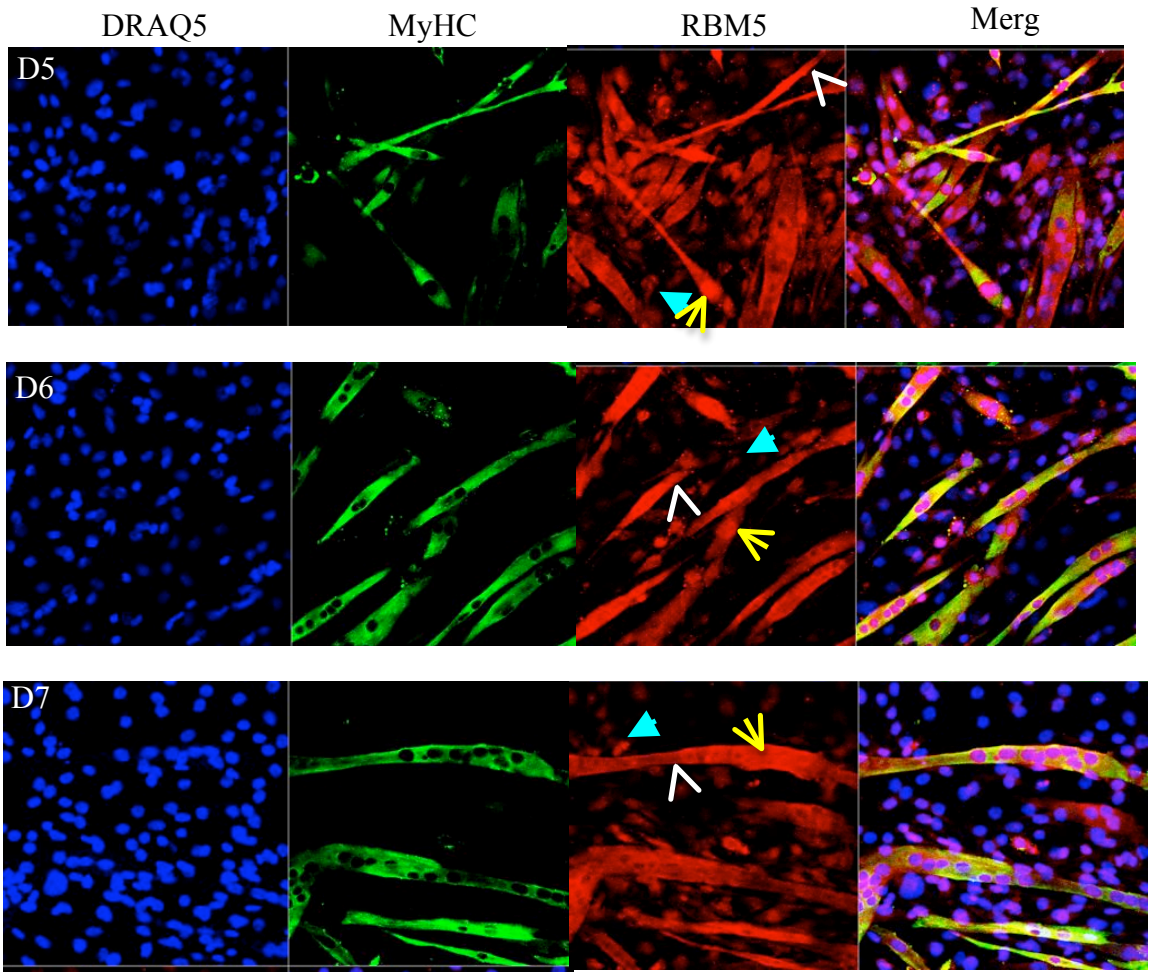

Figure 3.13 RBM5 cellular localization in D5, D6 and D7 differentiating C2C12 cells. Detection of RBM5 in the nucleus and cytoplasm during differentiation. Arrowheads (white) indicate cytosolic presence and arrows (yellow) indicate presence in the nucleus in myotubes. Arrows (cyan) indicate presence in the nucleus in MyHC-negative (reserve) cells. Images were acquired using 25x objective.

As evident from the higher magnification images (Figure 3.13A), the nuclear localization pattern of RBM5 was intra-nuclear but probably not in the nucleoli because some areas in the nucleus were not stained with RBM5. This observation is in line with the result obtained by (Gupta, 2006).

Next, in order to proceed with the immunofluorescence detection of RBM10, we had to ensure proper detection and specificity. Similar to RBM5, we performed control staining for RBM10 and MyHC (Figure 3.14). RBM10 immunoblots served as controls for the primary antibody, in which bands specific for RBM10v1 and RBM10v3 isoforms were seen when using Bethyl RBM10 antibody targeted against RBM10 (Appendix A, Fig A2). Controls with and without antibodies (primary and secondary) served as controls for staining specifically. All the signals detected were checked for specificity and cross-reactivity. Indeed, without RBM10 primary and secondary controls, there was no red color, which suggests that the MyHC antibody detected in the cytoplasm was specific. Similarly, when the cells were not stained with Mf-20 primary (MyHC) and secondary antibodies, only RBM10 (red color) was detected in the controls. No non-specific fluorescent signals were obtained.

This study is the first to determine the localization pattern of RBM10 in C2C12 cells, during proliferation as well as during the differentiation stages (Figures 3.15, 3.16, 3.17, 3.18). Previous reports have shown that the rat S1-1 was observed as a punctate structure in the nuclear bodies in the rat heart and skeletal muscle, besides being present in kidney, intestine, spleen and adrenal gland (Inoeu et al., 2008). We expected to see RBM10 to be distributed in the nucleus and as expected, at D0, RBM10 localization was nuclear, as indicated by the red color in the myoblasts (Figures 3.15, 3.16A). This nuclear localization is clearly evident in Figure 3.16A, RBM10 stained in the nucleus in the myoblasts. Our observation is in line with the result reported by Xiao et al., (2013), wherein S1-1 (the rat homologue) was localized in the nuclei in rat liver epithelial cells. They observed that RBM10 was absent in the nucleolus. We observed some areas in the nucleus that were not stained with anti-RBM10 anti-serum, which could be the nucleoli. Interestingly, as the myoblasts proceeded to differentiate, we observed that starting from D1, the RBM10

staining was distributed in the cytoplasm as well (Figure 3.15, 3.16B, 3.17, 3.18). Nuclear and cytoplasmic localization has been reported for RBM10 in a variety of normal (neutrophils and villi) and as well as cancerous cells (Hela, HL-60 and hepato cellular carcinoma) (Xiao et al., 2013; Inoue. 2013). In the present study, RBM10, like that of RBM5, localized in the nuclei of some of the reserve cells from D5 to D7 (Figure 3.18).

Interestingly, both RBM5 and RBM10 had a similar pattern of intracellular localization. Nuclear localization during the initial stages (in the myoblasts at D0 and in reserve cells in the myotube population on the proceeding days D5 to D7) and cellular localization in both cytoplasm and nucleus only during the later stages of differentiation indicates a level of functional regulation in these cells. The shift in intracellular distribution suggests that there is a potential need for these RBPs to be strategically positioned within the cell to perform site-specific functions. Furthermore, this mimics the localization profile of many myogenic factors such as MyoG, MyoD and Myf5 (Ferri et al., 2009) and indicates that nucleo-cytoplasmic shuttling of important proteins is a common occurrence in muscle.

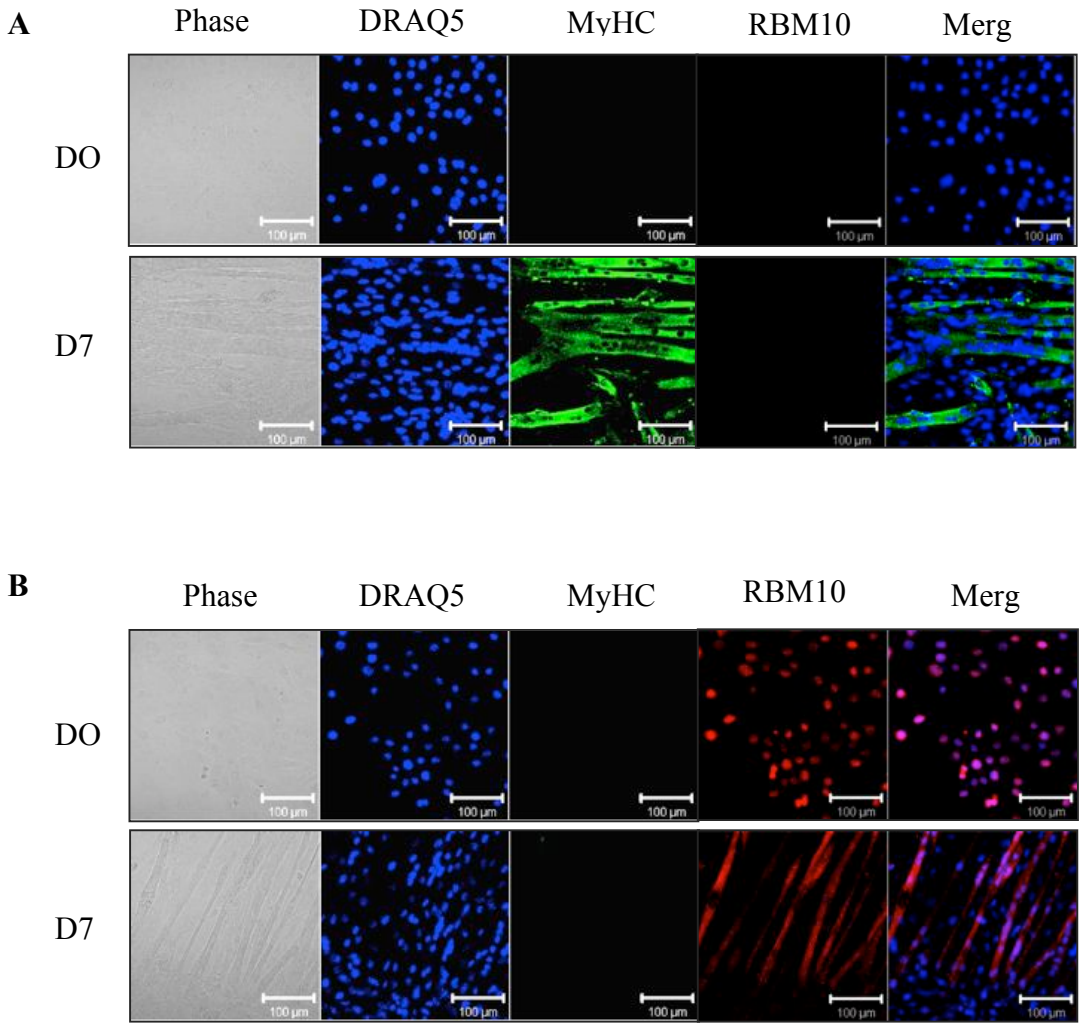

Figure 3.14 Controls for RBM10 and MyHC double IF staining. C2C12 myoblasts were induced to differentiate by changing GM to DM. The cells were grown on coverslips, fixed, permeabilized and stained. The staining procedure was verified using controls including **A**) No first rabbit anti-RBM10 primary antibody on D0 and D7 and **B**) no second mouse anti-Mf-20 primary antibody for MyHC on D0 and D7. Scale bar = 100µm

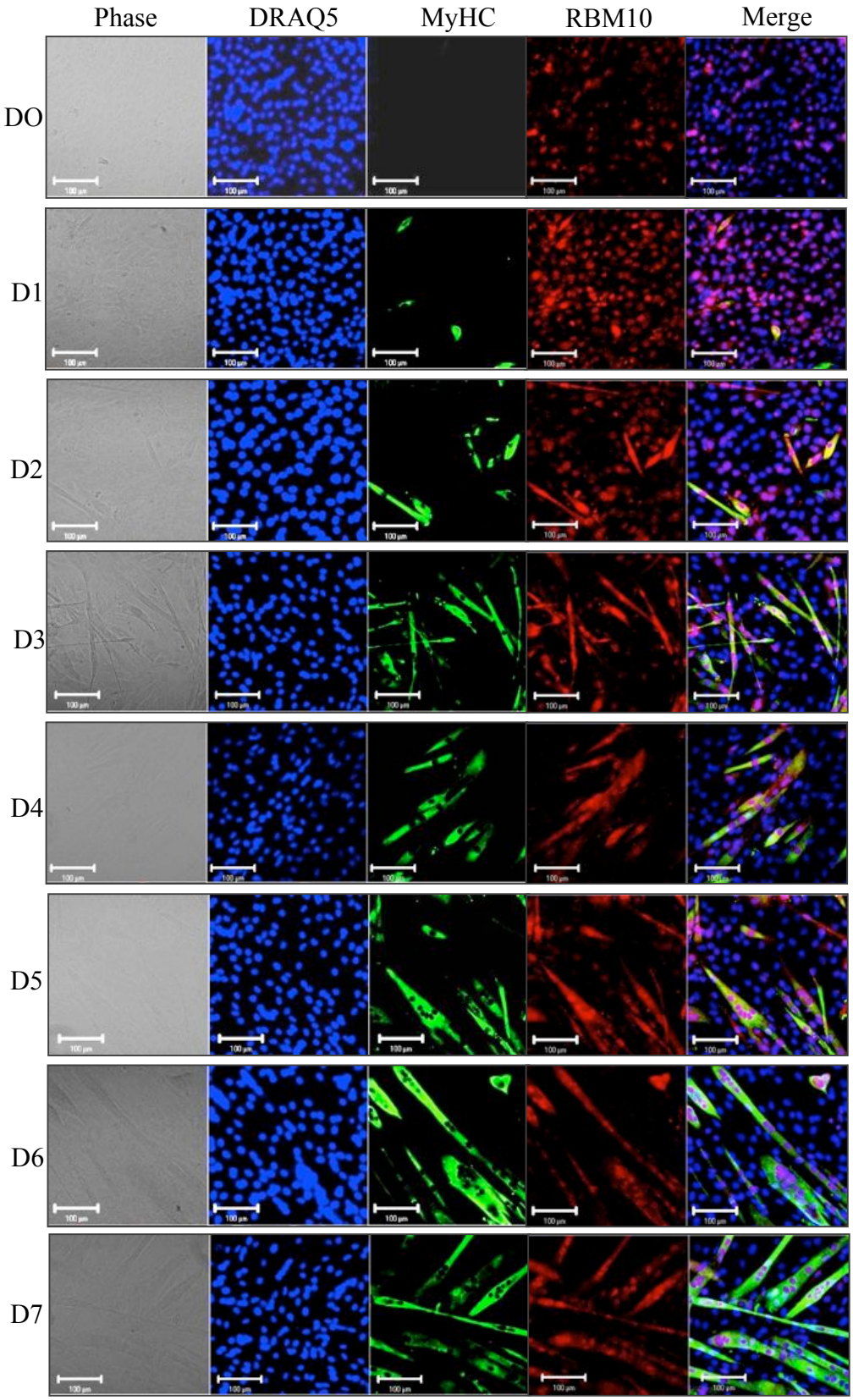

Figure 3.15 Intracellular distribution of RBM10 in differentiating C2C12 cells. RBM10 is differentially localized during C2C12 differentiation. C2C12 myoblasts were induced to differentiate for seven days, cells were fixed, permeabilized and stained. Phase contrast, DRAQ5, MyHC, RBM10 and merge panels showing the subcellular presence using IF staining. Scale Bar = 100µm

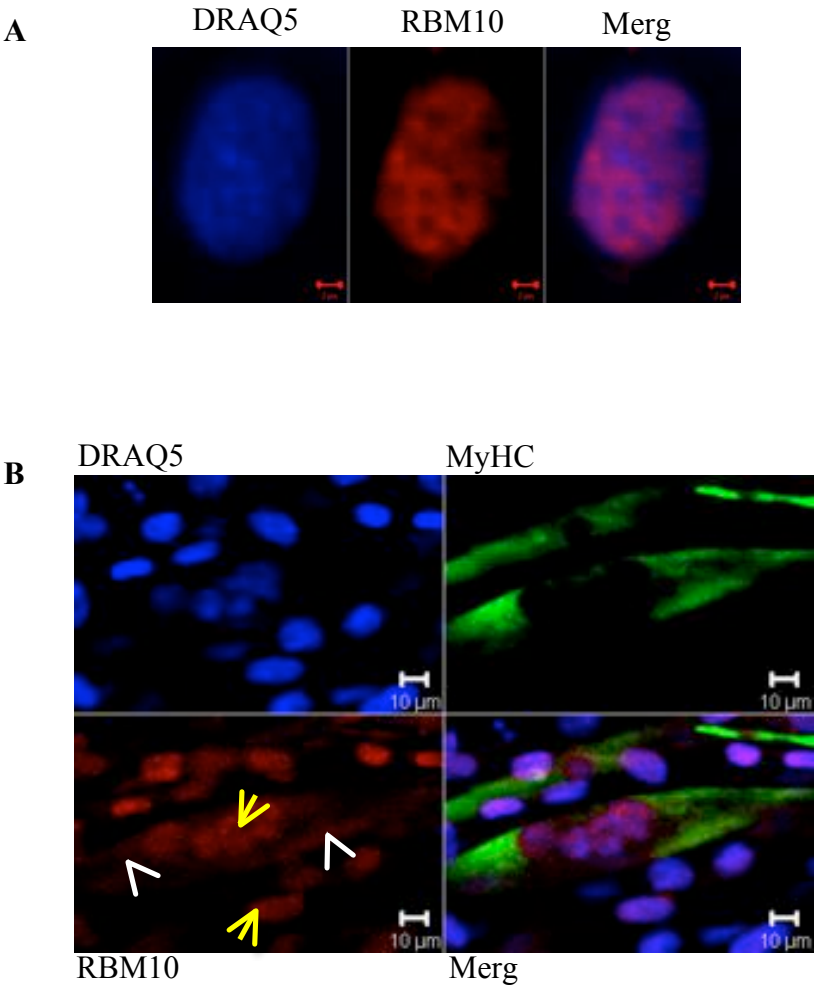

Figure 3.16 RBM10 cellular localization. Detection of RBM10 in the nucleus and cytoplasm. Nuclear localization on **A**) D0, Scale Bar=5µm and **B**) both nuclear and cytoplasmic localization on D7, Scale Bar=10µm. Arrowheads (white) indicate cytosolic presence and arrows (yellow) indicate presence in nucleus in differentiating myotubes. Images were acquired using 63x objective and electronically magnified.

A

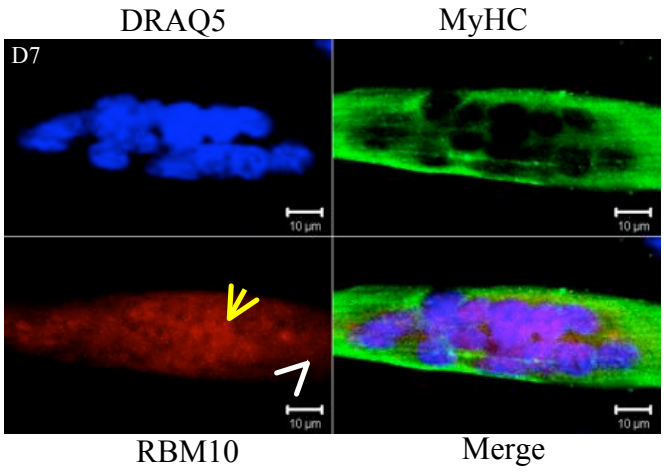

B

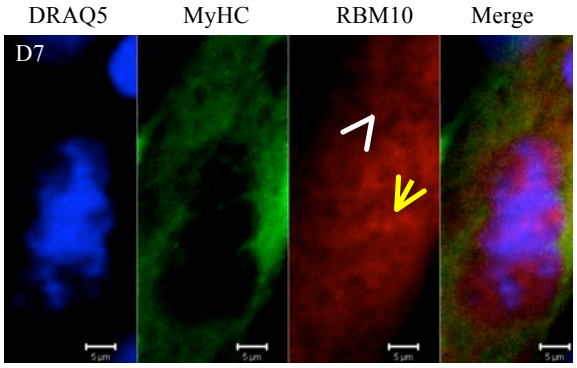

Figure 3.17 RBM10 cellular localization in differentiated myotubes. Detection of RBM10 in the nucleus and cytoplasm in D7 differentiated C2C12 cells. Arrowheads (white) indicate cytosolic presence and arrows (yellow) indicate presence in nucleus in differentiated myotubes. Scale Bar=10µm (**A**) and 5µm (**B**). Images were acquired using 63x objective and electronically magnified.

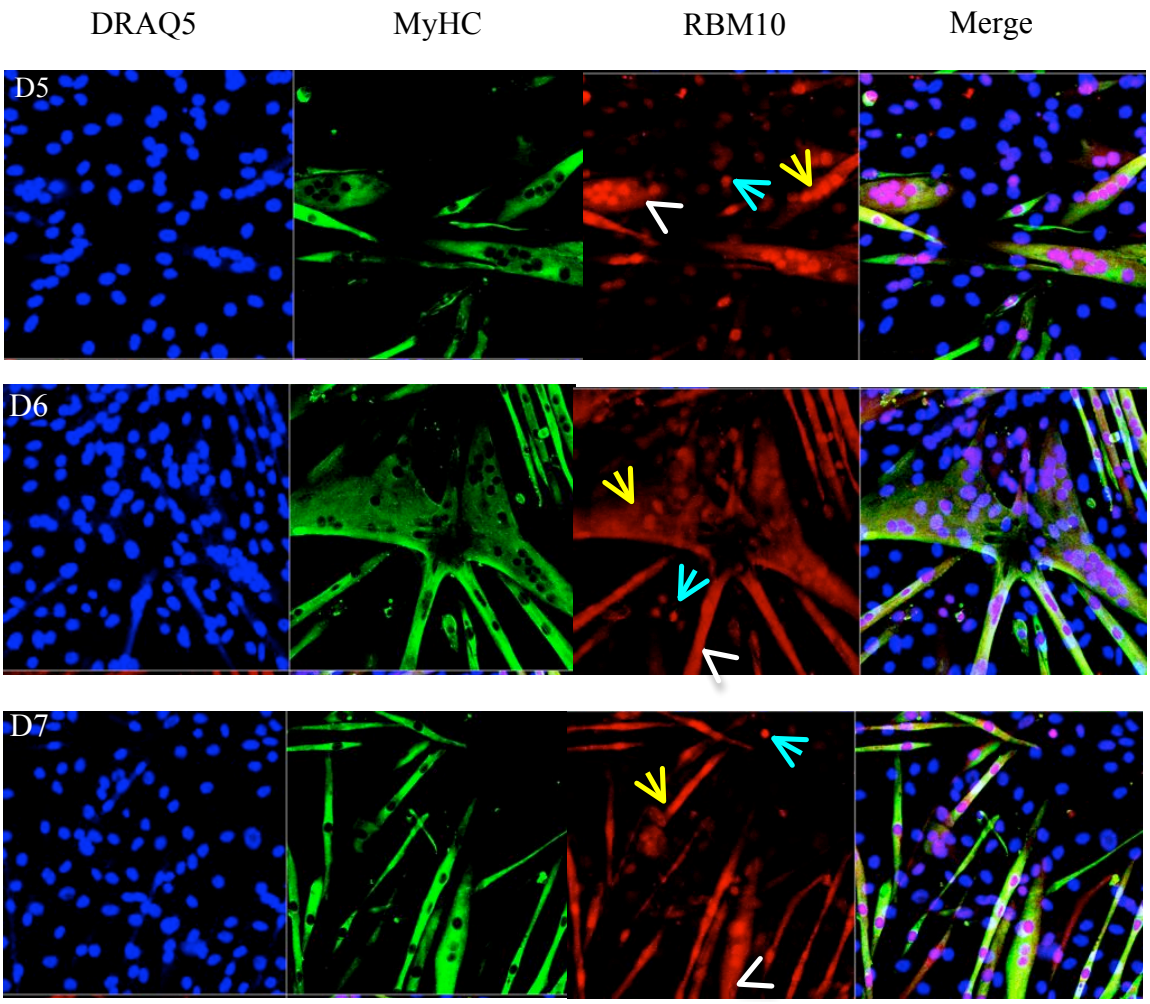

Figure 3.18 RBM10 cellular localization in D5, D6 and D7 differentiating C2C12 cells. Detection of RBM10 in the nucleus and cytoplasm during differentiation. Nuclear and cytosolic localization on Arrowheads (white) indicate cytosolic presence and arrows (yellow) indicate presence in nucleus in differentiating myotubes. Arrows (cyan) indicate presence in the nucleus in MyHC-negative (reserve) cells. Images were acquired using 25x objective.

3.3 Knockdown analysis

To elucidate the effect of RBM5 and RBM10 on skeletal muscle differentiation, we used a loss-of-function approach. More specifically, we performed three different knockdown (KD) experiments using RNA interference (RNAi): siRNA-mediated silencing of *Rbm5* or *Rbm10* or both *Rbm5* and *Rbm10* (double KD). When the C2C12 cells were 40-50% confluent, transient transfection using siRNA duplexes specific for *Rbm5* or *Rbm10* or *Rbm5* and *10* (*Rbm5+10*) were performed. A non-specific small interfering RNA (siRNA) duplex (scrambled control) was used as a control to eliminate off-target effects and to verify experimental specificity. Three trials of KD experiments were performed for each condition (i.e. RBM5, RBM10, RBM5+10). Rajan et al., (2012) have carried out shRNA knockdown screens of close to 400 genes and considered a KD cut off between 40-60% and omitted those which had 20% KD from their analysis. Knockdowns of >50 % at the protein level were considered to be acceptable for our experiments.

3.3.1 Knockdown efficiency

Proteins extracted from the cells collected at 24 and 48 hours post-transfections were subjected to immunoblot analysis using antibodies specific for RBM5, RBM10 and α-tubulin to assess the KD efficiency. Using densitometry the percentage of KD compared to control was calculated after normalizing the band intensity with α-tubulin (Blais et al., 2005). The results are presented for each trial individually as summarized in Table 6. This has been done for the following reasons, a) because N is only 2 or 3, it is more transparent to interpret from individual trials rather than using means and 2) each trial had different degrees of knockdown, for instance the coefficient of variation for RBM10 KD from 3 replicates was ~50% with a 4-fold difference in RBM10 expression, which would require 5 to 6 replicates to detect changes. Therefore the effect of the knockdown was also assessed separately rather than combining the trials together. The controls did not show depletion of the specific mRNA, thus allowing us to proceed further with our analysis of the effects of RBM KD during differentiation. Any effects observed due to reduction in RBM5 and RBM10 is directly or indirectly attributable to depletion of the corresponding RBP.

24 hours after transfection with siRBM5, RBM5 expression was decreased by 64%, 74% and 80% compared with scrambled siRNA control in the three transfections (Figure 3.19). 48 hours after transfection, the KD levels were 72%, 60% and 82% compared with scrambled siRNA control. The RBM5 KD levels were above 60% at both 24 and 48 hours post-transfection, thus meeting our expected degree of knockdown.

In RBM10 KD, 24 hours post-transfection, RBM10 expression was decreased by 62% for RBM10v1 and 67% for RBM10v3 in trial 1, 27% for RBM10v1 and 24% for RBM10v3 in trial 2 and 85% for RBM10v1 and 72% for RBM10v3 in trial 3, compared with scrambled siRNA controls, respectively **(**Figure 3.20). 48 hours after transfection, the KD levels were 77% for RBM10v1 and 67% for RBM10v3 in trial 1, 86% for RBM10v1 and 89% for RBM10v3 in trial 2 compared with scrambled siRNA control. The KD levels at 48 hours were comparatively higher than at 24 hours for both trial 1 and trial 2. The protein samples (siRBM10 and scrambled siRNA control) at 48 hours from trial 3 were not used in further analysis because they did not show a detectable band for RBM5 or RBM10 when probed with the specific antibody. The range of KD varied from 27% to 86% for RBM10v1 and 24% to 89% for RBM10v3 at 24 and 48 hours post-transfection, however, met our acceptable degree of KD. The two exceptions, RBM10v1- 27% and RBM10v3-24% at 24 hours (trial 2), met the acceptable degree of KD at 48 hours (RBM10v1- 86% and RBM10v3-89%).

In the RBM5+10 KD, the levels of both RBM5 and RBM10 were experimentally down-regulated as follows: trial 1, RBM5 was KD 67% (24h) and 52% (48h), RBM10v1 was KD 41% (24h) and 49% (48h), and RBM10v3 was KD 42% (24h) and 76% (48h); trial 2, RBM5 was KD 50% (24h) and 81% (48h), RBM10v1 was KD 47% (24h) and 85% (48h), and RBM10v3 was KD 49% (24h) and 83% (48h); and trial 3, RBM5 was KD 48% (24h), RBM10v1 was KD 83% (24h), and RBM10v3 was KD 59% (24h) (Figure 3.21). The protein samples (siRBM5+10 and scrambled siRNA control) at 48 hours for trial 3 were not used in further analysis because they did not show a detectable band for RBM5 or RBM10 when probed with the specific antibody. Except for trial 2, which had >80% KD of both RBM5 and RBM10 at 48 hours post-transfection, all the KD in trial 1 and trial 3 were variable and close to 50% and above. We also noticed that when both siRNAs were

introduced into the cells at the same time, the depletion of endogenous RBM5 and RBM10 proteins, is less comparable to the levels when each were individually knocked down.

To summarize, we were able to endogenously deplete RBM5 and RBM10 together in all the three trials for all three siRNA transfections and therefore proceeded to determine the effects of this depletion in C2C12 cells during differentiation.

Table 6
Knockdown levels of RBM5, RBM10 and RBM5+10 at 24h and 48h post-transfection

A) RBM5

siRBM5	Time Point	RBM5 % KD
Trial 1	24h	64
	48h	72
Trial 2	24h	74
	48h	60
Trial 3	24h	80
	48h	82

B) RBM10

siRBM10	Time Point	RBM10v1 % KD	RBM10v3 % KD
Trial 1	24h	62	67
	48h	77	67
Trial 2	24h	27	24
	48h	86	89
Trial 3	24h	85	72

C) RBM5+10

siRBM5+10	Time Point	RBM5 % KD	RBM10v1 % KD	RBM10v3 % KD
Trial 1	24h	67	41	42
	48h	52	49	76
Trail 2	24h	50	47	49
	48h	81	85	83
Trial 3	24h	48	83	59

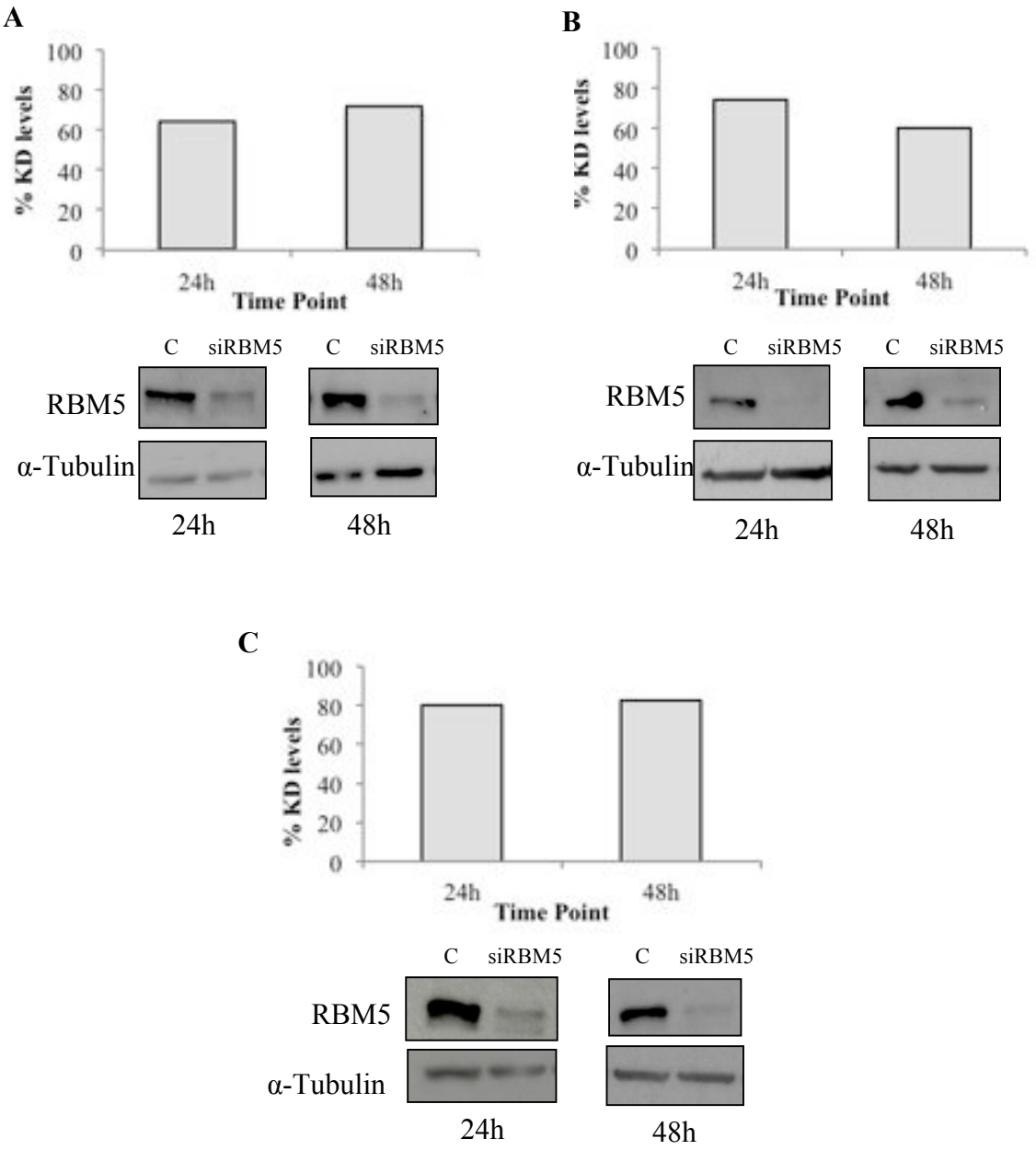

Figure 3.19 RBM5 KD levels in C2C12 cells 24h and 48h post-transfection. C2C12 cells were transfected with siRBM5 and the levels of KD were analyzed by immunoblots for **A**) Trial 1, **B**) Trial 2 and **C**) Trial 3. The KD percentage compared to scrambled siRNA control (C) was quantified using densitometry and plotted as a graph. α-tubulin was used for normalization.

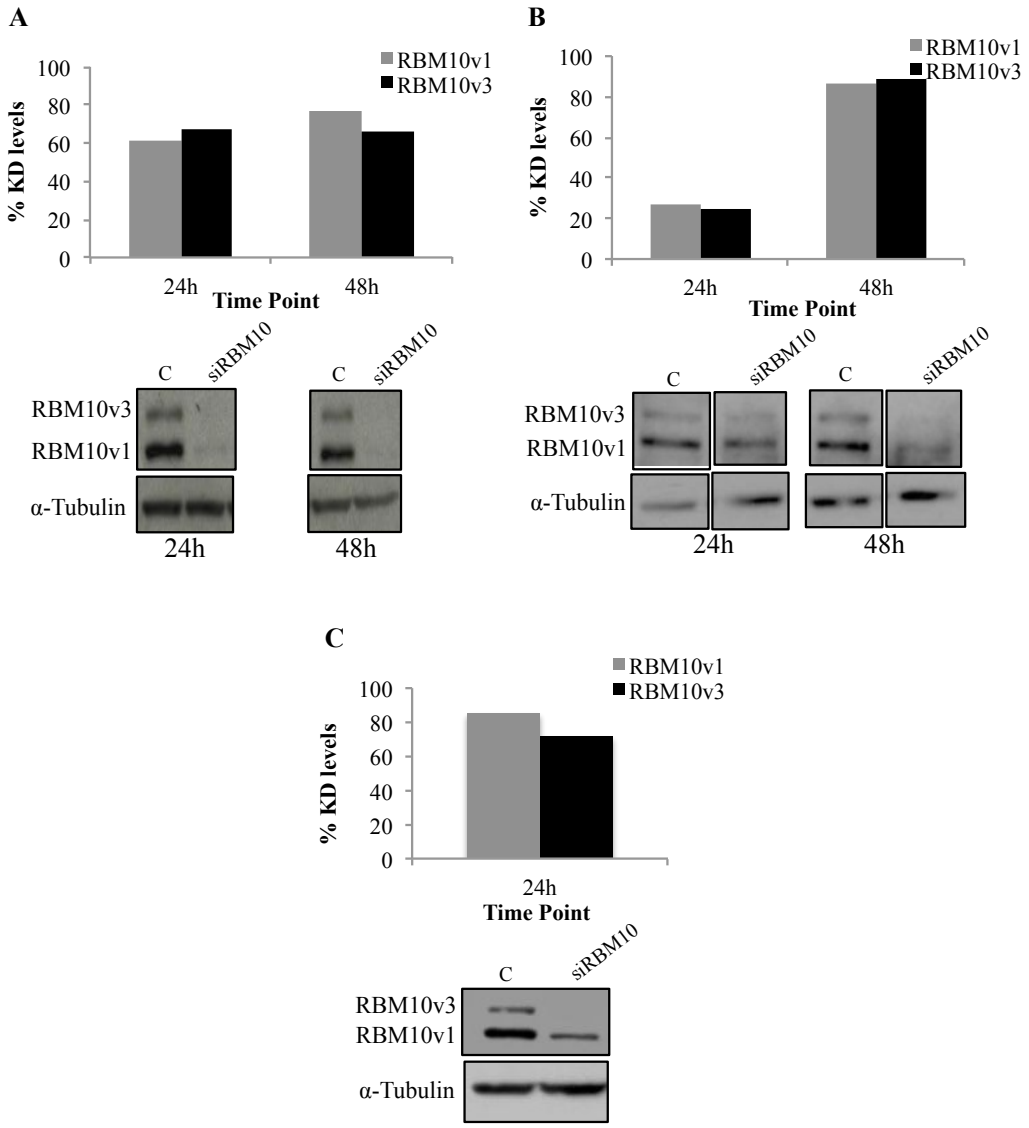

Figure 3.20 RBM10 KD levels in C2C12 cells 24h and 48h post-transfection. C2C12 cells were transfected with siRBM10 and the KD levels were analyzed by immunoblots for **A**) Trial 1, **B**) Trial 2 (whole blot in appendix A, Figures A6, A7 and A11) and **C**) Trial 3. The KD percentage compared to scrambled siRNA control (C) was quantified using densitometry and plotted as a graph. α-tubulin was used for normalization.

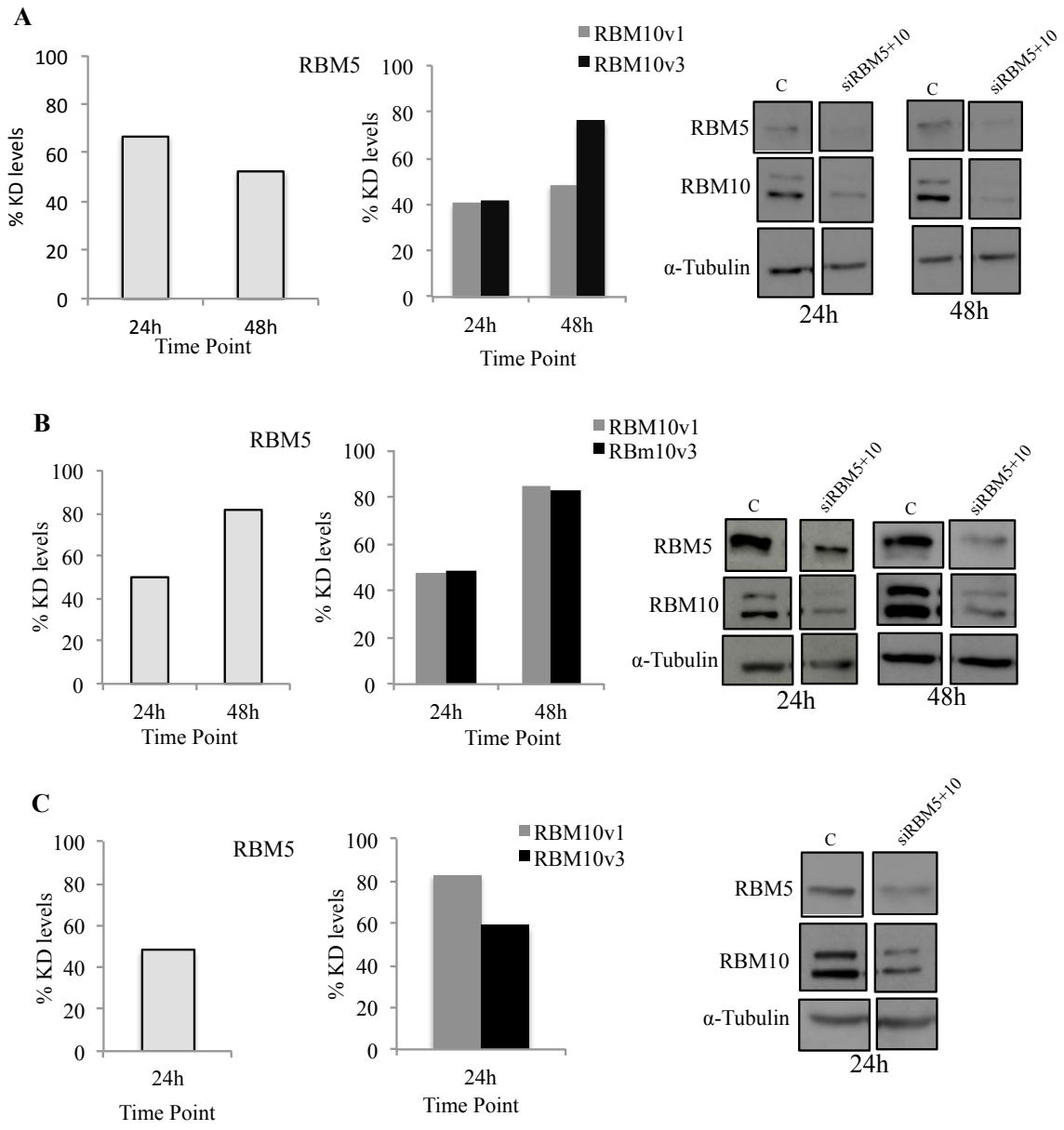

Figure 3.21 RBM5 and RBM10 KD levels in C2C12 cells 24h and 48h post-transfection. C2C12 cells were transfected with siRbm5 along with siRbm10 (siRBM5+10) and the KD levels were analyzed by immunoblots for **A**) Trial 1, **B**) Trial 2 and **C**) Trial 3. Whole blots in appendix A, Figures A9, A10 and A11. The KD percentage compared to scrambled siRNA control (C) was quantified using densitometry and plotted as a graph. α-tubulin was used for normalization.

3.3.2 Depleted RBM5 and RBM10 protein levels are replenished by D4

In order to assess the stage of functional involvement of these two RBPs in myogenic differentiation, it was necessary to determine the time-point of restoration. Therefore, the levels of RBM5 and RBM10 were estimated during differentiation (D0 to D4). Differentiation was induced by changing GM to DM 24 hours post-transfection. Immunoblotting was performed using protein extracted from transfected cells that were subjected to differentiation. Using densitometry, the band intensity measurements were obtained and the protein levels were calculated after normalizing with α-tubulin. The levels were compared to the control (scrambled siRNA) during each day and plotted as a graph. This measure of endogenous restitution is a physiological indicator of the effectiveness of transfection and the cell's ability to transcriptionally replenish the depleted mRNAs. We expected that over time, normal expression levels should occur, more specifically 3 to 7 days after transfection (Leung and Whittaker, 2005).

In RBM5 transfection experiments, RBM5 protein levels were measured from D0 until D4 (Figure 3.22). RBM5 protein levels in trial 1 remained depleted until D3 and restoration trend was not seen until D3 (did not have D4 samples and therefore was not able to measure the level of restoration on D4 for this trial) (Figure 3.22A); in trial 2, were beginning to reach normal levels by D3 and reached control levels on D4 (Figure 3.22B); and in trial 3 reached normal levels by D3 (Figure 3.22C). This indicates that restoration of RBM5 protein occurs in two trials and KD is effective for at least for three days for trials 1 and 2, and at least for two days for trial 3. Furthermore, the effect of depletion during differentiation until D3 in two trials and D2 in one trial is probably accounted for by reduction in RBM5. In addition, the KD levels were 72% (trial 1), 60% (trial 2) and 82% (trial 3) and the restoration was not dependent on the KD levels.

In RBM10 transfection experiments, when RBM10 protein levels were measured from D0 until D4, restoration to scrambled control levels occurred at different days for each trial (Figure 3.23). The RBM10v1 and RBM10v3 isoform levels were back to normal by D3 for trial 1 (Figure 3.23A); reached levels similar to control by D2 for trial 2 (Figure 3.23B) and

was not restored to normal levels even by D3 for trial 3 (Figure 3.23C). This indicates that the RBM10 isoform levels were restored at least on D2 and D3 in two trials, the KD was effective for these days and the effect observed in the KD during differentiation is accounted for by reduction in RBM10. In addition, the KD levels were 77% (RBM10v1) and 67% (RBM10v3) (trial 1), 86% (RBM10v1) and 89% (RBM10v3) (trial 2) at 48h and 85% (RBM10v1) and 72% (RBM10v3) (trial 3) at 24h and the restoration was not dependent on the KD levels.

In RBM5+10 KDs, restoration of RBM5 and RBM10 occurred to varying degrees in all of the three trials. RBM5 reached normal levels by D3 for trial 2 (Figure 3.24B) but was not restored in trial 1 and trial 3 (Figure 3.24 A and C). RBM10 reached normal levels by D3 for trial 1 (Figure 3.24A) but was not restored in trial 1 and trial 3 (Figure 3.24 B and C). Therefore, the KD was effective for those days and the effect observed in the KD during differentiation is accounted for by reduction in RBM5 and RBM10.

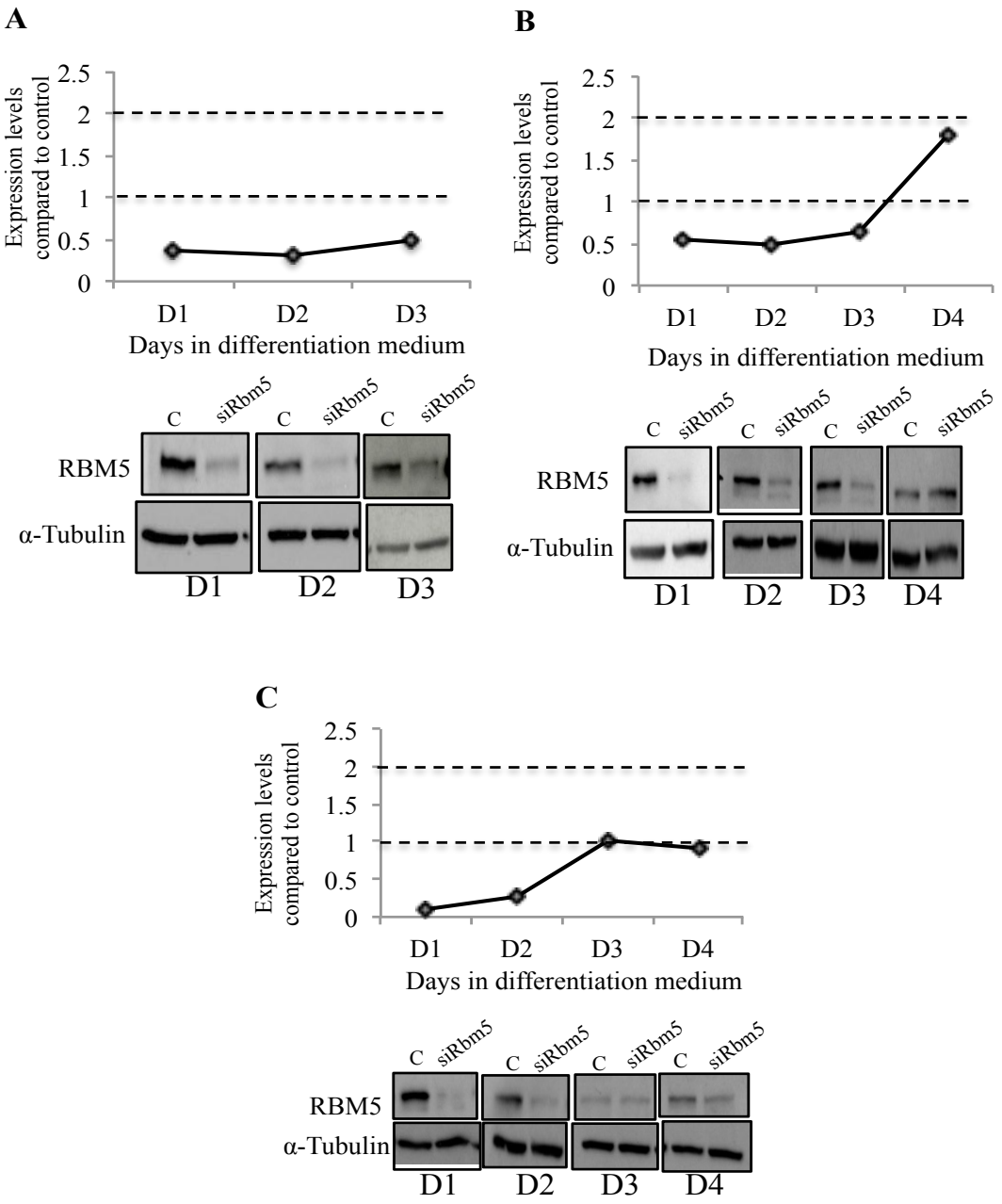

Figure 3.22 RBM5 restoration post-transfection in C2C12 cells. C2C12 cells were transfected with siRbm5 or scrambled siRNA and the levels of restoration were analyzed by immunoblots for **A**) Trial 1(did not have D4 samples), **B**) Trial 2 and **C**) Trial 3. The protein expression levels compared to scrambled siRNA control (C) were quantified using densitometry and plotted as a graph. α-tubulin was used for normalization.

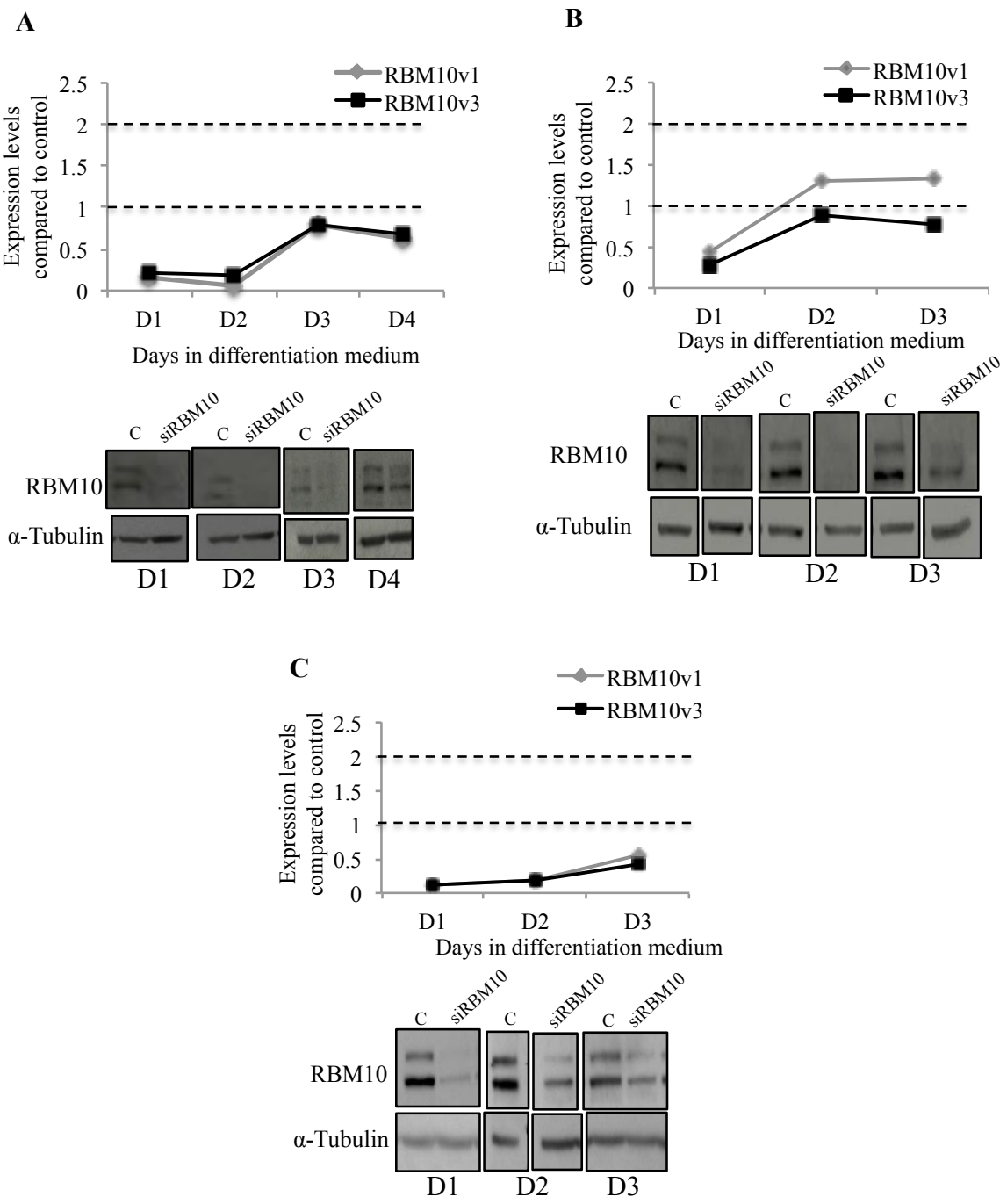

Figure 3.23 RBM10 restoration post-transfection in C2C12 cells. C2C12 cells were transfected with siRbm10 or scrambled siRNA and the levels of restoration were analyzed by immunoblots for **A**) Trial 1, **B**) Trial 2 (whole blots in appendix A, Figure A7) (did not have D4 samples) and **C**) Trial 3 (whole blots in appendix A, Figure A11) D4 -RBM10 immunoblotting did not work. The protein expression levels compared to scrambled siRNA control (C) were quantified using densitometry and plotted as a graph. α-tubulin was used for normalization.

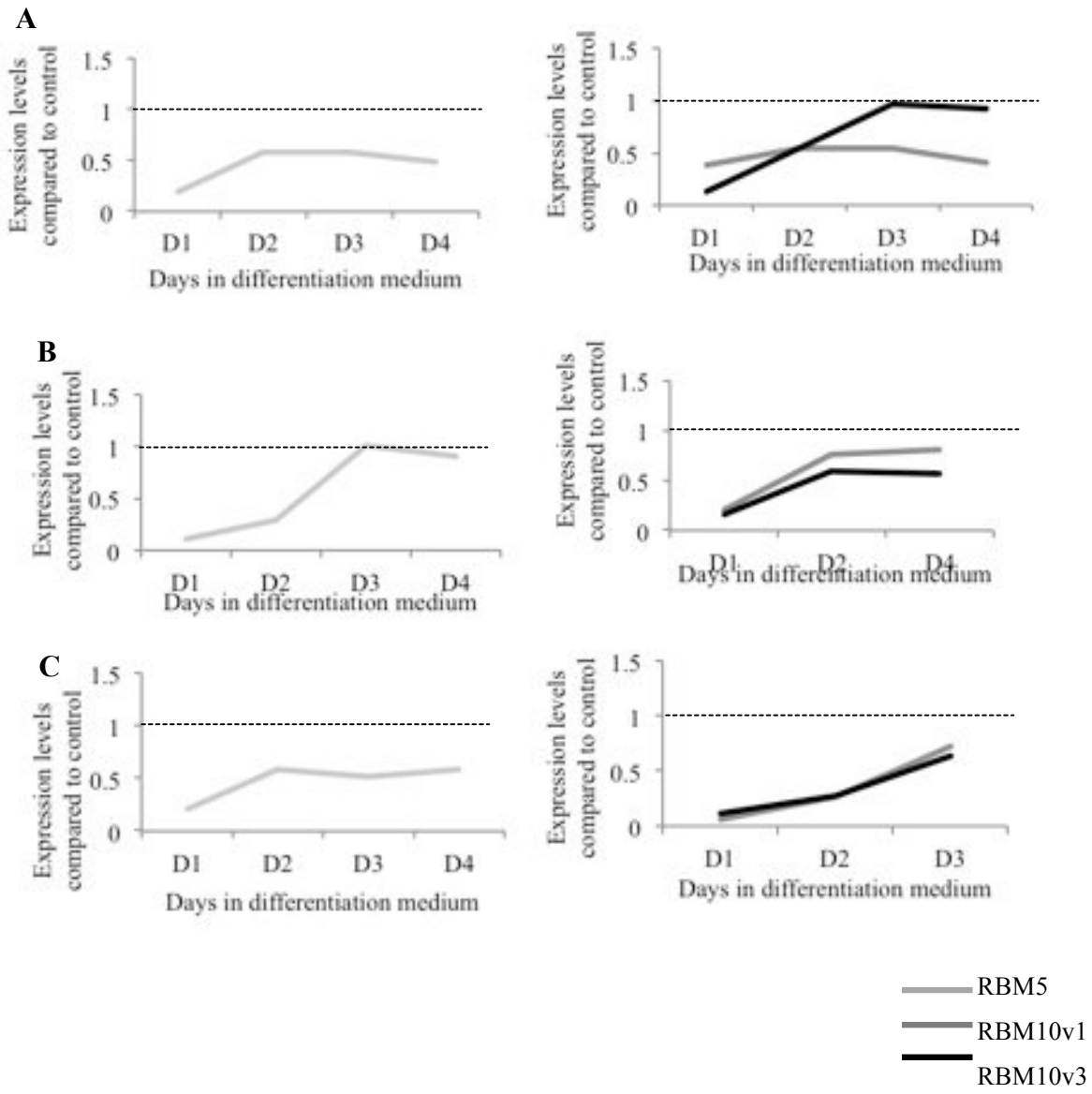

Figure 3.24 RBM5 and RBM10 restoration post-transfection in C2C12 cells. C2C12 cells were transfected with Rbm5 and Rbm10 siRNAs and the level of restoration was analyzed by immunoblotting for **A**) Trial 1, **B**) Trial 2 and **C**) Trial 3 (Whole blots in appendix A, Figures A9, A10 and A11). D3 (trial 2) and D4 (trial 3) RBM10 immunoblotting did not work. The protein expression levels compared to scrambled siRNA control (C) were quantified using densitometry and plotted as a graph. α-tubulin was used for normalization.

3.3.3 Depletion of one RBP does not effect the protein expression of the other

Because the RBM5 and RBM10 proteins are 50% identical and have overlapping functions (apoptosis/cell proliferation) in cancer cells, there is a possibility that disrupting the expression of one may impact the expression of the other. There are a few studies that suggest such regulation (Wang et al., 2013). Therefore, in our mouse model system, we wanted to analyze the expression of each RBP when another one of the RBP was inhibited. Using immunoblots, we quantified the expression levels of RBM5 in RBM10 KDs, and RBM10v1 and RBM10v3 isoform expression levels in RBM5-depleted cells at both 24h and 48h post-transfection and during differentiation for all three trials. The expression levels of the KDs were compared to the scrambled siRNA control protein levels for each time-point. We did not see a significant increase or decrease in RBM5 levels in the RBM10 KDs (Figure 3.25). We did not see any significant changes in both the RBM10 isoform levels in RBM5 KD (Figure 3.26). The Western blotting for RBM10 was not successful for 24h, 48h and D1 samples for trial 3 RBM5 KDs. These results confirm that: (a) the repression in protein expression levels of one RBP is not regulated by the other RBP; (b) the KD is siRNA specific and the siRNAs are specific to the mRNA that they are intended to target; and, (c) reduction in one RBP is not compensated by an increase in the expression of the other RBP studied in the present investigation.

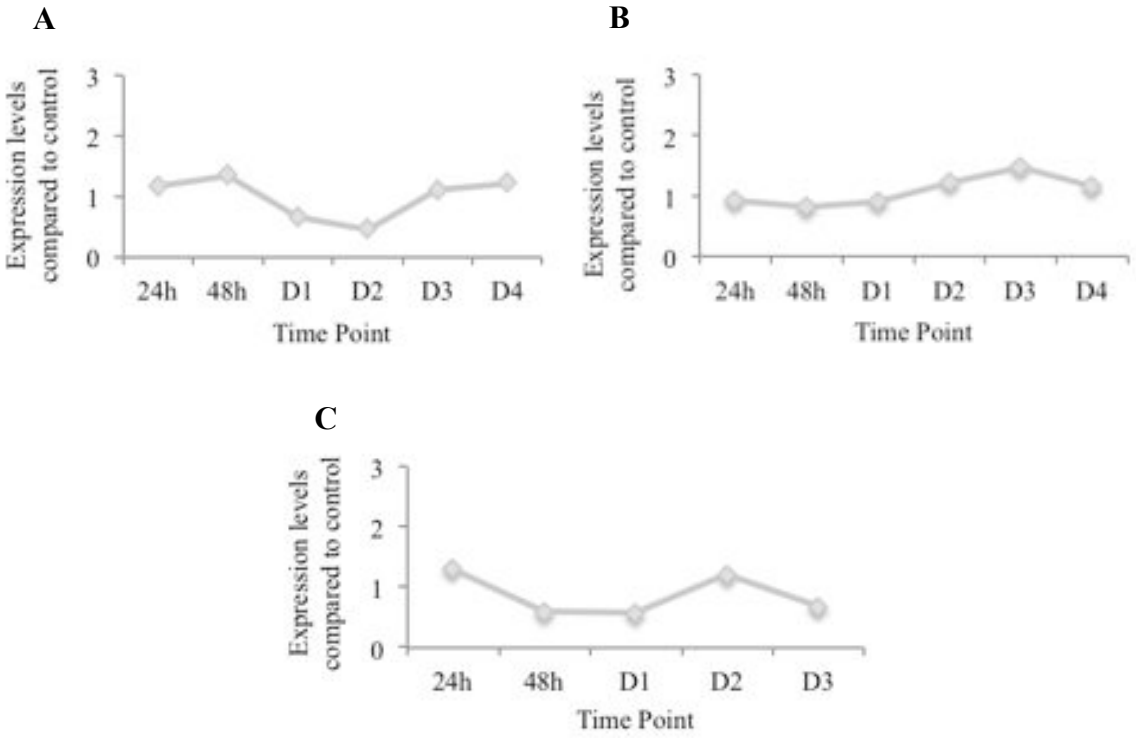

Figure 3.25 RBM5 protein levels in RBM10-depleted cells. Depletion of RBM10 does not significantly increase or decrease RBM5 protein levels, post-transfection and during differentiation. C2C12 cells were transfected with RBM10 or scrambled siRNAs (C). RBM5 protein levels compared to the control were quantified by densitometry from the immunoblots for **A**) Trial 1, **B**) Trial 2 and **C**) Trial 3. Whole blots in appendix A, Figures A6, A7 and A11. α-tubulin was used for normalization.

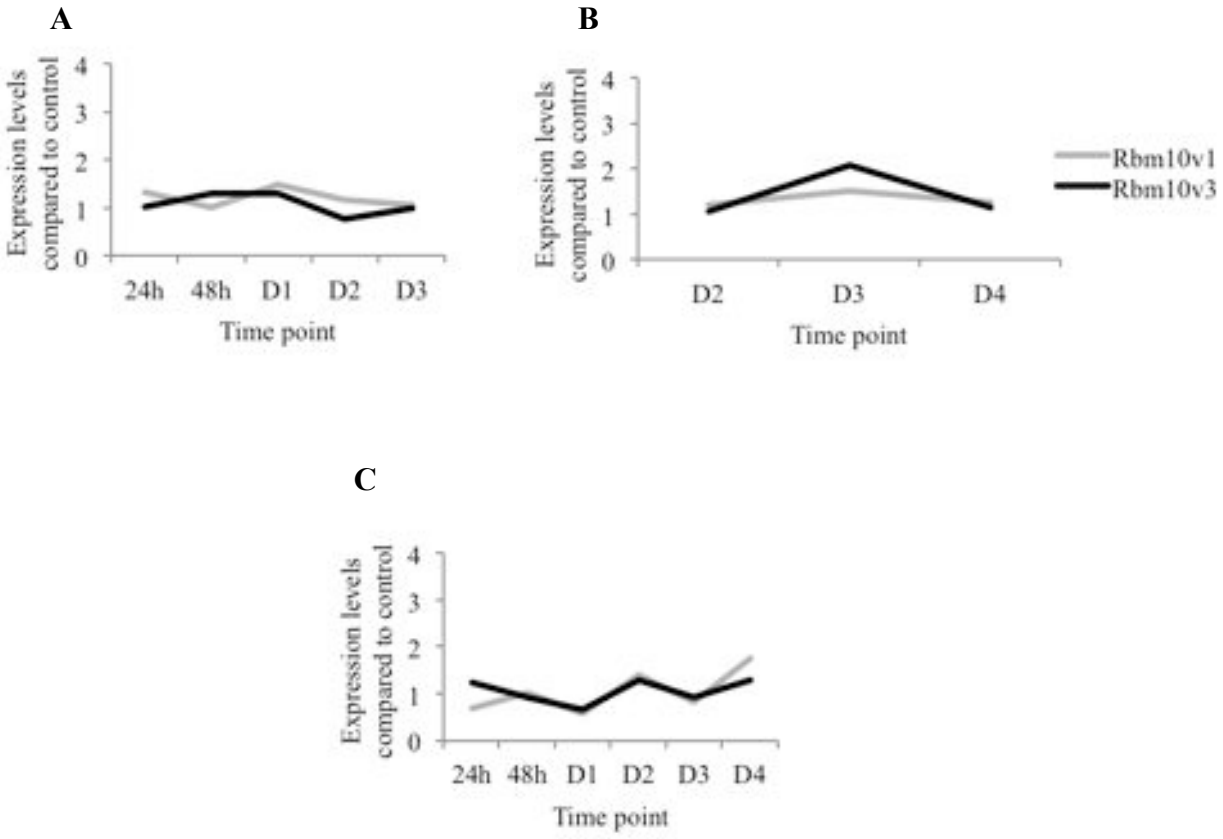

Figure 3.26 RBM10 protein levels in RBM5-depleted cells. Depletion of RBM5 does not significantly increase or decrease RBM10 protein isoform levels, post-transfection and during differentiation. C2C12 cells were transfected with RBM5 or scrambled siRNAs (C). RBM10 protein levels compared to the control were quantified by densitometry from the immunoblots for **A**) Trial 1, **B**) Trial 2 and **C**) Trial 3. Whole blots in appendix A, Figures A7, A8 and A10. α-tubulin was used for normalization.

3.3.4 Phenotypic consequences of RBM5 and RBM10 depletion

After verifying the KD levels in all the trials, we proceeded to analyze the phenotypic effects of RBM5 and RBM10 depletion in C2C12 myoblasts. This was attained by assessing the morphological changes in the depleted cells compared to scrambled control transfections during proliferation and differentiation. Using indirect immunofluorescence technique, the cells were immunostained for MyHC and counterstained with DRAQ5. Phenotypic assessment was performed for two trials and as indicated previously under section 3.3.1the results are presented for each trial individually. The two trials for RBM5 KD effect assessment are represented as Trial A (trial 2 in Table 6A) and Trial B (trial 3 in Table 6A); for RBM10 KD are represented as Trial A (trial 1 in Table 6B) and Trial B (trial 3 in Table 6B); for RBM5+10 KD are represented as Trial A (trial 2 in Table 6C) and Trial B (trial 3 in Table 6C). Statistically significant changes in both the trials are used for interpretation.

In our experiments, we have used the scrambled siRNA as our negative control because this acts as a control for transfection. Untransfected control was carried out along with scrambled siRNA control for the siRBM10 KD experiments. Comparable RBM10 levels were found in both untransfected controls and scrambled siRNA controls (Appendix A, Figure A6). This confirms at least at the protein level (target gene level), that any downstream effect of RBM KD is attributed to the silencing of the target protein, however does not eliminate any effect associated with baseline phenotype modifications such as cell density.

Results in untransfected cells (Figure 3.2) showed that proliferation stops at D1 and the differentiation changes start at D1, with an increase in the differentiation potential as the days progress until D5 ~30%, after which it reaches a plateau ~30-40%. At least 10% of cells were fused by D3 leading to an increase in the number of myotubes and myofibers starting from D4. The cells started expressing the differentiation-specific marker MyHC beginning from D1 and by D4, 25±2.9 cells/ hpf expressed MyHC.

During these experiments it was noticed that the specific timing at which some differentiation markers were expressed was different between our early non-transfected cells and the scrambled control siRNA transfected cells. This difference may be related to the effects of transfection on decreasing cell survival and on inhibiting cell cycle progression. It is well known that lipofectamine-based transfection is associated with cell death and would be expected to decrease the number of surviving cells. In addition, cell density-dependant effects affect the expression of several proteins such as myogenic markers like MyoG, MyoD, MyHC, and cell adhesion and cytoskeleton related proteins such as actin, talin and cadherin, and cell cycle related factors like decorin, cyclin D3 and p21 (Tanaka et al., 2011). Therefore for these experiments, all KD samples are compared only to the scrambled siRNA controls processed in parallel.

3.3.4.1 RBM5 depletion

When RBM5 is endogenously over-expressed in cancer cells, it is anti-proliferative and apoptotic, specifically, the inhibition of tumor growth by RBM5 is associated with the regulation of Cyclin A and retinoblastoma proteins leading to cell cycle arrest at G1 (Shao et al., 2012) and the p53 pathway (Kobayashi et al., 2011); and alternative splicing of targets involved in cell proliferation and apoptosis (Fushimi et al., 2008). Therefore, in our experiments, when we down-regulated Rbm5, we expected to see an effect on cell number, specifically an increase in proliferation in the KDs. Differentiation of C2C12 cells involves both cell cycle arrest and apoptosis; therefore, since RBM5 is pro-apoptotic, we expected that the scrambled controls would have a fewer number of cells than siRBM5 transfected cells.

The level of KD can be inferred from RBM5 IF staining in scrambled controls in comparison to RBM5 KDs, at 24 and 48 hours in one of the two trials (Appendix A-Figure A4). Fewer cells in the KD had RBM5 staining compared to the scrambled siRNA control cells. The RBM5 protein levels for trial A was reduced by 74% (trial 2 in Table 6A) and for trial B was reduced by 80% (trial 3 in Table 6A), as shown previously (Figure 3.19) by Western blots.

When RBM5-depleted and control cells were counted (DRAQ5 stained nuclei) 24 and 48 hours post-transfection, we found that the number of nuclei remained the same. There was no difference in the cell number between the control and RBM5 KD. The graph in Figure 3.27 depicts the average number of nuclei present in two separate trials. In trial A (Fig 3.27A), in each high power field (hpf), an average of 29±2 and 32±2 nuclei were present in the scrambled siRNA control and the RBM5 KD cultures, respectively, at 24 hours post-transfection. This increased to 76±5 and 84±8 nuclei / hpf in the scrambled siRNA control and RBM5 KD, respectively, at 48 hours post-transfection. In trial B (Fig 3.27B), in each high power field (hpf), an average of 39±4 and 46±4 nuclei were present in the scrambled siRNA control and the RBM5 KD cultures, respectively, at 24 hours post-transfection. This increased to 124±11 and 116±4 nuclei / hpf in the scrambled siRNA control and RBM5 KD, respectively, at 48 hours post-transfection. The difference between the control and RBM5 KD was not statistically significant at both 24 hours and 48 hours post-transfection. Therefore, RBM5 KD did not immediately effect C2C12 cell proliferation and/or apoptosis.

When RBM5-depleted and control cells were induced to differentiate and the cells were counted on D0, D1, D2, D3 and D4, we found that there was a difference in the number of nuclei (Figures 3.28A, 3.29A). An average of 176±6 (trial A) and 138±8 (trial B) nuclei / hpf were present in the control, whereas in the KDs the nuclei number was significantly reduced (P=0.0001 in both the trials) to 106±6 (trial A) and 97±2 (trial B) / hpf on D2. This drop in nuclei number was significant on D3 and D4 as well (P=0.0001). On D3, the nuclei number dropped from 190±8 (trial A) and 244±10 (trial B) nuclei / hpf to 102±5 (trial A) and 137±7 (trial B) nuclei / hpf in the KDs. On D4 the reduction was from 191±6 (trial A) and 168±12 (trial B) nuclei / hpf for the control to 118±2 (trial A) and 104±6 (trial B) nuclei / hpf in the KDs. Therefore, once differentiation was induced, the number of nuclei varied significantly between the control and RBM5 KD. These results, that silencing RBM5 resulted in reduction in the number of cells during differentiation suggest that RBM5 may be required during differentiation to maintain the necessary cell population in order to proceed with the differentiation process. Indirectly, this indicates an increase in apoptosis leading to loss of cells without RBM5. This result in C2C12 cells during differentiation therefore could possibly be associated with apoptosis because apoptosis in

C2C12 cells occurs between 48 hours of differentiation (Mercer et al., 2005) and proliferation stops prior to the beginning of differentiation.

Furthermore, we analyzed the phenotypic effects of RBM5 depletion on differentiation by counting the total number of nuclei, number of myotubes, number of myofibers, and number of nuclei within the myotubes and myofibers. Using these values other cell parameters such as differentiation potential, fusion index and maturation efficiency were calculated (Figures 3.28, 3.29). Interestingly, RBM5-depleted cells had a significant increase in differentiation potential on D2 with *P* values of 0.0001 (trial A) and 0.04 (trial B) compared to scrambled controls (Figures 3.28B, 3.29B). However by D4, there was a significant reduction in the percentage of differentiated myotubes [*P*=0.0001 (trial A) and 0.04 (trial B)] in the RBM5 KDs compared to scrambled controls. The number of MyHC-positive cells was greater on D2 but the number decreased on D3 and D4, thus the decrease in MyHC expression partly contributed to the decrease in differentiation potential (Table 7). The number of cells expressing the myogenic terminal differentiation marker MyHC was reduced significantly when RBM5 was depleted. Indeed, for trial A, *P* values were 0.018 and 0.0001 for D3 and D4, respectively. For trial B, the *P* values for D3 and D4 were 0.0005 and 0.008, respectively. These results suggest that RBM5 may modulate MyHC expression during differentiation. Additionally, RBM5-depleted cells were slow to differentiate because of the difference in cell numbers. RBM5 transfected cells consistently showed a lower number of cells at D2-D4 compared to scrambled controls in both trials, which is evident from the decreased cell density. Cell density is an important determinant for C2C12 myoblasts to differentiate. Fewer cells causes less cell-cell contact thereby disrupting cell signalling pathways leading to delayed differentiation (Tanaka et al., 2011). The downstream effects associated with RBM5 depletion such as the delay in differentiation, fusion and maturation could be due to the decrease in cell density.

The reduction in the fusion index contributed to less myotubes on D4 (Figures 3.28C, 3.29C). The index was 20±2% in the controls, which was reduced to 10±2% in the RBM5 KDs in trial A, with a similar reduction from 21±5% in the controls to 11±1% in the RBM5 KDs in trial B. KD also affected maturation, as there were significantly less myofibers (5 or more nuclei) in the RBM5 KD cells (Figures 3.28D&E, 3.29D&E). In these cells, there was

a decrease in the number of nuclei in myotubes, as well as a decrease in myotube numbers (P=0.0027 (trial A) and 0.0002 (trial B)). There was a 10-fold difference in maturation when comparing the controls to the RBM5 KDs with a significant P value (0.0045 for trial A and 0.003 for trial B) .

Although the two trials of RBM5 KD are considered separately, and despite having different levels of KD and different RBM5 protein restoration time points, they both show similar changes in the timing of the expression of the differentiation markers. In both trials, cells transfected with the scrambled siRNA control showed higher differentiation potential, fusion index and myotubes/field at D4 while the RBM5 KD cells showed that this effect was blunted (although to different extents) in both the experiments. These results suggest that RBM5 plays an important role in C2C12 differentiation by (a) having an effect on the number of cells, which probably results in the delay in differentiation; and (b) modulating the expression of MyHC during muscle cell differentiation.

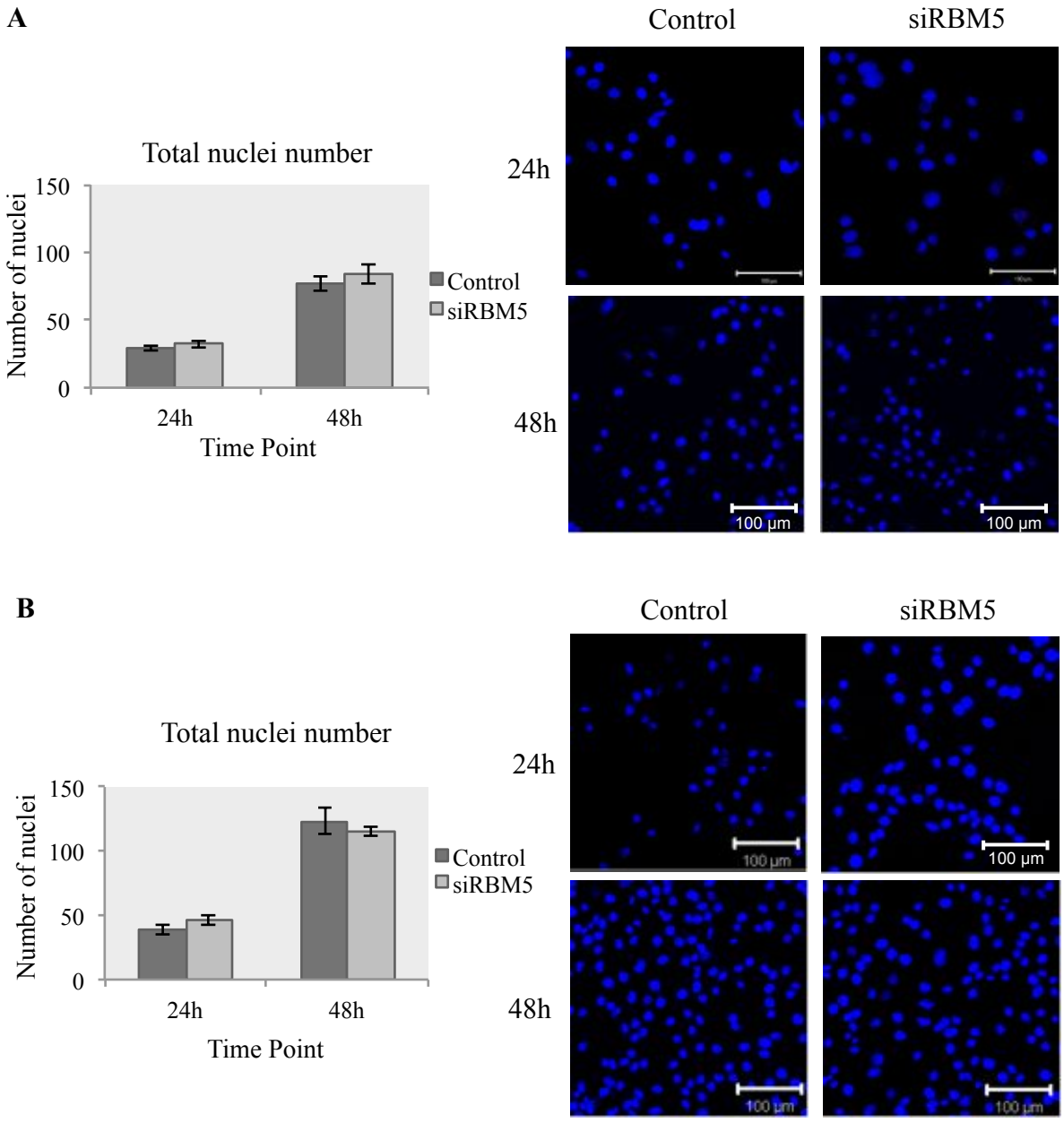

Figure 3.27 Effect of RBM5 depletion on C2C12 cell count. C2C12 myoblasts were transiently transfected with a scrambled siRNA control or siRBM5. At 24h and 48h post-transfection, the total cell count was estimated by counting the number of DRAQ5-stained nuclei in the field for **A**) Trial A and **B**) Trial B. The graph represents the average number of nuclei from 8-12 separate fields of view and the error bars represent SEM. The immunofluorescent images represent one representative field for the control and siRBM5 at 24h and 48h after transfection for the two trials. Scale bar = 100µm.

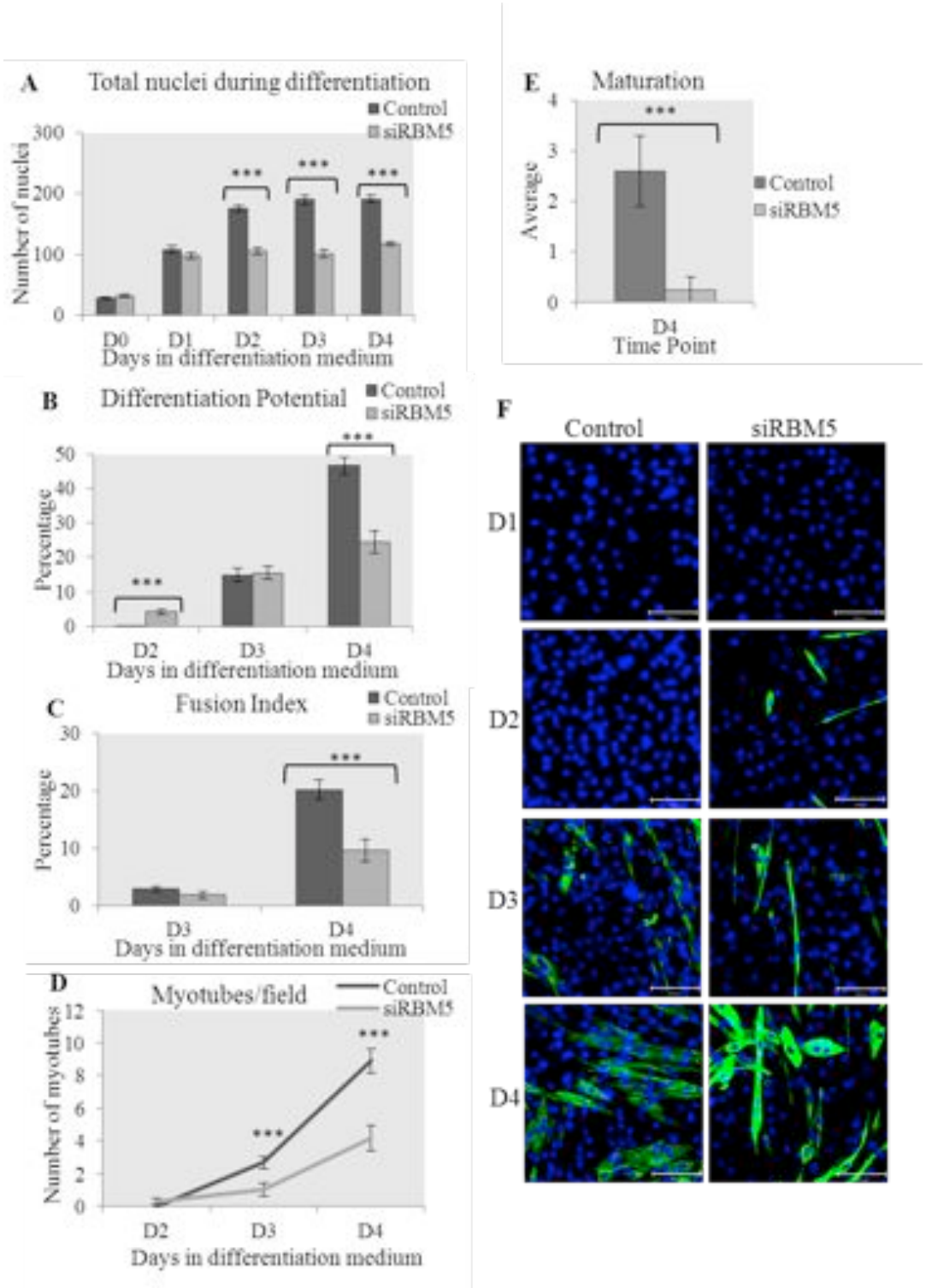

Figure 3.28 Quantitative analysis of RBM5 KD effect on C2C12 cell count, differentiation, fusion and maturation during differentiation (Trial A). A) The total number of cells was estimated by counting the number of DRAQ5-stained nuclei per field, **B**) Differentiation potential is the ratio of number of nuclei in MyHC-positive cells to the total number of nuclei in the field X 100, **C**) Fusion index is the ratio of the number of nuclei in myotubes (≥2 nuclei) to the total number of nuclei in MyHC-positive cells X 100, **D**) Average number of myotubes from all fields, **E**) Average number of myofibers (≥5 nuclei) from all fields and **F)** DRAQ5 and anti-MyHC stained merged images from a single representative field of view, Scale bar = 100µm. Error bars represent SEM. Unpaired students *t*-test was used to calculate the statistical significance. * = *P*< 0.05, ** = *P*< 0.001, *** = *P*< 0.0001. KD levels at 24h were 74%.

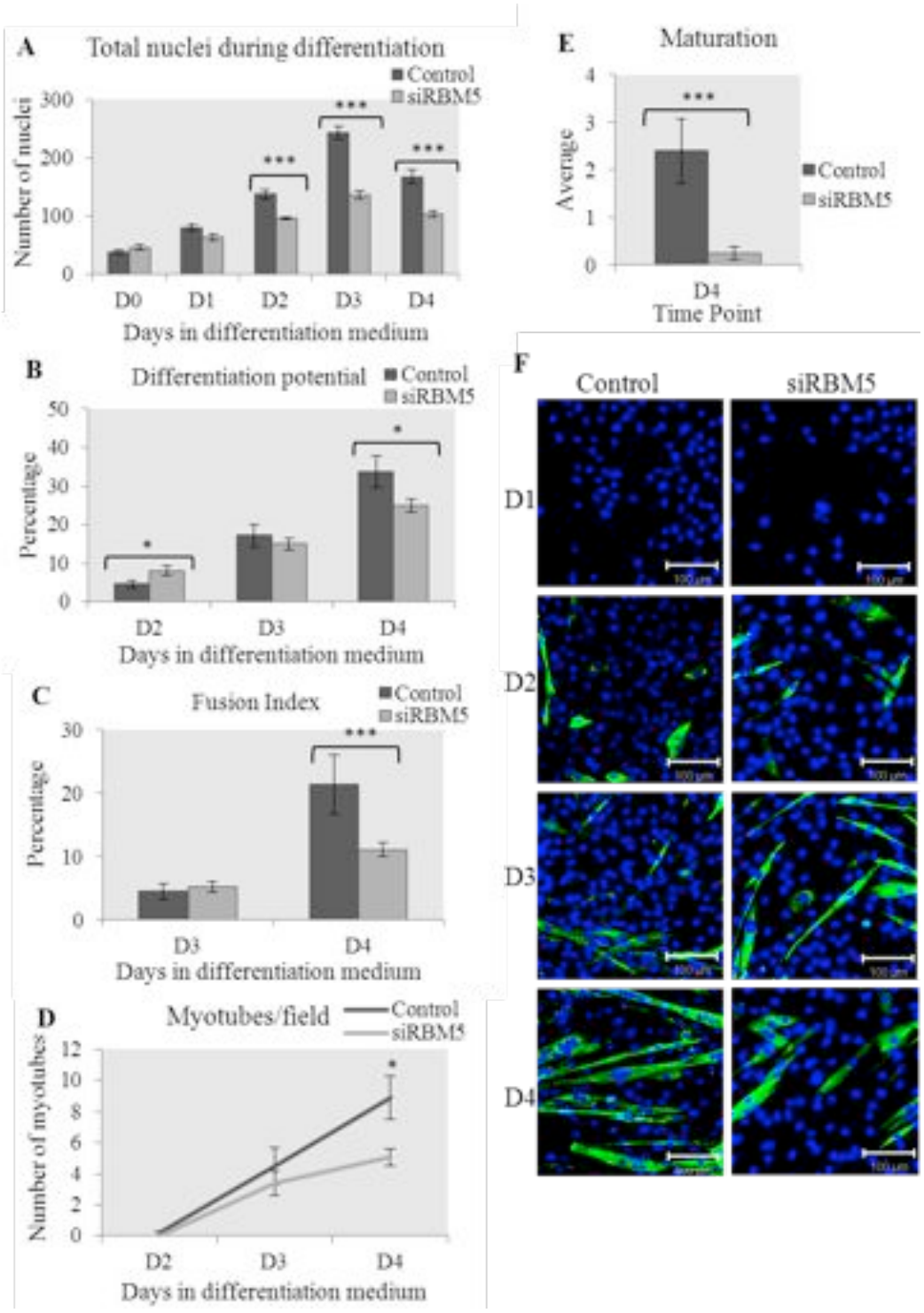

Figure 3.29 Quantitative analysis of RBM5 KD effect on C2C12 cell count, differentiation, fusion and maturation during differentiation (Trial B). **A**) The total number of cells was estimated by counting the number of DRAQ5-stained nuclei per field, **B**) Differentiation potential is the ratio of number of nuclei in MyHC-positive cells to the total number of nuclei in the field X 100, **C**) Fusion index is the ratio of the number of nuclei in myotubes (≥2 nuclei) to the total number of nuclei in MyHC-positive cells X 100, **D**) Average number of myotubes from all fields, **E**) Average number of myofibers (≥5 nuclei) from all fields and **F**) DRAQ5 and anti-MyHC stained merged images from a single representative field of view, Scale bar = 100µm. Error bars represent SEM. Unpaired students *t*-test was used to calculate the statistical significance. * = *P*< 0.05, ** = *P*< 0.001, *** = *P*< 0.0001. KD levels at 24h were 80%.

Table 7

MyHC-positive cells in RBM5-depleted differentiating C2C12 cells

	Trial A (74%)				**Trial B (80%)**			
	C		siRBM5		C		siRBM5	
	Ave	SEM	Ave	SEM	Ave	SEM	Ave	SEM
D2	0.1	0.1	5	1.1	6.5	1.4	8.3	1.2
D3	23	2.5	15*	2.1	33.6	2.4	19**	2.2
D4	37	2.6	19***	2.2	29.2	3.3	19*	1.6

* = $P< 0.05$, ** = $P< 0.001$, *** = $P< 0.0001$.

Percentage in brackets indicates the RBM5 KD % at 24 hours post-transfection.

3.3.4.2 RBM10 depletion

When RBM10 is depleted (mutated/KD/absent), it affects cancer cell proliferation. Specifically, RBM10 has been shown to be splicing NUMB to increase exon exclusion, which is anti-proliferative (Bechara et al., 2013). Therefore, when RBM10 is depleted we expected to see an increase in proliferating myoblasts.

The level of KD was inferred from RBM10 IF staining in scrambled controls in comparison to RBM10 KDs, at 24 and 48 hours in one of the two trials (Appendix A Figure A5). Fewer cells in KD had RBM10 staining compared to the scrambled siRNA control cells. The KD levels for this trial A (trial 1 in Table 6B) at 24h were 62% (RBM10v1) and 67% (RBM10v3) and for trial B (trial 3 in Table 6B) at 24h were 85% (RBM10v1) and 72% (RBM10v3) as shown previously (Figure 3.20) by Western blots.

Immediately following the transient transfection, the number of cell nuclei in RBM10 depleted cells, were different from the number of nuclei in the control. As expected, during proliferation (i.e. 24 and 48 hours post-transfection) when the cells are actively dividing, there was a significant increase in the number of nuclei in the RBM10 KDs, although there were differences between the trials (Figure 3.30). Specifically, in trial A (Figure 3.30A), the number of nuclei in the control was 42±3.5 / hpf and 103±6.9 / hpf at 24 and 48 hours post-transfection, respectively. There were 57.8±5 nuclei / hpf at 24 hours and 158±8.9 nuclei / hpf at 48 hours post-transfection in the RBM10-depleted cells. This difference was significant with P=0.02 at 24h and P=0.0001 at 48h. In trial B (Figure 3.30B), the total nuclei number was 54.6±6 / hpf at 24h and 135±23 / hpf at 48h in the control compared to 95.5±10 / hpf at 24h and 153±16.6 / hpf at 48h in the RBM10 KDs. Though the same trend was observed in trial B, only the 24 hour post-transfection was significant (P=0.0019). The initial plate density in trial B was high as evident from the difference in cell nuclei with 42±3.5 in trial A compared to 57.8±5 in trial B, and therefore we speculate that the effect on proliferation was more pronounced a day earlier in more confluent cultures.

When the RBM10-depleted and control cells were induced to differentiate (D1 to D4) there was no significant difference in the number of nuclei present (Figures 3.29A, 3.30A). The number of nuclei remained the same in the control and RBM10 KD cells during differentiation in both trials. Proliferation stops after D2 in both experiments.

In addition, we assessed other cell parameters such as the differentiation potential (Figures 3.29B, 3.30B), fusion index (Figures 3.29C, 3.30C) and maturation efficiency (Figures 3.29D and E, 3.30D and E). Controls showed differences in the differentiation markers between trials: D3 vs D4, which may depend on plating density. Our results indicated that there was no significant change in either the fusion potential, the number of myotubes per field and the maturation capacity between the control and RBM10-depleted cells, in both of the trials. However, we did observe a difference in significantly lower number of MyHC-positive cells on for trial A on D3 (P=0.0005) and on D4 (P=0.0004), and on D3 (P=0.0012) for trial B in the RBM10 KDs when compared to control cells.

Because there was no significant difference seen in the number of RBM10 KD cells and control cells during differentiation, the significant decrease in differentiation potential at D3/D4 indicated that the fewer number of differentiating cells in the KDs was not an effect associated with proliferation or cell density. As reported by Bechara et al. (2013), RBM10 may be primarily involved in proliferation before induction of differentiation. The effect on the differentiation potential on D4 (trial A) and D3 (trial B), may be due to the decrease in the number of MyHC-positive cells (Table 8), thereby indicating that, like RBM5, RBM10 possibly modulates MyHC expression during differentiation.

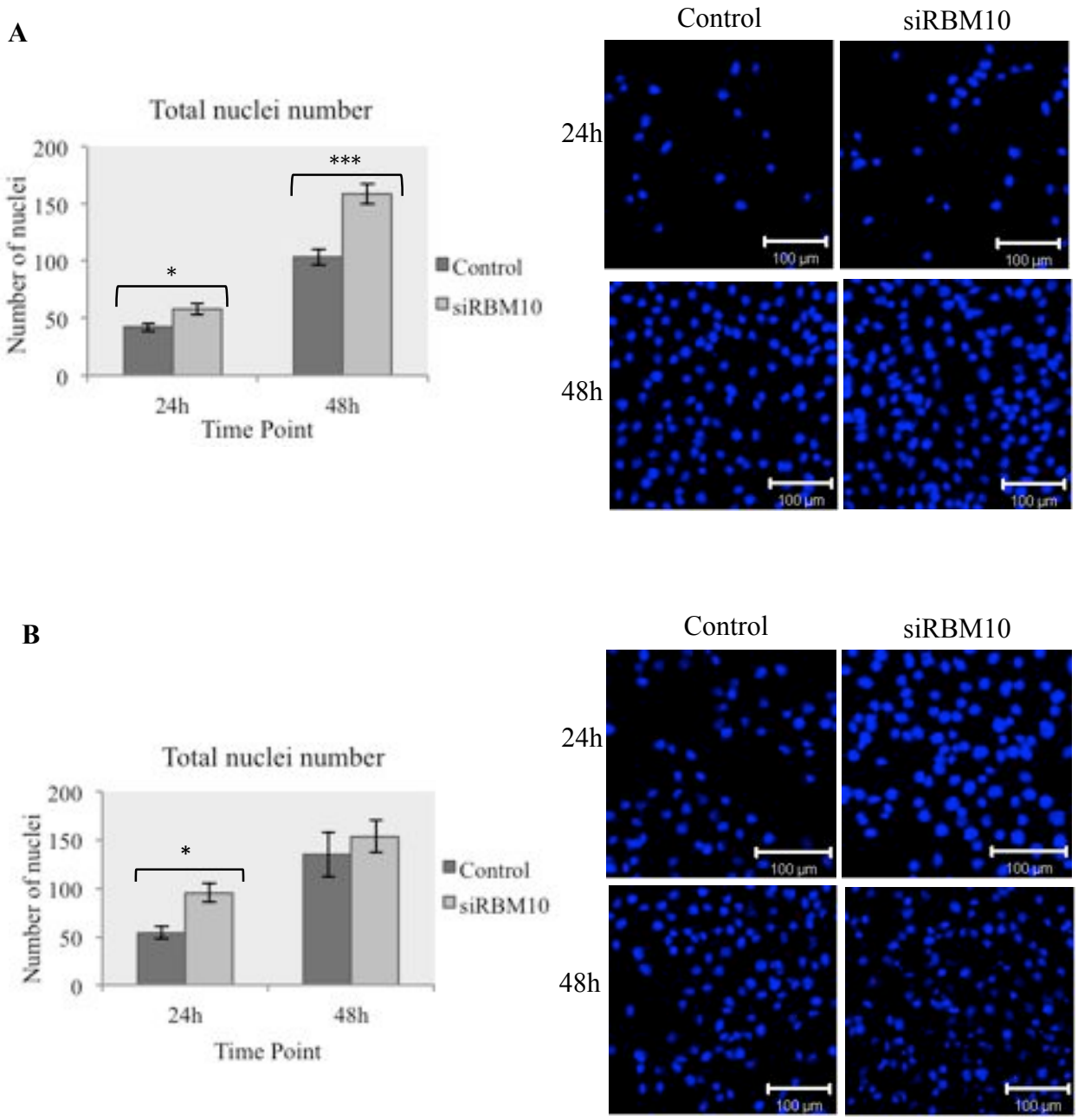

Figure 3.30 Effect of RBM10 depletion on C2C12 cell count. C2C12 myoblasts were transiently transfected with a scrambled siRNA control or siRBM10. At 24h and 48h post-transfection, the total cell count was estimated by counting the number of DRAQ5-stained nuclei in the field for **A)** Trial A and **B**) Trial B. The graph represents the average number of nuclei from 8-12 separate fields of view and the error bars represent SEM. The immunofluorescent images represent one representative field for the control and siRBM10 at 24h and 48h after transfection for the two trials. Scale bar = 100µm. Unpaired Students' *t*-test was used to calculate the statistical significance. * = $P< 0.05$, ** = $P< 0.001$, *** = $P< 0.0001$

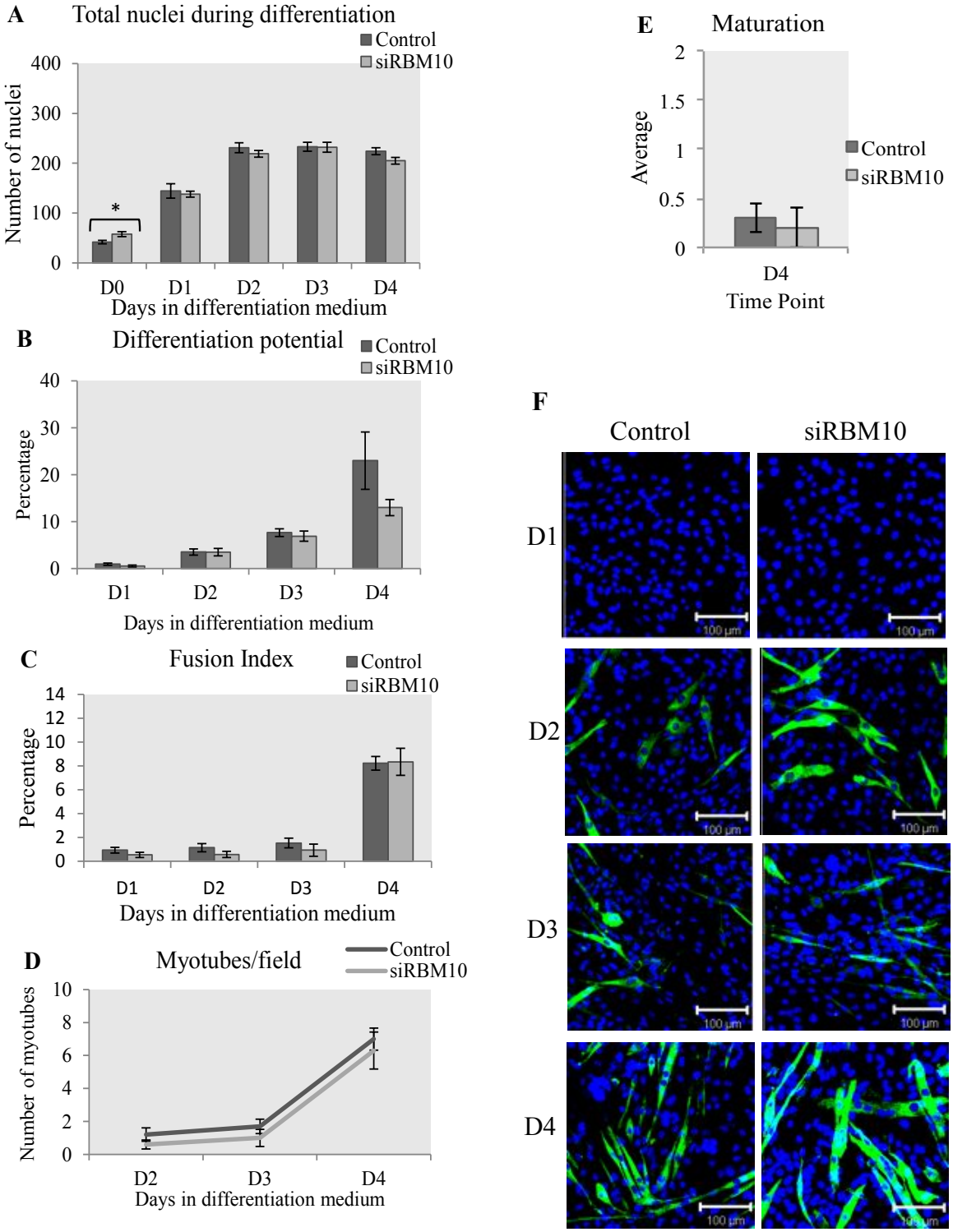

Figure 3.31 Quantitative analysis of RBM10 KD effect on C2C12 cell count, differentiation, fusion and maturation during differentiation (Trial A). A) The total number of cells was estimated by counting the number of DRAQ5-stained nuclei per field, **B**) Differentiation potential is the ratio of number of nuclei in MyHC-positive cells to the total number of nuclei in the field X 100, **C**) Fusion index is the ratio of the number of nuclei in myotubes (≥2 nuclei) to the total number of nuclei in MyHC-positive cells X 100, **D**) Average number of myotubes from all fields, **E**) Average number of myofibers (≥5 nuclei) from all fields and **F**) DRAQ5 and anti-MyHC stained merged images from a single representative field of view, Scale bar = 100µm. Error bars represent SEM. Unpaired students *t*-test was used to calculate the statistical significance. * = $P < 0.05$. KD levels at 24h were 62% (RBM10v1) & 67% (RBM10v3).

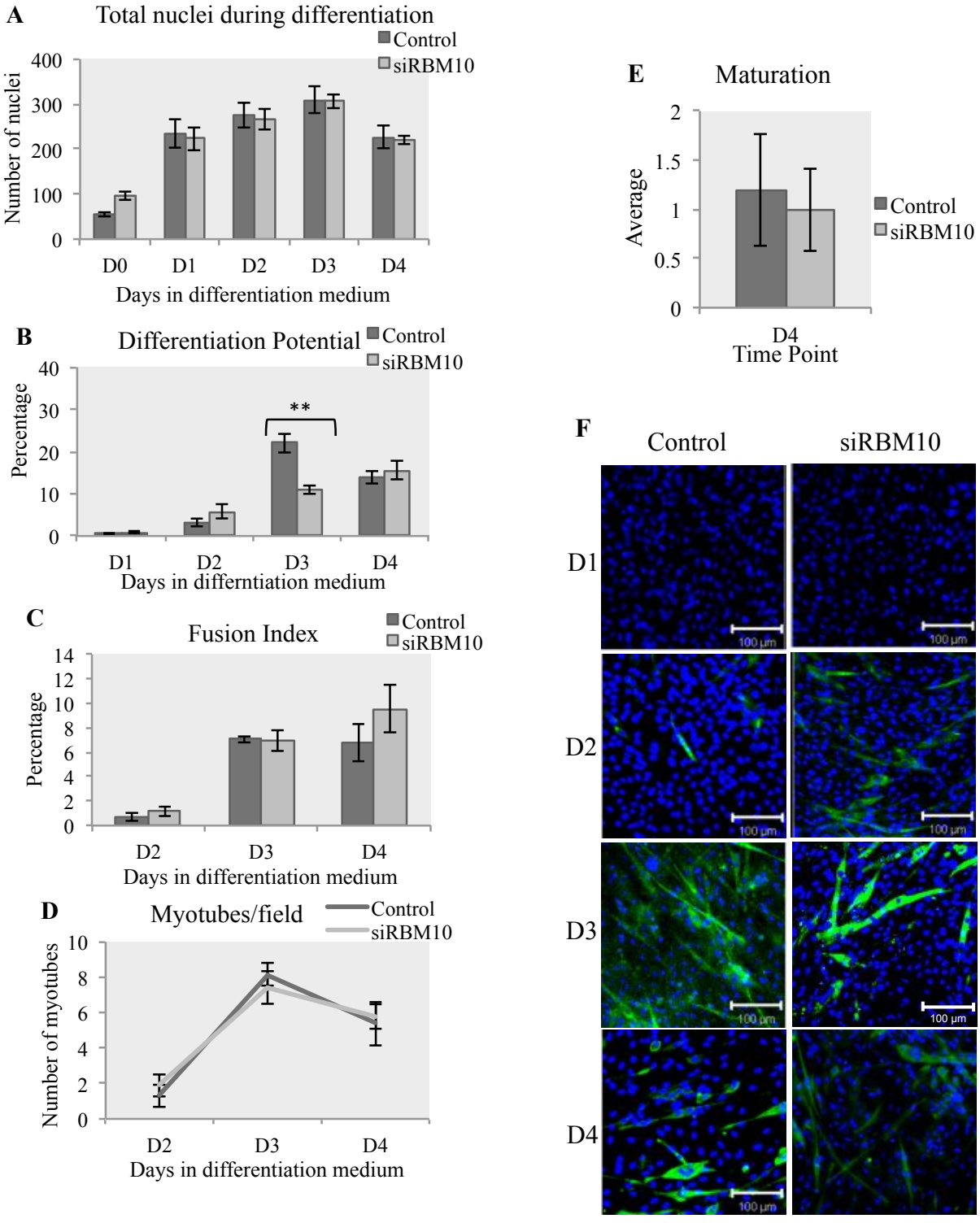

Figure 3.32 Quantitative analysis of RBM10 KD effect on C2C12 cell count, differentiation, fusion and maturation during differentiation (Trial B). A) The total number of cells was estimated by counting the number of DRAQ5-stained nuclei per field, **B**) Differentiation potential is the ratio of number of nuclei in MyHC-positive cells to the total number of nuclei in the field X 100, **C**) Fusion index is the ratio of the number of nuclei in myotubes (≥2 nuclei) to the total number of nuclei in MyHC-positive cells X 100, **D**) Average number of myotubes from all fields, **E**) Average number of myofibers (≥5 nuclei) from all fields and **F**) DRAQ5 and anti-MyHC stained merged images from a single representative field of view, Scale bar = 100µm. Error bars represent SEM. Unpaired Students' *t*-test was used to calculate the statistical significance. ** = $P < 0.001$. KD levels at 24h were 85% (RBM10v1) & 72% (RBM10v3).

Table 8
MyHC-positive cells in RBM10-depleted differentiating C2C12 cells

	Trial A (62% & 67%)				**Trial B (85% & 72%)**			
	C		siRBM10		C		siRBM10	
	Ave	SEM	Ave	SEM	Ave	SEM	Ave	SEM
D1	1.5	0.4	0.9	0.5	1.1	0.51	2.1	0.5
D2	6.9	1.5	6.9	1.5	11	3.9	15.8	4.7
D3	16	1.5	15	1.9	37	3.6	22.5**	1.6
D4	29	2.2	17**	1.6	26	4.3	17.8**	1.2

* = $P< 0.05$, ** = $P< 0.001$, *** = $P< 0.0001$.

Percentage in brackets indicates the RBM10v1 and RBM10v3 KD %, respectively at 24 hours post-transfection.

3.3.4.3 RBM5 and RBM10 combined depletion

Next, changes in morphology associated with depleting both RBM5 and RBM10 were examined. The KD levels for the two trials, trial A (trial 2 in Table 6C) at 24h were 50% (RBM5), 47% (RBM10v1) and 49% (RBM10v3) and for trial B (trial 3 in Table 6C) at 24h were 48% (RBM5), 35% (RBM10v1) and 59% (RBM10v3) as shown previously (Figure 3.20) by Western blots.

The number of nuclei in RBM5+10 KDs had a similar effect to that observed in RBM5-depleted cells. At 24 and 48 hours post-transfection, the number of cells did not vary between the control and RBM5+10-depleted cells in both the trials (Figure 3.33A,B). The number of starting cells in the scrambled siRNA controls was larger compared to the KDs in trial B.

When the cells were subjected to differentiation after transfection, the number of nuclei present were significantly lower in the RBM5+10 KDs (Figures 3.34, 3.35). Specifically, there were significant reductions on D1 (P=0.029), D3 (P=0.0001) and D4 (P=0.0037) for trial A (Figure 3.34A) and on D1 (P=0.0054), D2 (P=0.0002) and D4 (P=0.0036) for trial B. (Figure 3.35A). This effect was similar to that seen in RBM5-depleted cells suggesting that RBM5 is likely exerting a predominant role during C2C12 differentiation.

Next, we proceeded to assess the differentiation potential, fusion index and maturation index. The percentage of differentiating cells was lower in the RBM5+10 KDs. On D4, there was significant decrease in the differentiation potential (P=0.001) for trial A (Figure 3.34B) and (P=0.0007) for trial B (Figure 3.35B). The percentage of differentiating cells was 33.7±4 % for trial A and 25±2.25 % for trial B in the control, which was reduced to 23.5±3.6 % for trial A and 15±1.3 % for trial B in the RBM5+10 KDs.

Interestingly, we did not see a statistically significant difference in the fusion index in the RBM5+10 KDs. Although a lower fusion index was noted for the KDs, it was not statistically significant. However, we observed that RBM5+10 siRNA silenced myoblasts fused into myotubes more slowly than the controls because there were less myotubes in the KDs. The number of myotubes in control cells were 4.5±1.2 cells / hpf, which was reduced

to 1.2±0.35 cells / hpf in the KDs on D3 for trial A, with a significant *P* value of 0.016. For trial B, the number of myotubes on D2 (*P*=0.0008) was 9.6±1.12 cells / hpf and 3.5±1 cells / hpf in the control and KDs, respectively, and on D4 (*P*=0.0091) were 8.7±0.86 cells / hpf and 5.7±0.6 cells / hpf in the control and KDs, respectively. In both trials, there were significantly less MyHC-positive cells on D3 (*P*=0.0003) in trial A and on D2 (*P*=0.045) and D4 (*P*=0.0001) for trial B (Table 9) in the KDs compared to control. The difference in the starting cell number between the two trials could account for the differences seen amongst the two trials, especially in the MyHC-positive cells and myotubes /hpf.

We also observed that there were significantly less myofibers (≥5 nuclei) / high power field in the double KDs compared to control. The maturation potential was at least eight-fold less in trial A (2.4± 0.7 in control and 0.3± 0.21 in KD) with a significant *P* value of 0.0093 (Figure 3.34E)and four-fold less in trial B (1.8±0.5 control and 0.4±0.3 KD) with a significant *P* value of 0.025 (Figure 3.35E).

To summarize, depletion of both RBM5 and 10 resulted in (a) a decrease in cell number during differentiation, (b) a decrease in the number of cells differentiating, (c) fewer myotubes and myofibers formation and (d) lower MyHC expression.

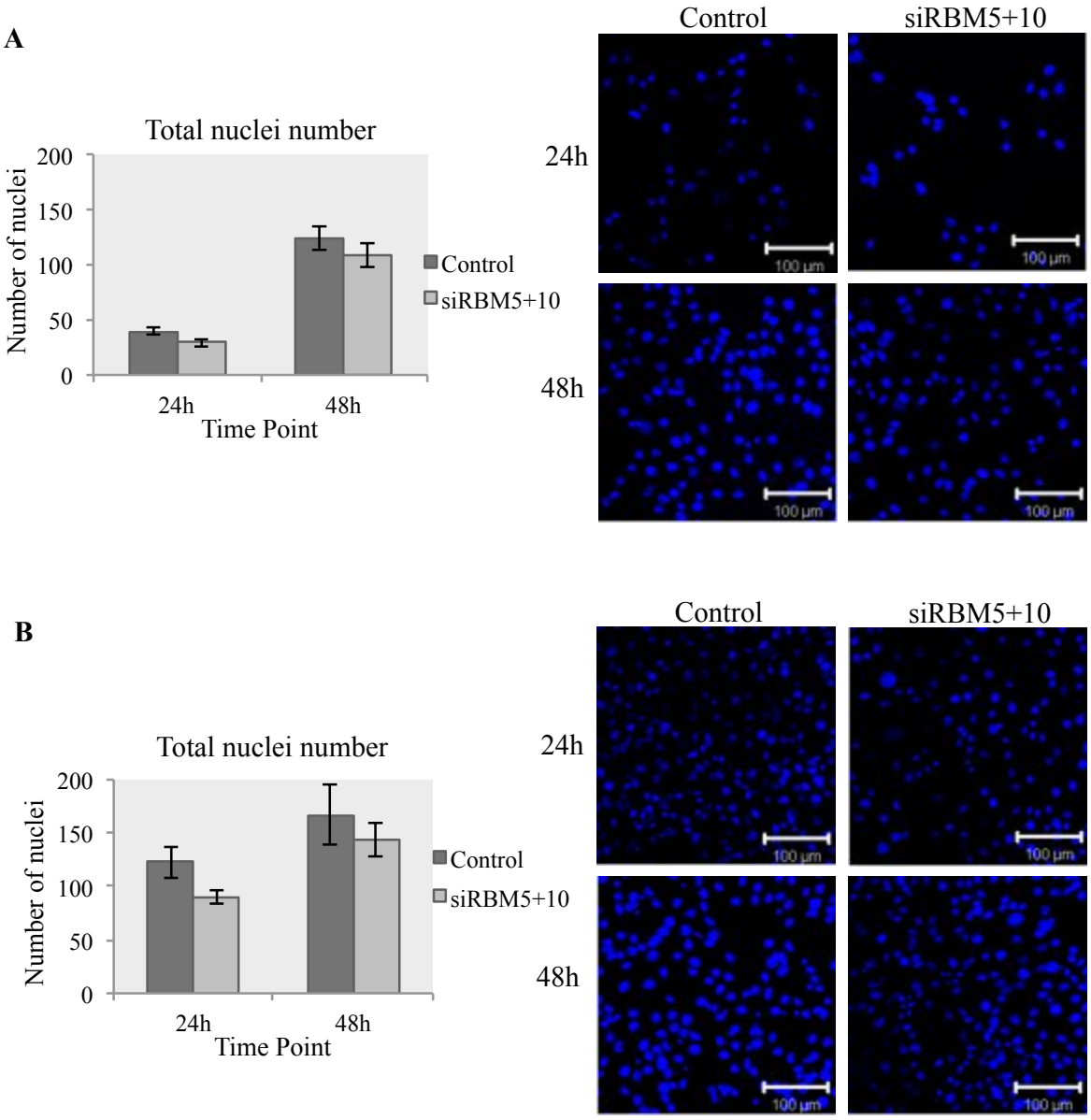

Figure 3.33 Effect of RBM5 and RBM10 depletion on C2C12 cell count. C2C12 myoblasts were transiently transfected with a scrambled siRNA control or siRBM5+10. At 24h and 48h post-transfection, the total cell count was estimated by counting the number of DRAQ5-stained nuclei in the field for **A**) Trial A and **B**) Trial B. The graph represents the average number of nuclei from 8-12 separate fields of view and the error bars represent SEM. The immunofluorescent images represent one representative field for the control and siRBM5+10 at 24h and 48h after transfection for the two trials. Scale bar = 100µm.

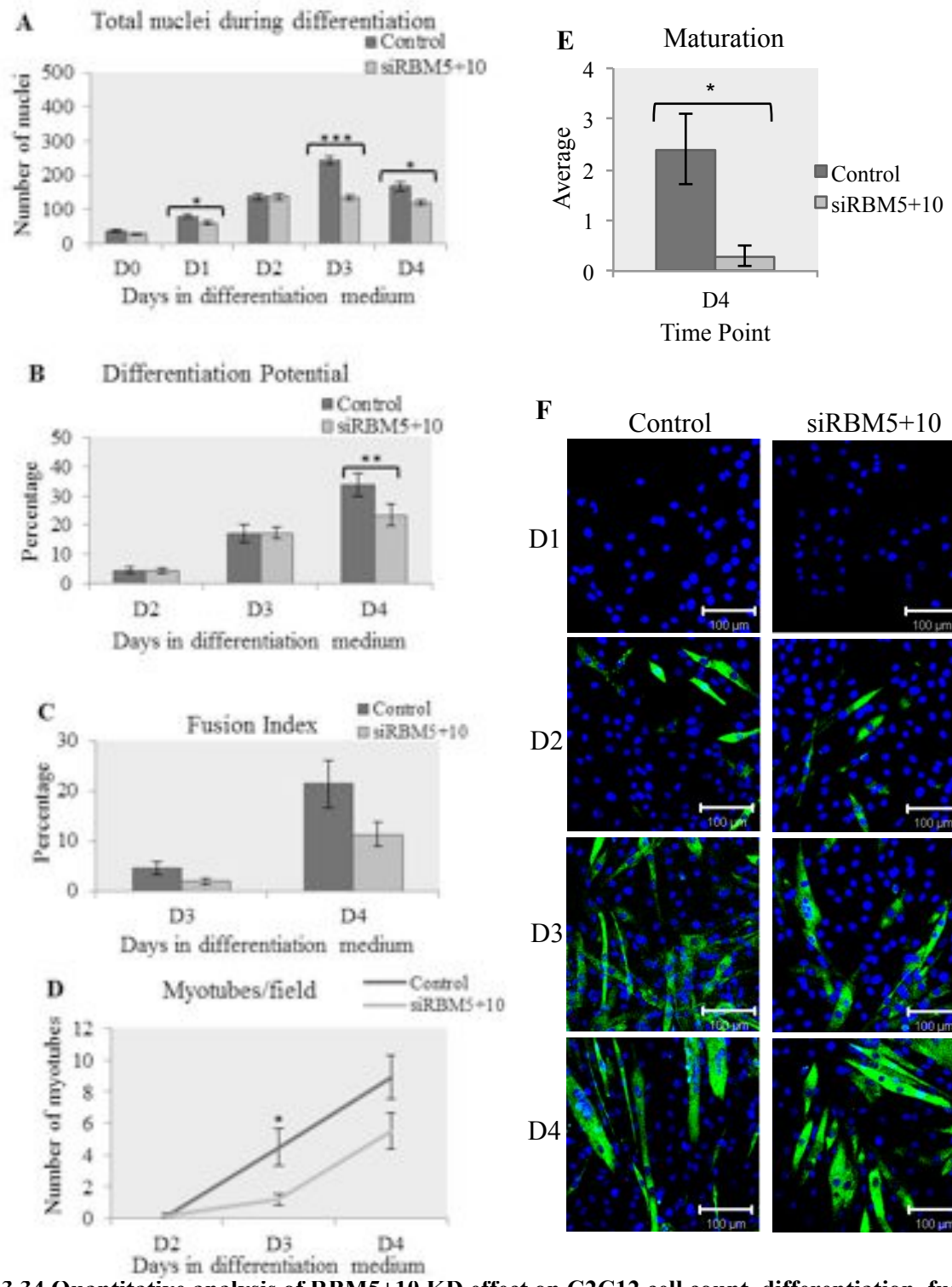

Figure 3.34 Quantitative analysis of RBM5+10 KD effect on C2C12 cell count, differentiation, fusion and maturation during differentiation (Trial A). A) The total number of cells was estimated by counting the number of DRAQ5-stained nuclei per field, **B**) Differentiation potential is the ratio of number of nuclei in MyHC-positive cells to the total number of nuclei in the field X 100, **C**) Fusion index is the ratio of the number of nuclei in myotubes (≥2 nuclei) to the total number of nuclei in MyHC-positive cells X 100, **D**) Average number of myotubes from all fields, **E**) Average number of myofibers (≥5 nuclei) from all fields and **F**) DRAQ5 and anti-MyHC stained merged images from a single representative field of view, Scale bar = 100µm. Error bars represent SEM. Unpaired Students' *t*-test was used to calculate the statistical significance. * = $P< 0.05$, ** = $P< 0.001$, *** = $P< 0.0001$. KD levels at 24h were 82% (RBM5), 42% (RBM10V1) & 55% (RBM10V3).

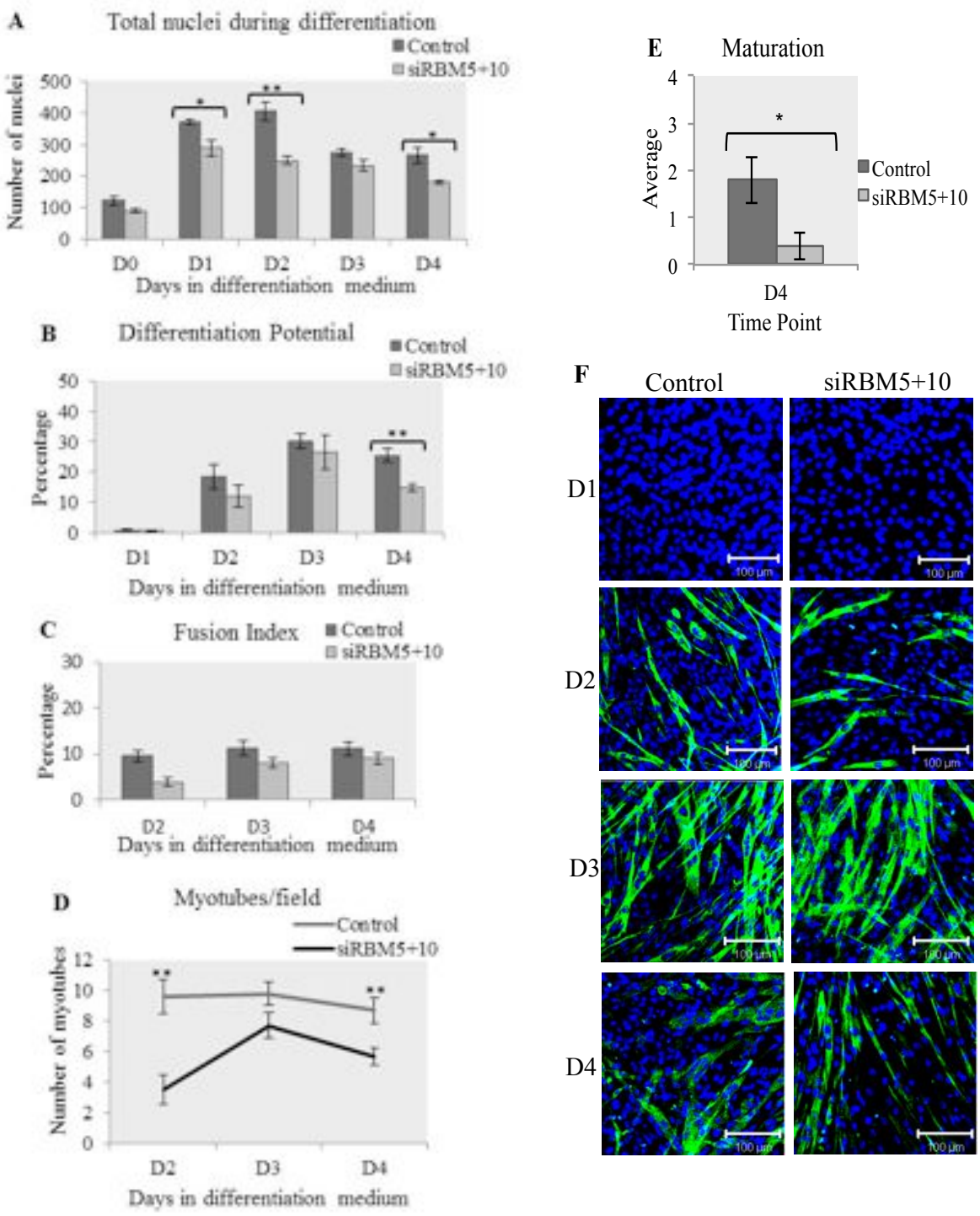

Figure 3.35 Quantitative analysis of RBM5+10 KD effect on C2C12 cell count, differentiation, fusion and maturation during differentiation (Trial B). A) The total number of cells was estimated by counting the number of DRAQ5-stained nuclei per field, **B**) Differentiation potential is the ratio of number of nuclei in MyHC-positive cells to the total number of nuclei in the field X 100, **C**) Fusion index is the ratio of the number of nuclei in myotubes (≥2 nuclei) to the total number of nuclei in MyHC-positive cells X 100, **D**) Average number of myotubes from all fields, **E**) Average number of myofibers (≥5 nuclei) from all fields and **F**) DRAQ5 and anti-MyHC stained merged images of a single representative field of view, Scale bar = 100µm. Error bars represent SEM. Unpaired Students' *t*-test was used to calculate the statistical significance. * = $P < 0.05$, ** = $P < 0.001$, *** = $P < 0.0001$. KD levels at 24h were 48% (RBM5), 83% (RBM10V1) & 59% (RBM10V3).

Table 9
MyHC-positive cells in RBM5+10-depleted differentiating C2C12 cells

	Trial A (50%, 47% & 49%)				**Trial B (48%, 83% & 59%)**			
	C		siRBM5+10		C		siRBM5+10	
	Ave	SEM	Ave	SEM	Ave	SEM	Ave	SEM
D2	6.5	1.3	6.1	0.8	37.8	5.8	21.9*	4.6
D3	33.6	2.8	19.8**	1.4	52.2	3.6	45.5	5.8
D4	29.2	3.3	22.9	3.7	37.6	2.7	18.9***	1.7

* = $P< 0.05$, ** = $P< 0.001$, *** = $P< 0.0001$.

Percentage in brackets indicates the RBM5, RBM10v1 and RBM10v3 KD %, respectively, at 24 hours post-transfection.

3.3.5 Expression of myogenic proteins (MyoD, Myf5, MyoG and MyHC) during differentiation in RBM5- and RBM10-depleted cells.

Inhibiting myogenesis (delay in differentiation, fusion and maturation) is a downstream phenotypic effect of gene expression changes in muscle specific factors. Previous results have shown that changes in the MRFs results in this delay (Sabourin and Rudnicki, 2000). Therefore, because of the inhibition in differentiation seen when RBM5 was KD, we expected to see changes in myogenic protein levels. When RBM5 was depleted in C2C12 cells and they were induced to differentiate, there was a decrease in MyHC expression (Figures 3.28, 3.29 and Table 7). Proteins extracted from these cells were then processed for immunoblot analysis to determine the expression levels of MyoD, Myf5 and MyoG. Our results indicated that neither RBM5 nor RBM10 depletion affected the expression of MyoD and Myf5 (Appendix A-Figures A19 and A20). Interestingly, RBM5 suppression selectively reduced expression of MyoG (Figure 3.32). In the scrambled siRNA control cells, MyoG was barely detectable on D0, present on D1, increased on D2, reached the highest levels on D3 and then decreased on D4 (by which time fusion has already started). In RBM5-depleted cells, although, MyoG was absent on D0 and present on D1, it was reduced on D2, D3 and D4 compared to the scrambled siRNA control.

As mentioned previously, when the RBM5 depleted cells were stained for MyHC, the number of MyHC-positive cells was significantly reduced (Table 7). This reduction was seen on D3 and D4 for trial 1 and trial 2. Therefore, these results suggest that RBM5 participates in the differentiation process by regulating the expression of MyHC and MyoG but not MyoD and Myf5.

In contrast, the RBM10-depleted cells did not show any change in MyoD, Myf5 and MyoG protein expression (Appendix A-Figures A18, A19 and A20). Interestingly, the same results were obtained in RBM5+10 combined KDs (Appendix A-Figures A18, A19 and A20). There was no change in MyoD, Myf5 and MyoG expression. With regard to MyHC expression, RBM10 and RBM5+10 KDs had down-regulated expression from that

observed in controls. As reported previously, the number of MyHC-positive cells was reduced during differentiation (Tables 8 and 9).

Therefore, our results show that MyoD and Myf5 expression levels remains stable in the KDs and indicate that the effect of RBM5 and RBM10 in the differentiating cells probably occurs at the post-specification/determination stages.

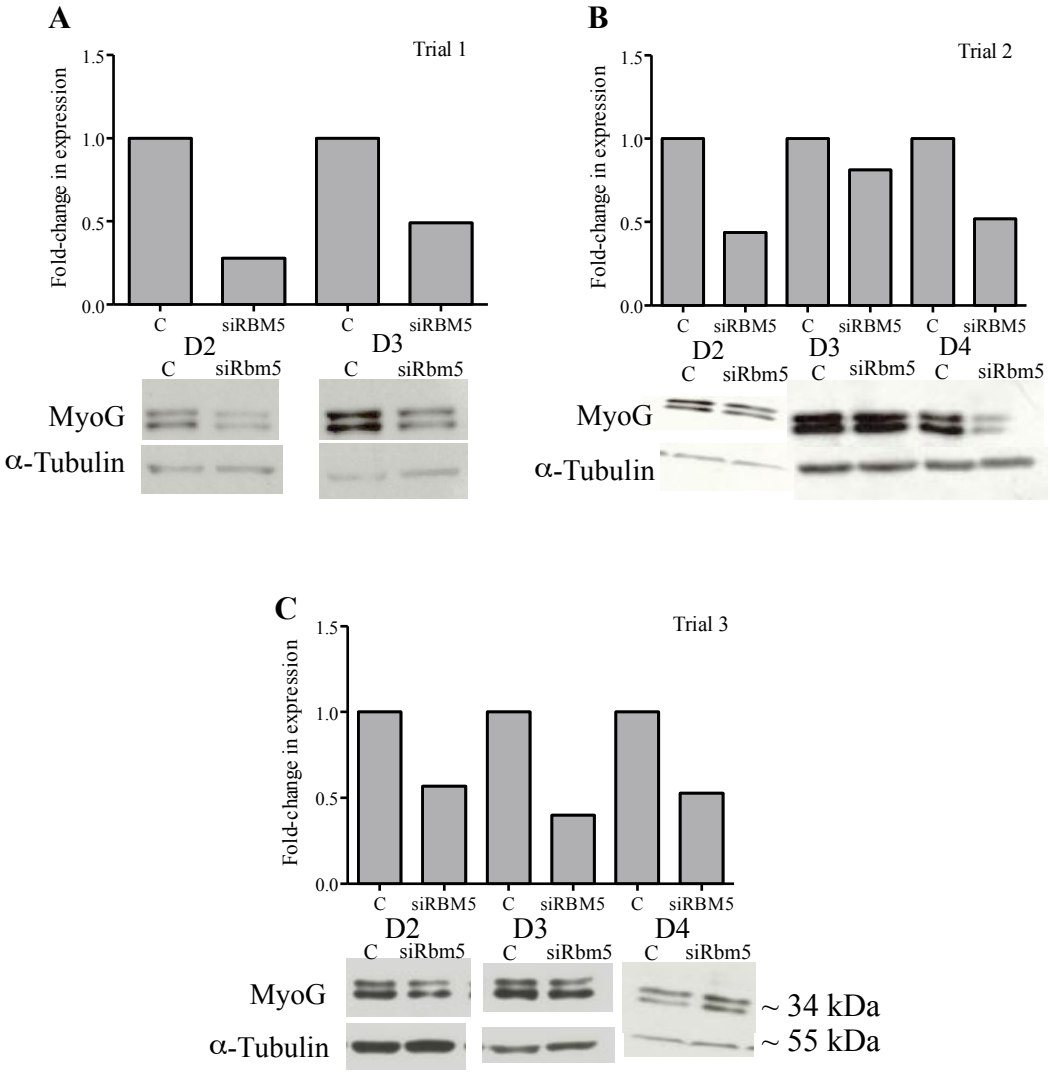

Figure 3.36 MyoG expression in RBM5-depleted differentiating C2C12 cells. RBM5 assists in myogenesis by modulating the expression of the MRF MyoG. Immunoblotting was performed using total protein extracted from scrambled siRNA control (C) and siRBM5 KD cells from three trials. Whole blots in Appendix A, Figure A18. α-tubulin was used as the normalization control. The graph depicts the fold-change in MyoG expression compared to the control levels, calculated using densitometry from technical duplicates.

3.3.6 Alternative splicing events that correlates with RBM5 and RBM10 depletion

After morphologically characterizing the effect of the KD of RBM5 and RBM10 during differentiation, we proceeded to characterize few splicing changes induced by RBM5, RBM10 and RBM5+10 KD. In our experiments, we chose three splicing transitions that have been previously shown to occur during C2C12 differentiation and proceeded directly to check if there is alternative splicing of these specific mRNAs (alpha-dystrobrevin, myocyte enhancer factor 2c and beta-integrin) and whether these events are affected by RBM5 and RBM10 depletion. The three mRNAs are involved in the differentiation program and are shown to be associated with preferential inclusion or exclusion of exons.

Alternative splicing constitutes an additional level of regulation in gene expression of many muscle-specific isoforms during the myogenic program (Bland et al., 2010). Because, RBM5 and RBM10 are splicing regulators and have been shown to be involved in mRNA splicing, we speculated that altering the levels of these two RBM proteins would affect the splicing of the three mRNAs, either by targeting exon inclusion in one variant and promoting the suppression of the other variant, which could delay differentiation or increase proliferation, as evident from the phenotypic effects associated during differentiation. We expected to see a change in timing and/or a change in the pattern of splicing (in early-expressed transcripts).

3.3.6.1 Alpha-Dystrobrevin (DTNA)

During C2C12 differentiation, the exon 11 of Alpha-Dystrobrevin gene is alternatively spliced. This splicing occurs after D2 and the detection of the exon 11 variant, reaches 78% in differentiated myotubes on D5 of differentiation. The increase in exon inclusion as differentiation progresses was shown to be associated with fusion during C2C12 differentiation (Bland et al., 2010). We proceeded to test the alternative splicing of the *Dtna* mRNA variants in all three KD experiments (RBM5/RBM10 and RBM5+10) (Table 10, Figure 3.33). In our experiments, we expected to see a delay in the expression of the exon 11 inclusion variant in the KDs.

In siRBM10-transfected cells, on D2, there was about 15.5%, 21.1% and 17.6% inclusion of exon 11 when compared to 16.6%, 29.5% and 21.2% in the scrambled siRNA control

(C), respectively, from three trials. This trend was observed on D3, with 28.2%, 49.6% and 32.2% inclusion in the KDs compared to 30.7%, 55.9% and 50.0% in the scrambled siRNA controls. Interestingly, we found that as differentiation progressed, KD of RBM10 led to a decrease in the inclusion of exon 11, which correlates with the inhibition seen in myogenic differentiation process. Therefore our data suggest that RBM10 promotes inclusion of exon 11 in *Dtna* mRNA transcript during C2C12 skeletal muscle differentiation. We did not find any change in AS of *Dtna* that corresponded to all 3 trilas in the RBM5 and RBM5+10 KDs. In our experiements, due to technical issues some data points are missing from the table, such as D4 differentiation for RBM5 KD (trial 1), RBM10 KDs (trial 2) and D2 RBM5+10KD (trial 3).

We observed a delay in splicing changes in the exon 11 variant in RBM10 KD trial 1 wherein we see 32.9% inclusion, compared to trial 3, which has 43.6% inclusion. This delay was observed starting from D2. This could be due to a low initial plating density, as evident from the presence of 42±3.5 cells/hpf in trial 1 compared to 54.6±6 cells/ hpf in trial 3.

These results indicate that RBM10 may regulate the alternative splicing of *Dtna* either directly or indirectly but additional experiments with stringent plating would be required to further elucidate the contributions of RBM10 in regulating the alternative splicing of this transcript.

3.3.6.2 Myocyte enhancer factor 2c (MEF2C)

Mef2c is responsible for maintaining the C2C12 cells in the differentiated state (Bachinski et al., 2010). Mef2cγ (-) activates transcription and Mef2cγ (+) represses transcription. Further, Mef2cγ (-) is associated with MyoD and cdk5 activity, which are involved in cell cycle arrest during the initial-stages of differentiation (Zhu and Gulick, 2004). The AS of *Mef2cγ* exon begins from D0 and continues to increase as differentiation progresses. Rajan et al. (2012) found that when the Mef2c mRNA was KD by shRNA, C2C12 cells had a lower fusion index of 8.25±3.42 with a mean cell count of 210.7±11.3 compared to scrambled control. Therefore, we expected to see an increase in Mef2cγ (+) variant in the RBM5 and RBM5+10 KDs.

When the alternative splicing of *Mef2cγ* was assessed in the RBM5, RBM10 and RBM5+10-depleted cells, as expected RBM5+10 KD showed an increase in *γ* exon inclusion when compared to the scrambled siRNA control (C) (Tables 11, 12, 13, Figure 3.38). This increase was observed on D4 in the two trials. Specifically, trial 1 showed an increase from 73.7% in the scrambled siRNA controls to 76.7% in the KDs, trial 2 showed an increase from 65.3 % in the scrambled siRNA controls to 71.9% in the KDs and trial 3 showed an increase from 76.3% in the scrambled siRNA controls to 80.3% in the KDs. In our experiements, due to technical issues some data points are missing from the table and therefore require additional biological replicates to confirm the AS changes observed in *Mef2cγ ,* during the other time-points.

Our results show that both RBM5 and RBM10 together could be potentially acting as splicing regulators during differentiation. We also observed that either RBM5 or RBM10 did not have an effect on the alternative splicing of *Mef2cγ* exon. Therefore, these findings demonstrate that the alternative splicing of *Mef2cγ* is regulated by either synergistic or additive association of these two RBPs.

3.3.6.3 Integrinβ1

During C2C12 differentiation, expression of the β1A integrin isoform decreases while the β1D isoform levels increase and replaces β1A in mature myotubes (Belkin et al., 1996; (Quach et al., 2009). Functionally, isoform-specific functions have been identified for these two isoforms in myogenesis; specifically, when β1A was replaced with β1D by knock-in experiments in mice, primary myogenesis was affected (Belkin et al., 1996). When β1D was over expressed in C2C12 cells, there was a delay in myotubes formation and when β1A was over expressed it affected myotube maturation (Cachaco et al., 2003).

Based on the importance of alternative splicing of Integrinβ1 during differentiation, we analyzed their alternative splicing pattern using exon-specific primers by end-point PCR. We compared the inclusion or exclusion of the β1A and β1D variants in the RBM5 and RBM10 KDs and controls (Figure 3.39). When the PCR products were analyzed, an integrin β1A variant at 282 bp was detected. This is the expected result since, during C2C12 differentiation, the β1D variant usually appears during the terminal-stages. In our

case, since our differentiation conditions did not proceed past D4, we can conclude that there was no integrin β1D (363 bp) detection until D4 in the KDs. This therefore indicates that neither RBM5 nor RBM10 is involved in the alternative splicing of integrin at least until D4 of differentiation.

To conclude, the alternative splicing transitions that are affected by inhibiting these two RBPs either individually or dually are the exon 11 inclusion of *Dtna* (reduced) and the γ exon inclusion of *Mef2c* (enhanced). The depletion did not affect integrin β1A and β1D alternative splicing. Our results reveal a potentially new role for RBM10 and RBM5&10 as a splicing regulator during myogenesis.

Overall, combining our expression and KD studies, we can infer that RBM5 is potentially crucial for differentiation, fusion and maturation. RBM10 likely has an alternative splicing role during differentiation and is required during proliferation before differentiation induction and for differentiation as well.

Table10.
Dtna exon inclusion percentage during C2C12 differentiation

RBM5KD	Trial 1 (72% KD)	Trial 2 (60% KD)	Trial 3 (82% KD)
C D2	29.5	35.0	41.8
siRBM5 D2	26.6	35.6	40.9
C D3	55.9	48.0	50.2
siRBM5 D3	58.4	54.1	54.4
C D4		59.2	61.0
siRBM5 D4		54.3	62.8

RBM10KD	Trial 1 (77% 10v1, 67% 10v3 KD)	Trial 2 (86% 10v1, 89% 10v3 KD)	Trial 3 (85% 10v1, 72% 10v3 KD)#
C D2	16.6	29.5	21.2
siRBM10 D2	15.5	21.1	17.6
C D3	30.7	55.9	50.0
siRBM10 D3	28.2	49.6	32.2
C D4	32.9		43.6
siRBM10 D4	36.5		46.8

siRBM5+10KD	Trial 1 (52% 5, 49% 10v1, 76% 10v3 KD)	Trial 2 (81% 5, 85% 10v1, 83% 10v3 KD)	Trial 3 (48% 5, 83% 10v1, 59% 10v3 KD)#
C D2	30.6	41.8	21.2
siRBM5+10 D2	21.2	30.0	
C D3	35.3	50.2	50.0
siRBM5+10 D3	38.6	50.2	38.9
C D4	46.9	61.0	43.6
siRBM5+10 D4	37.3	61.9	41.0

Percentage in brackets indicates the KD % at 48 hours post-transfection. # indicates the KD % at 24 hours. 5- RBM5, 10v1- RBM10V1 and 10v3- RBM10V3.

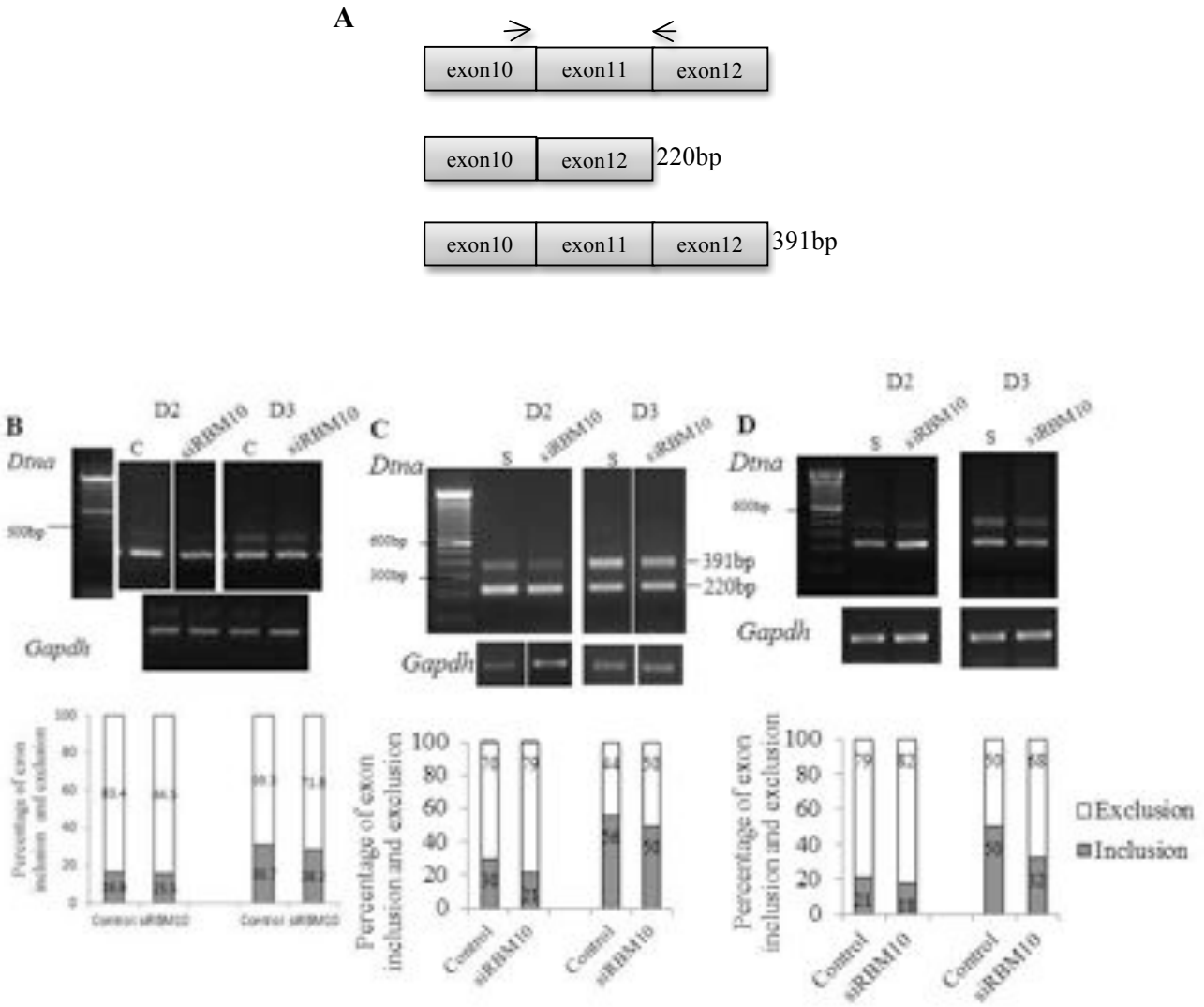

Figure 3.37 Alternative splicing of *Dtna* in RBM10 deficient differentiating C2C12 cells. RBM10 promotes inclusion of exon 11 of *Dtna* during muscle differentiation. **A**) Diagram illustrating the formation of the two variants, the location of primers used in this study and the expected product sizes. Semi-quantitative end-point PCR was performed on total RNA extracted from control (C) and siRBM10 KD cells from 3 trials, **B**) Trial 1, **C**) Trial 2 and **D**) Trial 3. (Raw data in appendix A-Figures A12 – A17). *Gapdh* was used as normalization control. The graphs show the percentage of exon inclusion and exclusion calculated using densitometry from technical quadruplicates.

Table 11
Mef2c*γ* exon inclusion percentage in Rbm5-depleted C2C12 cells

RBM5KD	Trial 1 (72% KD)	Trial 2 (60%KD)	Trial 3 (82% KD)
	%inc	%inc	%inc
C D0/24h	64.1		54.1
siRBM5 D0/24h	61.4		51.6
C 48h		65.5	53.5
siRBM5 48h		65.1	49.4
C D1	65.2	77.5	65.2
siRBM5 D1	69.2	74.3	67.1
C D2	76.1	82.5	67.2
siRBM5 D2	75.1	82.5	69.1
C D3	78.3	84.2	73.5
siRBM5 D3	73.4	83.2	74.0
C D4		74.1	65.3
siRBM5 D4		76.4	71.9

Percentage in brackets indicates KD % at 48 hours post-transfection. %inc is the percent of exon inclusion.

Table 12
Mef2c*γ* exon inclusion percentage in Rbm10-depleted C2C12 cells

RBM10KD	Trial 1 (77% 10v1, 67% 10v3)	Trial 2 (86% 10v1, 89% 10v3)	Trial 3 (85% 10v1, 72%10v3)#
	%inc	%inc	%inc
C D0/24h	67.8	64.1	80.9
siRBM10 D0/24h	71.8		70.2
C 48h	75.0		71.9
siRBM10 48h	69.7		76.9
C D1	75.3	65.2	76.3
siRBM10 D1	74.7	72.1	69.7
C D2	74.5	76.1	80.3
siRBM10 D2	73.3	75.0	78.7
C D3	74.3	78.3	80.4
siRBM10 D3	82.2	81.3	80.2
C D4	84.1		76.3
siRBM10 D4	80.2		79.5

Percentage in brackets indicates the KD % at 48 hours, # indicates the KD % at 24 hours. %inc is the percent of exon inclusion.

Table 13
Mef2c*γ* exon inclusion percentage in Rbm5- and Rbm10-depleted C2C12 cells

RBM5+10KD	Trial 1 (52% 5, 49% 10v1, 76% 10v3)	Trial 2 (81% 5, 85% 10v1, 83% 10v3)	Trial 3 (48% 5, 83% 10v1, 59% 10v3)#
	%inc	%inc	%inc
C D0/24h	59.0	54.1	80.9
siRBM5+10 D0/24h		54.2	75.1
C 48h		53.5	71.9
siRBM5+10 48h		49.4	70.4
C D1	71.8	65.2	76.3
siRBM5+10 D1	70.6	59.2	77.0
C D2	71.6	67.2	80.3
siRBM5+10 D2	71.1	66.0	
C D3	75.4	73.5	80.4
siRBM5+10 D3	75.8	69.6	77.7
C D4	73.7	65.3	76.3
siRBM5+10 D4	76.7	71.9	80.3

Percentage in brackets indicates KD %, # indicates the KD % at 24 hours, the rest are at 48 hours. %inc is the percent of exon inclusion.

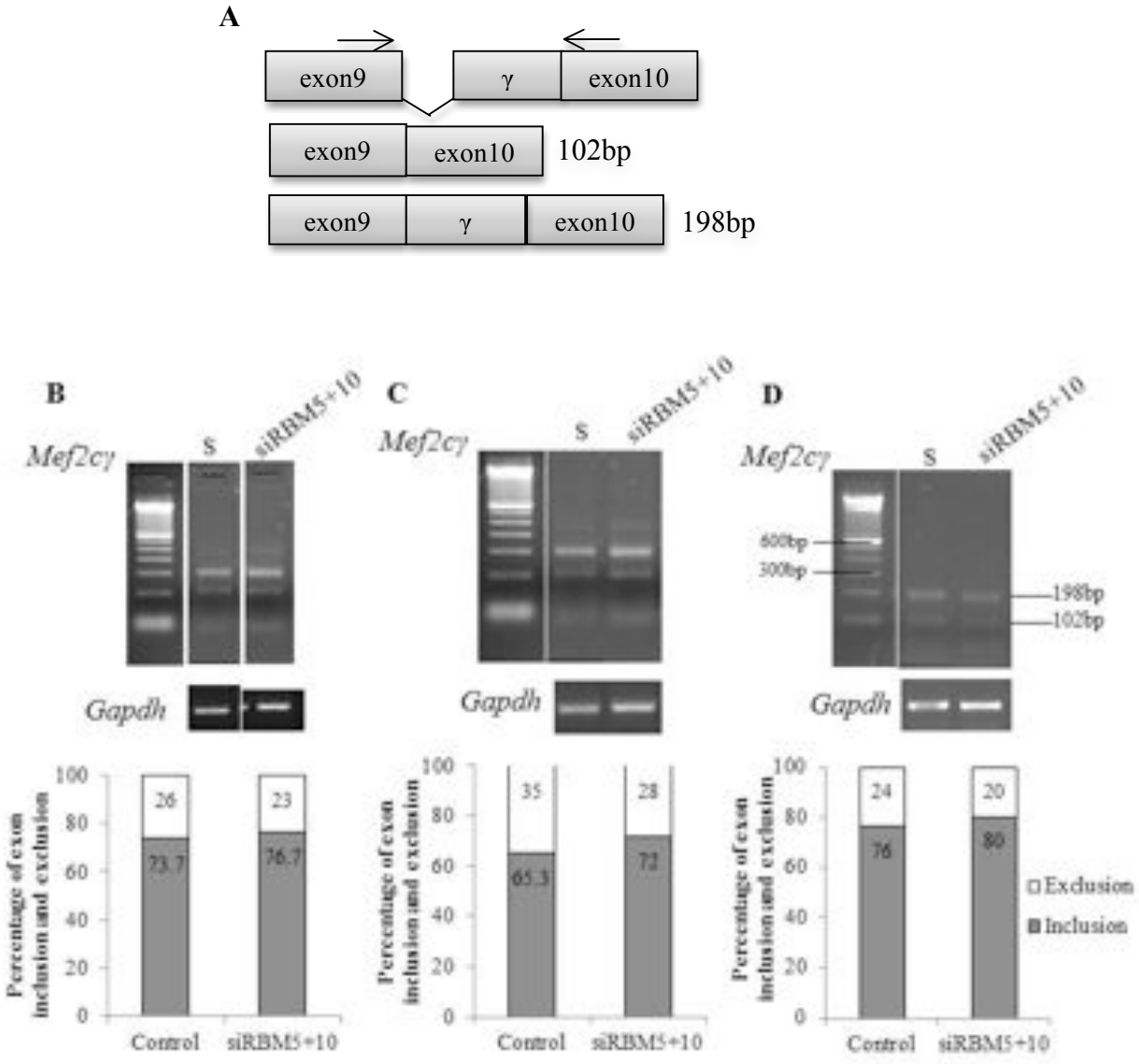

Figure 3.38 Alternative splicing of *Mef2cγ* in RBM5+10-depleted cells during C2C12 differentiation. RBM5 and RBM10 collectively modulate alternative splicing of *Mef2cγ* during differentiation. **A)** Diagram illustrating the formation of Mef2c γ+ and γ- spliced variants, the location of primers used in this study and the expected product sizes. Semi-quantitative end-point PCR was performed on total RNA extracted from control (C) and siRBM5+10 KD cells on D4 differentiation from three trials, **B**) Trial 1, **C**) Trial 2 and **D**) Trial 3 (Raw data in appendix A-Figures A15, A16, A17). *Gapdh* was used as normalization control. The graphs show the percentage of exon inclusion and exclusion calculated using densitometry from technical quadruplicates.

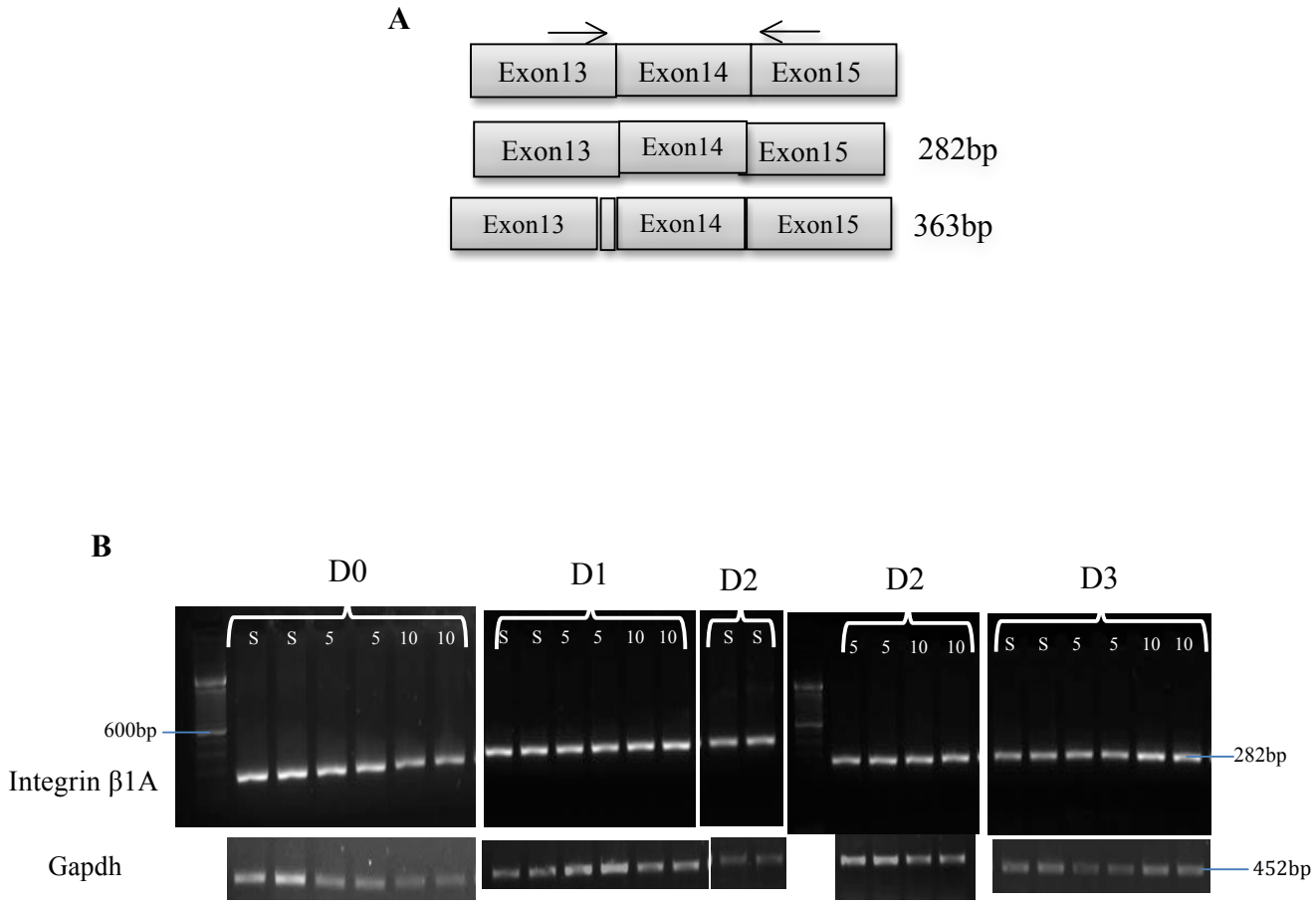

Figure 3.39 Alternative splicing of *Integrin β1A / β1D* events in RBM5- or RBM10- depleted cells during C2C12 differentiation. RBM5 and RBM10 have no effect on the alternative splicing of Integrin β variants. **A)** Diagram illustrating the formation of *Integrin β1A* and *Integrin β1D* spliced variants, the location of primers used in this study and the expected product sizes. Semi-quantitative end-point PCR was performed on total RNA extracted from control (S) and siRBM5 (5) and siRBM10 (10) KD cells from one trial (Trial 1) **B**) Agarose gel image showing Integrin β1A (282 bp) PCR product from D0-D3 in technical duplicates, but the other variant Integrin β1D (363 bp) was not detected.

Chapter 4

4 Discussion

4.1 C2C12 mouse myoblasts are appropriate model for determining the role of RBM5 and RBM10 during skeletal differentiation

Different model systems have been used to understand the molecular intricacies of the myogenic program (Miller, 1990). The C2C12 model is a representative model as judged by the following factors: (a) it is a well-characterized model, and (b) the time-course of differentiation can be accurately studied. In addition, several alternative splicing patterns, which are dynamic and necessary for myogenesis, have been extensively studied in this model system. C2C12 myoblasts were grown in DMEM supplemented with growth serum, which provided the cells with essential growth factors. When the percentage of serum was reduced, it resulted in deprivation of growth factors, which triggered a cascade of numerous molecular signalling pathways. This led to induction and execution of the myogenic differentiation process, thereby causing the transition from myoblasts to myotubes.

Many laboratories use different serum conditions for growth and differentiation such as varying the serum concentration and use of serum derived from different animals. For instance, some grow myoblasts in 10% fetal calf serum (FCS) and induce differentiation with 1% FCS (Ferri et al., 2009); others use 20% FBS in GM to 1% HS or 2% HS in DM (Ono et al., 2006, Mei et al., 2011), while some use 10% FBS for growth with differing concentrations (1%, 2% and 5%) of HS for differentiation (Louis et al., 2008, Sun et al., 2005, Velica and Bunce, 2011). For our experiments, we used 10% FBS to grow the myoblasts and 2% HS to induce differentiation. When the proliferating C2C12 myoblasts in growth medium grown to 80% cell density were exposed to reduced serum they started differentiating. The effect of changing serum concentration in the C2C12 myoblasts was assessed. The differentiation landmarks were examined visually, and in addition, the expression of muscle differentiation-specific markers such as MyoD and MyoG

(Myogenin) were analyzed. Assessing the muscle differentiation-specific markers was necessary to determine the progress of differentiation and also to confirm antibody specificities. MyoD, a component of the bHLH myogenic transcription factor, is necessary for the regulated expression of early (adhesion and extracellular proteins), intermediate (transcription factors) and late-stage genes (myofibril and cytoskeletal proteins) (Ishibashi et al., 2005, Tapscott, 2005). On the other hand, a decrease in MyoD levels are observed in quiescent cells, in fact, down-regulated expression of MyoD and Myf5 can direct the C2C12 cells to become reserve cells (Yoshida et al., 1998). When serum depletion occurs, MyoD-positive cells should show an increase in MyoG expression (Yoshida et al., 1998). Different observations have been recorded concerning the expression levels of MyoD in C2C12 cells. For instance, Ferri et al. (2009), observed that the mRNA levels of MyoD did not change but there was a significant increase in protein levels on D1 when compared to D0, D3 and D7. According to Miller (1990), MyoD levels increased on D3 but this increase was seen in mRNA levels. In addition, the mRNA expression levels of MyoD were shown to be cell density-dependant; the mRNA levels during differentiation fluctuated depending on the confluence of the C2C12 cells at the time of seeding (Tanaka et al., 2001). Others have reported steady-state MyoD protein levels during differentiation (Mal and Harter, 2003, Shen et al., 2003). Our experiments, agrees with these two reports; we detected MyoD in both undifferentiated myoblasts and the myotubes and MyoD protein levels remained same throughout the differentiation process.

Our assessments showed that differentiation was generated in the C2C12 cells treated with the lower concentration of HS and that the time-points of the differentiation morphology differed slightly from previously published reports. Tomczak et al. (2003), reported that by D2, the number of nuclei in multi-nucleated cells was 9±3% and by D4, the fusion index was 40±5% and by D6, the fusion index increased to 48±5%, with a marginal increase upto 52±3% by D10. In their experiment, 20% FBS-containing media was used for growth and 2% HS was used for differentiation. In our experiments, when using 10% FBS and 2% HS, we observed that the differentiation potential was at 9% between D2 and D3, and the fusion index was at 40% between D5 and D6 of differentiation. According to Ferri et al. (2009), wherein the experiments were performed using C2C12 cells, which were induced to

differentiate at 80% confluence, by changing 10% FCS to 1% FCS, the differentiation started 24 hours post-serum reduction. The fusion index was 8±3% on D2. On D3-D5, the fusion index increased to 35±5% and reached 60±6% at D7-D10. These suggest that based on the cell density and the percentage of serum used for growth and differentiation, there could be differences in the exact timing and the number of cells undergoing differentiation transformation.

Down-regulated expression of RBM5 and RBM10 during differentiation in this model tests the importance of time-dependant regulation and aligns with previous studies demonstrating that this intricate process is highly controlled. Thus, overall we can infer that the murine C2C12 myogenic differentiation cell line is a suitable model to study the role of RBM5 and RBM10 during the differentiation phase of skeletal myogenesis.

There are limitations associated with using this C2C12 model system. This *in vitro* mouse muscle differentiation model has some differences compared to normal skeletal myogenesis that occurs *in vivo*; the differences being exhibited in the timing of MyoD expression, the role of "satellite-like" reserve cells, the myofibers formed are not mature myofibers and the differentiation phase is part of both embryonic and regenerative myogenesis. In addition, the C2C12 cells are capable of differentiating if they reach high confluence even when being maintained in GM.

4.2 RBM5 and RBM10 are differentially expressed and tightly regulated during skeletal muscle differentiation

RBM5 and RBM10 are important RNA-binding proteins implicated in functions such as cell proliferation, apoptosis and alternative splicing in transformed cells (Edamatsu et al., 2000; Oh et al., 2002; Sutherland et al., 2000; Zhao et al., 2012; Shao et al., 2012; Fushimi et al., 2008; Bonnal et al., 2008; Wang et al., 2012). These two RBPs are associated with disease states such as tumors, including but not limited to lung, breast, ovarian, pancreas, etc. (Bechara et al., 2013). The precise mechanism of action of these RBPs in non-transformed systems is beginning to be deciphered. RBM5 has recently been shown to be involved in spermatid differentiation (O'Bryan et al., 2013). Although RBM5 and RBM10 are highly expressed in skeletal muscle, their exact role in muscle development has never

been explored. Our research has focused on the expression and the regulatory role played by RBM5 and RBM10 during the normal skeletal muscle differentiation. We are the first to report an important role for these two RBPs in skeletal myogenesis.

Firstly, we analyzed the expression levels for RBM5 and RBM10 in the mouse C2C12 myogenic differentiation model. We found that both RBM5 and RBM10 are expressed in C2C12 cells and the expression decreased progressively during differentiation. From these results, we can infer that (a) the presence of these two RBPs throughout differentiation signifies their potential importance during the entire process of C2C12 differentiation, (b) their differential expression suggests effective regulation during myogenic differentiation and (c) there is a likely possibility that these RBPs might exert specific functions in myogenesis. These experiments also revealed that the protein abundance of RBM5 and RBM10 had similar trends, from which we can deduce that RBM5 is co-expressed with its paralogue RBM10 during myogenic differentiation, which suggests both proteins could possibly possess distinct functions. Lastly, the change in expression validates that the C2C12 differentiation model is a useful model to elucidate the role of RBM5 and RBM10 in skeletal myogenesis.

We were able to detect Rbm5 and Rbm10 mRNA variants during differentiation, however, we cannot determine if these levels were comparable to previous observations that showed high mRNA expression in mature human skeletal muscle. Different types of myofibers constitute the mature adult muscle and there are many gene expression changes associated with mature muscle fibre *in vivo* (Gunning and Hardeman, 1991). For instance, the G protein subunit, $G\alpha_z$, which interacts with G protein-coupled receptors (GPCRs) and can modulate myogenin, was expressed during differentiation but was absent in adult muscle (Mei et al., 2011). SMAD3 and Notch3 are other muscle-related proteins that have shown transient expression (Kislinger et al., 2005). Some of the diversity is in part due to isoform-specific expression and function. For instance, even though there are multiple MyHC isoforms, different isoforms are required for specific functions (Wells et al., 1996). Spatio-temporal expression is not only associated with heterogeneity in fiber types but also with muscle-specific mechanical properties (Babu et al., 2000). In addition, inter-species variations, such as species-dependant fiber type specification are reported. For instance, in

rodents and birds, the myoblasts fuse in two stages generating the primary myotubes and the secondary myotubes, however, in humans, a third stage occurs leading to the formation of tertiary myotubes (Gunning and Hardeman, 1991). It is therefore possible that the down-regulated expression in humans corresponds to additional regulation.

We found an apparent discrepancy between the differential down-regulation of protein levels and the steady state mRNA levels for all of the variants suggesting that expression is regulated at a post-transcriptional and/or post-translational level. Differences in the mRNA stability and degradation of differentiation-specific transcripts when compared to proliferating and differentiating cells, indicates that when there is no functional requirement, these mRNA can be destroyed ('t Hoen et al., 2011). When they measured mRNA half-life, albeit for only 8 hours in proliferating and differentiating cells, factors such as decay rate and splice variants were shown to control the mRNA stability of many muscle-related mRNAs. Furthermore, our results are in line with the skeletal-specific differential expression (of both Rbm5 and Rbm10) observed in the rat H9c2 model (Loiselle and Sutherland, 2014). Thus, these findings indicate that the levels of RBM5 and RBM10 are tightly regulated during skeletal differentiation, suggesting an important role for these two RBM proteins in the myogenic process, and denoting functional specificity.

During C2C12 differentiation, the two RBM10 isoforms were differentially expressed where RBM10v3 was more highly expressed than RBM10v1. Our results are similar to that observed in H9c2 cells, in which RBM10v2 (Human/Rat RBM10v2 is equivalent to the mouse RBM10v3) was two-fold higher than RBM10v1 (at both protein and mRNA levels) during skeletal-specific differentiation (Loiselle and Sutherland, 2014). This trend was observed in cardiac lineage-specific differentiation as well (Loiselle and Sutherland, 2014). This may specify functional differences between cancer and normal cells. In human transformed cell lines, which are associated with lung adenocarcinomas (A549, GLC20), only one RBM10 variant (RBM10v1) is abundant and the other variant is nearly undetectable (Loiselle and Sutherland, 2014). Thus, our results clearly indicate that the level of regulation and functional implications of RBM10 in normal cells is different than in transformed cells. Many RBPs are alternatively spliced leading to isoform-specific functions (Glisovic et al., 2008). For instance, a spliced isoform of the RBP, hnRNP A/B

protein is involved in the regulation of alternative splicing during erythropoiesis (Glisovic et al., 2008). The human RBM10v2 isoform lacks certain domains such as the RNP2 motif region (Xiao et al., 2013), which suggests that this isoform may not be important during tumorigeneis, however, it may be required during myogenic differentiation. As suggested by Xiao et al., (2013), the presence of both isoforms in certain cellular systems, denoting binding to different RNA targets or different RNA-binding ability, could hold true for differentiation as well.

The expression of *Rbm5* variants is regulated post-transcriptionally in myogenesis, which is a normal cell developmental condition, unlike in cancer cells where it is regulated in relation to tumorigenesis (Sutherland et al., 2005). Similarly, the expression of Rbm10 variants and isoforms are regulated during normal cell development, which however correlates with a previous result that RBM10 is expressed during mid-gestation embryos (Johnston et al., 2010). RBPs are regulated depending on tissue-specific functions (Dreyfuss et al., 2002, Reed and Hurt, 2002). Post-transcriptional regulation of myogenic events is a necessary component for muscle differentiation. The presence of both RBPs during the initial stages of differentiation is therefore thought to provide better control.

Protein and mRNA levels do not always correlate (Greenbaum et al., 2003). In addition, the discrepancy between the mRNA and protein levels have been previously reported for myogenic proteins such as Myf5, Myogenin, MyoD and MRF4 during C2C12 differentiation and this has been accounted for by post-transcriptional mechanisms (Ferri et al., 2009). Furthermore, the relative difference between protein and mRNA expression during differentiation, suggests that micro RNAs (miRNAs) could regulate RBM5 and RBM10 accumulation. This argument stems from two observations. Firstly, miRNAs play a role in myogenesis by either repressing translation or promoting mRNA degradation (Soleimani and Rudnicki, 2011, Ge and Chen, 2011). Secondly, RBM5 is one of the lung-carcinoma associated putative target genes of hsa-miR-151a-3p (Pang et al., 2014). It is also shown that the expression of human RBM5 is repressed by miRNA (miR-660) and hence, is down-regulated (-1.96 fold) during myoblast differentiation (Dmitriev et al., 2013). No reports have thus far identified miRNA repression of RBM10.

The steady-state *Rbm5* mRNA levels measured in the differentiating C2C12 cells are different from the down-regulation observed during *in vitro* myogenic differentiation of human primary myoblasts (Dmitriev et al., 2013). However in those microarray experiments, the RNA was isolated from CD56+ myoblasts, which eliminates non-myogenic cells, whereas C2C12 cells are heterogenous population. In addition, there are possible differences in expression that could exist between species.

Post-translational modifications such as phosphorylation, sumoylation and ubiquitinylation of these muscle-specific regulators have also been shown to contribute to the discrepancy in the protein and mRNA levels (Naya and Olson, 1999). Based on the localization studies of MRFs such as Myf5, Myogenin, MyoD and MRF4, Ferri et al., (2009) have suggested the occurrence of stage-specific post-translational regulation of these myogenic proteins during differentiation. In addition, post-translational changes such as phosphorylation, arginine methylation and sumoylation are responsible for altering the localization, binding specificity/capacity and thus the function of many RBPs (Glisovic et al., 2008). Further research is warranted to elucidate the regulation of these two RBPs at the post-transcriptional and post-translational levels during myogenesis.

Accurate timing in the expression of MRFs is an important factor in myogenesis. As stated earlier, MRFs are expressed in a distinct manner, which denotes that the myogenic program is highly detailed and co-ordinated. We have therefore determined the approximate time-period when these RBM5 and RBM10 variants/isoforms are expressed during C2C12 differentiation to gain a better insight into their function, using our experimental conditions, specifically growing the C2C12 myoblasts in GM containing 10% FBS and inducing differentiation by changing to DM containing 2% HS. Based on the expression profile, RBM5 and RBM10 show potential involvement during the early- and mid- stages but not the terminal-stage. Therefore, our results on stage-specific expression of RBM5 and RBM10 led us to explore further their importance during myogenic differentiation. These expression studies therefore enabled us to proceed with our knockdown studies to validate our conclusion regarding the stage-specific expression and to determine a possible regulatory role for these two RBPs during myogenesis.

4.3 RBM5 and RBM10 are differentially localized in differentiating C2C12 cells

Intracellular localization of RBM5 and RBM10 in the differentiating cells revealed that both RBM5 and RBM10 were localized to the nucleus in the myoblasts and, as differentiation proceeds, they were present in both the cytosol and nucleus of the differentiating myotubes. This is the first report to show the subcellular distribution of RBM5 and RBM10 in a mouse myogenic differentiating cell line. Localization studies help in predicting functions, identifying interactions with the cellular machinery and to some extent, deducing the mechanism of action. The differential localization observed for RBM5 and RBM10 suggests a potential regulatory role in biological processes. The nuclear localization during the initial-stages, and both nuclear and cytosolic detection during the mid- and late- stages of differentiation implies multiple functions potentially related to mRNA biogenesis. Specifically, nuclear and cytoplasmic localization during the later stages of differentiation, especially in the myotubes, suggests potential involvement in export of mRNA targets. Many hnRNP proteins travel between the nucleus and cytoplasm, necessitated by their involvement in multiple functions at different stages, either during transcriptional pre-mRNA packaging, and/or post-transcriptional transport (Pinol-Roma and Dreyfuss, 1993, Dreyfuss et al., 1993). Furthermore, binding of RBPs to their target mRNAs is stage-specific; binding can occur to mRNAs at different stages and in different locations (Glisovic et al., 2008). Therefore, the presence of these two RBPs in specific cellular compartments suggests RNA binding, leading to involvement in transcriptional/post-transcriptional regulation. Based on the RBM5 and RBM10 expression profiles, we speculated their functional involvement during the early- stages of differentiation. The cytosolic (sarcomeric) localization observed after differentiation induction, during the mid- and late- stages of differentiation denotes that it could be a possible mechanism to confer functional control, specifically to retain these two RBPs in the cytoplasm and to prevent their splicing activity in the nucleus.

Previously, localization studies for RBM5 in non-transformed cells were carried out in adult testis through IHC, where both nuclear and cytosolic expression was observed (O'Bryan et al., 2013). The RBM5 plant homolog, SUA, was detected in the nucleus of

developing plant embryo tissue (Sugliani et al., 2010). Our results on the differential distribution of RBM5 during differentiation are in accord with previous studies (conducted in other cell types); while most have reported a nuclear presence, some have also found cytosolic localization.

The subcellular localization of RBM10 is initially in the nucleus of the proliferating myoblasts and then becomes localized in both the nucleus and cytoplasm as the cells differentiate. This indicates that the localization is stage-specific. Only a few reports have investigated the localization pattern of RBM10 in the cell (Inoue et al., 2008, Xiao et al., 2013). RBM10 was present in both dividing and non-dividing cells, as well as in terminally differentiated cells (Inoue et al., 2008). Transcriptional and post-transcriptional states of the cell induced reversible changes in the subcellular localization of RBM10 to the nucleus. In C2C12 differentiating cells, RBM10 was detected in the nucleus in reserve cells. Reserve cells exist in a dormant state (Montarras et al., 2013). Our result is in line with previous observation that RBM10 is expressed regardless of the state of the cell (proliferating/quiescent) (Inoue et al., 2008).

The percentage of differentiated C2C12 cells ranges between 40% and 60% (Yoshida et a., 1998) and the remaining are reserve cells (Miller, 1990). Interestingly, the myogenic proteins such as MyoD and Myf5 are localized specifically in the nuclei of undifferentiated C2C12 myoblasts, but in differentiated cells were mostly present in myocytes and myotubes and only in trace amounts in the reserve cells (Yoshida et al., 1998). The detection of RBM5 and RBM10 in these reserve cells, albeit not in all of them, does place them as important RNA-binding factors necessary for adult myogenesis.

The functional relevance of these two RBPs during differentiation is further supported by this specific localization patterns in the myoblasts and in differentiating myotubes. Additionally, it does not rule out the possibility of an involvement during regenerative myogenesis when necessary because both RBM5 and RBM10 are expressed in reserve cells, thus warranting further studies of their role in tissue injury and repair.

4.4 Possible functions of RBM5 and RBM10 during myogenesis

Several lines of evidence are presented in this dissertation to support the hypothesis that Rbm5 and Rbm10 are involved in regulating myogenesis. The expression profiles of Rbm5 and Rbm10 are consistent with a potential regulatory role during the initial- and mid- stages of differentiation. The functional regulation was predominantly examined by analysing the changes in cell morphology, expression of myogenic proteins and changes in alternative splicing following down-regulation of these RBPs using siRNAs (loss-of-RBM5 and -RBM10 functions). Depleted RBM5 and RBM10 levels altered expression and alternative splicing of several targets, which affected differentiation and led to the delay in fusion, respectively, thus indicating that both RBM5 and RBM10 might be essential during myogenesis. These effects during myogenesis may be due in part to their effects on MyoG and MyHC expression, and on alternative splicing of *Dtna* and *Mef2c*.

The last few years have witnessed a plethora of studies exploring the regulation of expression and function of RBM5 and RBM10 in many different systems in order to deduce their role. RBPs functioning in cell growth, proliferation and differentiation can also be involved in tumorigenesis (Kim et al., 2009). Therefore, these two RBPs, which have a functional role in cancer cell proliferation and apoptosis, may also possess a possible role in normal muscle cell differentiation. We were able to identify a stage-specific involvement. Thus, RBM5 and RBM10 are now emerging as multi-functional proteins possessing a wide range of functions in transformed as well as non-transformed cells.

4.4.1 RBM5 and RBM10 have functional role in the myogenic program

In order to elucidate the role of RBM5 in muscle cell differentiation, we decreased the level of RBM5 in C2C12 cells using siRNA transfection. Subsequently, differentiation was induced and the changes in cell morphology were assessed. Staining with DRAQ5 (an anthroquinone), the nuclear marker that intercalates to A-T of DNA, allowed us to count all the cells present in the field of view. This method of assessing cell number correlates with other cell counting methods such as the 5-Bromo 2'-deoxyuridine (BrdU) assay with the exception that DRAQ5 intercalates to DNA at any stage of the cell cycle whereas BrdU incorporation occurs only in newly synthesized DNA.

The results indicated that in differentiated C2C12 cells (D2-D4), RBM5 KD cells had fewer nuclei than controls and were slow in differentiating. In the RBM5 KD cells, the reduction in nuclei number during differentiation could be due to death of unfused cells. Fewer cells (nuclei) led to availability of less nuclei for fusion and thus affected the myogenic fusion process. Based on previous studies, there is enough evidence to suggest a putative tumor suppressor role for RBM5 by modulating both apoptosis and cell cycle arrest (Sutherland et al., 2005). The function of RBM5 in myogenesis is different from its tumor-specific anti-proliferative function. In tumorigenesis, RBM5 inhibits cell growth, however in differentiating C2C12 cells, RBM5 depletion has an opposite effect, and cell number is drastically reduced rather than being increased.

Similarly, the function of RBM5 in differentiation is different from its pro-apoptotic role in cancer cells (Sutherland et al., 2005). In our C2C12 cell system, higher RBM5 expression during the initial days of culture indicates a possible role in apoptosis, however, in the RBM5-depleted cells there were fewer nuclei rather than the expected increase in cell number. During C2C12 differentiation, apoptosis occurs during the initial stages of differentiation (approximately between D0 to D2) and apoptosis could either promote differentiation (positive role) or could also cause the cells to die leading to a delay (negative role) (Sandri and Carraro, 1999). We have not determined directly if RBM5 depletion affects cell proliferation or apoptosis. However, our results reveal that RBM5 likely functions in a different manner in non-tumor cells (C2C12) compared to tumor cells.

In addition, C2C12 myoblasts with transiently depleted RBM5 exhibited impaired fusion into myotubes. The RBM5 KD cells had decreased MyoG as evidenced by immunoblot and reduced MyHC protein levels from confocal analysis, which shows that the decrease in the expression of these myogenic proteins may be linked to this delay in myotubes formation.

Changes in expression of many cell cycle proteins such as Ccnd1, Ccna2, Ccne2 (down-regulation) and Ccnd3 and Cdkn1a (up-regulation), occurs during the first two days of induction of differentiation (Shen et al., 2003). Between 12-24 hours after induction, C2C12 cells showed an increase (over four-fold) in expression, which demonstrates that this is the critical period for gene expression regulation during differentiation (Rajan et al., 2012). The reduction in cell number detected two days after induction of differentiation is

the downstream effect of RBM5 inhibition, indicating either a direct or indirect effect on cell cycle or apoptotic genes to be the likely mechanism by which RBM5 affects cell density during C2C12 differentiation. In addition, the antagonistic function of two other Rbm5 mRNA variants *RBM5△6* (Mourtada-Maarabouni et al., 2003) and *RBM5-AS1* (Je2 cDNA antisense fragment) (Mourtada-Maarabouni et al., 2006) in comparison to the full length *Rbm5* mRNA transcript, especially in progression of tumor growth is another likely mechanism by which this RBP could regulate the cell number during differentiation. Hence, additional mechanistic studies are required to determine the level of regulation of RBM5 during C2C12 differentiation. `

Next, we down-regulated RBM10 in C2C12 cells using siRNA. The cells were analyzed morphologically. Interestingly, unlike RBM5 KD, we observed increased nuclei number in the post-transfection phase, during which time the cells were still proliferating. Without RBM10, the cells were increasing in number compared to the control, which indicates that the effect of RBM10 during differentiation is either to control cell proliferation rate or induce apoptosis. This is in accord with the observations seen in smooth muscle cells and cancer cells wherein overexpressed RBM10 induces apoptosis and reduces proliferation (Mueller et al., 2009). RBM10 is definitely not associated with late stages but is a contributor in early-stages of differentiation. These results suggest that RBM10 possibly plays an important role in C2C12 differentiation by aiding in maintaining the necessary cell population prior to induction and additional modulation of MyHC expression.

To reiterate, the pattern of RBM5 expression is similar to that observed in cancer cells but was functionally different in normal cells. In the case of RBM10, there was a difference in expression between cancer and normal cells but functionally they were similar. Therefore, this discord in expression pattern and in function observed during differentiation highlights the importance of regulation of these two RBPs during myogenesis.

Our results show that RBM5 functions in a different manner from RBM10. Our results are similar to the results of Bechara et al. (2013) where depletion of RBM5 was anti-proliferative, and the depletion of RBM10 was proliferative. RBM5 and RBM10 possibly coordinate with regulators of cell cycle withdrawal, apoptosis and muscle-specific factors; perhaps one is needed for initiation and the other for maintenance of the myogenic

differentiation process. The presence of RRMs and other domains involved in mRNA splicing mechanisms are not only indicators of functional association, but could provide an insight into the mechanisms of action. RBM5 and RBM10 are almost 50% identical; the remaining unique regions likely cause structural differences that could contribute to unique functions and binding targets. The difference in function between RBM5 and RBM10 observed during myogenesis would support this latter statement. From our findings, we can infer that although RBM5 and RBM10 have 50% homology, it is likely that they do not have redundant function in muscle cells.

Bechara et al. (2013) have shown that RBM5/6 and 10 have specific fuctions and are antagonistic in regulating cell proliferation; this effect was mostly related to NUMB alternative splicing. The two variants generated from the inclusion/exclusion of exon 9 has distinct roles; one is involved in proliferation whereas the other enhances differentiation. This study suggests that the effect (observed phenotypically) is an indirect effect of RBM5/10 through the regulation of AS of gene targets associated with cell proliferation, apoptosis and muscle differentiation.

In order to identify the transitions that are alternatively spliced by RBPs, usually, as a first step, high throughput techniques such as microarrays (splice-sentisitive/exon-exon junctions) and RNA sequencing could be employed, which would enable identification of a large cohort of potential splicing and expression changes (Blanchette et al., 2009, Kechavarzi and Janga, 2014, Katz et al., 2010). Once splicing events are identified, they are confirmed using end-point PCR (Venables et al., 2009). There are thousands of splicing changes that occur during differentiation. In this dissertation, we directly assessed three splicing events. These three targets were chosen because (a) studies have already showed that these are alternatively spliced during differentiation (in C2C12 cells) and (b) preference for one variant over another has been suggested to have a functional association with myogenesis. For example, the integrinβ1A isoform, which is expressed in proliferating myoblasts, decreases during differentiation while integrinβ1D expression takes precedence (Belkin et al., 1996), however integrinβ1A is associated with primary myogenesis (Cachaco et al., 2003).

4.4.2 RBM5 possibly affects the myogenic program by modulating the expression of muscle specific proteins (MyoG and MyHC)

Our results allow the characterization of possible mechanisms by which RBM5 modulates differentiation. To determine whether the delay in differentiation in the RBP-depleted cells was mediated through MRFs, we analyzed MyoG, MyoD and Myf5 protein expression levels by immunoblot analysis. MyHC levels were assessed by counting the nuclei of MyHC-positive cells after immunostaining. Expression of MRFs is critical for skeletal myogenesis (Berkes and Tapscott, 2005). MyoD and Myf5 are required for specification and MyoG is required for directing the myoblasts towards muscle specific lineage and terminal differentiation (Francetic and Li, 2011). Mutations in MyoD and Myf5 does not affect normal muscle formation but leads to defective and delayed development (Rudnicki et al., 1993). Similarly, MyoG knockout mice show defective muscle formation; indeed the myocytes in MyoG null mice are not able to fuse into myotubes (Francetic and Li, 2011). MyHC is a sarcomeric terminal differentiation marker expressed along with muscle creatinine kinases, which leads to fusion of myocytes and the formation of a functional myotube (Clegg et al., 1987). In our RBM5 KD experiments, the expression of MyHC and the major muscle-specific transcription factor MyoG were down-regulated and there was no change in Myf5 and MyoD expression. The decrease in MyHC and MyoG levels in the RBM5 KDs possibly indicates a mechanistic interaction between RBM5 and these two muscle-specific proteins at the molecular level and thereby promote a delay in differentiation, fusion and maturation phenotypically. RBM5 is likely to exert its function prior to MyoG induction, which correlates with the high expression levels of RBM5 in the initial-stage of differentiation because MyoG expression occurs later, but before the terminal-stages of differentiation.

The increase in MyHC expression on D2 contributed to the increase in differentiation potential. However, the levels of MyHC decreased significantly by D3 and D4 thereafter. This increase on D2 did not likely have any downstream association with fusion or maturation.

These results provide evidence that RBM5 is one of the RBPs involved in regulating expression of muscle-specific proteins such as MyoG and MyHC during myogenesis. Our

findings also show that RBM5 is related to regulating the expression of a specific subset of MRFs in a distinctive manner.

RBM5- and 10- depleted cells were slow in differentiating as evidenced by the decrease in MyHC protein levels and significantly reduced myotubes/myofibers. Our results also indicated that RBM5 and RBM10 are probably functionally different in the myogenic differentiation program except in modulating the expression of MyHC. Overall these results indicate that RBM5 and RBM10 slows the rate of differentiation, however it does not completely prevent the myoblasts from forming myotubes. Furthermore, when both RBM5 and 10 are KD together, only the effect of RBM5 were predominant. This was evident despite the different degrees of RBM5 KD levels, i.e. depletion of minimal levels of RBM5 in C2C12 cells was enough to produce the observed phenotypic modifications.

These effects for RBM5 and/or 10 could be direct or indirect. RBM5/10 could act directly affecting cell proliferation or apoptosis to alter the timing of differentiation or act indirectly by having an effect on splicing of critical differentiation mediators that in turn affect the timing of differentiation.

4.4.3 RBM10 affects the myogenic program by modulating the alternative splicing of *Dtna*

In this study, we attempted to identify the changes in alternative splicing events promoted by these two RBMs during C2C12 differentiation and therefore looked at the exon inclusion/exclusion of *Dtna*, *Mef2c* and *Integrin*. Depletion of RBM10 in C2C12 myoblasts resulted in three specific changes. Firstly, RBM10-depleted cells showed increased proliferation. Depletion of RBM10 maintained the myoblasts in a proliferative state. The idea is that, before differentiation is induced, RBM10 is required to maintain the necessary cell population. It still remains to be elucidated whether this results from changes in apoptosis or cell proliferation. The downstream consequences of RBM10 depletion during differentiation can affect the ability to differentiate (differentiation potential), but there was no delay in fusion or maturation.

Secondly, RBM10 modulates the expression of MyHC on D3/D4. Cells with a RBM10 KD did not have an impact on myogenesis-related gene expression, especially MyoG, MyoD and Myf5, however they did decrease MyHC expression.

Thirdly, RBM10-depleted cells had decreased inclusion of exon 11 in *Dtna*, which implies that RBM10 is involved in the alternative splicing of *Dtna* by promoting inclusion of exon 11. α-dystrobrevin is a predominant muscle-related component of DGC and has a crucial role in muscular dystrophies when it is aberrantly expressed (Metzinger et al., 1997). *Dtna* knockout mice show a mild form of myopathy (Grady et al., 1999). The change in the pattern of splicing in Dtna during C2C12 myogenic differentiation has been described previously (Bland et al., 2010). During differentiation, the exon 11(+) transcript increases as the exon 11(-) transcript decreases. Therefore, involvement of RBM10 to preferentially direct splicing to one variant that is important for promoting differentiation indicates that RBM10 does indeed act as a splicing regulator. It appears that the change in splicing pattern is temporal. The limitations of this study are that the effect seen is observed in only two out of three trials and therefore requires additional biological replicates.

4.4.4 Rbm5 and10 together affect the myogenic program by modulating the alternative splicing of *Mef2cγ*

When both RBM5 and RBM10 were depleted, we observed an increase in γ exon inclusion of a key transcription factor, Mef2c on D4. The Mef2 group of transcription factors are involved in skeletal muscle and neural differentiation, and heart and bone development (Hakim et al., 2010). Mef2c is specifically associated with muscle differentiation and the formation of synapses in the brain, and is mainly regulated by alternative splicing (Zhu and Gulick, 2004). Mef2c splicing is complex, selective and is dependent on the stage of development, tissue and other specific conditions such as calcium dependence or presence of co-regulators (Zhu and Gulick, 2004). In addition, Mef2c was responsible for maintaining the C2C12 cells in the differentiated state (Bachinski et al., 2010). The γ exon of Mef2c contains sequences involved in repression of transcription and is phospho-serine dependent (Zhu and Gulick, 2004). Therefore, Mef2cγ (-) is a transcription activator, while Mef2cγ (+) is a transcription repressor. Further, Mef2cγ (-) is associated with MyoD and cdk5 activity, which are involved during the initial-stages of differentiation (Zhu and

Gulick, 2004). Furthermore, both γ exon inclusion and exclusion were present and were expressed equally in undifferentiated and differentiated P19 cells, P19CL6 cells and in adult skeletal muscle (Hakim et al., 2010). However, in the control C2C12 myoblasts, at 24 and 48 hours post-transfection and during differentiation, we observed the presence of more γ; there was more inclusion as differentiation proceeded (Appendix A-Figures A12-A17). The significant increase in exon inclusion in the RBM5+10 KDs on D4, thus, supports the idea that this alternative splicing is not necessarily involved in delaying differentiation and that the reduction in abundance of one variant possibly has downstream effects during the differentiation process. Our results indicate that both RBM5 and RBM10 together act in a synergistic/additive fashion to modulate the alternative splicing of these transcripts because neither RBM5 nor RBM10 alone favoured the generation of more *Mef2cγ* (+). Previous studies have shown that other RBPs are involved in regulating the alternative splicing of Mef2c. For instance, the PTB protein is responsible for β exon inclusion of Mef2c (Lin and Tarn, 2011). It is possible that different RBPs are needed that target different splice sites to generate many variants of Mef2c during differentiation.

4.4.5 Proposed model for regulatory role

Based on our results and previous binding/regulatory studies, a model is proposed to explain how RBM5 could regulate the delay in differentiation and how RBM10 could regulate cell proliferation before induction (Figure 4.1).

The role of RBM5 during differentiation is possibly mediated through p21 and MyoG expression and stability. RBM5 could regulate the expression of p21 because in RBM5 KDs, both cell number and fusion were affected. During C2C12 differentiation, when cell-cell contact was inhibited because of the reduction in cell density, one of the proteins that was affected is p21 (Tanaka et al., 2011). Furthermore, p21 regulates the expression of MyoG (Halevy et al., 1995). Many RBPs are involved in stabilizing mRNA. mRNA stability depends on the stage of differentiation and on the status of the differentiating cell. Importantly, the half-life of certain proteins involved in myogenesis increased as differentiation proceeded. For instance, MyoG and p21 had increased half-lives, thus were stabilized during differentiation (Figueroa et al., 2003). Another aspect of mRNA stability

is binding to 3' UTRs. Many MRFs have specific sequences (destabilizing elements) in their 3' UTR, which are either AU rich elements (AREs) or GU rich elements (GREs) (Apponi et al., 2011). These MRFs are depleted by certain decay mechanisms set up to have a tight control over differentiation. These specific sequence elements are targets for many RBPs. For example, HuR protein, which is a RBP and a splicing regulator, binds with the 3'UTR of *Myogenin* mRNA (van der Giessen et al., 2003). The Hu family of proteins binds to AU rich regions in 3' UTRs and are involved in degrading Myogenin. Hence, we speculate that RBM5 is another RBP involved in regulating p21 expression and/or stability and *Myogenin* mRNA stability.

The effect of RBM10 during proliferation is possibly mediated through Notch signalling. The Notch pathway is important for tissue development, maintenance and repair with significant involvement in skeletal muscle (Nye et al., 1994). When Notch is activated, there is inhibition of differentiation especially through the NCID factor and via down-regulation of MyoG and Myosin light chain expression (Luo et al., 2005). Another important component of this Notch-mediated signalling pathway during differentiation is Mef2c. Notch inhibits Mef2c and its activation. Mef2c interacts with MAML1 (Mastermind-like protein 1) and is responsible for crosstalk between Notch and Mef2 during differentiation (Shen et al., 2006). Mef2 acts as a positive regulator and is involved in regulating the expression of MyoG and other transcription factors such as MyoD. During muscle injury, Notch activates satellite cell proliferation, especially during the early phase to direct the quiescent satellite cells to generate progenitor cells (Luo et al., 2005). When a sufficient progenitor population is reached, the Notch inhibitor NUMB is activated to produce regenerated muscle tissue. During myogenesis, isoform specific regulation of NUMB occurs (Beres et al., 2011). A recent study identified that Rbm5, 6 and 10 were responsible for NUMB alternative splicing in cancer cells (Bechara et al., 2013). The RBM10-depleted cells showed increased proliferative capacity and regulated alternative splicing of exon 9 in *NUMB* (induced exon inclusion). We speculate that the effect of RBM10 in regulating the initial phase of cell proliferation before differentiation is mediated through the alternative splicing of NUMB and the related downstream effects such as MyHC expression associated with the involvement of the Notch signalling pathway.

The effect of RBM5 and RBM10 combined mechanism of action is possibly mediated through alternative splicing of Mef2c. *Mef2cγ* (+) transcript is a transrepressor. Regulated transcription is required during differentiation, and multiple transcription activators and repressors are involved during the entire myogenic differentiation process. Based on the increase in *Mef2cγ* (+) inclusion on D4 observed in our experiment, we speculate that there are downstream effects associated with the transcription repression of Mef2c target genes such as structural proteins, enzymes, transporters and stress signalling molecules (Zhu and Gulick., 2004).

4.4.6 siRNA specificity

Because RBM5 and RBM10 levels were already high during the initial stages of differentiation, in order to functionally characterize their involvement during myogenesis, we depleted the expression of endogenous RBM5 and RBM10 in myoblasts using siRNAs. We believe that this is an effective approach rather than exogenously overexpressing the proteins. KD reduces the endogenous levels of the RBPs while overexpression would create super-physiological levels.

siRNA directed towards RBM5 and RBM10 was effective at lowering the levels of target mRNA because of the different effects such as the effect of RBM5 on fusion and maturation index and the effect of RBM10 on cell number before induction, were observed between the RBM5 and RBM10 KDs. This indicates that the siRNAs used were target-specific.

Although RBM5 depletion in some of the KD experiments was only close to 40 -50%, the observed inhibition of myogenic differentiation process indicates that the C2C12 differentiating cells need only a minimal amount (a threshold) to proceed with differentiation. In addition, phenotypic changes did not correlate directly to the level of KD because either the relationship is not linear or because of off-target non-specific effects. The latter is not likely the case because the effects of RBM5 and RBM10 on cell proliferation are entirely different.

During C2C12 differentiation, the transition from cell proliferation (prior to induction) to the progression of differentiation is a highly governed process. Maintaining the adequate number of cells during proliferation is crucial because proper cell-to-cell contact is required for fusion and maturation. Factors such as passage number, initial plating density, confluence of the cells at induction (serum deprivation) and transfection could be deteriments to differention, hence could be limiting factors in the KD experiments. Although, passage number is not a limiting factor in the current study; we know that plating density-dependant variations were observed in two of the KD trials. Transient KD meant that RBM5/10 expression was restored during differentiation, which could have some effect on cell behaviour. Therefore, these limitations should be considered while performing the KD experiments.

Transient transfection experiments are practically quick and easy way to characterize the function of RBM5/10 in the muscle system. However, our transient KD studies are limited in their ability to identify the potential effect of both these RBPs in differentiation because of the turn-over rate. The siRNA approach creates only a short-term reduction (restoration seen by D4 in our experiments). The entire C2C12 differentiation process can take up to 8 to 10 days and therefore in order to fully characterize their role in differentiation future experiments might utilize stable transfectants. The potential off-target effects if any, should be verified, either by performing "rescue" approach of the target gene by over expressing to validate the target-specific effect or use more than one siRNA to target different areas of the gene. Inclusion of negative controls, not only scrambled siRNA control but a combination of mismatched and scrambled siRNA, untransfected control and mock transfection controls in future experiments will increase the confidence in the results obtained.

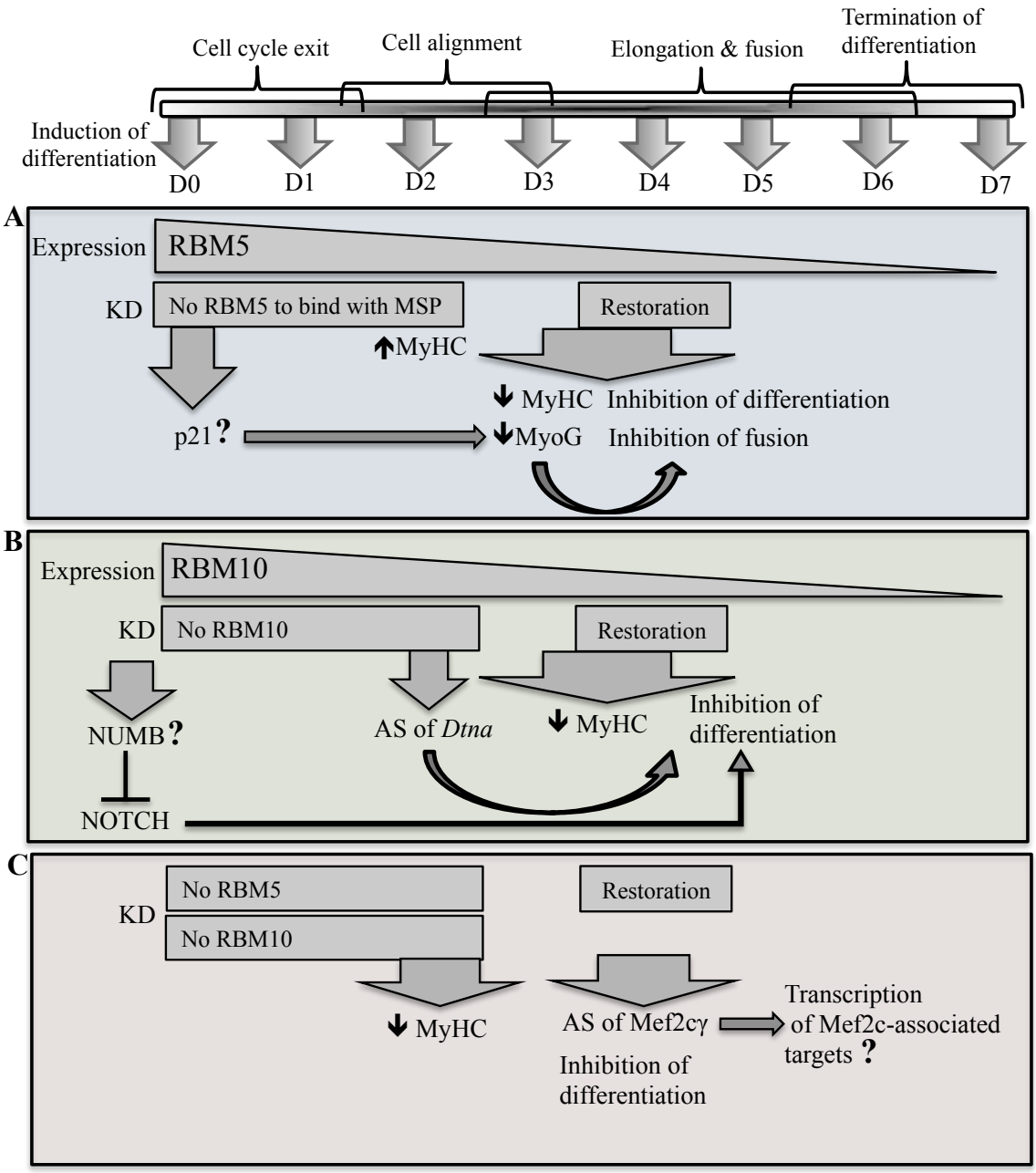

Figure 4.1 Proposed model of RBM5 and RBM10 mechanism of regulation during C2C12 differentiation. Model of regulation via p21 for RBM5 or NUMB for RBM10 or Mef2c for both RBM5 and 10 during differentiation. Expression of RBM5 and RBM10 is high during the initial-stages of differentiation indicating functional relevance at this stage. **A**) Depletion of RBM5 possibly affects p21, which has a direct effect on MyoG expression, thus causing the delay in fusion. **B**) Depletion of RBM10 possibly affects alternative splicing (AS) of NUMB during proliferation thereby targeting the NOTCH downstream pathways, along with AS of Dtna, both together causing the delay in differentiation. **C**) Depletion of RBM5 and 10 affects Mef2c, thus possibly affecting transcription of Mef2c-associated target factors such as structural proteins, enzymes, stress-signaling molecules and transporters.

4.5 Conclusion

The expression profile of Rbm5 and Rbm10 suggest a potential regulatory role during the initial phase of differentiation. This thesis demonstrates for the first time the role of the two RBPs, RBM5 and RBM10, in myogenic differentiation; in particular the association of RBM5, a putative tumor suppressor, as a mediator of delayed differentiation and inhibition of fusion through regulation of MyoG and MyHC expression, likely by stabilizing *Myogenin* or *MyHC* mRNA. In addition, we also show an association of RBM10 as a positive regulator of differentiation only, through modulating MyHC expression and as well regulating alternative splicing of *Dtna* mRNA. We further suggest that though both have specific and distinct functions, they possess some overlapping functions in differentiation and fusion by modulating the alternative splicing of *Mef2cγ* mRNA, amongst many others that still remain to be uncovered.

Given the previously identified role in cancer, especially in lung adenocarcinomas (RBM10) and NSCLCs (RBM5), this report on the role of RBM5 and RBM10 in normal muscle cell development hence provides a starting point for future functional characterization of these RBPs in muscle. This study has enabled us to determine the stage at which RBM5/10 exert their functions, however it will be of interest to carry out a detailed analysis on how precisely the regulation occurs, to identify the signalling pathways, binding partners and additional mRNA targets associated with these RBPs in differentiation. For instance, using this model system, we can carry out binding studies using gel-shift experiments to determine if RBM5 bind to the 3'UTRs of *Myogenin* and *MyHC* mRNA, and whether these interactions are direct or indirect. It will be of interest to determine the RNA-binding capacity of RBM5 and RBM10 using techniques such as (a) RNA-binding protein immunoprecipitation-microarray profiling (RIP-Chip) to identify RNAs that interact with these two RBPs (b) PAR-CLIP to identify binding sites of these two proteins and (c) Glutathione-S transferase (GST)-pull down assays to identify the binding partners. It would not be surprising to find additional target mRNAs that are alternatively spliced by these two RBPs during myogenesis, and furthermore, one would not find the same targets that were identified in a different system because there could be

tissue-specific regulation (O'Bryan et al., 2013). Future work can focus on identifying if it is cell proliferation or cell cycle arrest by which RBM10 perturbs the cell population during the proliferative stage before the myoblasts start differentiating, especially by performing BrdU incorporation assays to assess DNA synthesis or mitosis. Additional experiments are needed to determine if *NUMB* mRNA is alternatively spliced and the associated downstream effects on the Notch pathway when RBM10 is depleted. Similarly, if p21 levels are affected and to determine whether p21- dependent or independent mechanisms regulate MyoG expression when RBM5 is depleted. The physiological relevance of alternative splicing of Mef2c during differentiation in the RBM5+10 KDs needs further characterization.

Many RBPs are implicated in human diseases; hence it would also be worthwhile to explore RBM5 and RBM10 involvement in muscular atrophies and rhabdomyosarcoma. *In vivo* experiments using conditional knockout mice to look at the importance of these two in myogenesis could then be carried out in the long run.

RBM5 shares high sequence similarity with RBM6 and RBM10, with some overlapping functions (Sutherland et al., 2005). For example, when RBM5, RBM6 and RBM10 were depleted at the same time, they affected cell proliferation via alternatively splicing NUMB (Bechara et al., 2013). RBM6 is located adjacent to RBM5 on 3p21and also belongs to the homozygously deleted region in lung cancers. Expression patterns and *in vitro* RNA-binding studies show that RBM5, RBM10 and RBM6 are evolutionarily conserved RBPs (Drabkin et al., 1999). Therefore, there is a possibility of overlapping functions of all three during differentiation, so future studies can incorporate KD of all three RBPs to determine the combined regulatory role.

In summary, our findings provide a starting point to assess the role of these two RBPs in skeletal muscle differentiation. RBPs are key components in many cellular processes. With the recent increase in the identification of the multitude of RBPs, our findings are timely and provide a new insight into the functional involvement of these two RBPs in myogenesis.

REFERENCES

'T HOEN, P. A., HIRSCH, M., DE MEIJER, E. J., DE MENEZES, R. X., VAN OMMEN, G. J. & DEN DUNNEN, J. T. 2011. mRNA degradation controls differentiation state-dependent differences in transcript and splice variant abundance. *Nucleic Acids Res,* 39**,** 556-566.

ABMAYR, S. M. & PAVLATH, G. K. 2012. Myoblast fusion: lessons from flies and mice. *Development,* 139**,** 641-656.

AGAFONOV, D. E., DECKERT, J., WOLF, E., ODENWALDER, P., BESSONOV, S., WILL, C. L., URLAUB, H. & LUHRMANN, R. 2011. Semiquantitative proteomic analysis of the human spliceosome via a novel two-dimensional gel electrophoresis method. *Mol Cell Biol,* 31**,** 2667-2682.

APPONI, L. H., CORBETT, A. H. & PAVLATH, G. K. 2011. RNA-binding proteins and gene regulation in myogenesis. *Trends Pharmacol Sci,* 32**,** 652-658.

BABU, G. J., WARSHAW, D. M. & PERIASAMY, M. 2000. Smooth muscle myosin heavy chain isoforms and their role in muscle physiology. *Microsc Res Tech,* 50**,** 532-40.

BACHINSKI, L. L., SIRITO, M., BOHME, M., BAGGERLY, K. A., UDD, B. & KRAHE, R. 2010. Altered MEF2 isoforms in myotonic dystrophy and other neuromuscular disorders. *Muscle Nerve,* 42**,** 856-63.

BADER, D., MASAKI, T. & FISCHMAN, D. A. 1982. Immunochemical analysis of myosin heavy chain during avian myogenesis in vivo and in vitro. *J Cell Biol,* 95**,** 763-770.

BECHARA, E. G., SEBESTYEN, E., BERNARDIS, I., EYRAS, E. & VALCARCEL, J. 2013. RBM5, 6, and 10 Differentially Regulate NUMB Alternative Splicing to Control Cancer Cell Proliferation. *Mol Cell,* 52**,** 720-733.

BELKIN, A. M., ZHIDKOVA, N. I., BALZAC, F., ALTRUDA, F., TOMATIS, D., MAIER, A., TARONE, G., KOTELIANSKY, V. E. & BURRIDGE, K. 1996. Beta 1D integrin displaces the beta 1A isoform in striated muscles: localization at junctional structures and signaling potential in nonmuscle cells. *J Cell Biol,* 132**,** 211-226.

BENTZINGER, C. F., WANG, Y. X. & RUDNICKI, M. A. 2012. Building Muscle: Molecular Regulation of Myogenesis. *Cold Spring Harbor Perspectives in Biology,* 4.

BERES, B. J., GEORGE, R., LOUGHER, E. J., BARTON, M., VERRELLI, B. C., MCGLADE, C. J., RAWLS, J. A. & WILSON-RAWLS, J. 2011. Numb regulates Notch1, but not Notch3, during myogenesis. *Mech Dev,* 128**,** 247-57.

BERKES, C. A. & TAPSCOTT, S. J. 2005. MyoD and the transcriptional control of myogenesis. *Semin Cell Dev Biol,* 16**,** 585-95.

BERRIDGE, M. J. 2007. *Cell Signalling Biology*, Portland Press.

BHATTACHARYA, S., GIORDANO, T., BREWER, G. & MALTER, J. S. 1999. Identification of AUF-1 ligands reveals vast diversity of early response gene mRNAs. *Nucleic Acids Res,* 27**,** 1464-72.

BLACK, B. L. & OLSON, E. N. 1998. Transcriptional control of muscle development by myocyte enhancer factor-2 (MEF2) proteins. *Annu. Rev Cell Dev. Biol,* 14**,** 167-196.

BLAIS, A., TSIKITIS, M., COSTA-ALVEAR, D., SHARAN, R., KLUGER, Y. & DYNLACHT, B. D. 2005. An initial blueprint for myogenic differentiation. *Genes Dev,* 19**,** 553-569.

BLANCHETTE, M., GREEN, R. E., MACARTHUR, S., BROOKS, A. N., BRENNER, S. E., EISEN, M. B. & RIO, D. C. 2009. Genome-wide analysis of alternative pre-mRNA splicing and RNA-binding specificities of the Drosophila hnRNP A/B family members. *Mol. Cell,* 33**,** 438-449.

BLAND, C. S., WANG, E. T., VU, A., DAVID, M. P., CASTLE, J. C., JOHNSON, J. M., BURGE, C. B. & COOPER, T. A. 2010. Global regulation of alternative splicing during myogenic differentiation. *Nucleic Acids Res,* 38**,** 7651-7664.

BLAU, H. M., PAVLATH, G. K., HARDEMAN, E. C., CHIU, C. P., SILBERSTEIN, L., WEBSTER, S. G., MILLER, S. C. & WEBSTER, C. 1985. Plasticity of the differentiated state. *Science,* 230**,** 758-66.

BONNAL, S., MARTINEZ, C., FORCH, P., BACHI, A., WILM, M. & VALCARCEL, J. 2008. RBM5/Luca-15/H37 regulates Fas alternative splice site pairing after exon definition. *Mol Cell,* 32**,** 81-95.

BORYCKI, A. G. & EMERSON, C. P. 1997. Muscle determination: another key player in myogenesis? *Curr Biol,* 7**,** R620-R623.

BROSSEAU, J. P., LUCIER, J. F., LAPOINTE, E., DURAND, M., GENDRON, D., GERVAIS-BIRD, J., TREMBLAY, K., PERREAULT, J. P. & ELELA, S. A. 2010. High-throughput quantification of splicing isoforms. *RNA,* 16**,** 442-9.

BUCKINGHAM, M. 2001. Skeletal muscle formation in vertebrates. *Curr Opin Genet Dev,* 11**,** 440-8.

BUCKINGHAM, M. 2002. 15 The formation of skeletal muscle: from somite to hand. *J Anat,* 201**,** 421.

BUCKINGHAM, M. 2006. Myogenic progenitor cells and skeletal myogenesis in vertebrates. *Curr Opin Genet Dev,* 16**,** 525-32.

BUCKINGHAM, M., BAJARD, L., CHANG, T., DAUBAS, P., HADCHOUEL, J., MEILHAC, S., MONTARRAS, D., ROCANCOURT, D. & RELAIX, F. 2003. The formation of skeletal muscle: from somite to limb. *J Anat,* 202**,** 59-68.

BUCKINGHAM, M. & RIGBY, P. W. 2014. Gene regulatory networks and transcriptional mechanisms that control myogenesis. *Dev Cell,* 28**,** 225-38.

BURATTINI, S., FERRI, P., BATTISTELLI, M., CURCI, R., LUCHETTI, F. & FALCIERI, E. 2004. C2C12 murine myoblasts as a model of skeletal muscle development: morpho-functional characterization. *Eur. J Histochem,* 48**,** 223-233.

BURRY, R. W. 2011. Controls for immunocytochemistry: an update. *J Histochem. Cytochem,* 59**,** 6-12.

CACHACO, A. S., PEREIRA, C. S., PARDAL, R. G., BAJANCA, F. & THORSTEINSDOTTIR, S. 2005. Integrin repertoire on myogenic cells changes during the course of primary myogenesis in the mouse. *Dev Dyn,* 232**,** 1069-1078.

CACHACO, A. S., SM, C. D. S. L., KUIKMAN, I., BAJANCA, F., ABE, K., BAUDOIN, C., SONNENBERG, A., MUMMERY, C. L. & THORSTEINSDOTTIR, S. 2003. Knock-in of integrin beta 1D affects primary but not secondary myogenesis in mice. *Development,* 130**,** 1659-1671.

CASADEI, L., VALLORANI, L., GIOACCHINI, A. M., GUESCINI, M., BURATTINI, S., D'EMILIO, A., BIAGIOTTI, L., FALCIERI, E. & STOCCHI, V. 2009. Proteomics-based investigation in C2C12 myoblast differentiation. *Eur J Histochem,* 53**,** 261-268.

CASTELLO, A., FISCHER, B., EICHELBAUM, K., HOROS, R., BECKMANN, B. M., STREIN, C., DAVEY, N. E., HUMPHREYS, D. T., PREISS, T., STEINMETZ, L. M., KRIJGSVELD, J. & HENTZE, M. W. 2012. Insights into RNA biology from an atlas of mammalian mRNA-binding proteins. *Cell,* 149**,** 1393-1406.

CHAN, C. Y. X., MASUI, O., KRAKOVSKA, O., BELOZEROV, V. E., VOISIN, S., GHANNY, S., CHEN, J., MOYEZ, D., ZHU, P., EVANS, K. R., MCDERMOTT, J. C. & SIU, K. W. M. 2011. Identification of Differentially Regulated Secretome Components During Skeletal Myogenesis. *Molecular & Cellular Proteomics,* 10.

CHANG, N. C. & RUDNICKI, M. A. 2014. Satellite cells: the architects of skeletal muscle. *Curr Top Dev Biol,* 107**,** 161-81.

CHARGE, S. B. & RUDNICKI, M. A. 2004. Cellular and molecular regulation of muscle regeneration. *Physiol Rev,* 84**,** 209-238.

CHARRASSE, S., MERIANE, M., COMUNALE, F., BLANGY, A. & GAUTHIER-ROUVIERE, C. 2002. N-cadherin-dependent cell-cell contact regulates Rho GTPases and beta-catenin localization in mouse C2C12 myoblasts. *J. Cell Biol,* 158**,** 953-965.

CHEN, L. & ZHENG, S. 2009. Studying alternative splicing regulatory networks through partial correlation analysis. *Genome Biol,* 10**,** R3.

CLEGG, C. H., LINKHART, T. A., OLWIN, B. B. & HAUSCHKA, S. D. 1987. Growth factor control of skeletal muscle differentiation: commitment to terminal differentiation occurs in G1 phase and is repressed by fibroblast growth factor. *J Cell Biol,* 105**,** 949-956.

COLEGROVE-OTERO, L. J., MINSHALL, N. & STANDART, N. 2005. RNA-binding proteins in early development. *Crit Rev Biochem Mol. Biol,* 40**,** 21-73.

CONBOY, I. M. & RANDO, T. A. 2002. The regulation of Notch signaling controls satellite cell activation and cell fate determination in postnatal myogenesis. *Dev Cell,* 3**,** 397-409.

DEATO, M. D. & TJIAN, R. 2007. Switching of the core transcription machinery during myogenesis. *Genes Dev,* 21**,** 2137-2149.

DEDIEU, S., MAZERES, G., COTTIN, P. & BRUSTIS, J. J. 2002. Involvement of myogenic regulator factors during fusion in the cell line C2C12. *Int. J. Dev. Biol,* 46**,** 235-241.

DEDKOV, E. I., KOSTROMINOVA, T. Y., BORISOV, A. B. & CARLSON, B. M. 2003. MyoD and myogenin protein expression in skeletal muscles of senile rats. *Cell Tissue Res,* 311**,** 401-16.

DMITRIEV, P., BARAT, A., POLESSKAYA, A., O'CONNELL, M. J., ROBERT, T., DESSEN, P., WALSH, T. A., LAZAR, V., TURKI, A., CARNAC, G., LAOUDJ-CHENIVESSE, D., LIPINSKI, M. & VASSETZKY, Y. S. 2013. Simultaneous miRNA and mRNA transcriptome profiling of human myoblasts reveals a novel set of myogenic differentiation-associated miRNAs and their target genes. *BMC Genomics,* 14**,** 265.

DODOU, E., XU, S. M. & BLACK, B. L. 2003. mef2c is activated directly by myogenic basic helix-loop-helix proteins during skeletal muscle development in vivo. *Mech Dev,* 120**,** 1021-32.

DRABKIN, H. A., WEST, J. D., HOTFILDER, M., HENG, Y. M., ERICKSON, P., CALVO, R., DALMAU, J., GEMMILL, R. M. & SABLITZKY, F. 1999. DEF-

3(g16/NY-LU-12), an RNA binding protein from the 3p21.3 homozygous deletion region in SCLC. *Oncogene,* 18**,** 2589-2597.

DREYFUSS, G., KIM, V. N. & KATAOKA, N. 2002. Messenger-RNA-binding proteins and the messages they carry. *Nat Rev. Mol. Cell Biol,* 3**,** 195-205.

DREYFUSS, G., MATUNIS, M. J., PINOL-ROMA, S. & BURD, C. G. 1993. hnRNP proteins and the biogenesis of mRNA. *Annu. Rev. Biochem,* 62**,** 289-321.

EDAMATSU, H., KAZIRO, Y. & ITOH, H. 2000. LUCA15, a putative tumour suppressor gene encoding an RNA-binding nuclear protein, is down-regulated in ras-transformed Rat-1 cells. *Genes Cells,* 5**,** 849-858.

EDMONDSON, D. G., LYONS, G. E., MARTIN, J. F. & OLSON, E. N. 1994. Mef2 gene expression marks the cardiac and skeletal muscle lineages during mouse embryogenesis. *Development,* 120**,** 1251-1263.

EHMSEN, J., POON, E. & DAVIES, K. 2002. The dystrophin-associated protein complex. *Journal of Cell Science,* 115**,** 2801-2803.

EXETER, D. & CONNELL, D. A. 2010. Skeletal muscle: functional anatomy and pathophysiology. *Semin. Musculoskelet. Radiol,* 14**,** 97-105.

FARALLI, H. & DILWORTH, F. J. 2012. Turning on myogenin in muscle: a paradigm for understanding mechanisms of tissue-specific gene expression. *Comp Funct. Genomics,* 2012**,** 836374.

FAVREAU, C., HIGUET, D., COURVALIN, J. C. & BUENDIA, B. 2004. Expression of a mutant lamin A that causes Emery-Dreifuss muscular dystrophy inhibits in vitro differentiation of C2C12 myoblasts. *Mol Cell Biol,* 24**,** 1481-92.

FERNANDO, P., KELLY, J. F., BALAZSI, K., SLACK, R. S. & MEGENEY, L. A. 2002. Caspase 3 activity is required for skeletal muscle differentiation. *Proc. Natl. Acad. Sci. U. S. A,* 99**,** 11025-11030.

FERRI, P., BARBIERI, E., BURATTINI, S., GUESCINI, M., D'EMILIO, A., BIAGIOTTI, L., DEL, G. P., DE, L. A., STOCCHI, V. & FALCIERI, E. 2009. Expression and subcellular localization of myogenic regulatory factors during the differentiation of skeletal muscle C2C12 myoblasts. *J Cell Biochem,* 108**,** 1302-1317.

FIGUEROA, A., CUADRADO, A., FAN, J., ATASOY, U., MUSCAT, G. E., MUNOZ-CANOVES, P., GOROSPE, M. & MUNOZ, A. 2003. Role of HuR in skeletal myogenesis through coordinate regulation of muscle differentiation genes. *Mol Cell Biol,* 23**,** 4991-5004.

FRANCETIC, T. & LI, Q. 2011. Skeletal myogenesis and Myf5 activation. *Transcription,* 2**,** 109-114.

FREITAS, N. & CUNHA, C. 2009. Mechanisms and signals for the nuclear import of proteins. *Curr. Genomics,* 10**,** 550-557.

FURUKAWA, T., KUBOKI, Y., TANJI, E., YOSHIDA, S., HATORI, T., YAMAMOTO, M., SHIBATA, N., SHIMIZU, K., KAMATANI, N. & SHIRATORI, K. 2011. Whole-exome sequencing uncovers frequent GNAS mutations in intraductal papillary mucinous neoplasms of the pancreas. *Sci Rep,* 1**,** 161.

FUSHIMI, K., RAY, P., KAR, A., WANG, L., SUTHERLAND, L. C. & WU, J. Y. 2008. Up-regulation of the proapoptotic caspase 2 splicing isoform by a candidate tumor suppressor, RBM5. *Proc. Natl Acad Sci U. S. A,* 105**,** 15708-15713.

GARCIA-BLANCO, M. A., BARANIAK, A. P. & LASDA, E. L. 2004. Alternative splicing in disease and therapy. *Nat Biotechnol,* 22**,** 535-46.

GE, Y. & CHEN, J. 2011. MicroRNAs in skeletal myogenesis. *Cell Cycle,* 10**,** 441-8.

GEIGL, J. B., LANGER, S., BARWISCH, S., PFLEGHAAR, K., LEDERER, G. & SPEICHER, M. R. 2004. Analysis of gene expression patterns and chromosomal changes associated with aging. *Cancer Res,* 64**,** 8550-8557.

GLISOVIC, T., BACHORIK, J. L., YONG, J. & DREYFUSS, G. 2008. RNA-binding proteins and post-transcriptional gene regulation. *FEBS Lett,* 582**,** 1977-1986.

GRADY, R. M., GRANGE, R. W., LAU, K. S., MAIMONE, M. M., NICHOL, M. C., STULL, J. T. & SANES, J. R. 1999. Role for alpha-dystrobrevin in the pathogenesis of dystrophin-dependent muscular dystrophies. *Nat Cell Biol,* 1**,** 215-220.

GREENBAUM, D., COLANGELO, C., WILLIAMS, K. & GERSTEIN, M. 2003. Comparing protein abundance and mRNA expression levels on a genomic scale. *Genome Biol,* 4**,** 117.

GRIPP, K. W., HOPKINS, E., JOHNSTON, J. J., KRAUSE, C., DOBYNS, W. B. & BIESECKER, L. G. 2011. Long-term survival in TARP syndrome and confirmation of RBM10 as the disease-causing gene. *Am. J. Med. Genet. A,* 155A**,** 2516-2520.

GUNNING, P. & HARDEMAN, E. 1991. Multiple mechanisms regulate muscle fiber diversity. *FASEB J,* 5**,** 3064-3070.

GUO, K., WANG, J., ANDRES, V., SMITH, R. C. & WALSH, K. 1995. MyoD-induced expression of p21 inhibits cyclin-dependent kinase activity upon myocyte terminal differentiation. *Mol Cell Biol,* 15**,** 3823-3829.

GUPTA, J. 2006. *Nuclear speckle localization of RNA binding motif protein 5: an immediate early gene up-regulated by vascular endothelial growth factor.* Ph.D, University of Maryland.

HAKIM, N. H., KOUNISHI, T., ALAM, A. H., TSUKAHARA, T. & SUZUKI, H. 2010. Alternative splicing of Mef2c promoted by Fox-1 during neural differentiation in P19 cells. *Genes Cells,* 15**,** 255-267.

HALEVY, O., NOVITCH, B. G., SPICER, D. B., SKAPEK, S. X., RHEE, J., HANNON, G. J., BEACH, D. & LASSAR, A. B. 1995. Correlation of terminal cell cycle arrest of skeletal muscle with induction of p21 by MyoD. *Science,* 267**,** 1018-1021.

HAWKE, T. J. & GARRY, D. J. 2001. Myogenic satellite cells: physiology to molecular biology. *J Appl. Physiol (1985.),* 91**,** 534-551.

HEYWOOD, S. M., THIBAULT, M. C. & SIEGEL, E. 1983. Control of gene expression in muscle development. *Cell Muscle Motil,* 3**,** 157-93.

HINMAN, M. N. & LOU, H. 2008. Diverse molecular functions of Hu proteins. *Cell Mol. Life Sci,* 65**,** 3168-3181.

IMIELINSKI, M., BERGER, A. H., HAMMERMAN, P. S., HERNANDEZ, B., PUGH, T. J., HODIS, E., CHO, J., SUH, J., CAPELLETTI, M., SIVACHENKO, A., SOUGNEZ, C., AUCLAIR, D., LAWRENCE, M. S., STOJANOV, P., CIBULSKIS, K., CHOI, K., DE, W. L., SHARIFNIA, T., BROOKS, A., GREULICH, H., BANERJI, S., ZANDER, T., SEIDEL, D., LEENDERS, F., ANSEN, S., LUDWIG, C., ENGEL-RIEDEL, W., STOELBEN, E., WOLF, J., GOPARJU, C., THOMPSON, K., WINCKLER, W., KWIATKOWSKI, D., JOHNSON, B. E., JANNE, P. A., MILLER, V. A., PAO, W., TRAVIS, W. D., PASS, H. I., GABRIEL, S. B., LANDER, E. S., THOMAS, R. K., GARRAWAY, L. A., GETZ, G. & MEYERSON, M. 2012. Mapping the hallmarks of lung adenocarcinoma with massively parallel sequencing. *Cell,* 150**,** 1107-1120.

INOUE, A., TAKAHASHI, K. P., KIMURA, M., WATANABE, T. & MORISAWA, S. 1996. Molecular cloning of a RNA binding protein, S1-1. *Nucleic Acids Res,* 24**,** 2990-2997.

INOUE, A., TSUGAWA, K., TOKUNAGA, K., TAKAHASHI, K. P., UNI, S., KIMURA, M., NISHIO, K., YAMAMOTO, N., HONDA, K. I., WATANABE, T., YAMANE, H. & TANI, T. 2008. S1-1 nuclear domains: characterization and dynamics as a function of transcriptional activity. *Biol Cell*.

INOUE, Y. 2013. RBM10 in complete hydatidiform mole: cytoplasmic occurrence of its 50 kDa polypeptide. *International Journal of Reproduction, Contraception, Obstetrics and Gynecology,* 2**,** 114-118.

ISHIBASHI, J., PERRY, R. L., ASAKURA, A. & RUDNICKI, M. A. 2005. MyoD induces myogenic differentiation through cooperation of its NH2- and COOH-terminal regions. *J Cell Biol,* 171**,** 471-82.

IWASAKI, K., HAYASHI, K., FUJIOKA, T. & SOBUE, K. 2008. Rho/Rho-associated kinase signal regulates myogenic differentiation via myocardin-related transcription

factor-A/Smad-dependent transcription of the Id3 gene. *J Biol Chem,* 283**,** 21230-21241.

JAMES, C. G., ULICI, V., TUCKERMANN, J., UNDERHILL, T. M. & BEIER, F. 2007. Expression profiling of Dexamethasone-treated primary chondrocytes identifies targets of glucocorticoid signalling in endochondral bone development. *BMC Genomics,* 8**,** 205.

JIN, D., HIDAKA, K., SHIRAI, M. & MORISAKI, T. 2010. RNA-binding motif protein 24 regulates myogenin expression and promotes myogenic differentiation. *Genes Cells,* 15**,** 1158-1167.

JIN, W., NIU, Z., XU, D. & LI, X. 2012. RBM5 promotes exon 4 skipping of AID pre-mRNA by competing with the binding of U2AF65 to the polypyrimidine tract. *FEBS Lett,* 586**,** 3852-3857.

JOHNSTON, J. J., TEER, J. K., CHERUKURI, P. F., HANSEN, N. F., LOFTUS, S. K., CHONG, K., MULLIKIN, J. C. & BIESECKER, L. G. 2010. Massively parallel sequencing of exons on the X chromosome identifies RBM10 as the gene that causes a syndromic form of cleft palate. *Am J Hum. Genet,* 86**,** 743-748.

KABLAR, B., KRASTEL, K., YING, C., ASAKURA, A., TAPSCOTT, S. J. & RUDNICKI, M. A. 1997. MyoD and Myf-5 differentially regulate the development of limb versus trunk skeletal muscle. *Development,* 124**,** 4729-4738.

KASSAR-DUCHOSSOY, L., GAYRAUD-MOREL, B., GOMES, D., ROCANCOURT, D., BUCKINGHAM, M., SHININ, V. & TAJBAKHSH, S. 2004. Mrf4 determines skeletal muscle identity in Myf5:Myod double-mutant mice. *Nature,* 431**,** 466-471.

KATZ, Y., WANG, E. T., AIROLDI, E. M. & BURGE, C. B. 2010. Analysis and design of RNA sequencing experiments for identifying isoform regulation. *Nat Methods,* 7**,** 1009-15.

KECHAVARZI, B. & JANGA, S. C. 2014. Dissecting the expression landscape of RNA-binding proteins in human cancers. *Genome Biol,* 15**,** R14.

KIM, M. Y., HUR, J. & JEONG, S. 2009. Emerging roles of RNA and RNA-binding protein network in cancer cells. *BMB. Rep,* 42**,** 125-130.

KIM, Y. S., HWAN, J. D., BAE, S., BAE, D. H. & SHICK, W. A. 2010. Identification of differentially expressed genes using an annealing control primer system in stage III serous ovarian carcinoma. *BMC Cancer,* 10**,** 576.

KISHORE, S., LUBER, S. & ZAVOLAN, M. 2010. Deciphering the role of RNA-binding proteins in the post-transcriptional control of gene expression. *Brief. Funct. Genomics,* 9**,** 391-404.

KNIGHT, J. D. & KOTHARY, R. 2011. The myogenic kinome: protein kinases critical to mammalian skeletal myogenesis. *Skelet. Muscle,* 1**,** 29.

KOBAYASHI, T., ISHIDA, J., MUSASHI, M., OTA, S., YOSHIDA, T., SHIMIZU, Y., CHUMA, M., KAWAKAMI, H., ASAKA, M., TANAKA, J., IMAMURA, M., KOBAYASHI, M., ITOH, H., EDAMATSU, H., SUTHERLAND, L. C. & BRACHMANN, R. K. 2011. p53 transactivation is involved in the antiproliferative activity of the putative tumor suppressor RBM5. *Int J Cancer,* 128**,** 304-318.

KOPAN, R., NYE, J. S. & WEINTRAUB, H. 1994. The intracellular domain of mouse Notch: a constitutively activated repressor of myogenesis directed at the basic helix-loop-helix region of MyoD. *Development,* 120**,** 2385-2396.

LANGE, A., MILLS, R. E., LANGE, C. J., STEWART, M., DEVINE, S. E. & CORBETT, A. H. 2007. Classical nuclear localization signals: definition, function, and interaction with importin alpha. *J. Biol. Chem,* 282**,** 5101-5105.

LARIONOV, A., KRAUSE, A. & MILLER, W. 2005. A standard curve based method for relative real time PCR data processing. *BMC Bioinformatics,* 6**,** 62.

LEE, M. H. & SCHEDL, T. 2006. RNA-binding proteins. *WormBook***,** 1-13.

LEUNG, R. K. & WHITTAKER, P. A. 2005. RNA interference: from gene silencing to gene-specific therapeutics. *Pharmacol Ther,* 107**,** 222-39.

LI, H. & BINGHAM, P. M. 1991. Arginine/serine-rich domains of the su(wa) and tra RNA processing regulators target proteins to a subnuclear compartment implicated in splicing. *Cell,* 67**,** 335-342.

LI, P., WANG, K., ZHANG, J., ZHAO, L., LIANG, H., SHAO, C. & SUTHERLAND, L. C. 2012. The 3p21.3 tumor suppressor RBM5 resensitizes cisplatin-resistant human non-small cell lung cancer cells to cisplatin. *Cancer Epidemiol,* 36**,** 481-489.

LI, S., GUO, W., DEWEY, C. N. & GREASER, M. L. 2013. Rbm20 regulates titin alternative splicing as a splicing repressor. *Nucleic Acids Res,* 41**,** 2659-2672.

LIANG, H., ZHANG, J., SHAO, C., ZHAO, L., XU, W., SUTHERLAND, L. C. & WANG, K. 2012. Differential expression of RBM5, EGFR and KRAS mRNA and protein in non-small cell lung cancer tissues. *J Exp Clin Cancer Res,* 31**,** 36.

LIN, J. C. & TARN, W. Y. 2011. RBM4 down-regulates PTB and antagonizes its activity in muscle cell-specific alternative splicing. *J Cell Biol,* 193**,** 509-520.

LIN, J. C. & TARN, W. Y. 2012. Multiple roles of RBM4 in muscle cell differentiation. *Front Biosci (Schol. Ed),* 4**,** 181-189.

LLORIAN, M. & SMITH, C. W. 2011. Decoding muscle alternative splicing. *Curr. Opin. Genet Dev,* 21**,** 380-387.

LOISELLE, J. J. & SUTHERLAND, L. C. 2014. Differential downregulation of Rbm5 and Rbm10 during skeletal and cardiac differentiation. *In Vitro Cell Dev. Biol. Anim,* 50**,** 331-339.

LONDHE, P. & DAVIE, J. K. 2011. Sequential association of myogenic regulatory factors and E proteins at muscle-specific genes. *Skelet. Muscle,* 1**,** 14.

LOUIS, M., ZANOU, N., VAN, S. M. & GAILLY, P. 2008. TRPC1 regulates skeletal myoblast migration and differentiation. *J Cell Sci,* 121**,** 3951-3959.

LUKONG, K. E., CHANG, K. W., KHANDJIAN, E. W. & RICHARD, S. 2008. RNA-binding proteins in human genetic disease. *Trends Genet,* 24**,** 416-425.

LUNDE, B. M., MOORE, C. & VARANI, G. 2007. RNA-binding proteins: modular design for efficient function. *Nat Rev Mol. Cell Biol,* 8**,** 479-490.

LUO, D., RENAULT, V. M. & RANDO, T. A. 2005. The regulation of Notch signaling in muscle stem cell activation and postnatal myogenesis. *Semin Cell Dev Biol,* 16**,** 612-22.

MAARABOUNI, M. M. & WILLIAMS, G. T. 2006. The antiapoptotic RBM5/LUCA-15/H37 gene and its role in apoptosis and human cancer: research update. *ScientificWorldJournal,* 6**,** 1705-1712.

MAKAROV, E. M., OWEN, N., BOTTRILL, A. & MAKAROVA, O. V. 2012. Functional mammalian spliceosomal complex E contains SMN complex proteins in addition to U1 and U2 snRNPs. *Nucleic Acids Res,* 40**,** 2639-2652.

MAL, A. & HARTER, M. L. 2003. MyoD is functionally linked to the silencing of a muscle-specific regulatory gene prior to skeletal myogenesis. *Proc Natl Acad Sci U S A,* 100**,** 1735-9.

MANSSON, R., TSAPOGAS, P., AKERLUND, M., LAGERGREN, A., GISLER, R. & SIGVARDSSON, M. 2004. Pearson correlation analysis of microarray data allows for the identification of genetic targets for early B-cell factor. *J Biol Chem,* 279**,** 17905-13.

MARTIN-GARABATO, E., MARTINEZ-ARRIBAS, F., POLLAN, M., LUCAS, A. R., SANCHEZ, J. & SCHNEIDER, J. 2008. The small variant of the apoptosis-associated X-chromosome RBM10 gene is co-expressed with caspase-3 in breast cancer. *Cancer Genomics Proteomics,* 5**,** 169-173.

MARTINEZ-ARRIBAS, F., AGUDO, D., POLLAN, M., GOMEZ-ESQUER, F., AZ-GIL, G., LUCAS, R. & SCHNEIDER, J. 2006. Positive correlation between the expression of X-chromosome RBM genes (RBMX, RBM3, RBM10) and the proapoptotic Bax gene in human breast cancer. *J Cell Biochem,* 97**,** 1275-1282.

MASILAMANI, T. J., LOISELLE, J. J. & SUTHERLAND, L. C. 2014. Assessment of reference genes for real-time quantitative PCR gene expression normalization during C2C12 and H9c2 skeletal muscle differentiation. *Mol. Biotechnol,* 56**,** 329-339.

MEI, H., HO, M. K., YUNG, L. Y., WU, Z., IP, N. Y. & WONG, Y. H. 2011. Expression of Galpha(z) in C2C12 cells restrains myogenic differentiation. *Cell Signal,* 23**,** 389-397.

MERCER, S. E., EWTON, D. Z., DENG, X., LIM, S., MAZUR, T. R. & FRIEDMAN, E. 2005. Mirk/Dyrk1B mediates survival during the differentiation of C2C12 myoblasts. *J Biol Chem,* 280**,** 25788-25801.

MERLIE, J. P., BUCKINGHAM, M. E. & WHALEN, R. G. 1977. Molecular aspects of myogenesis. *Curr Top Dev Biol,* 11**,** 61-114.

METZINGER, L., BLAKE, D. J., SQUIER, M. V., ANDERSON, L. V., DECONINCK, A. E., NAWROTZKI, R., HILTON-JONES, D. & DAVIES, K. E. 1997. Dystrobrevin deficiency at the sarcolemma of patients with muscular dystrophy. *Hum. Mol. Genet,* 6**,** 1185-1191.

MILLER, G., SOCCI, N. D., DHALL, D., D'ANGELICA, M., DEMATTEO, R. P., ALLEN, P. J., SINGH, B., FONG, Y., BLUMGART, L. H., KLIMSTRA, D. S. & JARNAGIN, W. R. 2009. Genome wide analysis and clinical correlation of chromosomal and transcriptional mutations in cancers of the biliary tract. *J Exp Clin Cancer Res,* 28**,** 62.

MILLER, J. B. 1990. Myogenic programs of mouse muscle cell lines: expression of myosin heavy chain isoforms, MyoD1, and myogenin. *J Cell Biol,* 111**,** 1149-1159.

MIYAMOTO, S., HIDAKA, K., JIN, D. & MORISAKI, T. 2009. RNA-binding proteins Rbm38 and Rbm24 regulate myogenic differentiation via p21-dependent and -independent regulatory pathways. *Genes Cells,* 14**,** 1241-1252.

MOLKENTIN, J. D. & OLSON, E. N. 1996. Defining the regulatory networks for muscle development. *Curr Opin Genet Dev,* 6**,** 445-453.

MONTARRAS, D., L'HONORE, A. & BUCKINGHAM, M. 2013. Lying low but ready for action: the quiescent muscle satellite cell. *FEBS J,* 280**,** 4036-4050.

MORAN, J. L., LI, Y., HILL, A. A., MOUNTS, W. M. & MILLER, C. P. 2002. Gene expression changes during mouse skeletal myoblast differentiation revealed by transcriptional profiling. *Physiol Genomics,* 10**,** 103-111.

MOURTADA-MAARABOUNI, M., KEEN, J., CLARK, J., COOPER, C. S. & WILLIAMS, G. T. 2006. Candidate tumor suppressor LUCA-15/RBM5/H37 modulates expression of apoptosis and cell cycle genes. *Exp. Cell Res,* 312**,** 1745-1752.

MOURTADA-MAARABOUNI, M., SUTHERLAND, L. C., CLARK, J. P., COOPER, C. S. & WILLIAMS, G. T. 2001. Regulation of T-cell apoptosis by sequences encoded at the luca-15 candidate tumour suppressor locus. *ScientificWorldJournal,* 1**,** 38.

MOURTADA-MAARABOUNI, M., SUTHERLAND, L. C., MEREDITH, J. M. & WILLIAMS, G. T. 2003. Simultaneous acceleration of the cell cycle and suppression of apoptosis by splice variant delta-6 of the candidate tumour suppressor LUCA-15/RBM5. *Genes Cells,* 8**,** 109-119.

MOURTADA-MAARABOUNI, M., SUTHERLAND, L. C. & WILLIAMS, G. T. 2002. Candidate tumour suppressor LUCA-15 can regulate multiple apoptotic pathways. *Apoptosis,* 7**,** 421-432.

MOURTADA-MAARABOUNI, M. & WILLIAMS, G. T. 2002. RBM5/LUCA-15 - Tumour Suppression by Control of Apoptosis and the Cell Cycle? *ScientificWorldJournal,* 2**,** 1885-1890.

MUELLER, C. F., BERGER, A., ZIMMER, S., TIYERILI, V. & NICKENIG, G. 2009. The heterogenous nuclear riboprotein S1-1 regulates AT1 receptor gene expression via transcriptional and posttranscriptional mechanisms. *Arch Biochem Biophys,* 488**,** 76-82.

MUSUNURU, K. 2003. Cell-specific RNA-binding proteins in human disease. *Trends Cardiovasc. Med,* 13**,** 188-195.

NAGASE, T., SEKI, N., TANAKA, A., ISHIKAWA, K. & NOMURA, N. 1995. Prediction of the coding sequences of unidentified human genes. IV. The coding sequences of 40 new genes (KIAA0121-KIAA0160) deduced by analysis of cDNA clones from human cell line KG-1. *DNA Res,* 2**,** 167-210.

NAKAMORI, M., KIMURA, T., KUBOTA, T., MATSUMURA, T., SUMI, H., FUJIMURA, H., TAKAHASHI, M. P. & SAKODA, S. 2008. Aberrantly spliced alpha-dystrobrevin alters alpha-syntrophin binding in myotonic dystrophy type 1. *Neurology,* 70**,** 677-685.

NAKAMORI, M. & TAKAHASHI, M. P. 2011. The role of alpha-dystrobrevin in striated muscle. *Int J Mol. Sci,* 12**,** 1660-1671.

NARYZHNY, S. N., DESOUZA, L. V., SIU, K. W. & LEE, H. 2006. Characterization of the human proliferating cell nuclear antigen physico-chemical properties: aspects of double trimer stability. *Biochem Cell Biol,* 84**,** 669-676.

NAYA, F. J. & OLSON, E. 1999. MEF2: a transcriptional target for signaling pathways controlling skeletal muscle growth and differentiation. *Curr Opin. Cell Biol,* 11**,** 683-688.

NGUYEN, C. D., MANSFIELD, R. E., LEUNG, W., VAZ, P. M., LOUGHLIN, F. E., GRANT, R. P. & MACKAY, J. P. 2011. Characterization of a family of RanBP2-type zinc fingers that can recognize single-stranded RNA. *J Mol Biol,* 407**,** 273-283.

NISHIMURA, M., MIKURA, M., HIRASAKA, K., OKUMURA, Y., NIKAWA, T., KAWANO, Y., NAKAYAMA, M. & IKEDA, M. 2008. Effects of dimethyl sulphoxide and dexamethasone on mRNA expression of myogenesis- and muscle proteolytic system-related genes in mouse myoblastic C2C12 cells. *J Biochem,* 144**,** 717-724.

NIU, Z., JIN, W., ZHANG, L. & LI, X. 2012. Tumor suppressor RBM5 directly interacts with the DExD/H-box protein DHX15 and stimulates its helicase activity. *FEBS Lett,* 586**,** 977-983.

NOFZIGER, D., MIYAMOTO, A., LYONS, K. M. & WEINMASTER, G. 1999. Notch signaling imposes two distinct blocks in the differentiation of C2C12 myoblasts. *Development,* 126**,** 1689-1702.

NYE, J. S., KOPAN, R. & AXEL, R. 1994. An activated Notch suppresses neurogenesis and myogenesis but not gliogenesis in mammalian cells. *Development,* 120**,** 2421-30.

O'BRYAN, M. K., CLARK, B. J., MCLAUGHLIN, E. A., D'SYLVA, R. J., O'DONNELL, L., WILCE, J. A., SUTHERLAND, J., O'CONNOR, A. E., WHITTLE, B., GOODNOW, C. C., ORMANDY, C. J. & JAMSAI, D. 2013. RBM5 Is a Male Germ Cell Splicing Factor and Is Required for Spermatid Differentiation and Male Fertility. *PLoS Genet,* 9**,** e1003628.

O'LEARY, D. A., SHARIF, O., ANDERSON, P., TU, B., WELCH, G., ZHOU, Y., CALDWELL, J. S., ENGELS, I. H. & BRINKER, A. 2009. Identification of small molecule and genetic modulators of AON-induced dystrophin exon skipping by high-throughput screening. *PLoS One,* 4**,** e8348.

OH, J. J., GROSSHANS, D. R., WONG, S. G. & SLAMON, D. J. 1999. Identification of differentially expressed genes associated with HER- 2/neu overexpression in human breast cancer cells. *Nucleic Acids Res,* 27**,** 4008-4017.

OH, J. J., RAZFAR, A., DELGADO, I., REED, R. A., MALKINA, A., BOCTOR, B. & SLAMON, D. J. 2006. 3p21.3 tumor suppressor gene H37/Luca15/RBM5 inhibits growth of human lung cancer cells through cell cycle arrest and apoptosis. *Cancer Res,* 66**,** 3419-3427.

OH, J. J., TASCHEREAU, E. O., KOEGEL, A. K., GINTHER, C. L., ROTOW, J. K., ISFAHANI, K. Z. & SLAMON, D. J. 2010. RBM5/H37 tumor suppressor, located at the lung cancer hot spot 3p21.3, alters expression of genes involved in metastasis. *Lung Cancer,* 70**,** 253-262.

OH, J. J., WEST, A. R., FISHBEIN, M. C. & SLAMON, D. J. 2002. A candidate tumor suppressor gene, H37, from the human lung cancer tumor suppressor locus 3p21.3. *Cancer Res,* 62**,** 3207-3213.

OLSON, E. N., BRENNAN, T. J., CHAKRABORTY, T., CHENG, T. C., CSERJESI, P., EDMONDSON, D., JAMES, G. & LI, L. 1991. Molecular control of myogenesis: antagonism between growth and differentiation. *Mol Cell Biochem,* 104**,** 7-13.

ONO, Y., SENSUI, H., SAKAMOTO, Y. & NAGATOMI, R. 2006. Knockdown of hypoxia-inducible factor-1alpha by siRNA inhibits C2C12 myoblast differentiation. *J. Cell Biochem,* 98**,** 642-649.

OZUEMBA, B. 2011. *Expression of RBM5 and RBM10 splice variants in mouse tissues.* M.Sc Thesis, Univesity of Skovde.

PANG, A. L., TITLE, A. C. & RENNERT, O. M. 2014. Modulation of microRNA expression in human lung cancer cells by the G9a histone methyltransferase inhibitor BIX01294. *Oncol Lett,* 7**,** 1819-1825.

PENG, J., VALESHABAD, A. K., LI, Q. & WANG, Y. 2013. Differential expression of RBM5 and KRAS in pancreatic ductal adenocarcinoma and their association with clinicopathological features. *Oncol Lett,* 5**,** 1000-1004.

PERRY, R. L. & RUDNICK, M. A. 2000. Molecular mechanisms regulating myogenic determination and differentiation. *Front Biosci,* 5**,** D750-D767.

PINOL-ROMA, S. & DREYFUSS, G. 1993. hnRNP proteins: localization and transport between the nucleus and the cytoplasm. *Trends Cell Biol,* 3**,** 151-5.

POTTHOFF, M. J., ARNOLD, M. A., MCANALLY, J., RICHARDSON, J. A., BASSEL-DUBY, R. & OLSON, E. N. 2007. Regulation of skeletal muscle sarcomere integrity and postnatal muscle function by Mef2c. *Mol. Cell Biol,* 27**,** 8143-8151.

POWNALL, M. E., GUSTAFSSON, M. K. & EMERSON, C. P., JR. 2002. Myogenic regulatory factors and the specification of muscle progenitors in vertebrate embryos. *Annu. Rev Cell Dev. Biol,* 18**,** 747-783.

QUACH, N. L., BIRESSI, S., REICHARDT, L. F., KELLER, C. & RANDO, T. A. 2009. Focal adhesion kinase signaling regulates the expression of caveolin 3 and beta1 integrin, genes essential for normal myoblast fusion. *Mol Biol Cell,* 20**,** 3422-3435.

RAJAN, S., CHU PHAM, D. H., DJAMBAZIAN, H., ZUZAN, H., FEDYSHYN, Y., KETELA, T., MOFFAT, J., HUDSON, T. J. & SLADEK, R. 2012. Analysis of early C2C12 myogenesis identifies stably and differentially expressed transcriptional regulators whose knock-down inhibits myoblast differentiation. *Physiol Genomics,* 44**,** 183-197.

RAMASWAMY, S., ROSS, K. N., LANDER, E. S. & GOLUB, T. R. 2003. A molecular signature of metastasis in primary solid tumors. *Nat. Genet,* 33**,** 49-54.

REED, R. & HURT, E. 2002. A conserved mRNA export machinery coupled to pre-mRNA splicing. *Cell,* 108**,** 523-531.

RINTALA-MAKI, N. D., ABRASONIS, V., BURD, M. & SUTHERLAND, L. C. 2004. Genetic instability of RBM5/LUCA-15/H37 in MCF-7 breast carcinoma sublines may affect susceptibility to apoptosis. *Cell Biochem. Funct,* 22**,** 307-313.

RINTALA-MAKI, N. D., GOARD, C. A., LANGDON, C. E., WALL, V. E., TRAULSEN, K. E., MORIN, C. D., BONIN, M. & SUTHERLAND, L. C. 2007. Expression of RBM5-related factors in primary breast tissue. *J Cell Biochem,* 100**,** 1440-1458.

RINTALA-MAKI, N. D. & SUTHERLAND, L. C. 2009. Identification and characterisation of a novel antisense non-coding RNA from the RBM5 gene locus. *Gene,* 445**,** 7-16.

RIQUELME, M. A., CEA, L. A., VEGA, J. L., PUEBLA, C., VARGAS, A. A., SHOJI, K. F., SUBIABRE, M. & SAEZ, J. C. 2015. Pannexin channels mediate the acquisition of myogenic commitment in C2C12 reserve cells promoted by P2 receptor activation. *Front Cell Dev. Biol,* 3**,** 25.

RUDNICKI, M. A., SCHNEGELSBERG, P. N., STEAD, R. H., BRAUN, T., ARNOLD, H. H. & JAENISCH, R. 1993. MyoD or Myf-5 is required for the formation of skeletal muscle. *Cell,* 75**,** 1351-9.

SABOURIN, L. A., GIRGIS-GABARDO, A., SEALE, P., ASAKURA, A. & RUDNICKI, M. A. 1999. Reduced differentiation potential of primary MyoD-/- myogenic cells derived from adult skeletal muscle. *J Cell Biol,* 144**,** 631-43.

SABOURIN, L. A. & RUDNICKI, M. A. 2000. The molecular regulation of myogenesis. *Clin Genet,* 57**,** 16-25.

SANDRI, M. & CARRARO, U. 1999. Apoptosis of skeletal muscles during development and disease. *Int. J. Biochem. Cell Biol,* 31**,** 1373-1390.

SCHMIDT, C., GRONBORG, M., DECKERT, J., BESSONOV, S., CONRAD, T., LUHRMANN, R. & URLAUB, H. 2014. Mass spectrometry-based relative quantification of proteins in precatalytic and catalytically active spliceosomes by metabolic labeling (SILAC), chemical labeling (iTRAQ), and label-free spectral count. *RNA,* 20**,** 406-20.

SCHNEIDER, C. A., RASBAND, W. S. & ELICEIRI, K. W. 2012. NIH Image to ImageJ: 25 years of image analysis. *Nat Methods,* 9**,** 671-5.

SCHONEICH, C., DREMINA, E., GALEVA, N. & SHAROV, V. 2014. Apoptosis in differentiating C2C12 muscle cells selectively targets Bcl-2-deficient myotubes. *Apoptosis,* 19**,** 42-57.

SEKIYAMA, Y., SUZUKI, H. & TSUKAHARA, T. 2012. Functional gene expression analysis of tissue-specific isoforms of Mef2c. *Cell Mol. Neurobiol,* 32**,** 129-139.

SHAFEY, D., COTE, P. D. & KOTHARY, R. 2005. Hypomorphic Smn knockdown C2C12 myoblasts reveal intrinsic defects in myoblast fusion and myotube morphology. *Exp Cell Res,* 311**,** 49-61.

SHAO, C., ZHAO, L., WANG, K., XU, W., ZHANG, J. & YANG, B. 2012. The tumor suppressor gene RBM5 inhibits lung adenocarcinoma cell growth and induces apoptosis. *World J Surg Oncol,* 10**,** 160.

SHEN, H., MCELHINNY, A. S., CAO, Y., GAO, P., LIU, J., BRONSON, R., GRIFFIN, J. D. & WU, L. 2006. The Notch coactivator, MAML1, functions as a novel coactivator for MEF2C-mediated transcription and is required for normal myogenesis. *Genes Dev,* 20**,** 675-88.

SHEN, X., COLLIER, J. M., HLAING, M., ZHANG, L., DELSHAD, E. H., BRISTOW, J. & BERNSTEIN, H. S. 2003. Genome-wide examination of myoblast cell cycle withdrawal during differentiation. *Dev Dyn,* 226**,** 128-138.

SIMPSON, R. J. 2006. SDS-PAGE of Proteins. *CSH Protoc,* 2006.

SMITH, M. I., HUANG, Y. Y. & DESHMUKH, M. 2009. Skeletal muscle differentiation evokes endogenous XIAP to restrict the apoptotic pathway. *PLoS One,* 4**,** e5097.

SMITH, T. H., KACHINSKY, A. M. & MILLER, J. B. 1994. Somite subdomains, muscle cell origins, and the four muscle regulatory factor proteins. *J Cell Biol,* 127**,** 95-105.

SOLEIMANI, V. D. & RUDNICKI, M. A. 2011. New insights into the origin and the genetic basis of rhabdomyosarcomas. *Cancer Cell,* 19**,** 157-159.

SONG, Z., WU, P., JI, P., ZHANG, J., GONG, Q., WU, J. & SHI, Y. 2012. Solution structure of the second RRM domain of RBM5 and its unusual binding characters for different RNA targets. *Biochemistry,* 51**,** 6667-6678.

SPLETTER, M. L. & SCHNORRER, F. 2014. Transcriptional regulation and alternative splicing cooperate in muscle fiber-type specification in flies and mammals. *Exp Cell Res,* 321**,** 90-8.

SUGLIANI, M., BRAMBILLA, V., CLERKX, E. J., KOORNNEEF, M. & SOPPE, W. J. 2010. The conserved splicing factor SUA controls alternative splicing of the developmental regulator ABI3 in Arabidopsis. *Plant Cell,* 22**,** 1936-1946.

SUN, L., TRAUSCH-AZAR, J. S., CIECHANOVER, A. & SCHWARTZ, A. L. 2005. Ubiquitin-proteasome-mediated degradation, intracellular localization, and protein synthesis of MyoD and Id1 during muscle differentiation. *J. Biol. Chem,* 280**,** 26448-26456.

SUTHERLAND, L. C., EDWARDS, S. E., CABLE, H. C., POIRIER, G. G., MILLER, B. A., COOPER, C. S. & WILLIAMS, G. T. 2000. LUCA-15-encoded sequence variants regulate CD95-mediated apoptosis. *Oncogene,* 19**,** 3774-3781.

SUTHERLAND, L. C., LERMAN, M., WILLIAMS, G. T. & MILLER, B. A. 2001. LUCA-15 suppresses CD95-mediated apoptosis in Jurkat T cells. *Oncogene,* 20**,** 2713-2719.

SUTHERLAND, L. C., RINTALA-MAKI, N. D., WHITE, R. D. & MORIN, C. D. 2005. RNA binding motif (RBM) proteins: a novel family of apoptosis modulators? *J. Cell Biochem,* 94**,** 5-24.

SUTHERLAND, L. C., WANG, K. & ROBINSON, A. G. 2010. RBM5 as a putative tumor suppressor gene for lung cancer. *J Thorac. Oncol,* 5**,** 294-298.

TAMBURINO, A. M., RYDER, S. P. & WALHOUT, A. J. 2013. A compendium of Caenorhabditis elegans RNA binding proteins predicts extensive regulation at multiple levels. *G3. (Bethesda.),* 3**,** 297-304.

TANAKA, K., SATO, K., YOSHIDA, T., FUKUDA, T., HANAMURA, K., KOJIMA, N., SHIRAO, T., YANAGAWA, T. & WATANABE, H. 2011. Evidence for cell density affecting C2C12 myogenesis: possible regulation of myogenesis by cell-cell communication. *Muscle Nerve,* 44**,** 968-977.

TANNU, N. S., RAO, V. K., CHAUDHARY, R. M., GIORGIANNI, F., SAEED, A. E., GAO, Y. & RAGHOW, R. 2004. Comparative proteomes of the proliferating C(2)C(12) myoblasts and fully differentiated myotubes reveal the complexity of the skeletal muscle differentiation program. *Mol Cell Proteomics,* 3**,** 1065-1082.

TAPSCOTT, S. J. 2005. The circuitry of a master switch: Myod and the regulation of skeletal muscle gene transcription. *Development,* 132**,** 2685-2695.

TIMMER, T., TERPSTRA, P., VAN DEN BERG, A., VELDHUIS, P. M., TER ELST, A., VOUTSINAS, G., HULSBEEK, M. M., DRAAIJERS, T. G., LOOMAN, M. W., KOK, K., NAYLOR, S. L. & BUYS, C. H. 1999. A comparison of genomic structures and expression patterns of two closely related flanking genes in a critical lung cancer region at 3p21.3. *Eur. J. Hum. Genet,* 7**,** 478-486.

TOMCZAK, K. K., MARINESCU, V. D., RAMONI, M. F., SANOUDOU, D., MONTANARO, F., HAN, M., KUNKEL, L. M., KOHANE, I. S. & BEGGS, A. H. 2004. Expression profiling and identification of novel genes involved in myogenic differentiation. *FASEB J,* 18**,** 403-405.

VAN DER GIESSEN, K., DI-MARCO, S., CLAIR, E. & GALLOUZI, I. E. 2003. RNAi-mediated HuR depletion leads to the inhibition of muscle cell differentiation. *J Biol Chem,* 278**,** 47119-28.

VELICA, P. & BUNCE, C. M. 2011. A quick, simple and unbiased method to quantify C2C12 myogenic differentiation. *Muscle Nerve,* 44**,** 366-370.

VENABLES, J. P., KLINCK, R., KOH, C., GERVAIS-BIRD, J., BRAMARD, A., INKEL, L., DURAND, M., COUTURE, S., FROEHLICH, U., LAPOINTE, E., LUCIER, J. F., THIBAULT, P., RANCOURT, C., TREMBLAY, K., PRINOS, P., CHABOT, B. & ELELA, S. A. 2009. Cancer-associated regulation of alternative splicing. *Nat Struct. Mol Biol,* 16**,** 670-676.

WALLACE, R. B., SHAFFER, J., MURPHY, R. F., BONNER, J., HIROSE, T. & ITAKURA, K. 1979. Hybridization of synthetic oligodeoxyribonucleotides to phi chi 174 DNA: the effect of single base pair mismatch. *Nucleic Acids Res,* 6**,** 3543-3557.

WALSH, K. & PERLMAN, H. 1997. Cell cycle exit upon myogenic differentiation. *Curr Opin Genet Dev,* 7**,** 597-602.

WALTERS, E. H., STICKLAND, N. C. & LOUGHNA, P. T. 2000. MRF-4 exhibits fiber type- and muscle-specific pattern of expression in postnatal rat muscle. *Am J Physiol Regul. Integr. Comp Physiol,* 278**,** R1381-R1384.

WANG, K., BACON, M. L., TESSIER, J. J., RINTALA-MAKI, N. D., TANG, V. & SUTHERLAND, L. C. 2012. RBM10 Modulates Apoptosis and Influences TNA-a Gene Expression. *Journal of Cell Death,* 5**,** 1-19.

WANG, Y., GOGOL-DORING, A., HU, H., FROHLER, S., MA, Y., JENS, M., MAASKOLA, J., MURAKAWA, Y., QUEDENAU, C., LANDTHALER, M., KALSCHEUER, V., WIECZOREK, D., WANG, Y., HU, Y. & CHEN, W. 2013. Integrative analysis revealed the molecular mechanism underlying RBM10-mediated splicing regulation. *EMBO Mol Med,* 5**,** 1431-1442.

WEI, M. H., LATIF, F., BADER, S., KASHUBA, V., CHEN, J. Y., DUH, F. M., SEKIDO, Y., LEE, C. C., GEIL, L., KUZMIN, I., ZABAROVSKY, E., KLEIN, G., ZBAR, B., MINNA, J. D. & LERMAN, M. I. 1996. Construction of a 600-kilobase cosmid clone contig and generation of a transcriptional map surrounding the lung cancer tumor suppressor gene (TSG) locus on human chromosome 3p21.3: progress toward the isolation of a lung cancer TSG. *Cancer Res,* 56**,** 1487-1492.

WELLING, D. B., LASAK, J. M., AKHMAMETYEVA, E., GHAHERI, B. & CHANG, L. S. 2002. cDNA microarray analysis of vestibular schwannomas. *Otol. Neurotol,* 23**,** 736-748.

WELLS, L., EDWARDS, K. A. & BERNSTEIN, S. I. 1996. Myosin heavy chain isoforms regulate muscle function but not myofibril assembly. *EMBO J,* 15**,** 4454-9.

WURTH, L. 2012. Versatility of RNA-Binding Proteins in Cancer. *Comp Funct Genomics,* 2012**,** 178525.

XIAO, S. J., WANG, L. Y., KIMURA, M., KOJIMA, H., KUNIMOTO, H., NISHIUMI, F., YAMAMOTO, N., NISHIO, K., FUJIMOTO, S., KATO, T., KITAGAWA, S., YAMANE, H., NAKAJIMA, K. & INOUE, A. 2013. S1-1/RBM10: multiplicity and cooperativity of nuclear localisation domains. *Biol Cell,* 105**,** 162-174.

YAFFE, D. & SAXEL, O. 1977. A myogenic cell line with altered serum requirements for differentiation. *Differentiation,* 7**,** 159-166.

YOSHIDA, N., YOSHIDA, S., KOISHI, K., MASUDA, K. & NABESHIMA, Y. 1998. Cell heterogeneity upon myogenic differentiation: down-regulation of MyoD and Myf-5 generates 'reserve cells'. *J Cell Sci,* 111 (Pt 6)**,** 769-779.

YUSUF, F. & BRAND-SABERI, B. 2012. Myogenesis and muscle regeneration. *Histochem. Cell Biol,* 138**,** 187-199.

ZHANG, L., JIE, C., OBIE, C., ABIDI, F., SCHWARTZ, C. E., STEVENSON, R. E., VALLE, D. & WANG, T. 2007. X chromosome cDNA microarray screening identifies a functional PLP2 promoter polymorphism enriched in patients with X-linked mental retardation. *Genome Res,* 17**,** 641-648.

ZHANG, L., ZHANG, Q., YANG, Y. & WU, C. 2014. The RNA recognition motif domains of RBM5 are required for RNA binding and cancer cell proliferation inhibition. *Biochem Biophys. Res. Commun,* 444**,** 445-450.

ZHANG, P., WONG, C., LIU, D., FINEGOLD, M., HARPER, J. W. & ELLEDGE, S. J. 1999. p21(CIP1) and p57(KIP2) control muscle differentiation at the myogenin step. *Genes Dev,* 13**,** 213-24.

ZHAO, L., LI, R., SHAO, C., LI, P., LIU, J. & WANG, K. 2012. 3p21.3 tumor suppressor gene RBM5 inhibits growth of human prostate cancer PC-3 cells through apoptosis. *World J Surg Oncol,* 10**,** 247.

ZHENG, S., DAMOISEAUX, R., CHEN, L. & BLACK, D. L. 2013. A broadly applicable high-throughput screening strategy identifies new regulators of Dlg4 (Psd-95) alternative splicing. *Genome Res,* 23**,** 998-1007.

ZHU, B. & GULICK, T. 2004. Phosphorylation and alternative pre-mRNA splicing converge to regulate myocyte enhancer factor 2C activity. *Mol. Cell Biol,* 24**,** 8264-8275.

Appendices

Appendix A

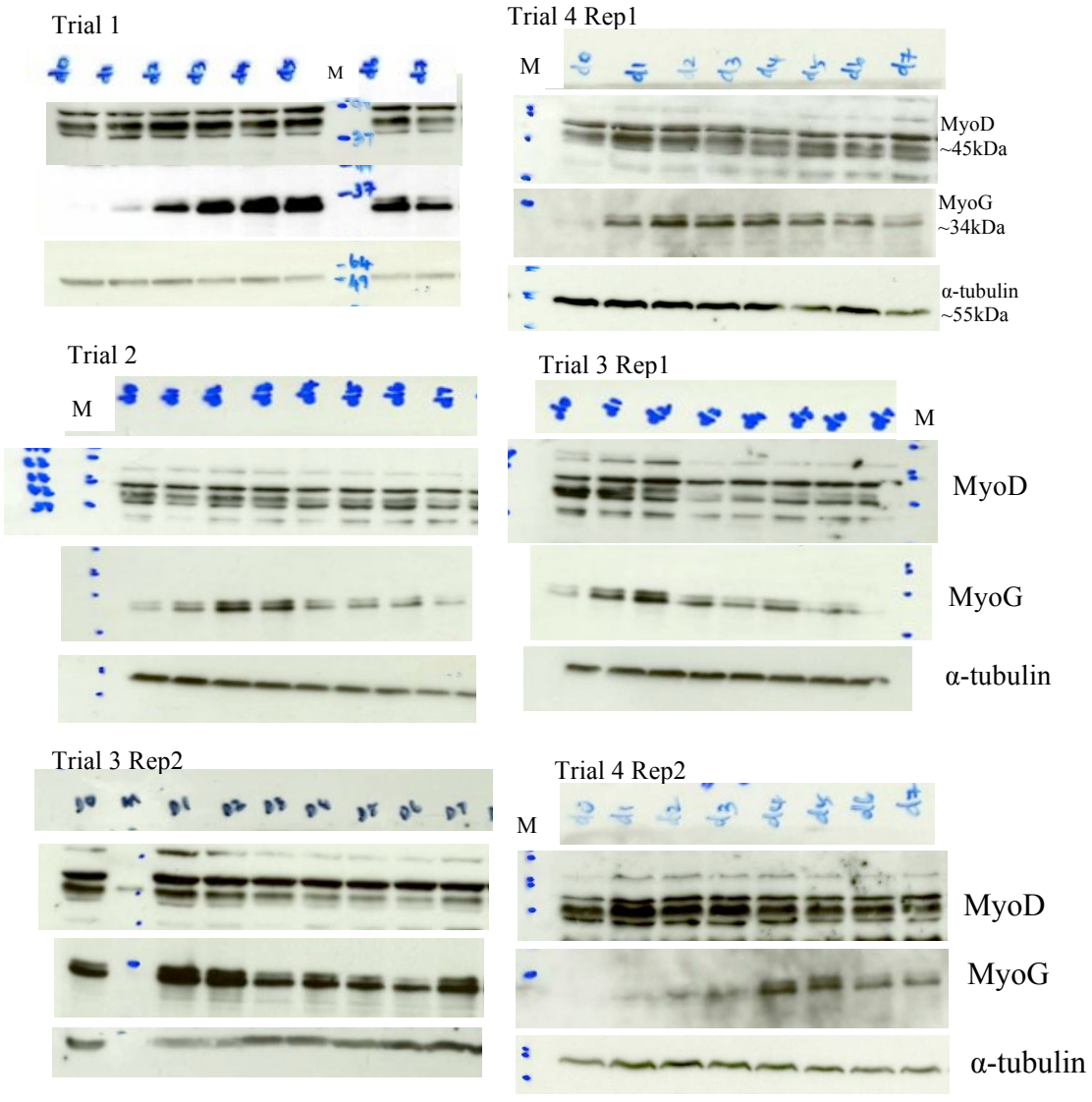

Figure A1. **MYOD, MYOG and α-tubulin during C2C12 differentiation**. Raw Western blot images for MyoD, MyoG and α-tubulin from D0 to D7 differentiating C2C12 cells. Presented here are 4 biological replicates in technical duplicates (for 2 trilas) that are representative of the replicates used in the analysis. BenchMark protein ladder (M) (Life Technologies) was used as the molecular weight (in kDa) standard.

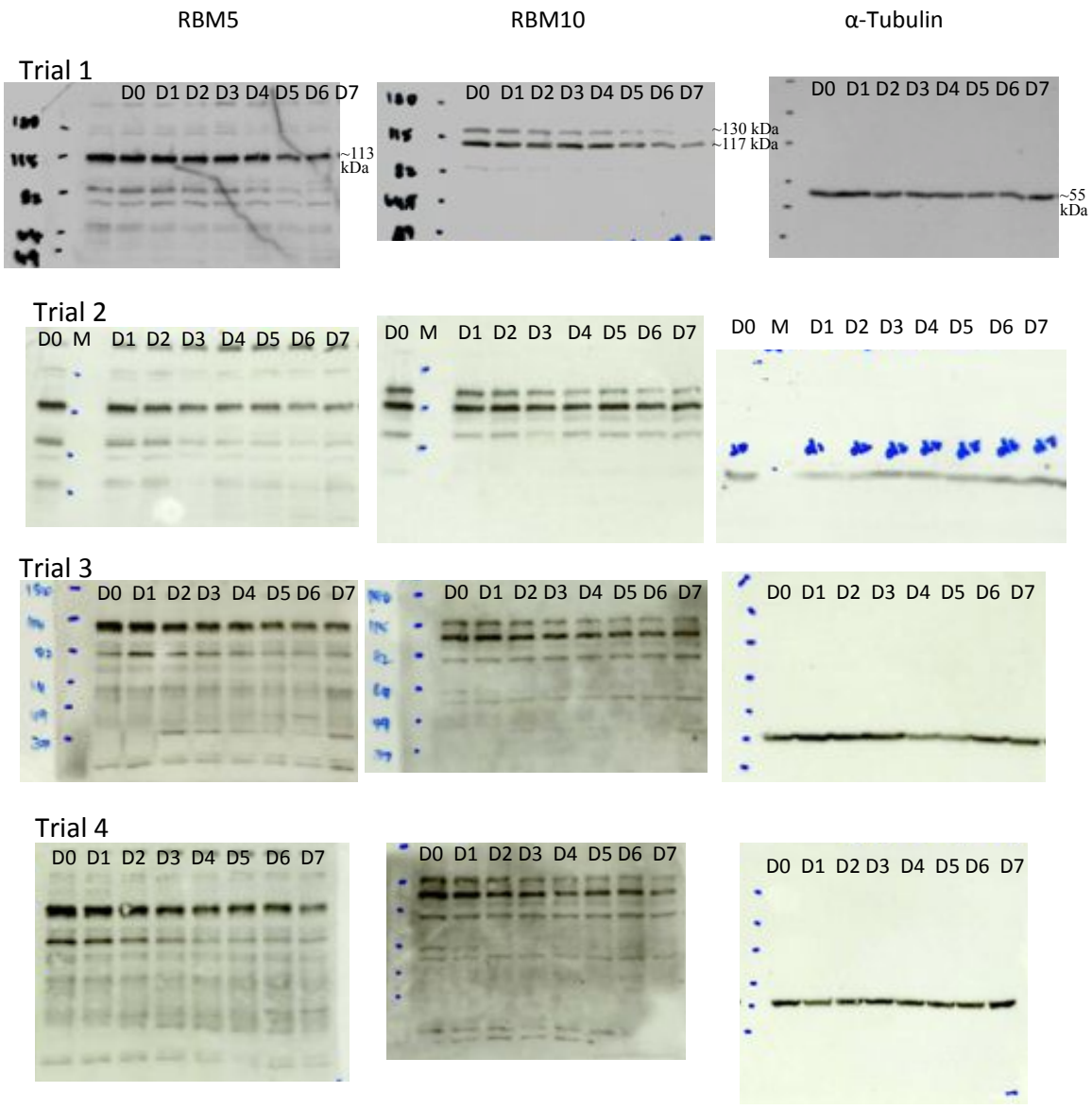

Figure A2. **RBM5, RBM10 and α-tubulin during C2C12 differentiation.** Raw Western blot images from four biological replicates for RBM5, RBM10 and α-tubulin from D0-D7 differentiating C2C12 cells. Full-length blots are shown to indicate only bands specific for RBM5 were seen when using LUCA-15 UK antibody targeted against RBM5 and for RBM10 isoforms when using Bethyl antibody targeted against both the isoforms. BenchMark protein ladder (Life Technologies) was used as the molecular weight (in kDa) standard.

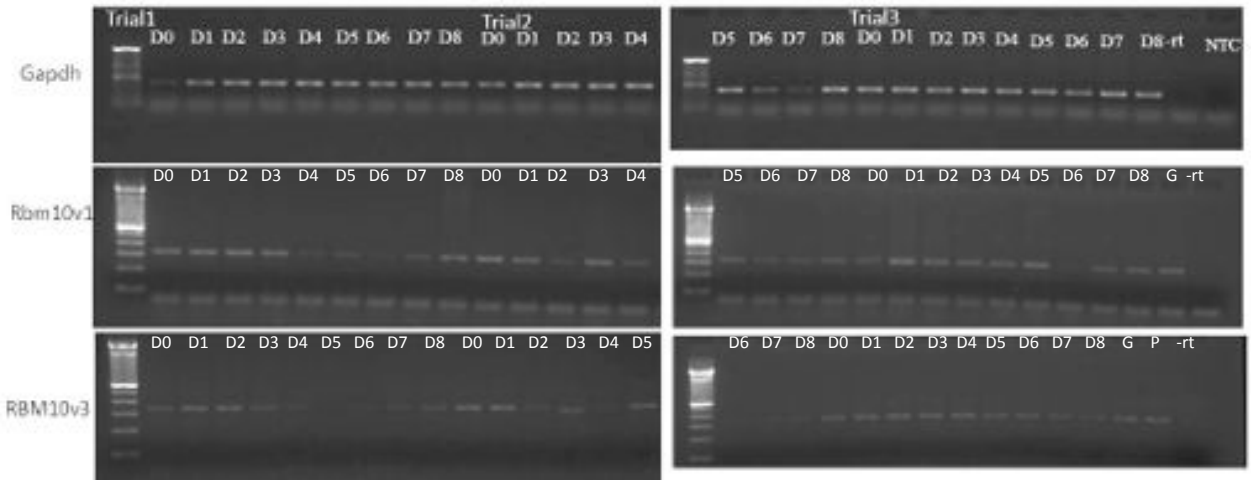

Figure A3. ***Rbm10v1*, *Rbm10v3* and *Gapdh* during C2C12 differentiation.** Raw end-point PCR images for *Rbm10v1*, *Rbm10v3* and *Gapdh* from D0-D7 differentiating C2C12 cells. Presented here are 3 biological replicates that are representative of the 4 biological replicates used in the analysis. –rt and NTC are negative controls; G (C2C12 cells in growth medium) and P (pooled cDNA) are positive controls. Amplified PCR products were visualized in a 1% agarose gel stained with SYBR® safe DNA gel stain. 100bp DNA ladder (Life Technologies).

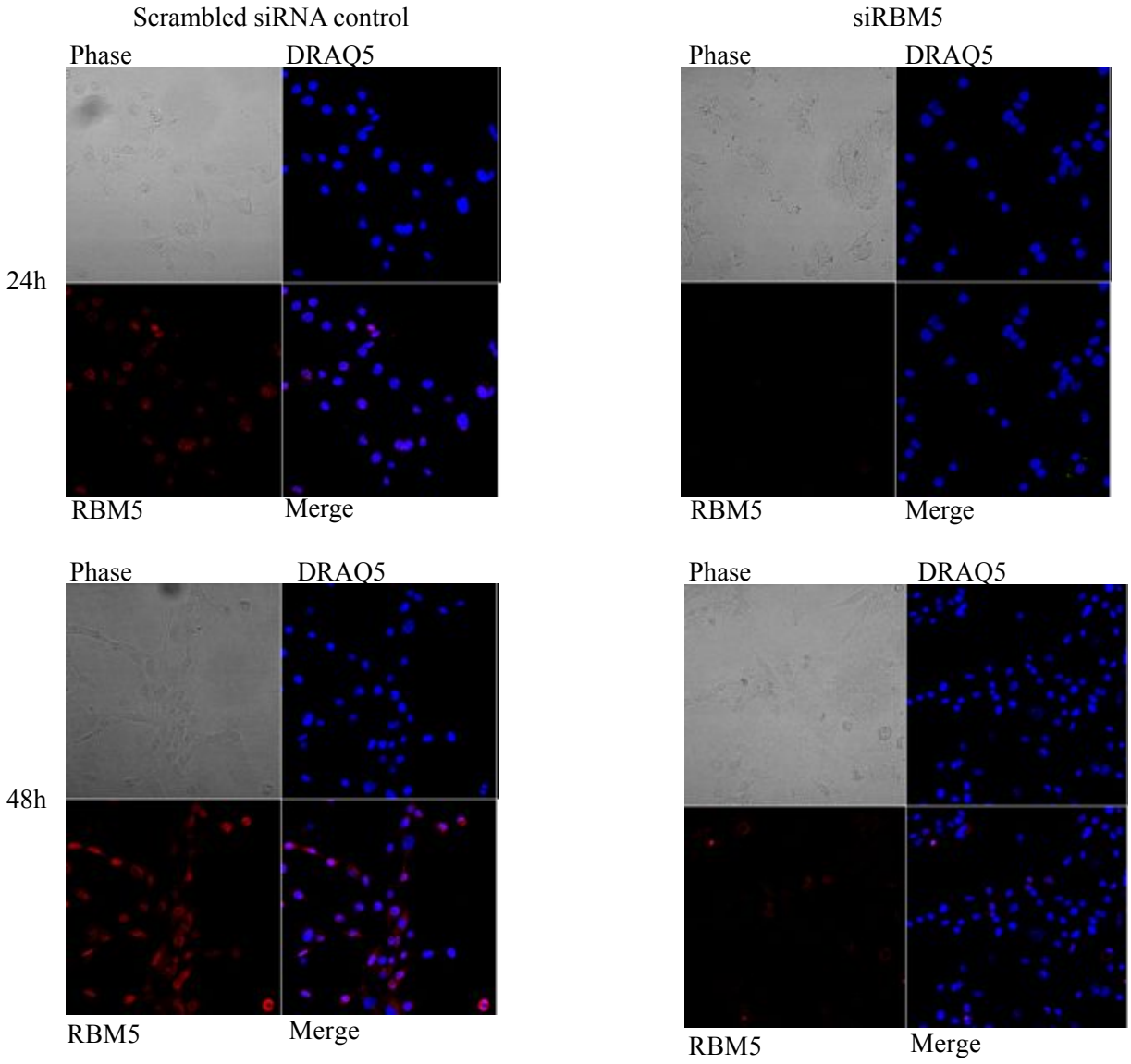

Figure A4. **RBM5 IF staining in the KDs.** IF images of Draq5 (blue) and RBM5 (red) staining in scrambled siRNA control and RBM5 KD C2C12 cells at 24h and 48h post-transfection from one trial. The KD levels measured by Western were 74% at 24h and 60% at 48(Trial A).

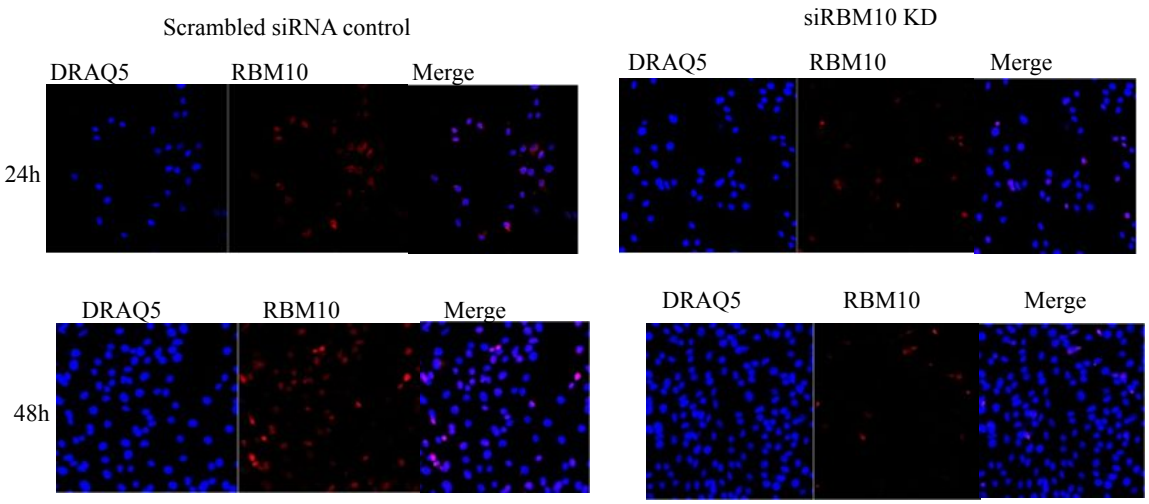

Figure A5. **RBM10 IF staining in the KDs.** IF images of Draq5 (blue) and RBM10 (red) staining in scrambled siRNA control and RBM10 KD C2C12 cells at 24h and 48h post-transfection from one trial (trial A). The KD levels measured by Western were 62% (RBM10v1) and 67% (RBM10v3) at 24h and 77% (RBM10v1) and 67% (RBM10v3) at 48h.

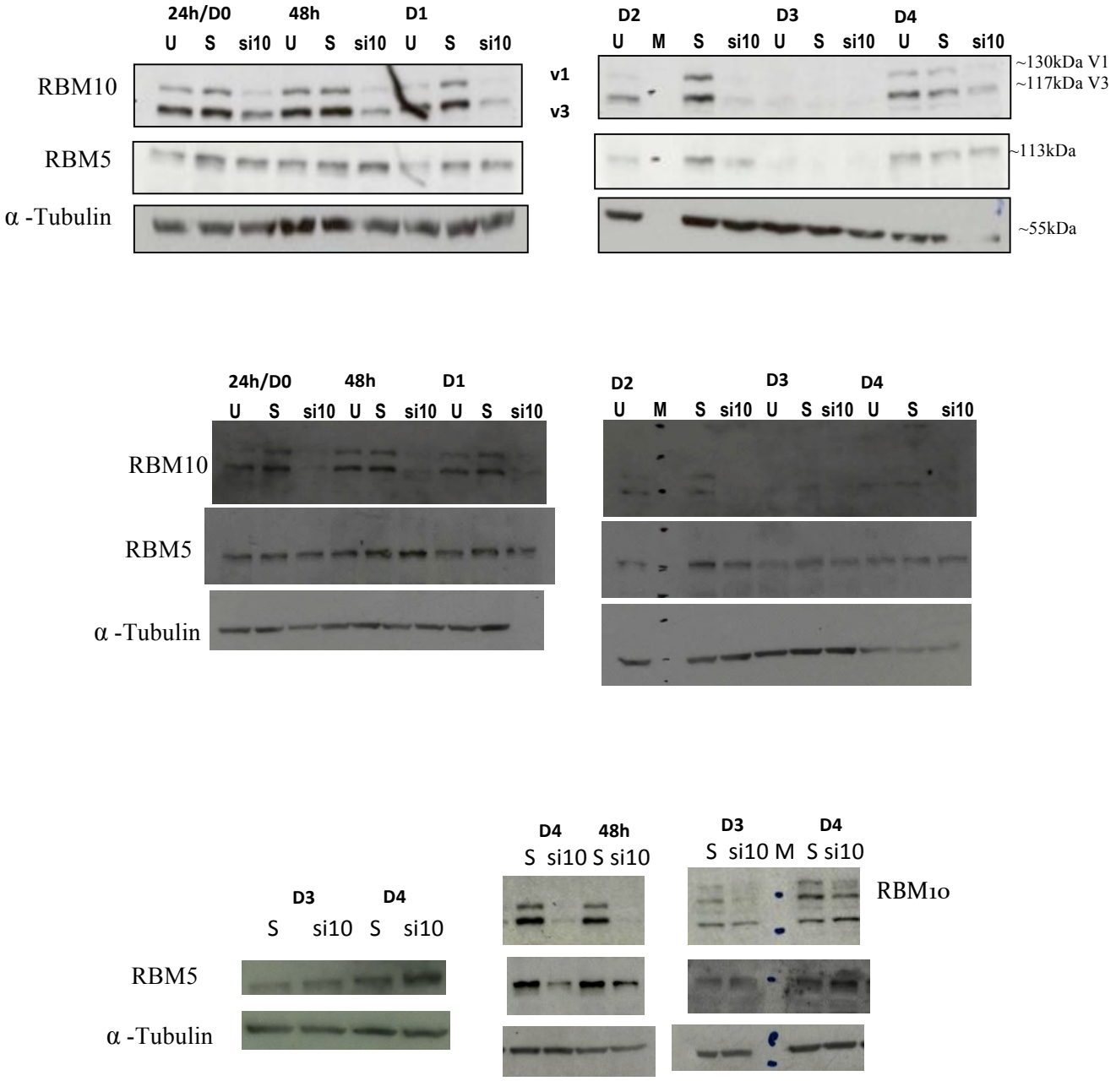

Figure A6. **RBM5, RBM10 and α-tubulin levels in RBM10 KDs:** Raw Western blot images for RBM5, RBM10 and α-tubulin from siRBM10 (si10), untransfected control (U) and siRNA scrambled control (S) C2C12 cells at 24h, 48h post-transfection and at D0-D4 differentiation, in technical replicates (Trial1). BenchMark protein ladder (M) (Life Technologies) was used as the molecular weight (in kDa) standard.

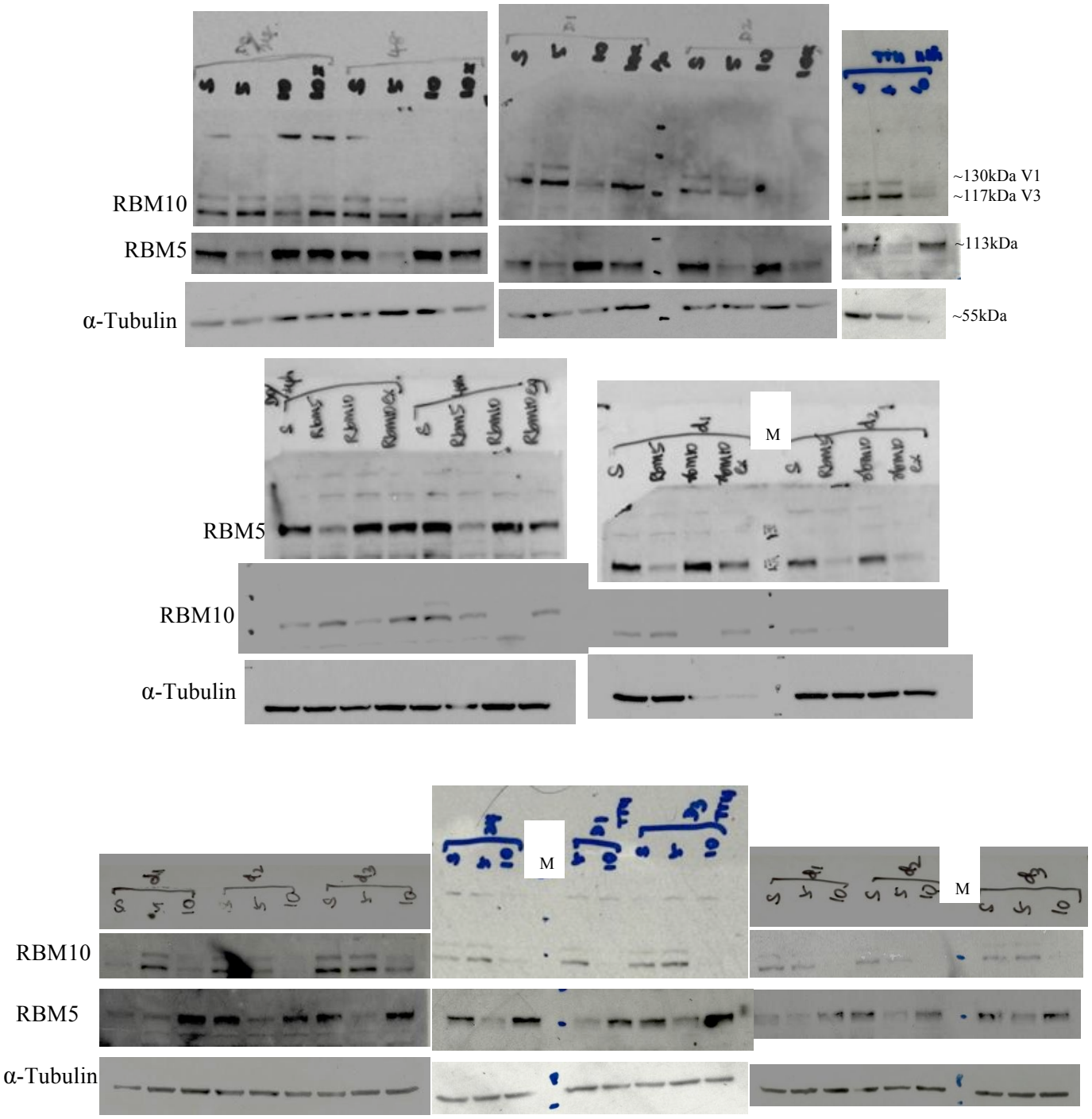

Figure A7. **RBM5, RBM10 and α-tubulin levels in RBM5 and RBM10 KDs**: Raw Western blot images for RBM5, RBM10 and α-tubulin from siRBM5 (5 or RBM5) (Trial 1), siRBM10 (10 or RBM10) (Trial 2) and siRNA scrambled control (S) C2C12 cells at 24h, 48h post-transfection and at D0-D3 differentiation, in technical replicates. 10x (or RBM10ex) is RBM10v1 specific KD and is not included in the scope of this thesis. BenchMark protein ladder (M) (Life Technologies) was used as the molecular weight (in kDa) standard.

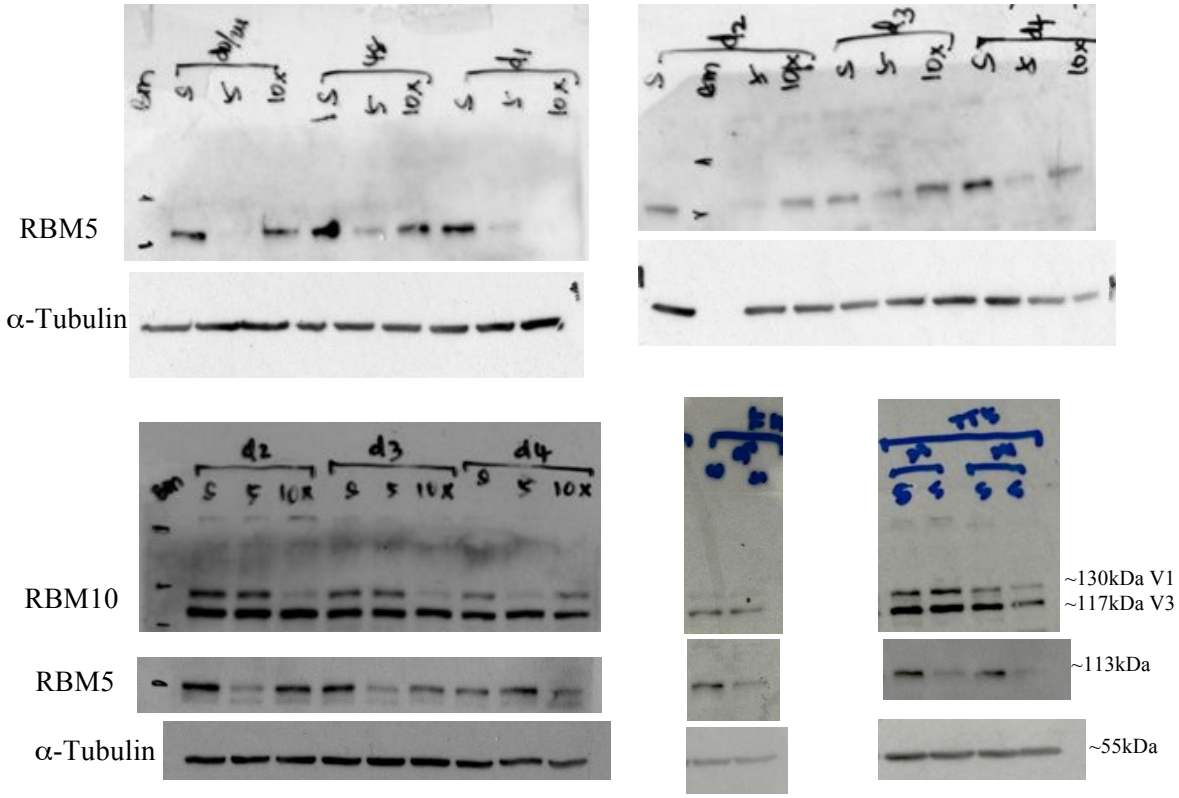

Figure A8. **RBM5, RBM10 and α-tubulin levels in RBM5 KDs.** Raw Western blot images for RBM5, RBM10 and α-tubulin from siRBM5 (5) and siRNA scrambled control (S) C2C12 cells at 24h, 48h post-transfection and at D0-D4 differentiation, in technical replicates (Trial 2). 10x is Rbm10v1 specific KD and is not included in the scope of this thesis. BenchMark protein ladder (BM) (Life Technologies) was used as the molecular weight (in kDa) standard.

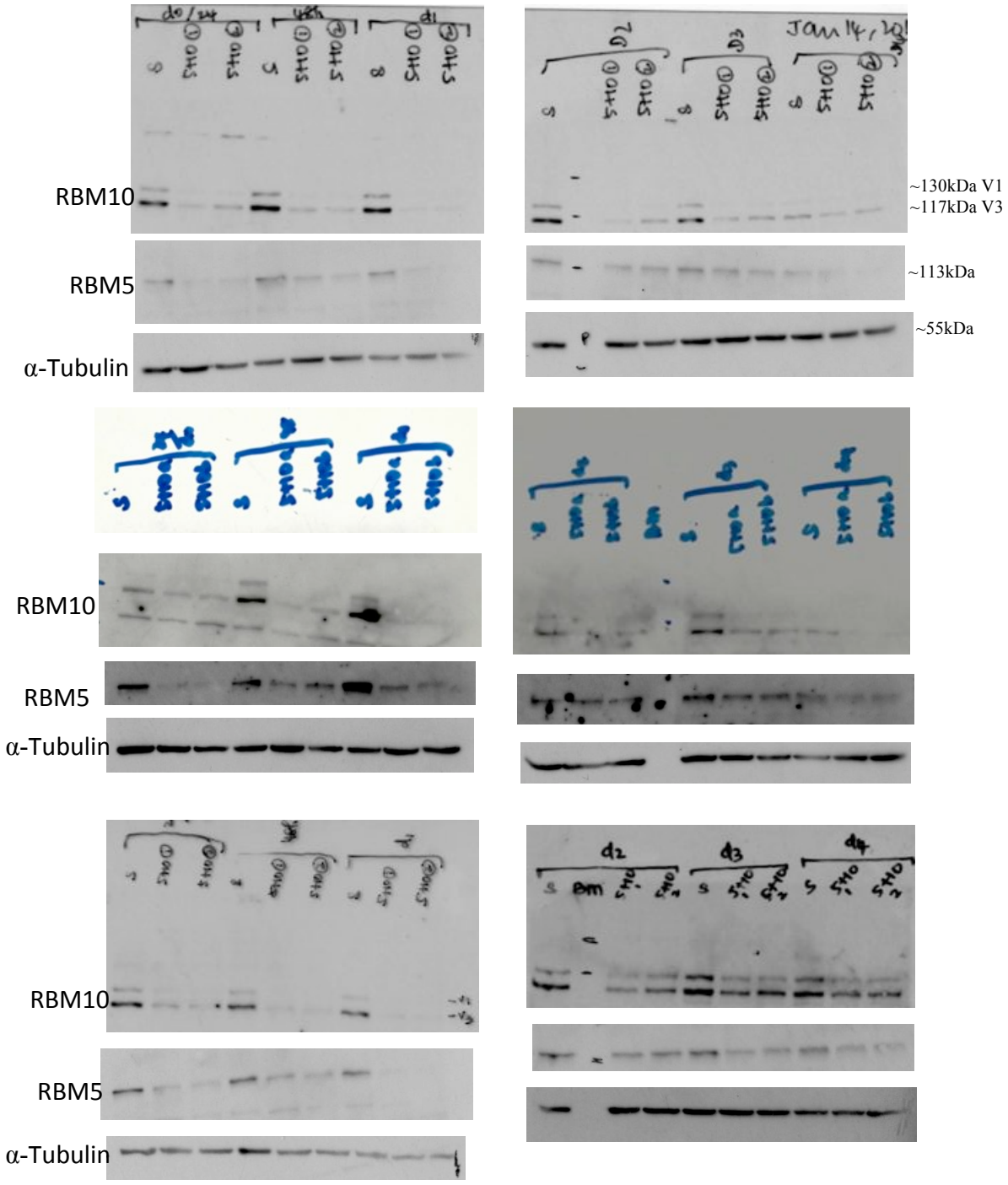

Figure A9. **RBM5, RBM10 and α-Tubulin levels in RBM5+10 KDs.** Raw Western blot images for RBM5, RBM10 and α-tubulin from siRBM5+10 and siRNA scrambled control (S) C2C12 cells at 24h, 48h post-transfection and at D0-D4 differentiation, in technical replicates (Trial 1). 5+10a (also labelled as 5+10 1) & 5+10b (also labeled as 5+10 2)- Two different concentrations of siRNA were used for RBM5+10 KD. For the purpose of this thesis only the results obtained from 5+10b are used for interpretation. BenchMark protein ladder (BM) (Life Technologies) was used as the molecular weight (in kDa) standard.

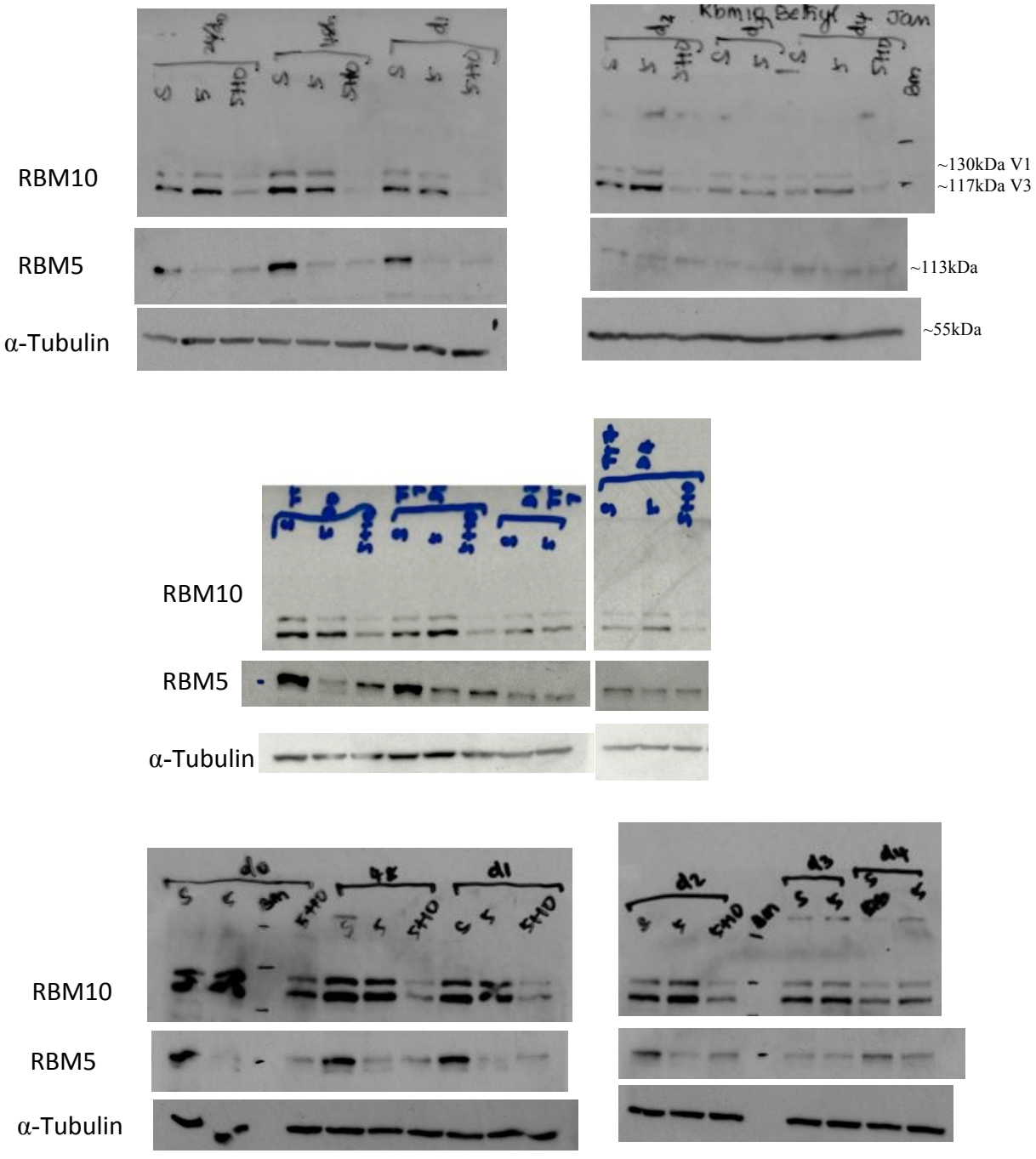

Figure A10. **RBM5, RBM10 and α-Tubulin levels in RBM5 and RBM5+10 KDs.** Raw Western blot images for RBM5, RBM10 and α-tubulin from siRBM5 (trial3), siRBM5+10 (5+10) (trial2), and siRNA scrambled control (S) C2C12 cells at 24h, 48h post-transfection and at D0-D4 differentiation, in technical replicates. BenchMark protein ladder (BM) (Life Technologies) was used as the molecular weight (in kDa) standard.

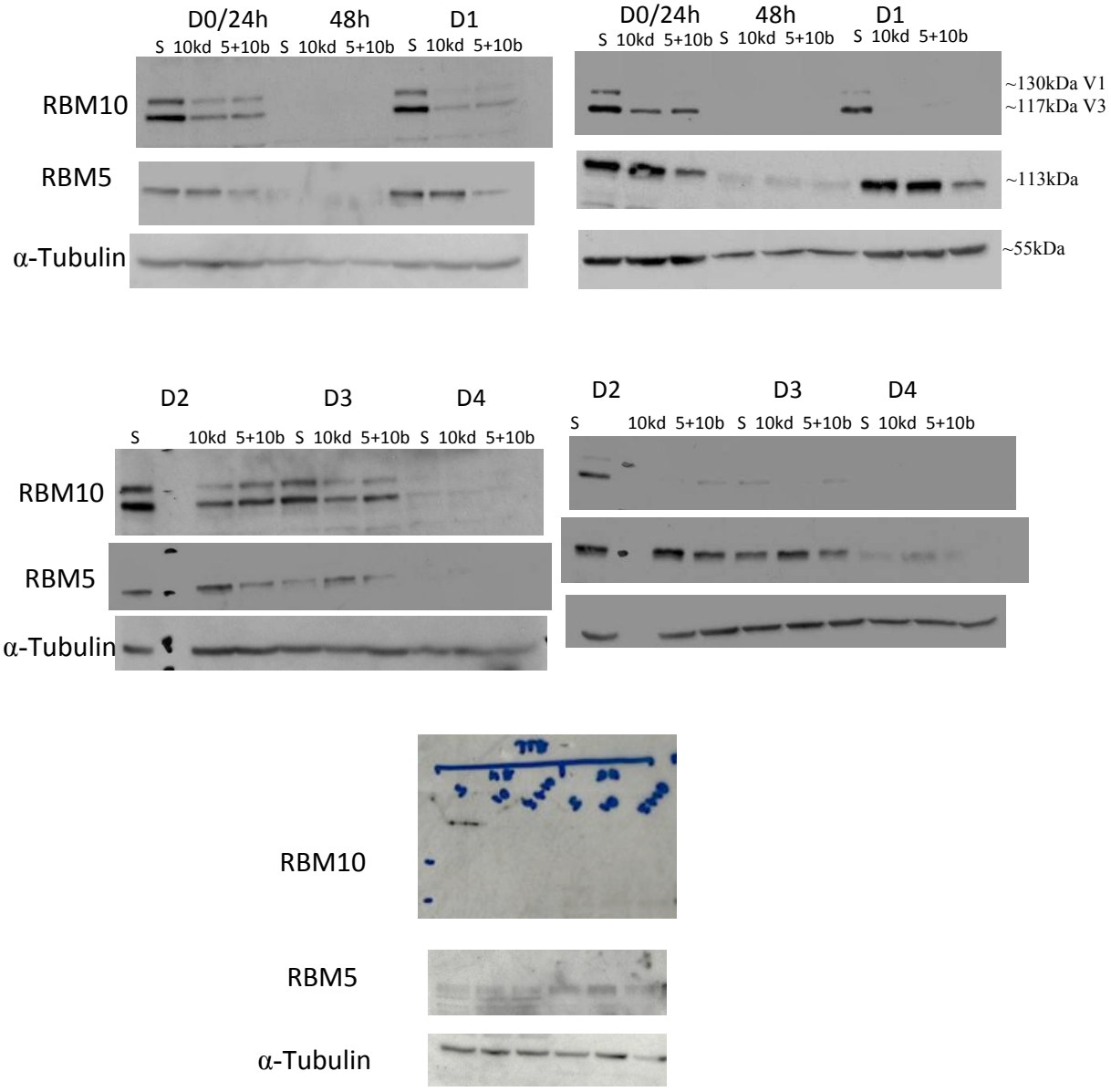

Figure A11. **RBM5, RBM10 and α-Tubulin levels in RBM10 and RBM5+10 KDs.** Raw Western blot images for RBM5, RBM10 and α-tubulin from siRBM10 (10), siRBM5+10 (5+10b) and siRNA scrambled control (S) C2C12 cells at 24h, 48h post-transfection and at D0-D4 differentiation, in technical replicates (Trial 3). BenchMark protein ladder (Life Technologies) was used as the molecular weight (in kDa) standard.

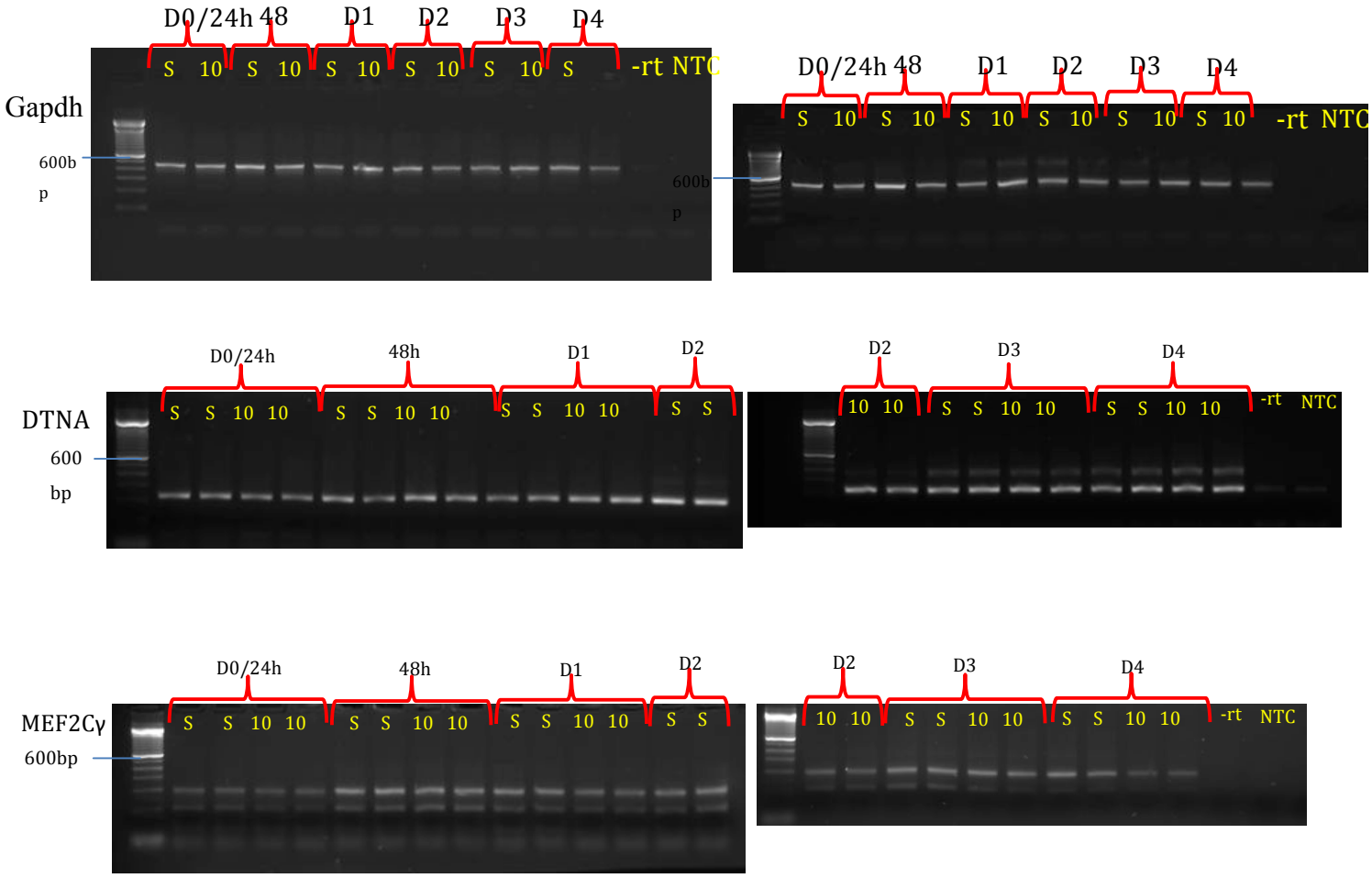

Figure A12. ***Gapdh*, *Dtna* and *Mef2cγ* levels in RBM10 KDs.** *Gapdh*, *DtnaA* and *Mef2cγ* end-point PCR products visualized in a 2% agarose gel stained with SYBR® safe DNA gel stain for determining the alternative splicing changes in RBM10-depleted (Trial1) C2C12 cells collected at 24h, 48h post-transfection and at D0-D4 differentiation. S- Scrambled control, 10- Rbm10 KD, -rt and NTC – negative controls. Presented here are technical duplicates that are representative of the technical quadruplicates. 100bp DNA ladder (Life Technologies).

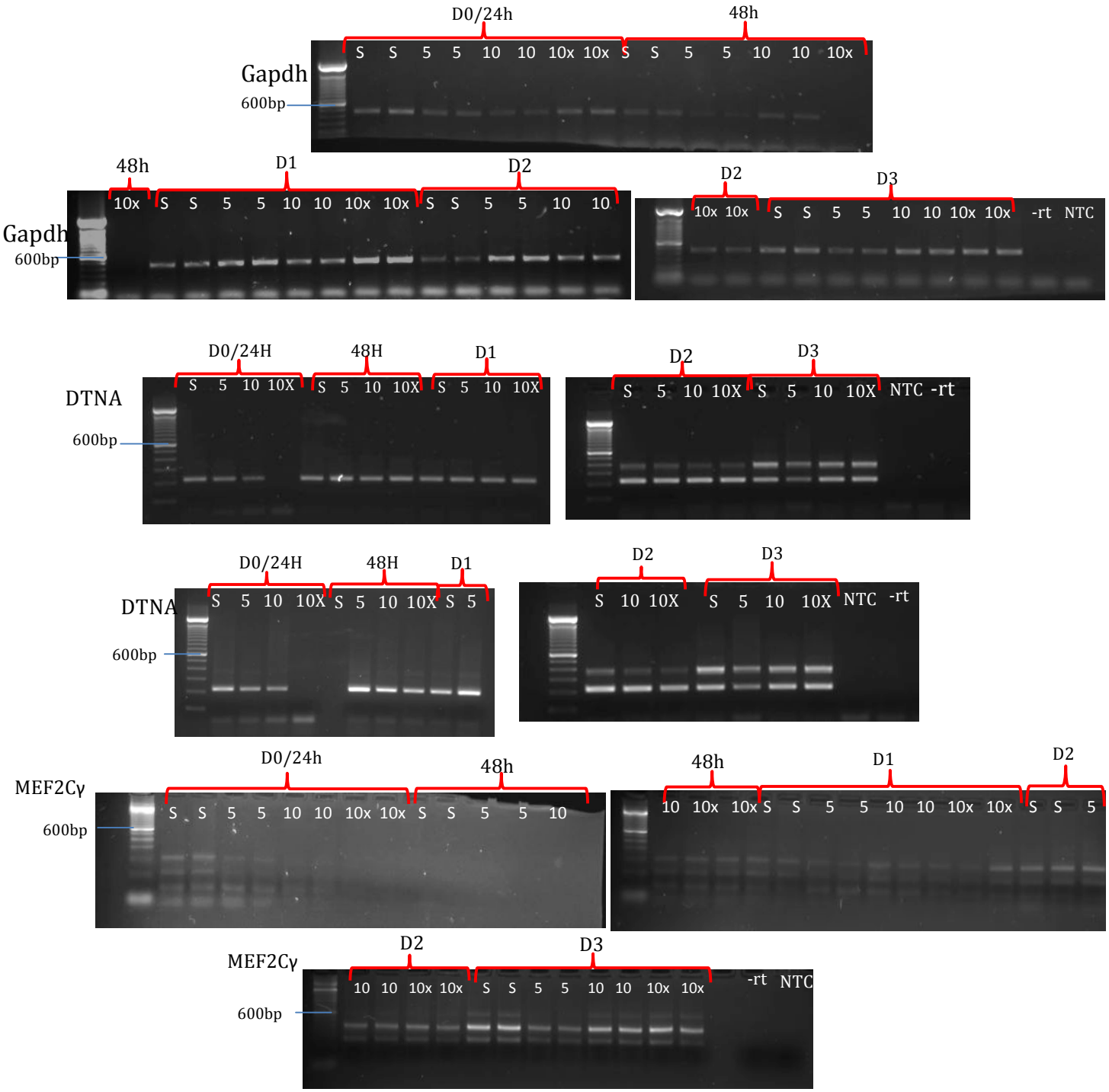

Figure A13. **Gapdh, Dtna and Mef2cγ levels in RBM5 and RBM10 KDs.** *Gapdh*, *Dtna* and *Mef2cγ* end-point PCR products visualized in a 2% agarose gel stained with SYBR® safe DNA gel stain for determining the alternative splicing changes in Rbm5-depleted (trial 1) and RBM10- depleted (trial2) C2C12 cells. S- Scrambled control, 5- Rbm5 KD, 10- Rbm10 KD and 10x- Rbm10 v1 KD. –rt and NTC-negative controls. Presented here are technical replicates that are representative of the technical quadruplicates used in the analysis. 100bp DNA ladder (Life Technologies).

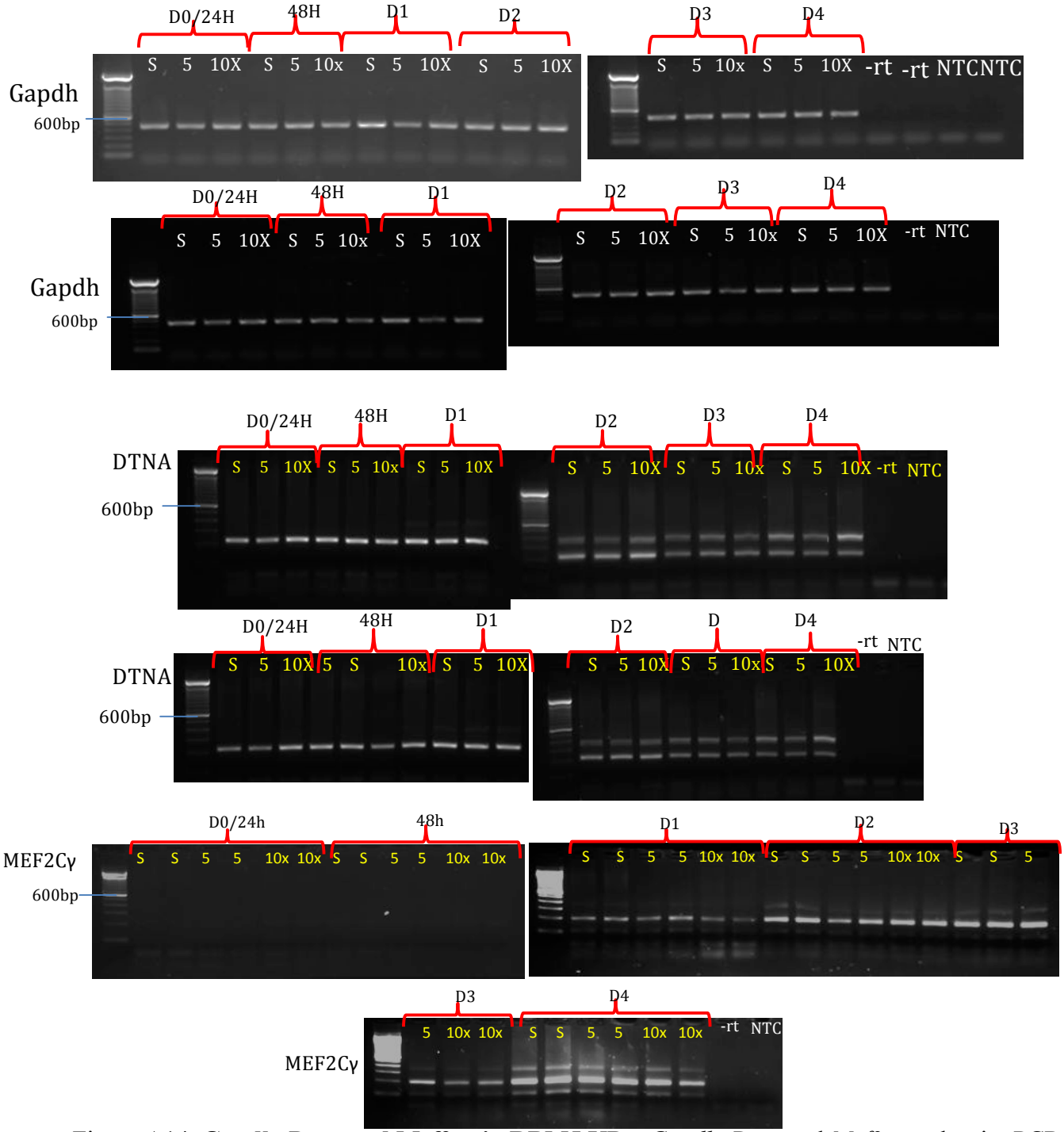

Figure A14. **Gapdh, Dtna and Mef2cγ in RBM5 KDs**. *Gapdh*, *Dtna* and *Mef2cγ* end-point PCR products visualized in a 2% agarose gel stained with SYBR® safe DNA gel stain for determining the alternative splicing changes in Rbm5-depleted (trial 2) C2C12 cells. S- Scrambled control, 5-Rbm5 KD and 10x- Rbm10 v1 KD. –rt and NTC-negative controls. Presented here are technical replicates that are representative of the technical quadruplicates used in the analysis. 100bp DNA ladder (Life Technologies).

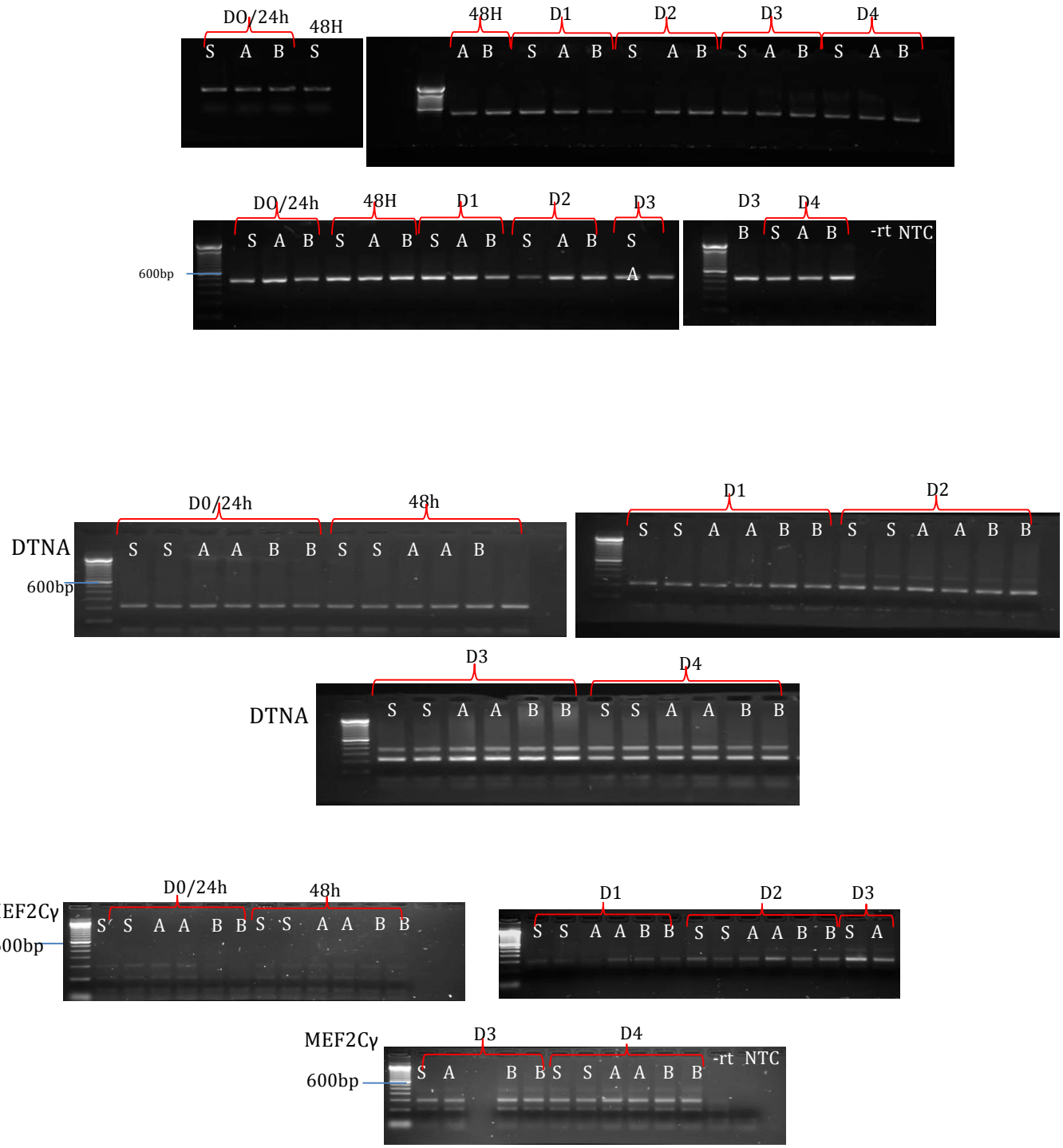

Figure A15. ***Gapdh*, *Dtna* and *Mef2cγ* levels in RBM5+10 KDs.** *Gapdh*, *Dtna* and *Mef2cγ* end-point PCR products visualized in a 2% agarose gel stained with SYBR® safe DNA gel stain for determining the alternative splicing changes in Rbm5&10-depleted C2C12 cells (trial1). S-Scrambled control, A&B- Two different concentrations of siRNA were used for RBM5+10 KD. For the purpose of this thesis only the results obtained from 'B' are used for interpretation. –rt and NTC- negative controls. 100bp DNA ladder (Life Technologies). Presented here are technical replicates that are representative of the technical quadruplicates used in the analysis.

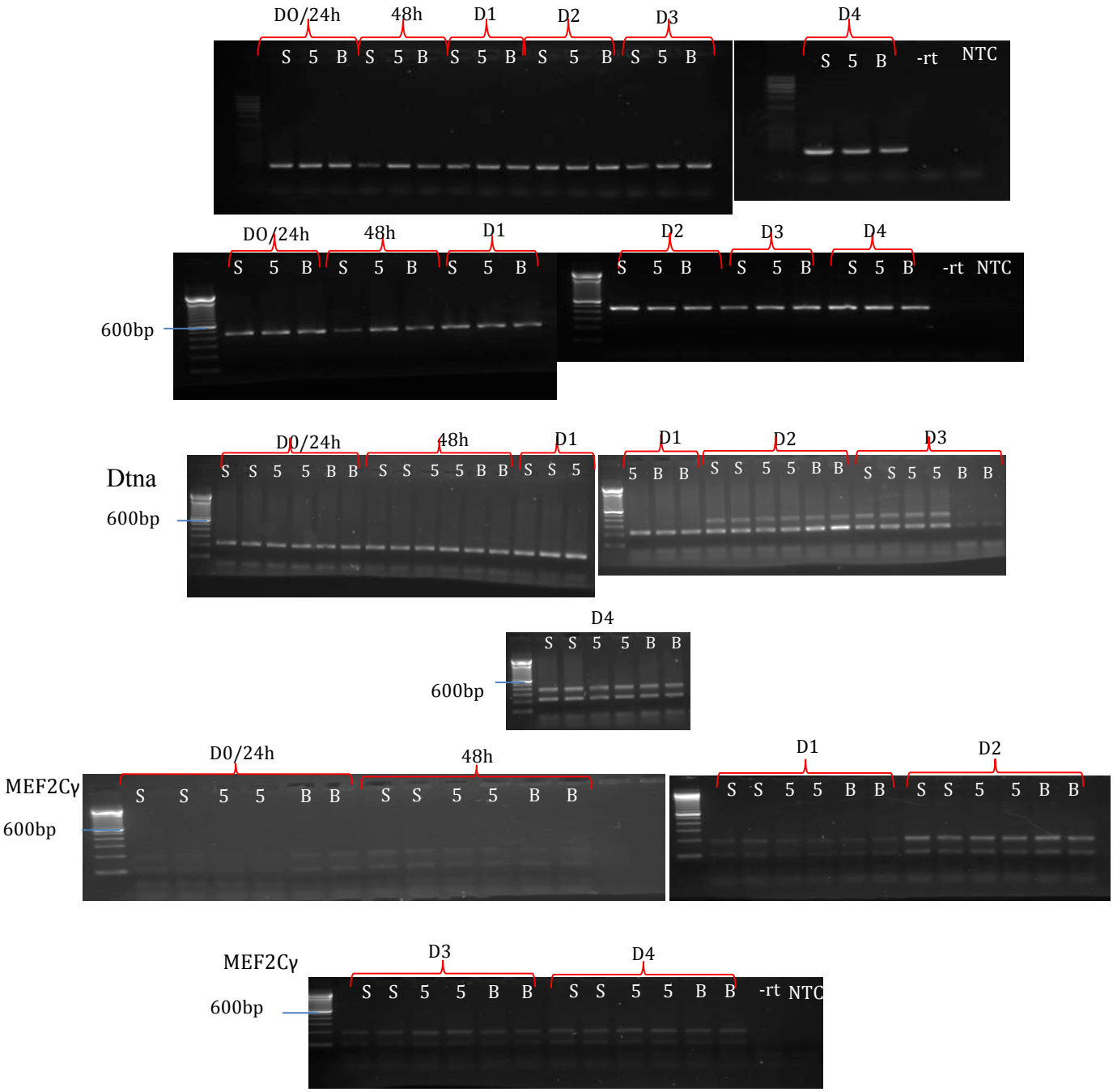

Figure A16. ***Gapdh*, *Dtna* and *Mef2cγ* levels in RBM5 and RBM5+10 KDs.** *Gapdh*, *Dtna* and *Mef2cγ* end-point PCR products visualized in a 2% agarose gel stained with SYBR® safe DNA gel stain for determining the alternative splicing changes in Rbm5-depleted (trial3)and RBM5&10- depleted (trial2) C2C12 cells. S- Scrambled control, 5- Rbm5 KD and B- Rbm5+10 KD. –rt and NTC- negative controls. 100bp DNA ladder (Life Technologies). Presented here are technical replicates that are representative of the technical quadruplicates used in the analysis.

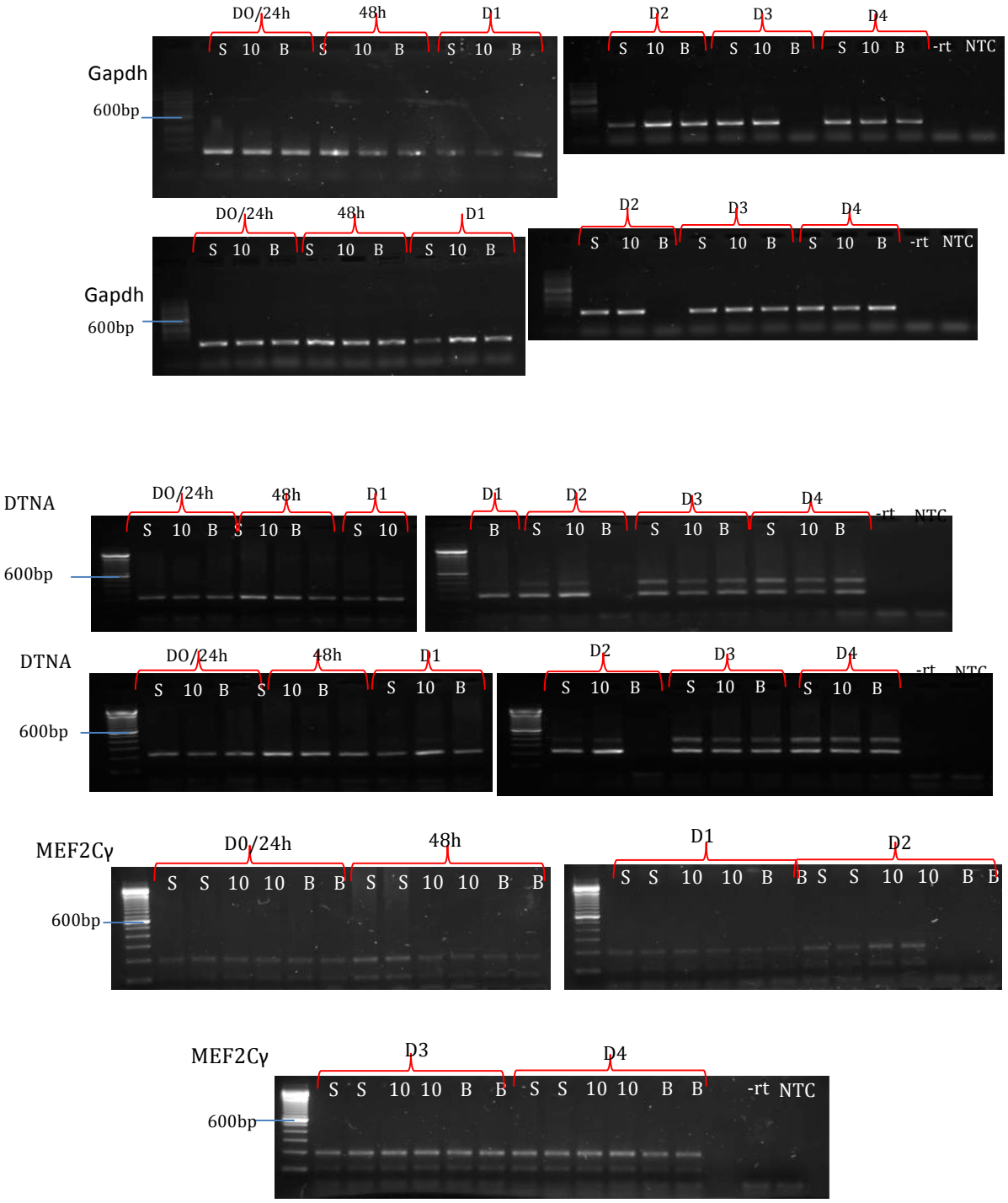

Figure A17. ***Gapdh*, *Dtna* and *Mef2cγ* in RBM10 and RBM5+10 KDs**. *Gapdh*, *DtnaA* and *Mef2cγ* end-point PCR products visualized in a 2% agarose gel stained with SYBR® safe DNA gel stain for determining the alternative splicing changes in Rbm10-depleted (trial 3) and RBM5&10- depleted (trial 3) C2C12 cells. S- Scrambled control, 10- Rbm10 KD and B- Rbm5+10 KD. –rt and NTC- negative controls. 100bp DNA ladder (Life Technologies). Presented here are technical replicates that are representative of the technical quadruplicates used in the analysis.

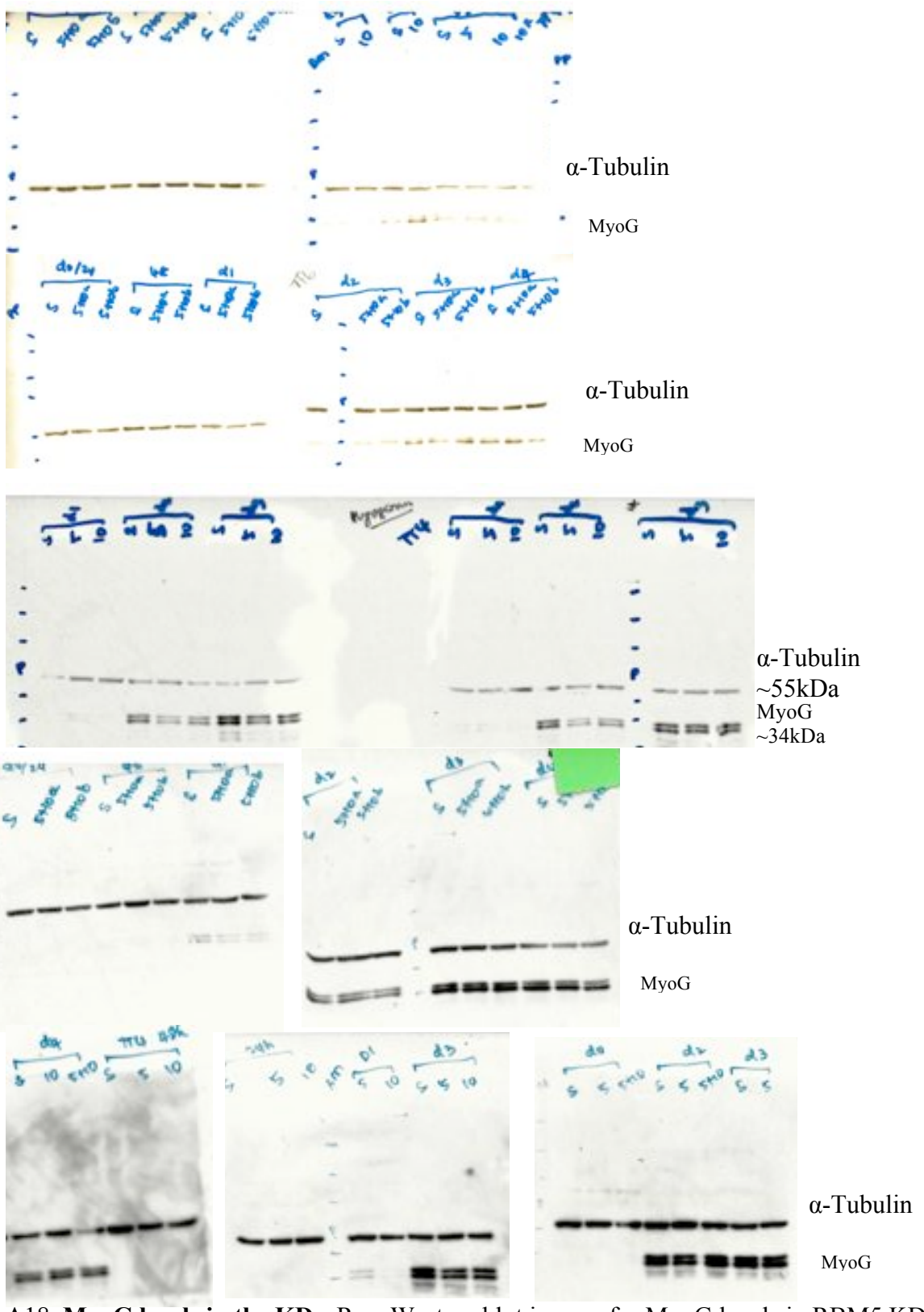

Figure A18. **MyoG levels in the KDs**. Raw Western blot images for MyoG levels in RBM5 KD, RBM10 KD and RBM5+10 KDs at 24h and 48h post-transfection and at D1-D4 differentiation from 3 trials. BenchMark protein ladder (Life Technologies) was used as the molecular weight standard. α-Tubulin levels are also shown in these images. Presented here are technical replicates that are representative of the technical quadruplicates used in the analysis.

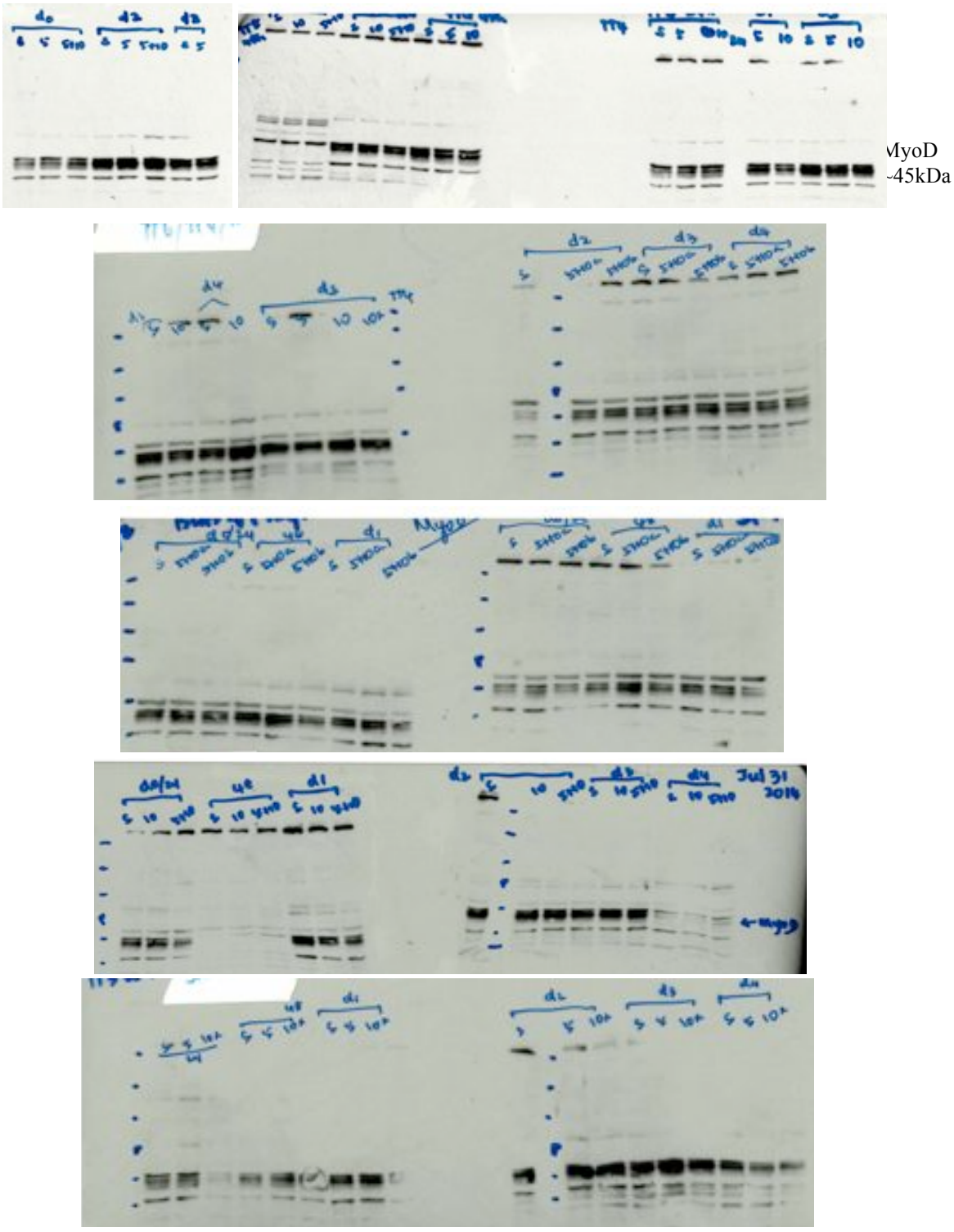

Figure A19. **MyoD levels in the KDs**. Raw Western blot images for MyoD levels in RBM5 KD, RBM10 KD and RBM5+10 KDs at 24h and 48h post-transfection and at D1-D4 differentiation. BenchMark protein ladder (Life Technologies) was used as the molecular weight standard. α-Tubulin levels are shown in Fig A18.

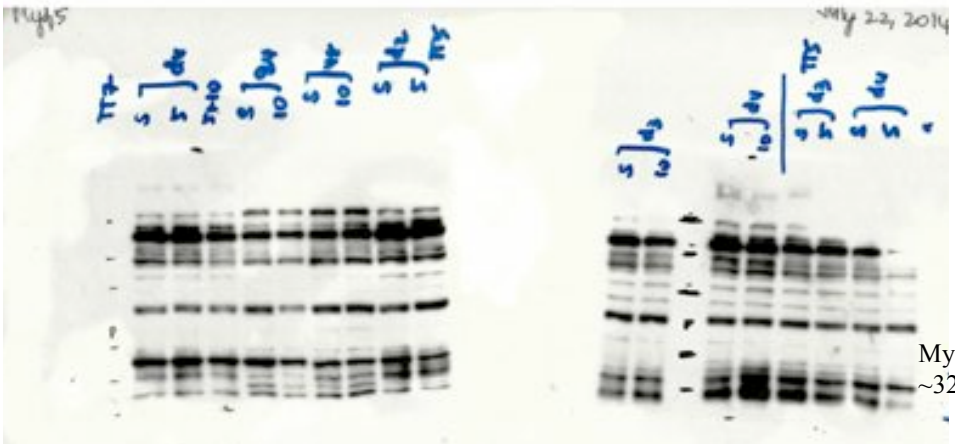

Figure A20. **Myf5 levels in the KDs**. Raw Western blot images for Myf5 levels in RBM5 KD, RBM10 KD and RBM5+10 KDs. BenchMark protein ladder (Life Technologies) was used as the molecular weight standard. α-Tubulin levels are shown in Fig A18.

Table A1: Passage number of the C2C12 cells used in the experiments

Passage number	**Experiment**
P13, P16, P13, P18	RBM5 and RBM10 expression during differentiation
P10	RBM5 and RBM10 expression during differentiation (IF)
P14	RBM10 (trial2) and RBM5 (trial1) KDs
P20	RBM10 KD (trial1)
P12	RBM5 KD (trial2)
P13	RBM5+10 KD (trial1)
P15	RBM5 (trial3) and RBM5+10 (trial2) KDs
P16	RBM10 (trial3) and RBM5+10 (trial3) KDs

Appendix B

Assessment of Reference Genes for Real-Time Quantitative PCR Gene Expression Normalization During C2C12 and H9c2 Skeletal Muscle Differentiation
Twinkle J. Masilamani • Julie J. Loiselle •Leslie C. Sutherland
Molecular Biotechnology, Volume 56, Issue 4, 2014, pp 329-339

Supplemental Material
Molecular Biotechnology, Volume 56, Issue 4, 2014, pp 329-339

Copyright Agreement

"Springer US / Molecular Biotechnology, Volume 56, Issue 4, 2014, pp 329-339, Assessment of Reference Genes for Real-time Quantitative PCR Gene Expression Normalization During C2C12 and H9c2 Skeletal Muscle Differentiation, Twinkle J. Masilamani, Julie J. Loiselle, Leslie C. Sutherland, full text, original copyright notice license number 3520470686229 is given to the publication in which the material was originally published, with kind permission from Springer Science and Business Media"

Co-Authorship Statement

All works pertaining to C2C12 cells were performed by TJM. JJL performed the experiments for H9c2 cells.

Mol Biotechnol (2014) 56:329–339
DOI 10.1007/s12033-013-9712-2

RESEARCH

Assessment of Reference Genes for Real-Time Quantitative PCR Gene Expression Normalization During C2C12 and H9c2 Skeletal Muscle Differentiation

Twinkle J. Masilamani · Julie J. Loiselle · Leslie C. Sutherland

Published online: 22 October 2013
© Springer Science+Business Media New York 2013

Abstract Skeletal muscle differentiation occurs during muscle development and regeneration. To initiate and maintain the differentiated state, a multitude of gene expression changes occur. Accurate assessment of these differentiation-related gene expression changes requires good quality template, but more specifically, appropriate internal controls for normalization. Two cell line-based models used for in vitro analyses of muscle differentiation incorporate mouse C2C12 and rat H9c2 cells. In this study, we set out to identify the most appropriate controls for mRNA expression normalization during C2C12 and H9c2 differentiation. We assessed the expression profiles of Actb, Gapdh, Hprt, Rps12 and Tbp during C2C12 differentiation and of Gapdh and Rps12 during H9c2 differentiation. Using NormFinder, we validated the stability of the genes individually and of the geometric mean generated from different gene combinations. We verified our results using Myogenin. Our study demonstrates that using the geometric mean of a combination of specific reference genes for normalization provides a platform for more precise test gene expression assessment during myoblast differentiation than using the absolute expression value of an individual gene and reinforces the necessity of reference gene validation.

Keywords Skeletal differentiation · C2C12 · H9c2 · Myogenesis · Real-time quantitative PCR · Reference genes · Normalization · Geometric mean

Introduction

Myogenesis, a multistep, highly orchestrated process that is inherently necessary for muscle development and regeneration, involves a multitude of gene expression changes [1]. Exploring the molecular pathways of skeletal and cardiac myogenesis involves quantifying the expression of transcription factors [2], growth factors [3], calcium channels

Electronic supplementary material The online version of this article (doi:10.1007/s12033-013-9712-2) contains supplementary material, which is available to authorized users.

T. J. Masilamani · L. C. Sutherland
Biomolecular Sciences Program, Laurentian University, 935 Ramsey Lake Road, Sudbury, ON P3E 2C6, Canada
e-mail: tmasilamani@amric.ca

T. J. Masilamani · J. J. Loiselle · L. C. Sutherland (✉)
AMRIC, Health Sciences North, 41 Ramsey Lake Road, Sudbury, ON P3E 5J1, Canada
e-mail: lsutherland@amric.ca

J. J. Loiselle
e-mail: jloiselle@amric.ca

J. J. Loiselle · L. C. Sutherland
Department of Biology, Laurentian University, 935 Ramsey Lake Road, Sudbury, ON P3E 2C6, Canada

L. C. Sutherland
Department of Chemistry and Biochemistry, Laurentian University, 935 Ramsey Lake Road, Sudbury, ON P3E 2C6, Canada

L. C. Sutherland
Division of Medical Sciences, Northern Ontario School of Medicine, Laurentian University, 935 Ramsey Lake Road, Sudbury, ON P3E 2C6, Canada

L. C. Sutherland
Division of Medical Oncology, Department of Medicine, University of Ottawa, Ottawa, ON, Canada

[4] and kinases [5] that play a major role during initiation and maintenance of the differentiated state. Murine C2C12 and rat H9c2 cells are secondary cell line-based models that are used for the study of gene expression during the differentiation phase of myogenesis [6–10]. Real-time quantitative PCR (qPCR) is an effective and reliable method for the accurate assessment of gene expression changes. Using qPCR, the normal differentiation-associated changes in gene expression, as well as disease-associated changes, equivalent to those that occur in muscular dystrophy and cancer, can be investigated [11–13].

In qPCR, good RNA integrity and the use of reference genes whose expression levels (a) do not change, and (b) are similar to those of the test gene, are vital for the accurate assessment of gene expression. RNA integrity can be determined using gel electrophoresis to visually assess the amount of ribosomal RNA degradation, or using a bioanalyzer that calculates the RNA Integrity Number (RIN) [14]. Purity is generally assessed using a spectrophotometer to determine the 260/280 absorbance ratio. Any variability in sample preparation attributed to, e.g., sample purity, handling and enzyme efficiencies, is minimized by the use of a normalization control, typically either a reference gene or input foreign RNA. Reference genes for expression normalization are usually "housekeeping" genes, genes that are ubiquitously and constitutively expressed, and required for cell viability [15].

A major criterion for a reference gene is that its expression levels remain constant without bias to treatment, age, tissue type, nutrition, gender, etc. Unfortunately, the expression of many genes is effected by the vagaries of experimental conditions [16, 17]. The use of more than one reference gene increases accuracy by reducing noise and error, and is becoming an accepted standard in expression studies [18]. Ideally, multiple reference genes would be empirically validated and the ones with minimal experimentally associated expression level variability would be used to normalize, either by averaging [19] or using the geometric mean [18] of the expression levels. Software programs, such as BestKeeper [20], GeNorm [18] and NormFinder [21], are available to help with reference gene validation, each using a different algorithm to calculate expression stability.

The two genes most commonly used for normalization in mouse and rat expression studies are β-actin (*Actb*) and glyceraldehyde-3-phosphate dehydrogenase (*Gapdh*) [8, 22, 23]. Mouse reference genes have also included hypoxanthine phosphoribosyltransferase (*Hprt)* [24], ribosomal protein S12 (*Rps12*) [25], TATA binding protein (*Tbp*) [26], β-glucuronidase (*GusB*) [27], ribosomal RNA small subunit (*18S*) [28], β-2 microglobulin *(B2 M)* [29] and cyclophilin D (*CycD*) [30].

The objective of our study was to examine the expression of various genes during C2C12 and H9c2 myoblast differentiation. To accomplish this, we needed to establish which genes would make optimal reference genes for expression normalization. We set out to identify a normalization control with (a) static RNA expression during differentiation, and (b) suitability for both high and low expressing test genes. For C2C12 differentiation, we chose to assess the suitability of Actb, Gapdh, Hprt, Rps12 and Tbp transcripts (Table 1). The Actb transcript encodes a cytoskeletal protein that is ubiquitously and highly expressed. As a component of cytoskeletal microfilaments, it functions in cell motility and the transport of organelles and chromosomes [31]. The Gapdh transcript encodes a major metabolic enzyme that is ubiquitously and highly expressed, and involved in many processes including apoptotic initiation, transcription activation and endoplasmic reticulum to Golgi shuttling [32]. Hprt encodes a transferase enzyme that is ubiquitously but not highly expressed, and is involved in the salvage pathway that generates purine nucleotides [33]. *Rps12* produces the ribosomal subunit 40S, and was identified by meta-analysis as one of the top fifteen novel candidate reference genes in humans and mice [25]. Tbp encodes a transcription factor that binds to the TATA box, and is a component of the pre-initiation transcription complex for all three RNA polymerases [34]. Gapdh and Hprt were previously used [35, 36] as individual reference genes and thus were included as study controls. Actb was included out of curiosity since, despite the fact that it was previously determined to be unsuitable for C2C12 differentiation studies [37, 38], many studies still incorporate it as a normalization control. For H9c2 differentiation, we chose to assess the suitability of Gapdh and Rps12 transcripts (Table 1). Gapdh was chosen since it has been routinely used for rat expression studies, but we found no prior publication validating its use as a reference gene for H9c2 differentiation studies. Rps12 was chosen as a second candidate gene for validation because in humans and mice it was identified as one of the top potential reference genes [25]. Following our examination of reference gene expression, we used the geometric mean for normalization of Myogenin levels.

Materials and Methods

Cell Culture and Differentiation

C2C12 murine myoblasts (a gift from Dr. Celine Boudreau-Larivière) were grown in Growth Medium (GM) containing Dulbecco's Modified Eagle's Medium (DMEM)-High Glucose (Life Technologies, Burlington, ON, USA) supplemented with 10 % Fetal Bovine Serum (FBS) (Life Technologies) and 1 % antibiotic–antimycotic (Life Technologies). Differentiation was induced, at 80 % confluence, by replacing the GM with differentiation medium (DM)

containing DMEM-High Glucose supplemented with 2 % horse serum (Life Technologies) and 1 % antibiotic–antimycotic. Day 0 (D0) indicates the day on which the cells were switched from GM to DM. H9c2 rat myoblasts (ATCC-CRL1446) were grown in DMEM-High Glucose supplemented with 10 % FBS (GM) and skeletal differentiation was induced at 80 % confluence by switching GM to DMEM-High Glucose containing 1 % FBS (DM). C2C12 and H9c2 cells were incubated at 37 °C with 5 % CO_2, and the medium was replaced every two days. Adherent cells were harvested using 2.5 % trypsin (Life Technologies). Trypsin was inactivated using GM; the cells were centrifuged at 16 200 × *g*, and then stored at −80 °C.

Immunofluorescence and Confocal Laser Scanning Microscopy (LSM)

C2C12 and H9c2 cells were grown on coverslips (VWR International LLC, Radnor, PA, USA). Differentiation was induced with the respective conditions and coverslips were collected on D0, D4 and D7. The cells were fixed with 4 % paraformaldehyde and permeabilized using 0.5 % Triton X-100. 5 % goat serum was used for blocking. Immunofluorescence was performed with a 1:100 dilution of Myosin Heavy Chain (MHC) mAb MF20-b (Developmental Studies Hybridoma Bank, Iowa City, IA) and probed with AlexaFluor 488 anti-mouse IgG secondary antibody (1: 200 dilution) (Molecular Probes, Life Technologies). The nucleus was stained with DRAQ5 (1:1 000 dilution) (Biostatus Ltd, Leicestershire, UK). Confocal pictures were taken on a Zeiss LSM 510 Meta confocal microscope using the same settings for D0, D4 and D7 (excitation at 633 nm for DRAQ5, 488 nm for Mf-20 and 543 nm for Phalloidin).

RNA Extraction and Reverse-Transcription (RT)

Total RNA was extracted from 80 % confluent cells grown in 10-cm plates using 1 ml Tri Reagent Solution (Molecular Research Centre Inc., Cincinnati, OH, USA), quantified using the Nano Drop 2 000 spectrophotometer (Thermo Scientific, Wilmington, DE, USA) and the integrity checked by electrophoresing through a 1 % agarose gel (Supplementary Figs. 1S, 2S). For C2C12 cells, we treated with DNase (Ambion®, Life Technologies Inc.) 20 µg of RNA in a 50-µl total volume, according to the manufacturer's instructions, then reverse-transcribed 2 µg of the DNase-treated RNA using 500 ng OligoDT (Alpha DNA, Montreal, QC, USA), 10 mM dNTPs (New England Biolabs, Whitby, ON), 5X First Strand Buffer, 0.1 mM DTT and 200 U Moloney Murine leukemia virus (MMLV) reverse transcriptase (Life Technologies) in a 40-µl reaction volume. cDNA was generated by denaturing the RNA at 65 °C for 5 min, reverse transcribing the RNA into cDNA for 2 min at 37 °C followed by 50 min at 37 °C, then terminating the transcription reaction at 70 °C for 10 min. In the case of H9c2 cells, only those time courses that showed genomic DNA contamination were DNase-treated. For H9c2 cells, 1 µg of RNA was used in a 20-µl reaction volume with the above-described RT conditions. For C2C12 and H9c2 cells, RT negative controls (cDNA synthesis without the addition of MMLV-RT enzyme) were also included to confirm the absence of genomic DNA contamination or the presence of pseudogenes.

End-Point PCR

C2C12 and H9c2 cDNA synthesis and genomic DNA contamination were verified using end-point PCR (Supplementary Figs. 3S, 4S). For C2C12 cells, we used Gapdh Forward: 5′-AACACAGTCCATGCCATCAC-3′ and Gapdh Reverse: 5′-TCCACCACCCTGTTGCTGTA-3′. The PCR reaction consisted of 100 ng of cDNA template, 0.2 mM dNTPs, 200 nm of forward and reverse oligos (Alpha DNA), 1.25 U Taq DNA polymerase and 10x reaction buffer in a 50-µl volume. The template was denatured for 5 min at 95 °C, amplified with 26 cycles of 95 °C for 30 s, 58 °C for 30 s and 72 °C for 1 min, and extended at 72 °C for 10 min. A 452-bp amplicon was visualized in a 1 % agarose gel stained with SYBR® safe DNA gel stain (Life Technologies). For H9c2 cells, we used Actin Forward: 5′ TGAGCGCAAGT ACTCTGTGTGGAT 3′ and Reverse: 5′ TAGAAGCATT TGCGGTGCACGATG 3′. The PCR reaction consisted of 50 ng of cDNA template, 0.67 mM dNTPs, 0.67 µM of forward and reverse oligos (Alpha DNA), 1 U Taq DNA polymerase and 10x reaction buffer in a 15-µl volume. The PCR conditions were 95 °C for 10 min, 40 cycles at 95 °C for 30 s, 62 °C for 30 s and 72 °C for 45 s, and an extension at 72 °C for 10 min. A 129-bp amplicon was visualized in a 2 % agarose gel stained with SYBR® safe DNA gel stain.

Real-Time Quantitative PCR (qPCR)

Expression levels of Actb, Gapdh, Hprt, Rps12 and Tbp were determined using qPCR with the primers (Alpha DNA) listed in Table 1. In silico specificity of these primers was determined using the NCBI Blast tool and the primers were confirmed to have 100 % specificity to either the gene for which it was generated or pseudogenes (which were not amplified due to DNase treatment [26]). qPCR was carried out using 12.5 µl of iTaq™ SYBR® Green Super Mix with ROX (Bio-Rad, Mississauga, ON), 300–400 nM of forward and reverse oligos and 11 ng (H9c2) and 21 ng (C2C12) cDNA template in a 25-µl reaction and an ABI Prism 7900T Thermocycler (Applied Biosystems, Life Technologies Inc.). For C2C12 cells, four independent differentiation time courses (D0–D7) with varying numbers of technical

replicates (*n* of 2–7) were analyzed. For H9c2 cells, three independent differentiation time courses with 3 technical replicates were analyzed. The qPCR conditions were; denaturation at 95 °C for 3 min, followed by 40 cycles of 95 °C for 30 s and a primer-dependent temperature for annealing (see Table 1) for 60 s. For H9c2 samples, the annealing was carried out for 30 s, followed by a 15 s extension at 72 °C. The annealing temperatures were optimized using gradient end-point PCR performed on pooled cDNA templates. A melt-curve (dissociation profile), with data acquisition at 95 °C for 15 s, 60 °C for 15 s and 95 °C for 15 s, was used to experimentally confirm primer specificity (Supplementary Figs. 5S, 6S). Standard curves were generated, using dilutions of the pooled cDNA samples throughout differentiation (Supplementary Figs. 7S, 8S). The coefficient of determination (R^2) of the standard curves, used to determine if the Cq of the dilutions are a proper fit to the standard curve, showed that all were in the range of 0.98–0.99 (Supplementary Figs. 9S, 10S). Reaction efficiencies, calculated from the standard curve slope, were in the range 1.69–2.26.

Statistical Analysis

RNA expression levels were quantified using the relative quantification method because of the differing qPCR efficiencies amongst all transcripts [39, 40] using ABI software (SDS 2.4) based on the formula log 10^[(Cq (sample)-y intercept)/(-slope)], where Cq is the cycle threshold value (previously termed Ct value, but now more accurately referred to as the Cq value) and the y intercept and slope values are derived from the standard curve [41]. Data analysis was carried out using Microsoft Excel and Graph Pad Prism®. The relative fold-change in reference gene RNA expression for the time (day) in DM was calculated from the quantity normalized to the reference gene RNA expression level on day 0. Inter-quartile range (IQR) analysis was used to identify outliers. IQR was calculated from the 25th (q1) and 75th (q3) percentile values. Values with a fold-change $>$ q3 and $<$ q1 were considered as outliers and were eliminated from the analysis.

One-way ANOVA was used to determine if differentiation induced statistically significant changes in the expression levels of the reference genes. A $P < 0.05$ represented a statistically significant change in expression. Pearson

Fig. 1 Confocal immunofluorescence pictures of differentiating C2C12 and H9c2 cells. Mouse C2C12 (**a**) and rat H9c2 (**b**), myoblasts on D0, differentiating myocytes on D4 and differentiated myotubes on D7. The nuclei are stained with DRAQ5 (*blue*), MHC is detected by Alexafluor-conjugated secondary antibody for the Mf-20 protein (*green*) and F-actin (showing the cell morphology) is stained with phalloidin (*red*). H9c2 cells are also shown using phase contrast. The mono-nucleated myoblasts on D0 proliferate, elongate and fuse to become multi-nucleated myotubes by D7 differentiation. *Scale bar* 100 μm

Table 1 qPCR parameters for 5 candidate reference genes

Gene	PubMed ID	Function	Primer sequence [5′ to 3′]	Annealing temperature (°C)	Amplicon length (bp)
Mouse					
Actb	NM_007393.3	Cytoskeletal protein	F: TCCTGACCCTGAAGTACCCCAT	61	131
			R: CTCGGTGAGCAGCACAGGGT		
Gapdh	NM_008084.2	Metabolic enzyme	F: ATGTTTGTGATGGGTGTGAA	50	122
			R: ATGCCAAAGTTGTCATGGAT		
Hprt	NM_013556	Enzyme	F: ATGGACTGATTATGGACAGGACTG	60	124
			R: TCCAGCAGGTCAGCAAAGAAC		
Rps12	NM_011295.6	Ribosomal protein	F: AAGGCATAGCTGCTGGAGGTGTAA	60	156
			R: AGTTGGATGCGAGCACACACAGAT		
Tbp	NM_013684.3	Transcription factor	F: TGCACAGGAGCCAAGAGTGAA	60	132
			R: CACATCACAGCTCCCCACCA		
Myogenin	NM_031189.2	Myogenesis marker	F: CAGGAGATCATTTGCTCG	50	122
			R: GGGCATGGTTTCGTCTGG		
Rat					
Gapdh	BC059110	Metabolic enzyme	F: ATGTTTGTGATGGGTGTGAA	63	122
			R: ATGCCAAAGTTGTCATGGAT		
Rps12	M18547	Ribosomal protein	F: TGAGCCCATGTATGTCAAGCTGGT	67	162
			R: ACTACAACGCAACTGCAACCAACC		
Myogenin	NM_017115.2	Myogenesis marker	F: CAACTGAGATTGTCTGCCAGGC	63	165
			R: GTCTTATGTGAATGGACGGTGGG		

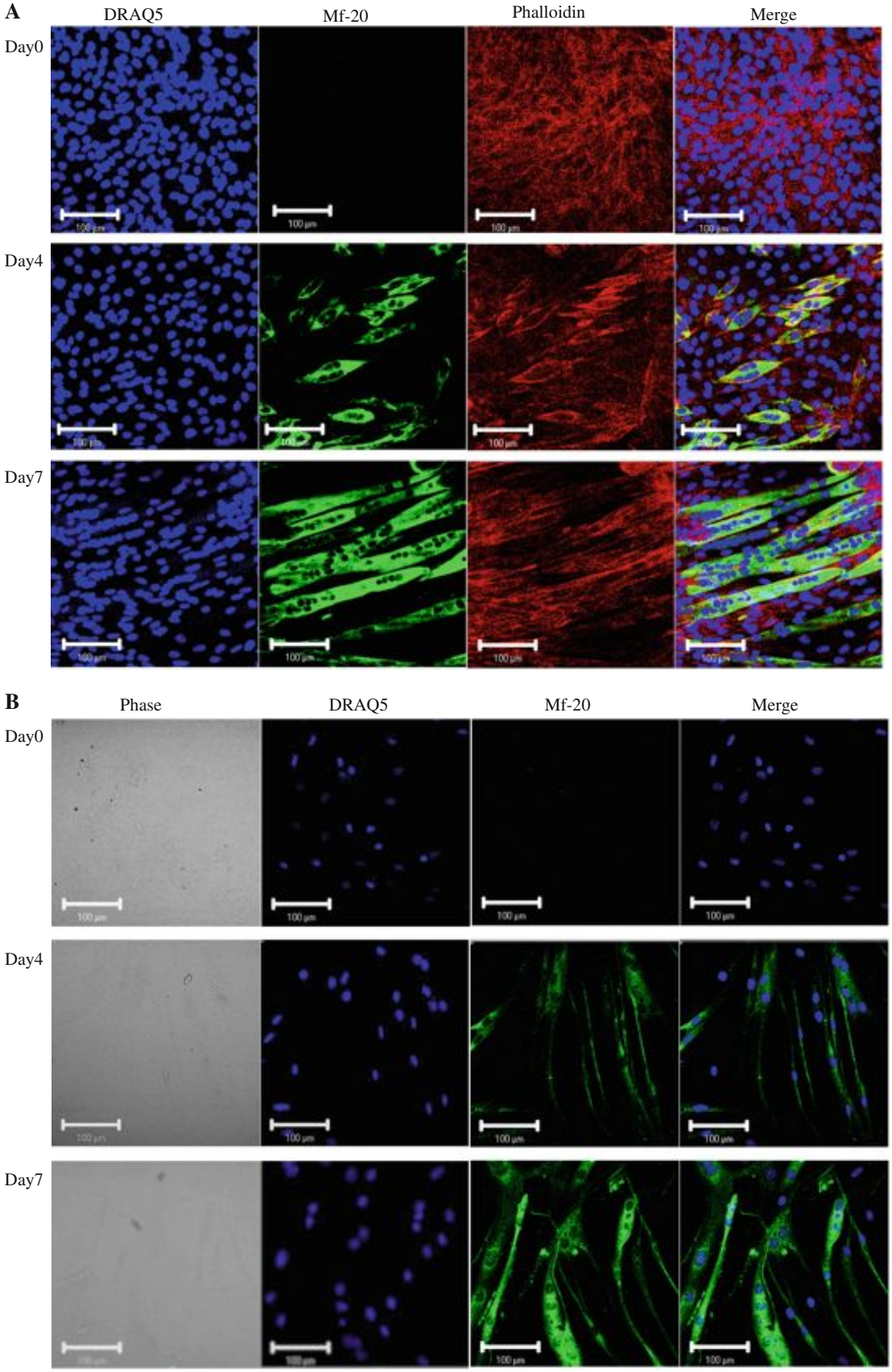
A
DRAQ5
Mf-20
Phalloidin
Merge
Day0
Day4
Day7
B
Phase
DRAQ5
Mf-20
Merge
Day0
Day4
Day7

correlation analysis (r) was used to examine the relationship between time in DM and reference gene expression changes, and a two-tailed Student's t test was used to determine the level of statistical significance. NormFinder [21], which determines the stability value based on the intra- and inter-group variations was used to verify the results obtained from the statistical analyses. It is a freeware available as an add-in for Microsoft Excel. Relative expression fold-change values were used in the analysis.

Results and Discussion

We set out to study gene expression changes during myoblast differentiation. C2C12 and H9c2 cells were induced to differentiate by serum withdrawal, resulting in cell cycle arrest, cell fusion and formation of multinucleated-myotubes. Many expression changes are associated with this phenotypic change between D0 and D7 as shown in Fig. 1a (C2C12) and Fig. 1b (H9c2). We ensured that any change in expression levels was not a result of decreased efficiency of RNA extraction in the more differentiated myotubes, or differences in RNA integrity, by visually assessing 28S, 18S and 5S RNA degradation using gel electrophoresis (Supplementary Figs. 1S,2S).

Expression Levels of Candidate Reference Genes in C2C12 Cells

Actb, Hprt, Gapdh, Rps12 and Tbp mRNA expression at each day of differentiation was assessed using real-time qPCR. The box plots in Fig. 2a show the fold-change in expression levels over time, before and after outlier elimination. (All subsequent calculations were minus outliers.) By grouping all the differentiation data for a particular gene (Fig. 2a), we see that expression of all the potential reference genes examined was less than expression at D0, a phenomenon not attributable to increased rRNA expression, which decreases during C2C12 differentiation [42]. By examining the data according to "days in DM" (Fig. 2b), we see that decreased expression occurred for each of the genes by D3; however, expression levels of Gapdh were closest to D0 and had a much smaller overall distribution than the other transcripts examined (Fig. 2a, b), thereby, demonstrating the least expression variability. Relative expression levels of all the five genes examined were of the order Gapdh > Actb > Rps12 > Hprt > Tbp (Supplementary Fig. 9S).

Expression Levels of Candidate Reference Genes in H9c2 Cells

During H9c2 skeletal myoblast differentiation, expression levels of both Gapdh and Rps12 were close to D0 with no significant variability during differentiation (Fig. 3). We did not, therefore, evaluate additional reference genes in H9c2 cells. Expression levels of Gapdh were higher than those of Rps12 (Supplementary Fig. 10S).

Statistical Analyses

To determine if the observed changes in expression levels during differentiation were significant (Supplementary Table 1S), for each day of each time course for each gene, a one-way analysis of variance (ANOVA) was performed (Table 2). There was no significant change in expression of Gapdh, Hprt and Tbp in C2C12 cells, or of Gapdh or Rps12 in H9c2 cells. To determine if a relationship existed between expression level changes and the length of time in DM, a Pearson correlation analysis was carried out (Table 2). In C2C12 cells, *Gapdh* was the only gene examined that did not demonstrate a significant correlation ($p = 0.0908$, $r^2 = 0.4030$) between expression changes and days in DM. Combined with the ANOVA analysis, these results suggest that Actb and Rps12 are unsuitable individual normalization controls for C2C12 differentiation studies using our parameters. Though a significant Pearson's correlation was observed for Hprt and Tbp, demonstrating a relationship between expression levels and the length of time in DM, the actual change in expression levels during differentiation was not significant (as determined by ANOVA), suggesting that Hprt and Tbp expression is stable during C2C12 differentiation, using our parameters. In H9c2 cells, no significant change in expression levels or significant correlations between expression levels and days in DM were observed for either Gapdh or Rps12.

Identification of Ideal Reference Genes Using NormFinder

We used NormFinder software to verify the results obtained by one-way ANOVA and Pearson's correlation analysis. NormFinder ranks the genes using a model-based approach, the lowest stability value indicating the most stable gene expression. NormFinder calculates this stability value using quantified gene expression values and not simply raw Cq values, as other software programs. This is important in our study since, as mentioned, certain primer pairs had lower efficiencies than others (this is taken into account when quantifying gene expression, but not when using raw Cq values).

In C2C12 cells, Hprt had the lowest stability value (0.069) which indicated that its transcript was the most stable (had the least variable expression) of the five candidate reference genes (Fig. 4a). Gapdh (0.142) was the next most stable, followed by Tbp (0.158), Rps12 (0.196) and

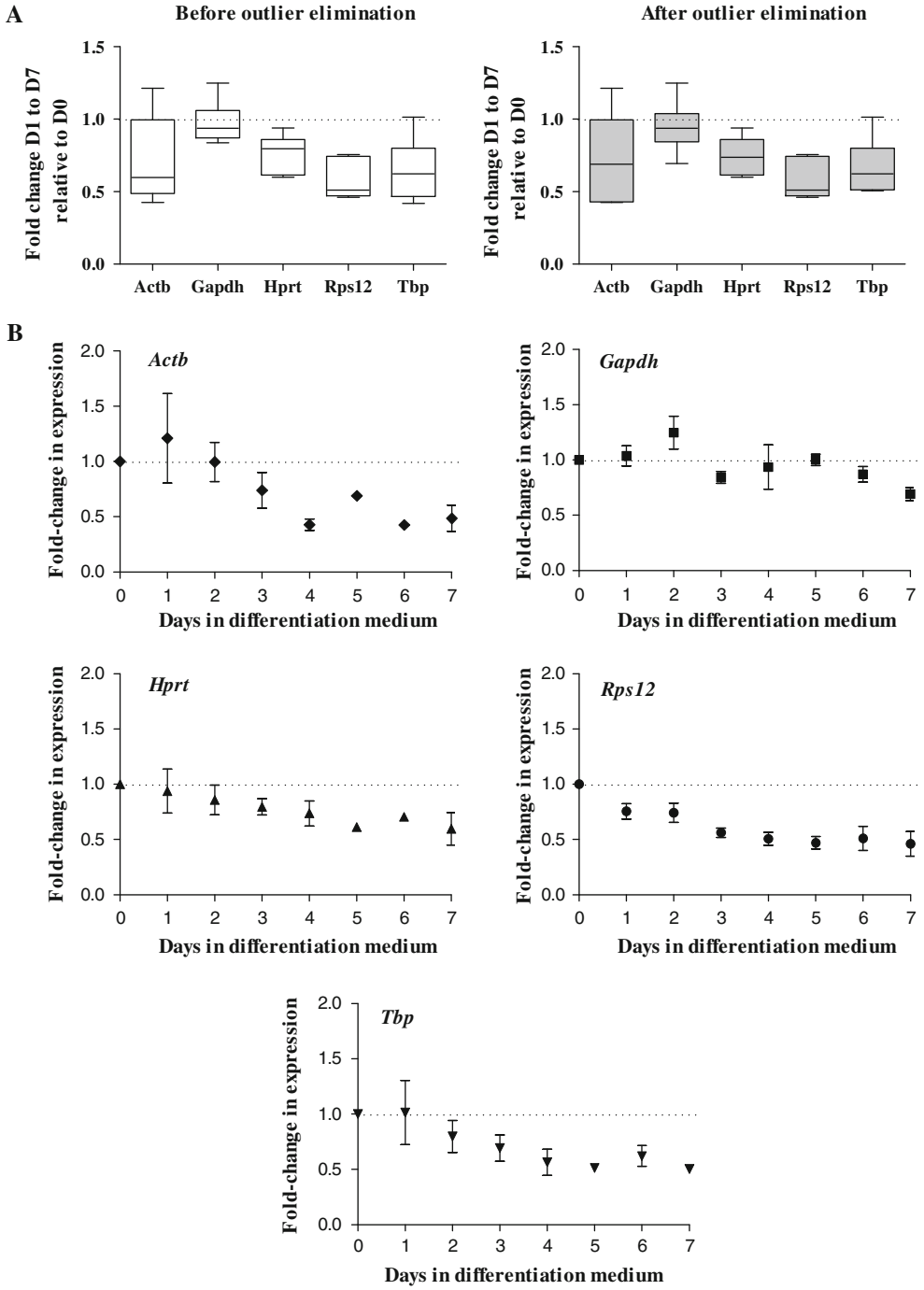

Fig. 2 qPCR expression profiles of five candidate reference genes in differentiating C2C12 cells. (**a**) *Box plots* showing distribution of the data before and after elimination of outliers. Whiskers represent the minimum and maximum fold-change values. (**b**) Individual gene expression profiles showing the fold-change in expression as compared to D0. *Error bars* represent ± SEM from four biological replicates. Data points are mean values plotted after removal of outliers

Actb (0.208). These NormFinder results were consistent with the results obtained from one-way ANOVA analysis in that they demonstrated Rps12 and Actb were the least stable transcripts (most variable). We also examined the stability values of various groupings of reference genes using the geometric mean because the geometric mean of multiple reference genes is another possibility for test gene expression normalization. Actb/Hprt/Gapdh/Rps12/Tbp, Actb/Gapdh/Hprt/Rps12, Actb/Gapdh/Rps12/Tbp, Actb/Gapdh/Hprt/Tbp, Actb/Hprt/Rps12/Tbp, Gapdh/Hprt/Rps12/Tbp, Gapdh/Hprt/Rps12, Actb/Hprt and Gapdh/Rps12 had lower stability values (<0.05) than all individual gene stability

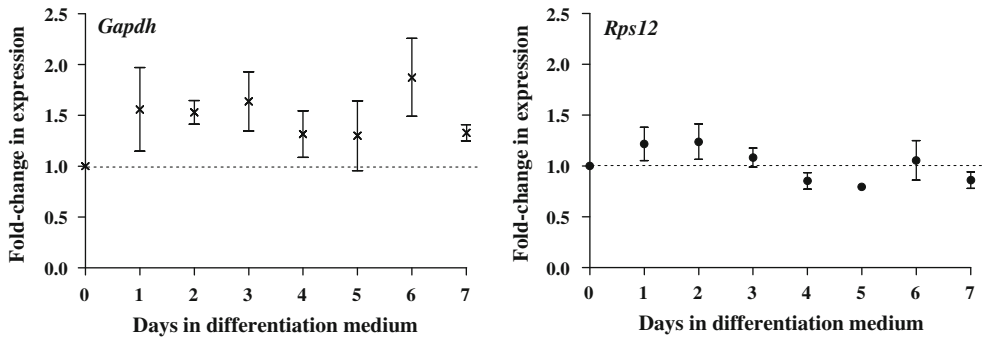

Fig. 3 qPCR expression profiles of two candidate reference genes in differentiating H9c2 cells. Individual gene expression profiles showing the fold-change in expression compared to D0. *Error bars* represent ± SEM from three biological replicates

Table 2 Results of statistical analyses

Tests performed	C2C12					H9c2	
	Actb	*Gapdh*	*Hprt*	*Rps12*	*Tbp*	*Gapdh*	*Rps12*
One-way ANOVA	0.022*	0.557	0.1756	0.0001***	0.1	0.4984	0.1634
Pearson correlation (r)	−0.9011	−0.6348	−0.9564	−0.9555	−0.9118	0.3160	−0.5831
p value (two-tailed)	0.0022**	0.0908	0.0002***	0.0002***	0.0016*	0.4457	0.1292
Pearson coefficient of determination (r^2)	0.8120	0.4030	0.9147	0.9130	0.8314	0.0998	0.3400

Significance: * $p < 0.05$; ** $p < 0.01$; *** $p < 0.001$

Pearson's correlation values closer to +1 or −1 indicate strong correlation

values (Fig. 4a, b), suggesting that multiple reference genes are the preferred method for normalizing test gene expression levels during C2C12 differentiation.

In H9c2 cells, the stability values for Gapdh (0.131) and Rps12 (0.131) were higher than the geometric mean of both these genes (0.046) (Fig. 4c), suggesting that the geometric mean is more suitable than the absolute expression level of either individual gene as a reference for test gene expression studies during differentiation.

Verification of the Suitability of the Chosen Reference Genes

To verify that the selected reference genes (based on NormFinder analysis) were suitable myoblast differentiation normalization controls, we used them to analyze expression of the myogenesis marker Myogenin during both C2C12 and H9c2 differentiation [43]. In C2C12 cells, using the geometric mean of the expression levels of all five selected reference genes (the most stable combination), only Actb/Gapdh/Hprt/Rps12 (the next most stable combination) or Gapdh/Hprt/Rps12, the fold-change in Myogenin mRNA expression was assessed, relative to Actb and Hprt (Fig. 5a). We observed that the geometric mean of five, four and three genes showed a gradual increase of Myogenin levels to D3, with a similar expression trend from D3 to D7, as previously reported by qPCR [44], RT-PCR [45] and Northern blot [46]. When Actb, the most variable of the five transcripts examined, was used as a reference gene we observed a different expression profile, with a four-fold greater increase on D1. Therefore, the geometric mean of the three reference genes Gapdh/Hprt/Rps12 was a reasonable normalization factor for Myogenin mRNA expression analysis in differentiating C2C12 cells. In H9c2 cells, using the geometric mean of Gapdh/Rps12 (Fig 5b), the induction and expression of Myogenin during differentiation was similar to that during C2C12 differentiation, suggesting that the geometric mean of these two transcripts is a suitable normalization factor for test gene expression analysis during H9c2 differentiation.

General Discussion of Results

The tremendous benefits provided by real-time qPCR technology for gene expression analysis in myogenic studies have been hampered by a serious lack of standards, making data interpretation a monumental task. Standards relating to data dissemination, including ambiguity in terminologies and experimental procedures, were addressed by the Minimal Information for publication of qPCR Experiments (MIQE) guidelines [47]. Standards relating to data collection, inherent in the experimental protocol,

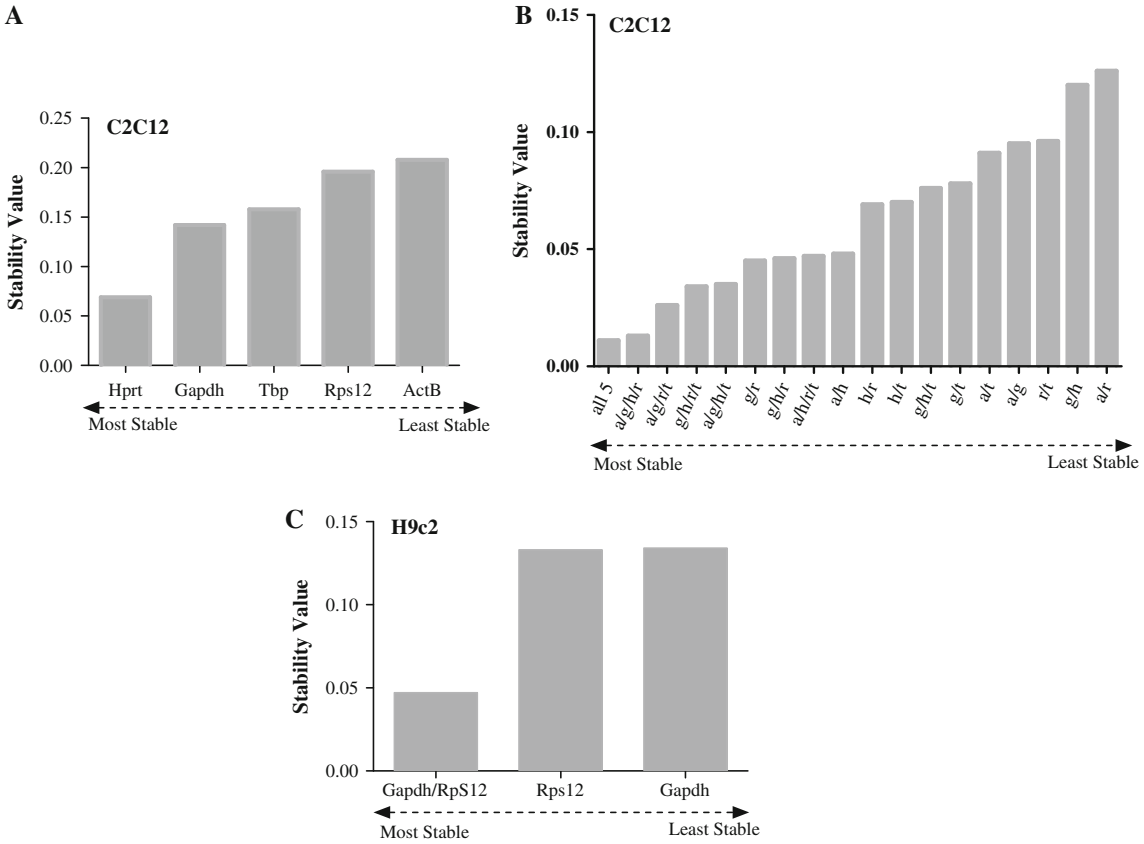

Fig. 4 Transcript stability values calculated using NormFinder. In C2C12 cells (**a**) graph representing the order of individual genes based on their transcript stability values (**b**) graph showing the order of different combinations of genes with their transcript stability values calculated based on the geometric mean. In H9c2 cells (**c**) graph showing the transcript stability values of Gapdh, Rps12 and the geometric mean of Gapdh/Rps12. The genes are ordered based on their transcript stability values (closer to 0 being the most stable). *A* Actb, g Gapdh, *h* Hprt, *r* Rps12, *t* Tbp

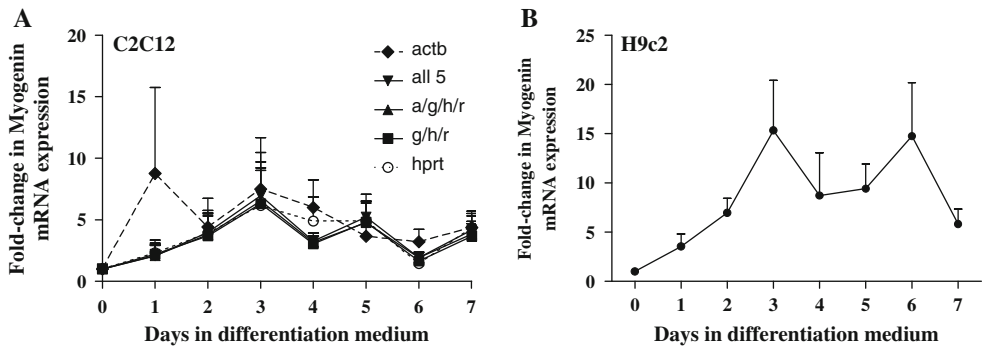

Fig. 5 qPCR expression level profile of Myogenin in differentiating C2C12 and H9c2 cells. (**a**) Myogenin expression in C2C12 cells, calculated after normalization using the individual reference genes (Actb or Hprt) or the geometric mean of three different reference gene combinations (Actb/Gapdh/Hprt/Rps12/Tbp, Actb/Gapdh/Hprt/Rps12, Gapdh/Hprt/Rps12). (**b**) Myogenin expression in H9c2 cells, calculated after normalization using the geometric mean of Gapdh and Rps12. In both the graphs, the fold-change in expression is compared to D0. *Error bars* represent ± SEM from four and three biological replicates in C2C12 and H9c2, respectively. *A* Actb, *g* Gapdh, *h* Hprt, *r* Rps12, *t* Tbp

remain to be addressed. This gap in data collection, accounted for mostly by incorrect normalization strategies, results in inaccurate quantification and interpretation of results. We have attempted to address the normalization issue in two commonly used in vitro models of differentiation and disease, C2C12 and H9c2 myoblasts.

Myoblast differentiation, most notably in C2C12 cells, is induced by different labs using a range of conditions. We

grew the C2C12 myoblasts in 10 % fetal bovine serum, induced differentiation using 2 % horse serum and examined expression over 7 days. Other labs may vary the percentage of serum in the GM and/or DM, the serum species in the DM and the number of days over which expression is analyzed [8, 48, 49]. It should be noted, therefore, that our results may not apply to all C2C12 differentiation protocols. Our results do support previous reports, however, showing that Actb expression decreases [37, 38] and Gapdh expression remains unchanged during C2C12 differentiation [37]. No previous reports have examined the suitability of the geometric mean of the gene combinations presented in this study as normalization controls during C2C12 differentiation. For H9c2 differentiation, the most commonly used reference gene is *Gapdh* [8, 48, 50]; however, we could find no reference to its validation as such. Thus, to our knowledge, this is the first assessment of either *Gapdh* or *Rps12* as a reference gene for H9c2 differentiation expression studies.

In summary, over seven days of C2C12 differentiation (from 10 % FBS to 2 % HS) and H9c2 skeletal differentiation (from 10 % FBS to 1 % FBS), our statistical and NormFinder analyses confirmed that a normalization factor obtained from the geometric averaging of multiple reference genes had the least expression level variability and was, therefore, the most suitable normalization control. The normalization data for C2C12 cells demonstrate that particular combinations of appropriate reference genes (as demonstrated in Fig. 4b) are more important than the number of reference genes used. This highlights the importance of using software programs like NormFinder, which allow accurate identification of the best combination of reference genes for a given system. Therefore, determination of the optimal normalization factor remains an important aspect of any expression study.

Acknowledgments This work was funded by an NSERC Vanier Canada Graduate Scholarship (CGS) to T.J.M., an NSERC Alexander Graham Bell Canada Graduate Scholarship to J.J.L., NSERC Grant # 9043429 to L.C.S. and the Northern Cancer Foundation. The authors would like to acknowledge some initial technical assistance from Tyler Kirwan, and reagents from - and discussions with - Celine Boudreau-Larivière.

Conflict of interest The authors declare no conflict of interest.

References

1. Molkentin, J. D., & Olson, E. N. (1996). Defining the regulatory networks for muscle development. *Current Opinion Genetics Development, 6*, 445–453.
2. Sabourin, L. A., & Rudnicki, M. A. (2000). The molecular regulation of myogenesis. *Clinical Genetics, 57*, 16–25.
3. Florini, J. R., Ewton, D. Z., & Coolican, S. A. (1996). Growth hormone and the insulin-like growth factor system in myogenesis. *Endocrine Reviews, 17*, 481–517.
4. Bijlenga, P., Liu, J. H., Espinos, E., Haenggeli, C. A., Fischer-Lougheed, J., Bader, C. R., et al. (2000). T-type alpha 1H Ca2 + channels are involved in Ca2 + signaling during terminal differentiation (fusion) of human myoblasts. *Proceedings National Academy Science USA, 97*, 7627–7632.
5. Knight, J. D., & Kothary, R. (2011). The myogenic kinome: protein kinases critical to mammalian skeletal myogenesis. *Skelet Muscle, 1*, 29.
6. Cabane, C., Englaro, W., Yeow, K., Ragno, M., & Derijard, B. (2003). Regulation of C2C12 myogenic terminal differentiation by MKK3/p38alpha pathway. *American Journal of Physiology Cell Physiology, 284*, C658–C666.
7. Casadei, L., Vallorani, L., Gioacchini, A. M., Guescini, M., Burattini, S., D'Emilio, A., et al. (2009). Proteomics-based investigation in C2C12 myoblast differentiation. *European Journal of Histochemistry, 53*, 261–268.
8. Ding, Y., Choi, K. J., Kim, J. H., Han, X., Piao, Y., Jeong, J. H., et al. (2008). Endogenous hydrogen peroxide regulates glutathione redox via nuclear factor erythroid 2-related factor 2 downstream of phosphatidylinositol 3-kinase during muscle differentiation. *American Journal of Pathology, 172*, 1529–1541.
9. Favreau, C., Delbarre, E., Courvalin, J. C., & Buendia, B. (2008). Differentiation of C2C12 myoblasts expressing lamin A mutated at a site responsible for Emery-Dreifuss muscular dystrophy is improved by inhibition of the MEK-ERK pathway and stimulation of the PI3-kinase pathway. *Experimental Cell Research, 314*, 1392–1405.
10. Wang, L., Ma, W., Markovich, R., Lee, W. L., & Wang, P. H. (1998). Insulin-like growth factor I modulates induction of apoptotic signaling in H9C2 cardiac muscle cells. *Endocrinology, 139*, 1354–1360.
11. Bland, C. S. Wang, E. T. Vu, A. David, M. P. Castle, J. C. Johnson, J. M. Burge, C. B. and Cooper, T. A. (2010) Global regulation of alternative splicing during myogenic differentiation. Nucleic Acids Residues 38, 7651–7664.
12. Bland, C. S. Wang, E. T. Vu, A. David, M. P. Castle, J. C. Johnson, J. M. Burge, C. B. and Cooper, T. A. (2010) Global regulation of alternative splicing during myogenic differentiation. Nucleic Acids Res 38, 7651–7664.
13. Soleimani, V. D., & Rudnicki, M. A. (2011). New insights into the origin and the genetic basis of rhabdomyosarcomas. *Cancer Cell, 19*, 157–159.
14. Fleige, S., & Pfaffl, M. W. (2006). RNA integrity and the effect on the real-time qRT-PCR performance. *Molecular Aspects of Medicine, 27*, 126–139.
15. Eisenberg, E., & Levanon, E. Y. (2003). Human housekeeping genes are compact. *Trends in Genetics, 19*, 362–365.
16. Dheda, K., Huggett, J. F., Bustin, S. A., Johnson, M. A., Rook, G., & Zumla, A. (2004). Validation of housekeeping genes for normalizing RNA expression in real-time PCR. *BioTechniques, 37*, 112–119.
17. Gutierrez, L., Mauriat, M., Pelloux, J., Bellini, C., & Van, W. O. (2008). Towards a systematic validation of references in real-time rt-PCR. *Plant Cell, 20*, 1734–1735.
18. Vandesompele, J. De, P. K. Pattyn, F. Poppe, B. Van, R. N. De, P. A. and Speleman, F. (2002) Accurate normalization of real-time quantitative RT-PCR data by geometric averaging of multiple internal control genes. Genome Biol 3, RESEARCH0034.
19. Tanaka, S., Terada, K., & Nohno, T. (2011). Canonical Wnt signaling is involved in switching from cell proliferation to myogenic differentiation of mouse myoblast cells. *J Mol Signal., 6*, 12.
20. Pfaffl, M. W., Tichopad, A., Prgomet, C., & Neuvians, T. P. (2004). Determination of stable housekeeping genes, differentially regulated target genes and sample integrity: BestKeeper–Excel-based tool using pair-wise correlations. *Biotechnology Letters, 26*, 509–515.

21. Andersen, C. L., Jensen, J. L., & Orntoft, T. F. (2004). Normalization of real-time quantitative reverse transcription-PCR data: a model-based variance estimation approach to identify genes suited for normalization, applied to bladder and colon cancer data sets. *Cancer Research, 64*, 5245–5250.
22. Sakiyama, K., Abe, S., Tamatsu, Y., & Ide, Y. (2005). Effects of stretching stress on the muscle contraction proteins of skeletal muscle myoblasts. *Biomedical Research, 26*, 61–68.
23. Stuelsatz, P., Pouzoulet, F., Lamarre, Y., Dargelos, E., Poussard, S., Leibovitch, S., et al. (2010). Down-regulation of MyoD by calpain 3 promotes generation of reserve cells in C2C12 myoblasts. *Journal of Biological Chemistry, 285*, 12670–12683.
24. Mamo, S., Gal, A. B., Bodo, S., & Dinnyes, A. (2007). Quantitative evaluation and selection of reference genes in mouse oocytes and embryos cultured in vivo and in vitro. *BMC Developmental Biology, 7*, 14.
25. de Jonge, H. J., de Fehrmann, R. S., Bont, E. S., Hofstra, R. M., Gerbens, F., de Kamps, W. A., et al. (2007). Evidence based selection of housekeeping genes. *PLoS One, 2*, e898.
26. Willems, E., Mateizel, I., Kemp, C., Cauffman, G., Sermon, K., & Leyns, L. (2006). Selection of reference genes in mouse embryos and in differentiating human and mouse ES cells. *International Journal of Developmental Biology, 50*, 627–635.
27. Lokireddy, S., Wijesoma, I. W., Teng, S., Bonala, S., Gluckman, P. D., McFarlane, C., et al. (2012). The ubiquitin ligase Mul1 induces mitophagy in skeletal muscle in response to muscle-wasting stimuli. *Cell Metabolism, 16*, 613–624.
28. Zhang, R., Edwards, J. R., Ko, S. Y., Dong, S., Liu, H., Oyajobi, B. O., et al. (2011). Transcriptional regulation of BMP2 expression by the PTH-CREB signaling pathway in osteoblasts. *PLoS One, 6*, e20780.
29. Ogawa, M., Mizofuchi, H., Kobayashi, Y., Tsuzuki, G., Yamamoto, M., Wada, S., et al. (2012). Terminal differentiation program of skeletal myogenesis is negatively regulated by O-GlcNAc glycosylation. *Biochimica et Biophysica Acta, 1820*, 24–32.
30. Diel, P., Baadners, D., Schlupmann, K., Velders, M., & Schwarz, J. P. (2008). C2C12 myoblastoma cell differentiation and proliferation is stimulated by androgens and associated with a modulation of myostatin and Pax7 expression. *Journal of Molecular Endocrinology, 40*, 231–241.
31. Dugina, V., Zwaenepoel, I., Gabbiani, G., Clement, S., & Chaponnier, C. (2009). Beta and gamma-cytoplasmic actins display distinct distribution and functional diversity. *Journal of Cell Science, 122*, 2980–2988.
32. Seidler, N. W. (2013). Basic biology of GAPDH. *Advances in Experimental Medicine and Biology, 985*, 1–36.
33. Gassmann, M. G., Stanzel, A., & Werner, S. (1999). Growth factor-regulated expression of enzymes involved in nucleotide biosynthesis: a novel mechanism of growth factor action. *Oncogene, 18*, 6667–6676.
34. Meyers, R. E., & Sharp, P. A. (1993). TATA-binding protein and associated factors in polymerase II and polymerase III transcription. *Molecular and Cellular Biology, 13*, 7953–7960.
35. Londhe, P., & Davie, J. K. (2011). Sequential association of myogenic regulatory factors and E proteins at muscle-specific genes. *Skelet. Muscle, 1*, 14.
36. Londhe, P., & Davie, J. K. (2011). Gamma interferon modulates myogenesis through the major histocompatibility complex class II transactivator, CIITA. *Molecular and Cellular Biology, 31*, 2854–2866.
37. Nishimura, M., Nikawa, T., Kawano, Y., Nakayama, M., & Ikeda, M. (2008). Effects of dimethyl sulfoxide and dexamethasone on mRNA expression of housekeeping genes in cultures of C2C12 myotubes. *Biochemical and Biophysical Research Communications, 367*, 603–608.
38. Lloyd, C., & Gunning, P. (2002). beta- and gamma-actin genes differ in their mechanisms of down-regulation during myogenesis. *Journal of Cellular Biochemistry, 84*, 335–342.
39. Schmittgen, T. D., & Livak, K. J. (2008). Analyzing real-time PCR data by the comparative C(T) method. *Nature Protocols, 3*, 1101–1108.
40. Souaze, F., Ntodou-Thome, A., Tran, C. Y., Rostene, W., & Forgez, P. (1996). Quantitative RT-PCR: limits and accuracy. *BioTechniques, 21*, 280–285.
41. Larionov, A., Krause, A., & Miller, W. (2005). A standard curve based method for relative real time PCR data processing. *BMC Bioinformatics, 6*, 62.
42. Ali, S. A., Zaidi, S. K., Dacwag, C. S., Salma, N., Young, D. W., Shakoori, A. R., et al. (2008). Phenotypic transcription factors epigenetically mediate cell growth control. Proc Natl Acad Sci U. *S. A, 105*, 6632–6637.
43. Charge, S. B., & Rudnicki, M. A. (2004). Cellular and molecular regulation of muscle regeneration. *Physiological Reviews, 84*, 209–238.
44. Janot, M., Audfray, A., Loriol, C., Germot, A., Maftah, A., & Dupuy, F. (2009). Glycogenome expression dynamics during mouse C2C12 myoblast differentiation suggests a sequential reorganization of membrane glycoconjugates. *BMC Genomics, 10*, 483.
45. Yang, J. H., Song, Y., Seol, J. H., Park, J. Y., Yang, Y. J., Han, J. W., et al. (2011). Myogenic transcriptional activation of MyoD mediated by replication-independent histone deposition. *Proceedings National Academy Science USA, 108*, 85–90.
46. Figueroa, A., Cuadrado, A., Fan, J., Atasoy, U., Muscat, G. E., Munoz-Canoves, P., et al. (2003). Role of HuR in skeletal myogenesis through coordinate regulation of muscle differentiation genes. *Molecular and Cellular Biology, 23*, 4991–5004.
47. Bustin, S. A., Benes, V., Garson, J. A., Hellemans, J., Huggett, J., Kubista, M., et al. (2009). The MIQE guidelines: minimum information for publication of quantitative real-time PCR experiments. *Clinical Chemistry, 55*, 611–622.
48. Kee, H. J., Kim, J. R., Joung, H., Choe, N., Lee, S. E., Eom, G. H., et al. (2012). Ret finger protein inhibits muscle differentiation by modulating serum response factor and enhancer of polycomb1. *Cell Death and Differentiation, 19*, 121–131.
49. Miller, J. B. (1990). Myogenic programs of mouse muscle cell lines: expression of myosin heavy chain isoforms, MyoD1, and myogenin. *Journal of Cell Biology, 111*, 1149–1159.
50. Leong, C. W., Wong, C. H., Lao, S. C., Leong, E. C., Lao, I. F., Law, P. T., et al. (2007). Effect of resveratrol on proliferation and differentiation of embryonic cardiomyoblasts. *Biochemical and Biophysical Research Communications, 360*, 173–180.

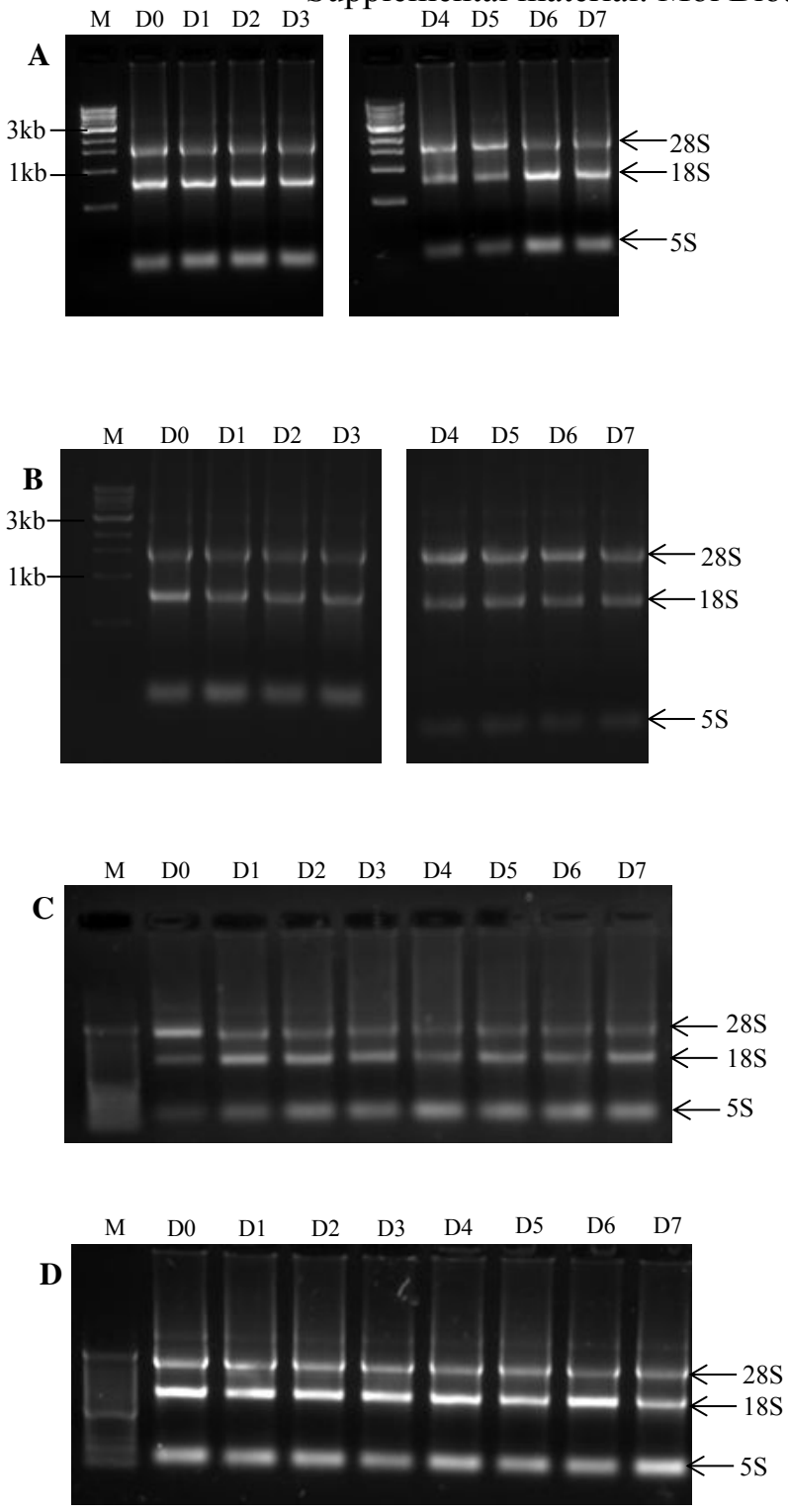

Figure 1S. Visualization of total RNA extracted from differentiating C2C12 cells (D0 to D7) following agarose gel electrophoresis. RNA samples from 4 biological replicates (A), (B), (C) and (D) from day 0 to day 7 visualized in a 1% agarose gel stained with SYBR® safe DNA gel stain. M: 1kb ladder (NEB)

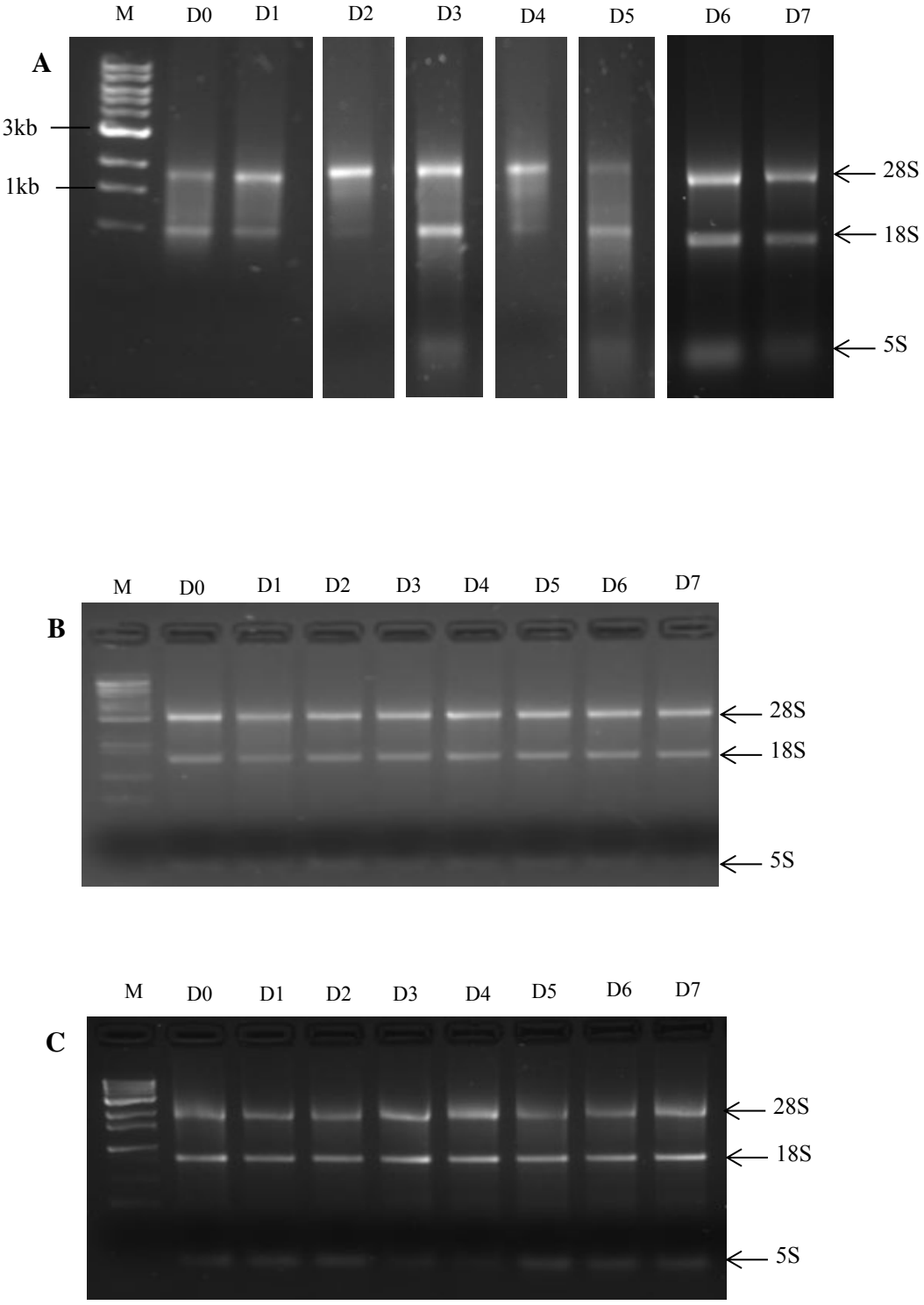

Figure 2S. Visualization of total RNA extracted from differentiating H9c2 cells (D0 to D7) following agarose gel electrophoresis. RNA samples from 3 biological replicates (A), (B) and (C) from day 0 to day 7 visualized in a 1% agarose gel stained with SYBR® safe DNA gel stain. M: 1kb DNA ladder (NEB)

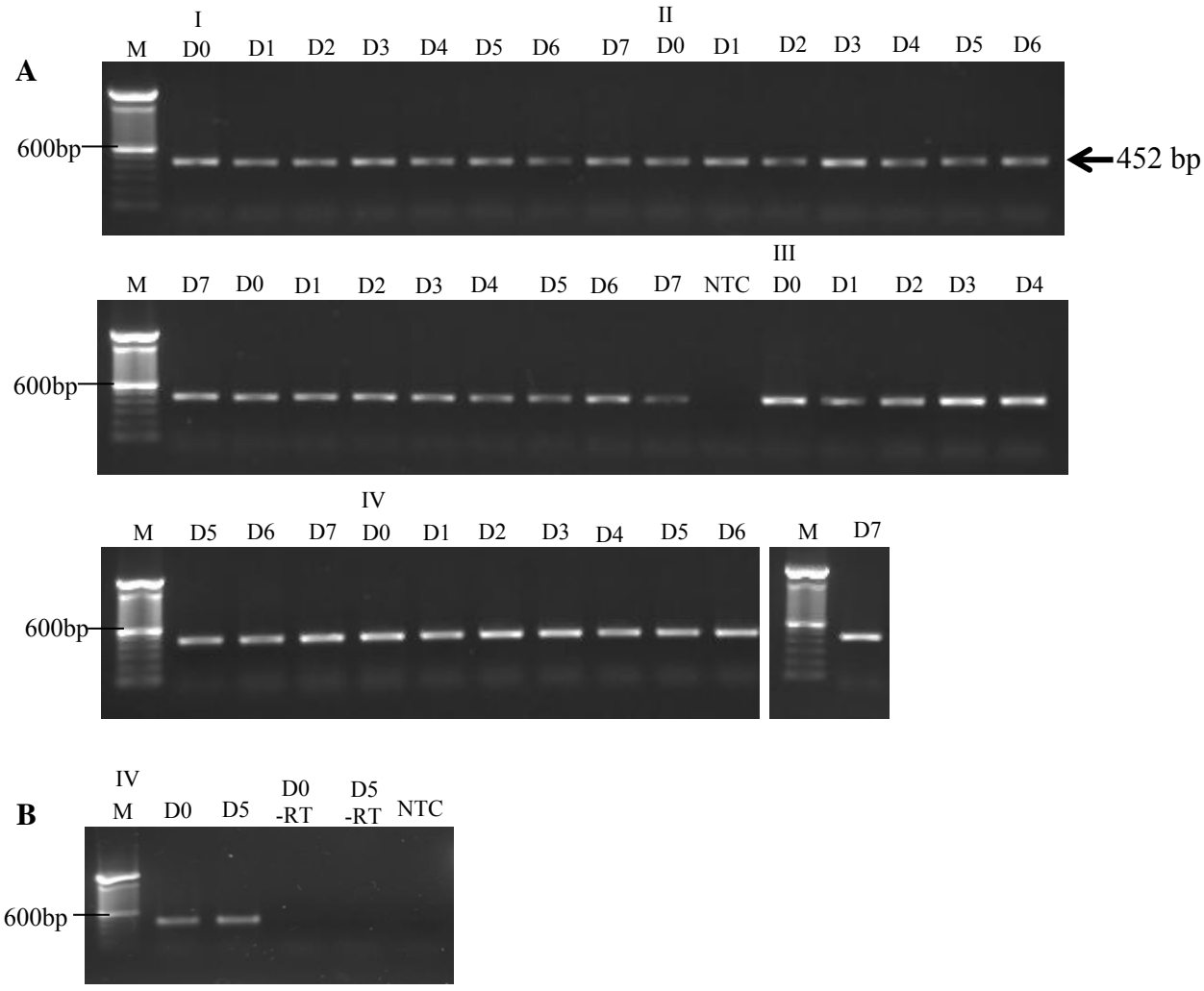

Figure 3S. End-point PCR for Gapdh in C2C12 cells. A) A 452 bp amplified fragment from four biological replicates (I, II, III and IV), visualized in a 1% agarose gel stained with SYBR® safe DNA gel stain. In case of genomic DNA contamination, a 646 bp fragment would be expected. B) Results of +RT enzyme and -RT enzyme of day 0 and day 5 samples from biological replicate IV. M: 100 bp DNA ladder (Life Technologies). NTC: No template control.

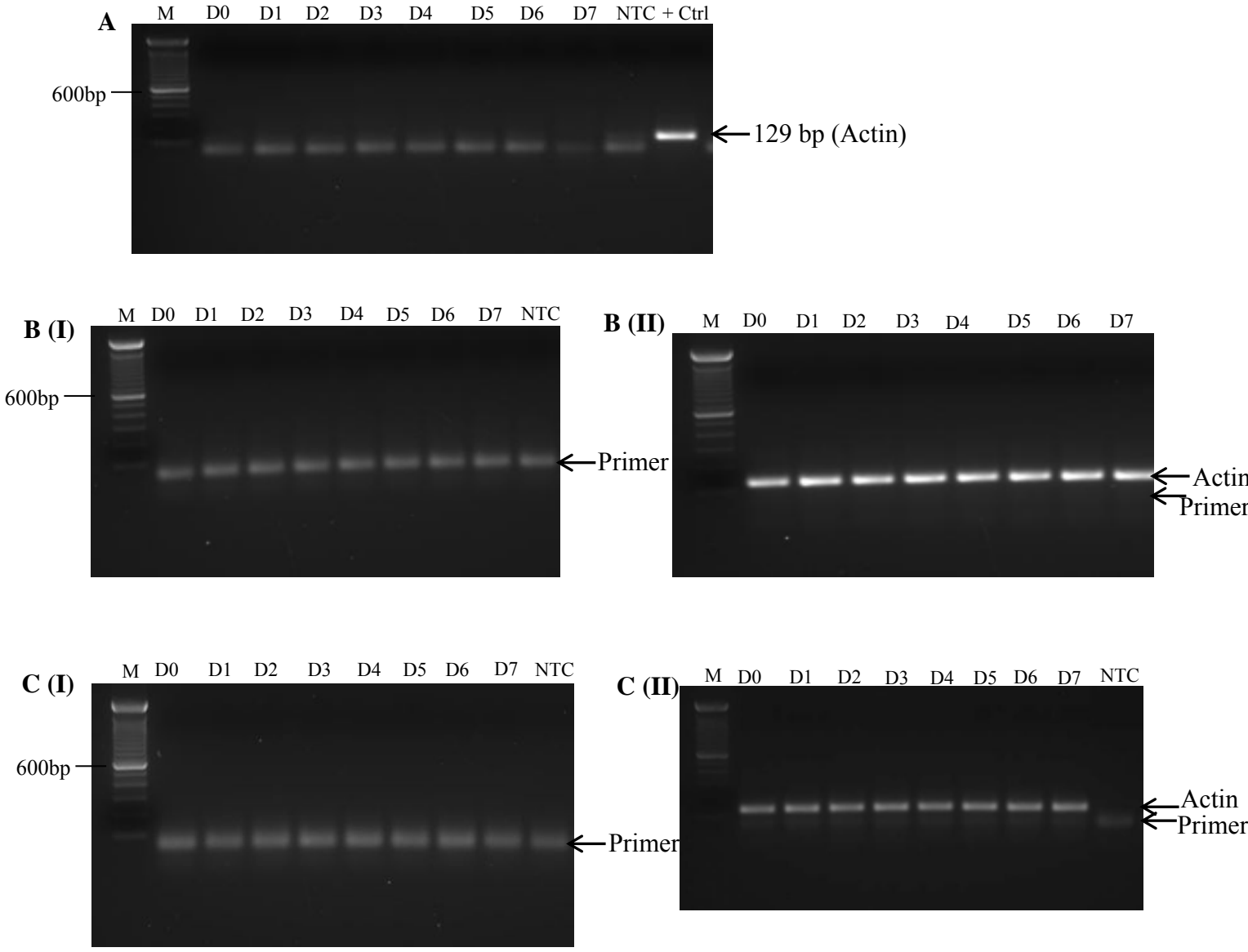

Figure4S. Actin amplification for genomic DNA contamination verification in H9c2 cells. RNA samples from three biological replicates were used to prepare cDNA with and without the addition of MMLV-RT reverse transcriptase enzyme. Actin was then amplified from the samples and visualized in a 2% agarose gel stained with SYBR® safe DNA gel stain to verify that there was no genomic contamination in the RNA samples. A) Results of –RT enzyme cDNA from day 0 to 7 of skeletal differentiation for biological replicate 1. Positive control refers to cDNA reaction to which the RT enzyme was added. B) Results of –RT enzyme cDNA (I) and +RT enzyme cDNA (II) following actin amplification from day 0 to 7 of skeletal differentiation cDNA samples from biological replicate 2. C) Results of –RT enzyme cDNA (I) and +RT enzyme cDNA (II) following actin amplification from day 0 to 7 of skeletal differentiation cDNA samples from biological replicate 3. M: 100 bp DNA ladder (Life Technologies). NTC: No template control.

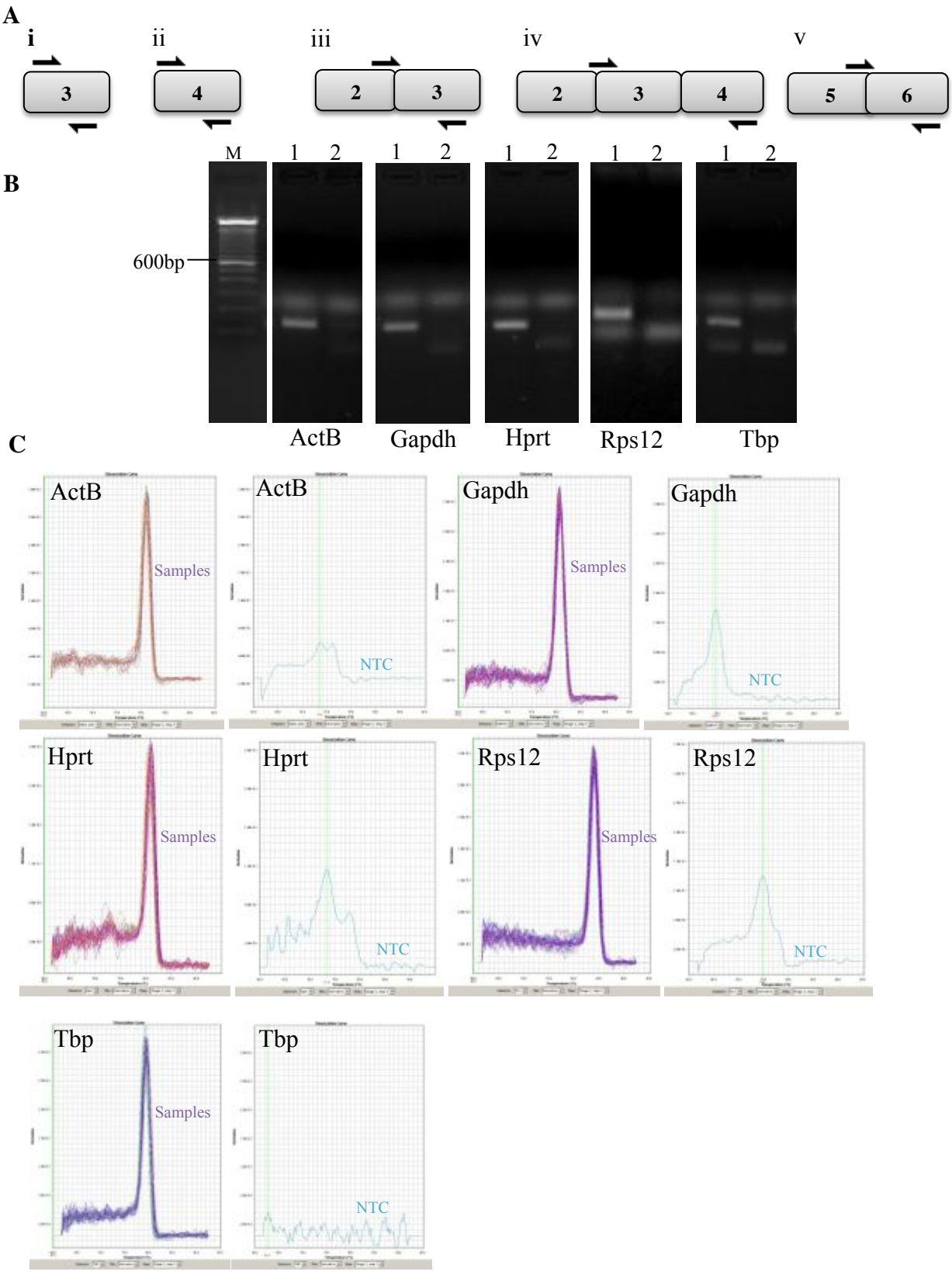

Figure 5S. Primer location, qPCR products and dissociation curve in C2C12 cells. A) The location of forward and reverse primer in relationship to exons for i) ActB, ii) Gapdh, iii) Hprt, iv) Rps12 and v) Tbp. B) qPCR products of (1) sample and (2) no template control (NTC) stained with SYBR® safe DNA gel stain and visualized in a 2% agarose gel. C) Dissociation curves of samples and NTC from one biological replicate showing the melt curve profile.

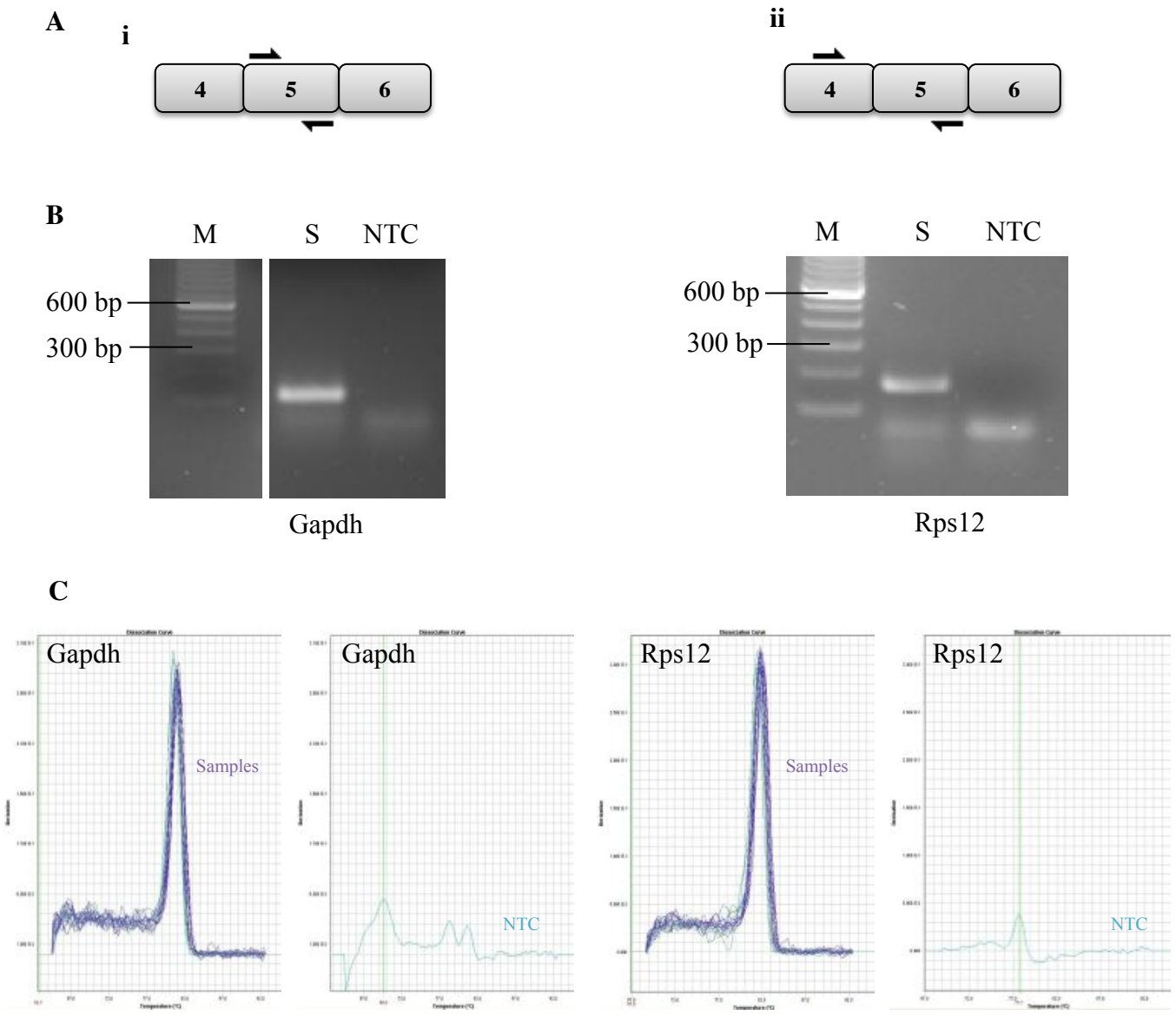

Figure 6S. Primer location, qPCR products and dissociation curve in H9c2 cells. A) The location of the forward and reverse primer in relationship to exons for i) Gapdh and ii) Rps12. B) qPCR products of (S) sample and (NTC) no template control stained with SYBR® safe DNA gel stain and visualized in a 2% agarose gel. C) Dissociation curves of samples and NTC from one biological replicate showing the melt curve profile.

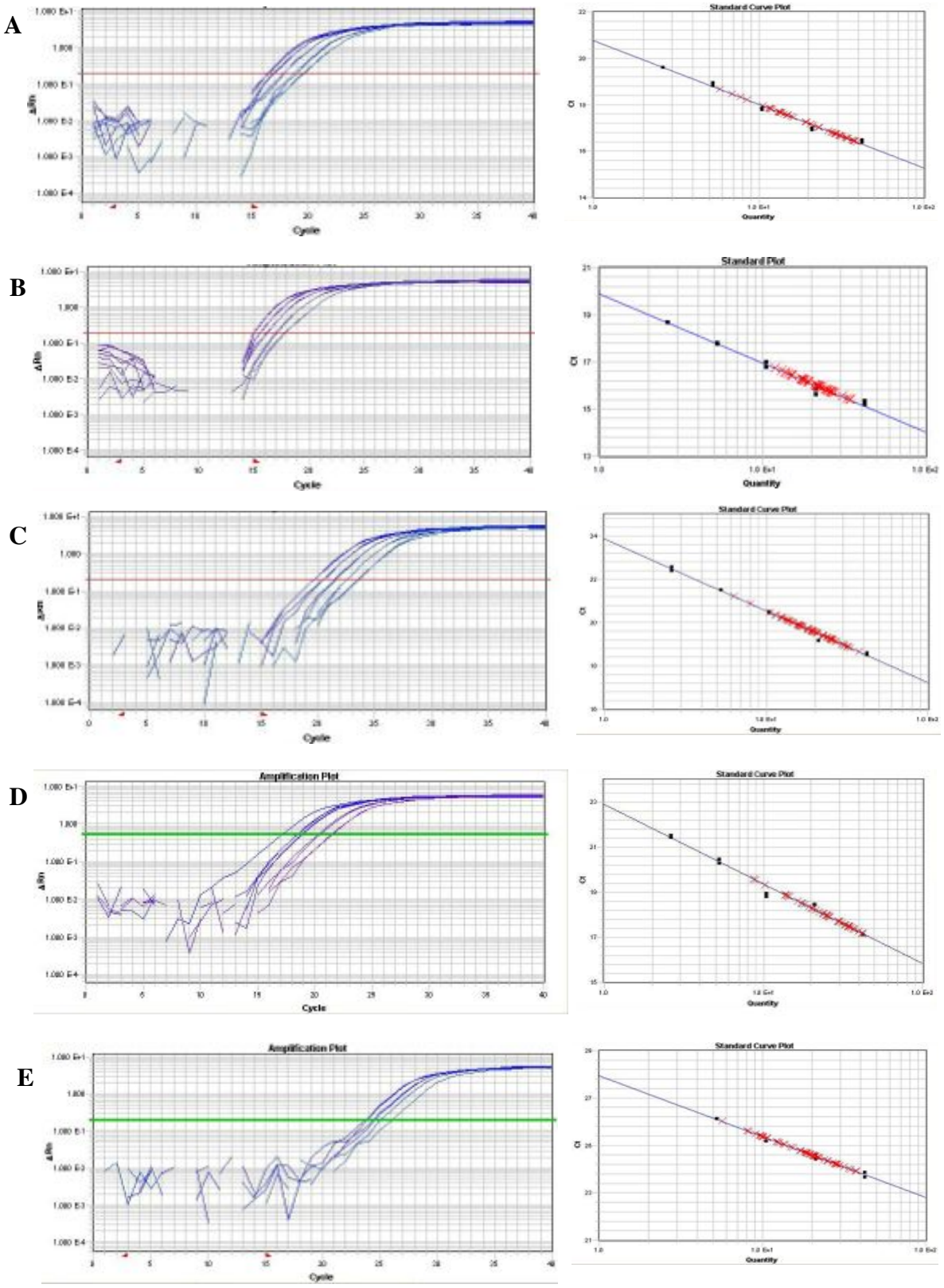

Figure 7S. **Amplification plot and standard curves in C2C12 cells.** Amplification plot showing the Cq of the standard dilutions for A) ActB, B) Gapdh, C) Hprt, D) Rps12 and E) Tbp. Standard curves generated using different dilutions of the pooled cDNA, the Cq values are plotted on the Y-axis and the logarithmic values of the quantity are plotted on the X-axis.

A

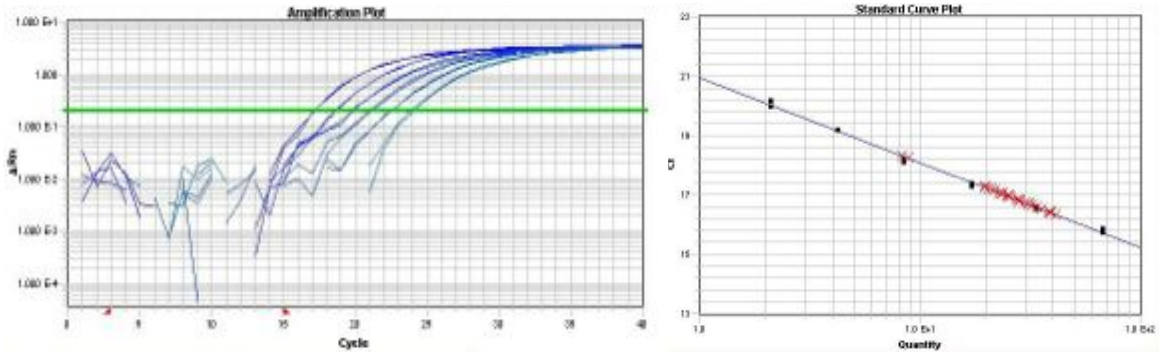

B

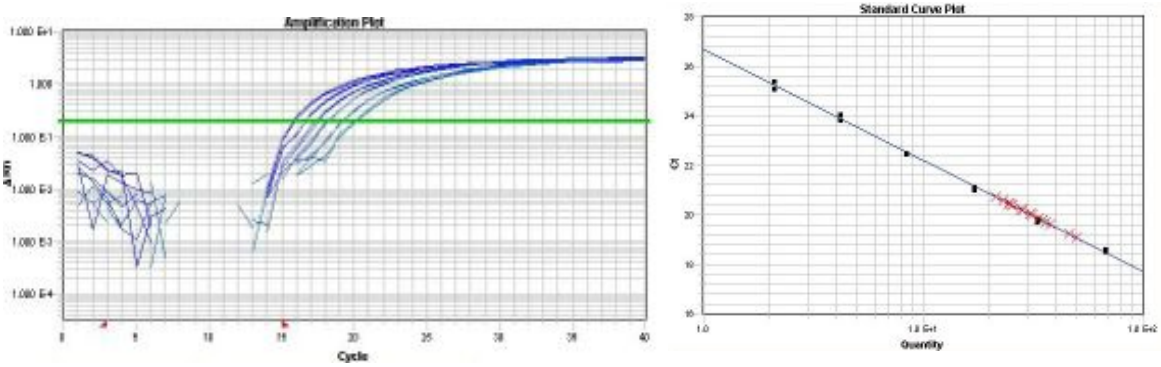

Figure 8S. **Amplification plots and standard curves in H9c2 cells.** Amplification plot showing the Cq of the standard dilutions for A) Gapdh, and B) Rps12. Standard curves generated using different dilutions of the pooled cDNA, the Cq values are plotted on the Y-axis and the logarithmic values of the quantity are plotted on the X-axis

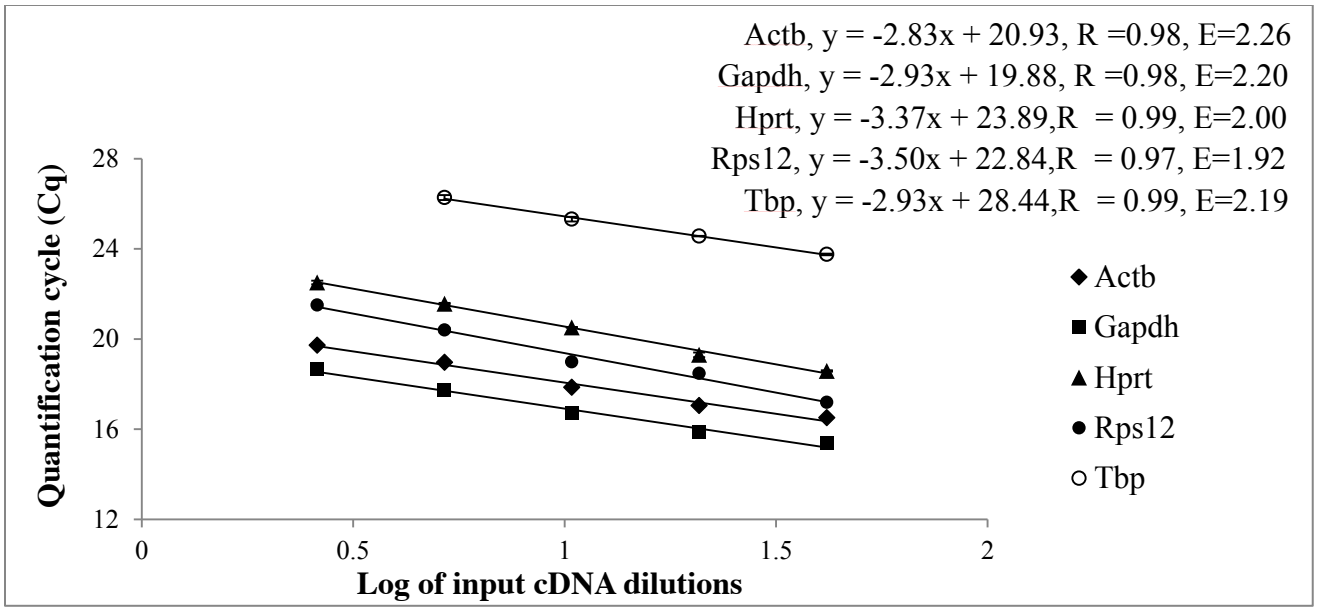

Figure 9S. C2C12 qPCR standard curves. Standard curves generated using dilutions of the pooled cDNAs for Actb, Gapdh, Hprt, Rps12 and Tbp in C2C12 cells. Y axis represents the Cq value and the x axis represents the logarithmic values of the concentration of input cDNA. Error bars represent SEM from technical replicates (n=4). The equation indicates the slope, y intercept, R^2 values and the efficiency of the qPCR reaction (E). E is calculated by the formula E= POWER (10,-(1/slope)).

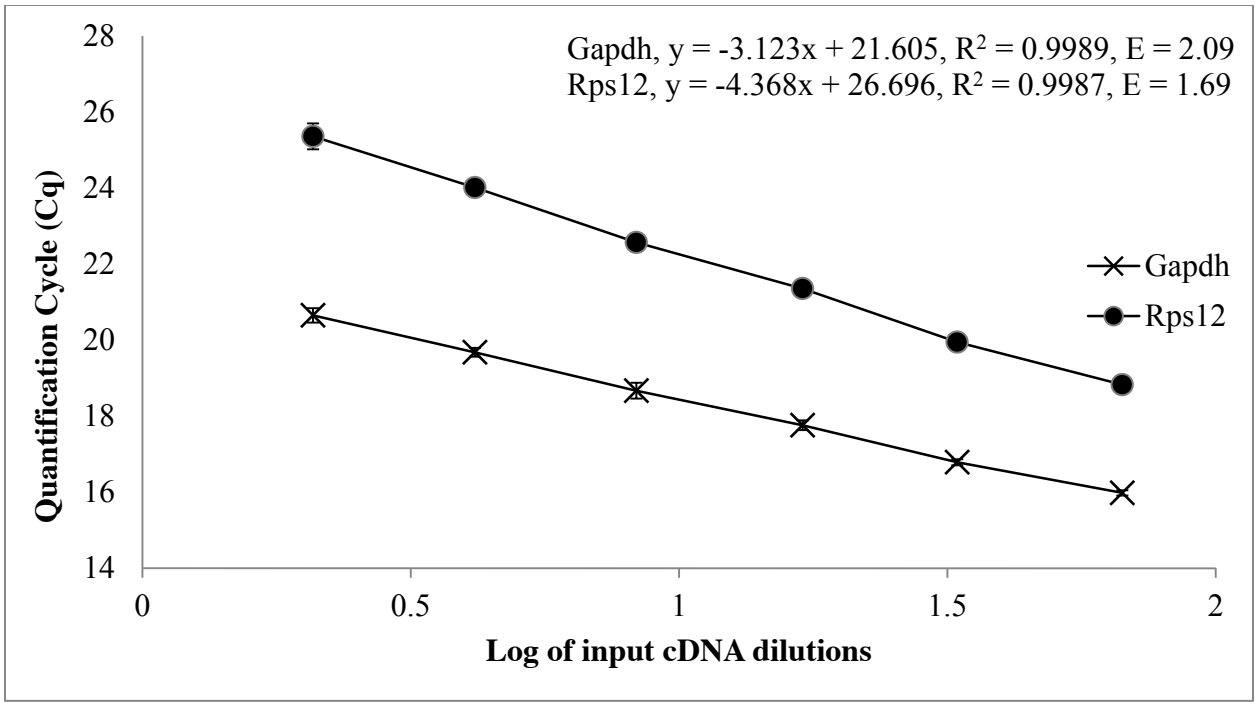

Figure 10S. H9c2 qPCR standard curves. Standard curves generated using dilutions of the pooled cDNAs for Gapdh and Rps12 in H9c2 cells. Y axis represents the Cq value and the x axis represents the logarithmic values of the concentration of input cDNA. Error bars represent SEM from technical duplicates. The equation indicates the slope, y intercept, R^2 values and the efficiency of the qPCR reaction (E). E is calculated by the formula E= POWER (10,-(1/slope)).

Supplementary Table 1S. Inter- and intra- assay variations
C2C12

ActB		D1 Mean ± SEM	D2 Mean ± SEM	D3 Mean ± SEM	D4 Mean ± SEM	D5 Mean ± SEM	D6 Mean ± SEM	D7 Mean ± SEM
Biological Replicate	**1**	1.556 ± 0.152	0.959 ± 0.067	0.937 ± 0.047	0.389 ± 0.035	0.318 ± 0.020	0.231 ± 0.022	0.322 ± 0.023
	2	0.741 ± 0.137	1.217 ± 0.110	0.465 ± 0.052	0.528 ± 0.189	0.630 ± 0.059	0.434 ± 0.108	0.244 ± 0.038
	3	0.374 ± 0.110	0.506 ± 0.091	0.461 ± 0.106	0.365 ± 0.166	0.749 ± 0.247	0.619 ± 0.020	0.695 ± 0.011
	4	2.173 ± 0.142	1.298 ± 0.142	1.090 ± 0.125	1.012 ± 0.199	0.687 ± 0.009	0.417 ± 0.133	0.682 ± 0.048
Overall Average		1.211 ± 0.404	0.995 ± 0.178	0.739 ± 0.161	0.574 ± 0.150	0.689 ± 0.034	0.425 ± 0.079	0.486 ± 0.118

Gapdh		D1 Mean ± SEM	D2 Mean ± SEM	D3 Mean ± SEM	D4 Mean ± SEM	D5 Mean ± SEM	D6 Mean ± SEM	D7 Mean ± SEM
Biological Replicate	**1**	1.168 ± 0.126	0.953 ± 0.066	0.930 ± 0.081	0.621 ± 0.063	0.618 ± 0.078	0.656 ± 0.059	0.611 ± 0.081
	2	0.907 ± 0.033	1.586 ± 0.102	0.714 ± 0.095	1.284 ± 0.051	1.096 ± 0.079	0.839 ± 0.031	0.631 ± 0.043
	3	0.324 ± 0.016	0.952 ± 0.054	0.886 ± 0.004	0.462 ± 0.0006	0.883 ± 0.064	1.013 ± 0.073	0.836 ± 0.034
	4	1.836 ± 0.016	1.507 ± 0.060	1.581 ± 0.062	1.379 ± 0.087	1.027 ± 0.004	0.975 ± 0.080	1.269 ± 0.251
Overall Average		1.059 ± 0.313	1.248 ± 0.171	0.843 ± 0.066	0.936 ± 0.231	0.906 ± 0.105	0.871 ± 0.080	0.837 ± 0.152

Hprt		D1 Mean ± SEM	D2 Mean ± SEM	D3 Mean ± SEM	D4 Mean ± SEM	D5 Mean ± SEM	D6 Mean ± SEM	D7 Mean ± SEM
Biological Replicate	**1**	1.198 ± 0.329	0.904 ± 0.586	0.997 ± 0.217	0.972 ± 0.212	0.602 ± 0.139	0.657 ± 0.094	0.527 ± 0.101
	2	0.652 ± 0.208	0.547 ± 0.138	0.629 ± 0.123	0.591 ± 0.073	0.536 ± 0.117	0.744 ± 0.056	0.145 ± 0.007
	3	0.466 ± 0.080	0.719 ± 0.079	0.680 ± 0.087	0.439 ± 0.105	0.694 ± 0.250	1.157 ± 0.279	0.889 ± 0.261
	4	1.441 ± 0.053	1.265 ± 0.046	0.878 ± 0.157	0.945 ± 0.050	0.621 ± 0.053	0.717 ± 0.047	0.832 ± 0.060
Overall Average		0.939 ± 0.228	0.859 ± 0.153	0.796 ± 0.085	0.737 ± 0.131	0.613 ± 0.032	0.706 ± 0.025	0.598 ± 0.170

Rps12		D1 Mean ± SEM	D2 Mean ± SEM	D3 Mean ± SEM	D4 Mean ± SEM	D5 Mean ± SEM	D6 Mean ± SEM	D7 Mean ± SEM
Biological Replicate	**1**	0.849 ± 0.092	0.655 ± 0.016	0.683 ± 0.018	0.655 ± 0.034	0.463 ± 0.017	0.436 ± 0.075	0.376 ± 0.033
	2	0.746 ± 0.003	0.593 ± 0.020	0.598 ± 0.000	0.588 ± 0.037	0.450 ± 0.001	0.463 ± 0.033	0.256 ± 0.003
	3	0.532 ± 0.013	1.039 ± 0.029	0.480 ± 0.014	0.396 ± 0.006	0.642 ± 0.006	0.867 ± 0.0321	0.838 ± 0.060
	4	0.895 ± 0.046	0.684 ± 0.024	0.485 ± 0.006	0.388 ± 0.011	0.328 ± 0.009	0.274 ± 0.003	0.371 ± 0.011
Overall Average		0.755 ± 0.081	0.644 ± 0.026	0.562 ± 0.048	0.507 ± 0.067	0.414 ± 0.042	0.392 ± 0.059	0.335 ± 0.039

Tbp		D1 Mean ± SEM	D2 Mean ± SEM	D3 Mean ± SEM	D4 Mean ± SEM	D5 Mean ± SEM	D6 Mean ± SEM	D7 Mean ± SEM
Biological Replicate	**1**	1.227 ± 0.162	0.926 ± 0.113	0.933 ± 0.081	0.829 ± 0.088	0.501 ± 0.013	0.542 ± 0.151	0.435 ± 0.024
	2	0.806 ± 0.213	0.546 ± 0.128	0.540 ± 0.198	0.464 ± 0.102	0.473 ± 0.131	0.762 ± 0.084	0.138 ± 0.008
	3	0.219 ± 0.026	0.476 ± 0.022	0.369 ± 0.027	0.212 ± 0.015	0.520 ± 0.024	0.800 ± 0.036	0.594 ± 0.094
	4	1.818 ± 0.0007	1.204 ± 0.198	0.894 ± 0.041	0.720 ± 0.047	0.325 ± 0.013	0.336 ± 0.032	0.467 ± 0.013
Overall Average		1.015 ± 0.338	0.799 ± 0.170	0.694 ± 0.138	0.565 ± 0.138	0.512 ± 0.012	0.621 ± 0.106	0.407 ± 0.047

H9c2

Rps12		D1 Mean ± SEM	D2 Mean ± SEM	D3 Mean ± SEM	D4 Mean ± SEM	D5 Mean ± SEM	D6 Mean ± SEM	D7 Mean ± SEM
Biological Replicate	**1**	1.433 ± 0.226	1.532 ± 0.269	1.261 ± 0.109	0.721 ± 0.294	0.758 ± 0.092	1.446 ± 0.150	0.942 ± 0.148
	2	0.896 ± 0.072	1.259 ± 0.055	1.057 ± 0.073	1.000 ± 0.089	0.774 ± 0.081	0.863 ± 0.041	0.699 ± 0.048
	3	1.326 ± 0.116	0.928 ± 0.052	0.936 ± 0.101	0.843 ± 0.064	0.850 ± 0.079	0.059 ± 0.041	0.942 ± 0.088
Overall Average		1.218 ± 0.164	1.240 ± 0.174	1.084 ± 0.095	0.855 ± 0.081	0.794 ± 0.029	1.056 ± 0.195	0.861 ± 0.081

Gapdh		D1 Mean ± SEM	D2 Mean ± SEM	D3 Mean ± SEM	D4 Mean ± SEM	D5 Mean ± SEM	D6 Mean ± SEM	D7 Mean ± SEM
Biological Replicate	**1**	2.137 ± 0.184	1.419 ± 0.156	1.660 ± 0.092	1.130 ± 0.066	0.634 ± 0.059	2.443 ± 0.183	1.229 ± 0.336
	2	0.765 ± 0.034	1.763 ± 0.055	2.013 ± 0.024	1.772 ± 0.353	1.787 ± 0.058	2.037 ± 0.038	1.272 ± 0.038
	3	1.777 ± 0.193	1.406 ± 0.133	1.122 ± 0.016	1.045 ± 0.073	1.482 ± 0.126	1.143 ± 0.120	1.487 ± 0.099
Overall Average		1.560 ± 0.411	1.530 ± 0.117	1.598 ± 0.259	1.315 ± 0.229	1.301 ± 0.345	1.874 ± 0.384	1.329 ± 0.080